Cranfield University

Vitor Emanuel M. Loureiro S. Pereira

Computer Model to Predict Electron Beam-Physical Vapour Deposition (EB-PVD) Thermal Barrier Coating (TBC) Deposition on Substrates with Complex Geometry

School of Industrial and Manufacturing Science

PhD Thesis

Cranfield University

School of Industrial and Manufacturing Science

PhD Thesis

Academic Year 1999-2000

Vitor Emanuel M. Loureiro S. Pereira

Computer Model to Predict Electron Beam-Physical Vapour Deposition (EB-PVD) Thermal Barrier Coating (TBC) Deposition on Substrates with Complex Geometry

Supervisors: Prof. J. R. Nicholls
Dr. T. W. Shaw

July 2000

This thesis is submitted in fulfilment of the
requirements for the Degree of Doctor in Philosophy

ALL
MISSING
PAGES ARE
BLANK

Abstract

For many decades gas turbine engineers have investigated methods to improve engine efficiency further. These methods include advances in the composition and processing of materials, intricate cooling techniques, and the use of protective coatings. Thermal barrier coatings (TBCs) are the most promising development in superalloy coatings research in recent years with the potential to reduce metal surface temperature, or increase turbine entry temperature, by 70-200°C.

In order for TBCs to be exploited to their full potential, they need to be applied to the most demanding of stationary and rotating components, such as first stage blades and vanes. Comprehensive reviews of coating processes indicate that this can only be achieved on rotating components by depositing a strain-tolerant layer applied by the electron beam-physical vapour deposition (EB-PVD) coating process.

A computer program has been developed in Visual C++ based on the Knudsen cosine law and aimed at calculating the coating thickness distribution around any component, but typically turbine blades. This should permit the controlled deposition to tailor the TBC performance and durability. Various evaporation characteristics have been accommodated by developing a generalised point source evaporation model that involves real and virtual sources.

Substrates with complex geometry can be modelled by generating an STL file from a CAD package with the geometric information of the component, which may include shadow-masks. Visualisation of the coated thickness distributions around components was achieved using OpenGL library functions within the computer model.

This study then proceeded to verify the computer model by first measuring the coating thickness for experimental trial runs and then comparing the calculated coating thickness to that measured using a laboratory coater. Predicted thickness distributions are in good agreement even for the simplified evaporation model, but can be improved further by increasing the complexity of the source model.

Contents in Brief

Table of Contents

List of Figures

List of Tables

Abbreviations

3D	three-dimensional
Å	angstrom(s)
API	application programming interface
APS	air (or atmospheric) plasma spraying
ASCII	American standard code for information interchange
ATCS	atmosphere and temperature controlled spraying
C	degrees centigrade
CAD	computer-aided design
CAM	computer-aided manufacturing
cc	cubic centimetre(s)
CEC	Commission of European Communities
COST	collaboration in science and technology
CTE	coefficient of thermal expansion
CVD	chemical vapour deposition
DS	directional solidification (or directionally solidified)
EB	electron beam
e-beam	electron beam
EB-PVD	electron beam-physical vapour deposition
F	degrees Fahrenheit
FEA	finite element analysis
FOD	foreign object damage
g	gram(s)
GDI	graphics device interface
GE	General Electric
GT	gas turbine
IGES	initial graphics exchange specification
K	degrees Kelvin
kg	kilogram
LPCVD	low pressure chemical vapour deposition
LPPS	low pressure plasma spray
M	metre(s)
mbar	millibar

MFC	Microsoft Foundation Classes
μm	micrometre(s) (10^{-6} m)
MSZ	magnesia stabilised zirconia
NASA	National Aeronautics and Space Administration
NGV	nozzle guide vane
nm	nanometre(s) (10^{-9} m)
OOA	object-oriented analysis
OOD	object-oriented design
OOP	object-oriented programming
OPEC	Organisation of Petroleum Exporting Countries
Pa	pascals
PACVD	plasma assisted CVD (another name for PECVD)
PAPVD	plasma assisted physical vapour deposition
PECVD	plasma enhanced chemical vapour deposition
PHIGS	programmer's hierarchical interactive graphics system
ppm	part(s) per million (1 in 10^6)
PS	plasma spray
PVD	physical vapour deposition
r.p.m.	revolutions per minute
RP	rapid prototyping
SC	single crystal
STEP	standard for the exchange of product model data
TBC	thermal barrier coating
TET	turbine entry temperature
TGO	thermally grown oxide
TIT	turbine inlet temperature
TS	thermal spray
VIA	vapour incidence angle (or vapour-impact angle)
VPS	vacuum plasma spray
W	Watt
wt.%	weight percent
YPSZ	yttria partially stabilised zirconia
YSZ	yttria stabilised zirconia

Acknowledgements

Throughout the long and arduous process involved in completing this study, many people have assisted, directed and supported me.

At the top of my list of acknowledgements I would like to thank my supervisors, Prof. J. R. Nicholls and Dr. T. W. Shaw, for their advice and encouragement, which enabled me to complete this document.

I would like to express my thanks to Tony Gray, Denis Timpson, Andrew Dyer and Collin Matthews who exercised abundant patience over an extended period of time in the preparation of the physical experiments and specimens.

Special thanks also go to various people for informal discussions on CAD, file formats, and OpenGL, including Fernando Ribeiro, Graham Jared and Peter Sherar. Their comments and suggestions were of considerable value in the preparation of the final document.

I would also like to thank my monitor, Dr. Fan, for his kindness and for always being interested in the progress of this thesis.

The financial support of Fundação para a Ciência e Tecnologia (FCT) is gratefully acknowledged.

I also appreciate the efforts of Heather Stephenson who proof-read the document.

Finally, a big "THANK YOU" to all those people who, directly or indirectly, asked: "How's the thesis going?"

This work is specifically dedicated to my parents who probably suffered more than I did and for believing that education was an important component in their son's development.

"The eventual goal of science is to provide a single theory that describes the whole universe."

Stephen Hawking *A Brief History of Time, 1988*

Structure of the Thesis

The structure of this thesis covers all relevant aspects concerned with the modelling of electron beam-physical vapour deposition (EB-PVD) thermal barrier coatings (TBCs).

- Chapter one introduces both the economical and ecological reasons that force the thermal efficiency of a gas turbine engine to be increased and its specific fuel consumption to be decreased.

- Chapter two discusses the various types of protective coatings as well as the different materials used with particular emphasis to metallic and ceramic coatings.

- Chapter three describes and characterises in detail the most promising development in superalloy coatings in recent years: thermal barrier coatings (TBCs) with regard to their history, applications, advantages/disadvantages, properties, and failure modes.

- Chapter four is devoted to some of the most important coating processes for depositing both diffusion and overlay type coatings for high-temperature materials.

- Chapter five characterises the process that potentially meets the requirement for attaining higher temperature capability – electron beam-physical vapour deposition.

- Chapter six identifies the need to control thickness distribution and thus modelling vacuum evaporation, which can be done using an inverse square law and based on the cosine of the deposition angle.

- Chapter seven gives an overview of the computer model and highlights it in two parts: the evaporation model and the deposition model. Moreover, it underlines the need for object oriented programming and discusses the structure of the model.

- Chapter eight formulates the evaporation model and the associated source variations investigated such as the theoretical point source evaporator, modelling of sources with large dimensions, multiple sources, and the virtual source concept.

- Chapter nine concerns the deposition aspect of the computer model including, substrate rotation, shadow masking, and substrate manipulation.

- Chapter ten is dedicated to the software tool developed, how it is used to predict the thickness profile around a component, and its advantages and limitations.

- Chapter eleven discusses how the results of the computer model compare to those measured from physical experiments.

- Chapter twelve draws conclusions about the modelling undertaken.

- Chapter thirteen suggests areas of future development in addition to other possible research, in order to define the physics of the evaporation and deposition more precisely.

CHAPTER

1

1. Introduction

For many decades gas turbine engineers have investigated methods to improve engine efficiency (Meetham, 1981). The efficiency of advanced gas turbine engines is continually being improved by increasing turbine inlet temperature (TIT). The main drives behind increasing operating temperature are an increase in engine power or a decrease in fuel consumption, or a combination of these (Driver et al., 1981). Even small increases in operating temperature yield big payoffs in turbine performance, efficiency, and pollution reduction (Brown, 1996). In addition, it also affects economics.

Design trends for advanced gas turbine engines are, therefore, toward ever increasing turbine inlet temperature. This is important because the hotter the exhaust gases the more efficient is the operation of the jet engine. However, within one of the most hostile environments ever created by man, superalloy turbine blades and vanes routinely operate at 90% of their melting point (Gell et al., 1987; Brown, 1996; NMAB, 1996). Nevertheless, further improvements are always necessary to accommodate the new demands. For example, the aircraft business is expected to undergo significant growth over the next two decades. New engines, to be competitive, must have significantly improved performance and durability (Gell, 1995; Howse, 1998).

In a typical gas turbine engine two contradictory objectives must be met: high thermal efficiency, on the one hand, which can be achieved by increasing the operating temperature, as reported earlier, and component durability, on the other. However, the latter objective would normally require lower operating temperatures, or structural materials possessing inherently greater temperature performance.

It is clear, then, that increased thermal efficiency has to be accomplished without component structural failure. For instance, the surface temperature of engine components must, therefore, be maintained low enough for the materials used to retain their properties within acceptable bounds (Bose, 1995). Many approaches have been used to increase the operating temperature limit of the turbine blades and vanes. The composition and processing of the materials themselves have been improved. In another approach low surface temperature is partially met by innovative component cooling schemes using compressor discharge air. Notwithstanding this, it is desirable to keep the proportion of cooling air to a minimum in order that the overall efficiency of the engine is maximised. Still another method of protecting components is by applying a surface layer of material capable of protecting the component against the potentially damaging environment.

Over the last 60 years, thanks to the innovative efforts of engineers and designers, the gas turbine has earned an impressive reputation for very good fuel flexibility (Mukherjee, 1997). Efficient combustion has become increasingly important because of the rapid rise in commercial aircraft traffic and the consequent increase in atmospheric pollution and noise (Rolls-Royce, 1986).

1.1. Increasing Engine Thermal Efficiency and Decreasing Fuel Consumption

Economic reasons force the development of a new gas turbine with a lower specific fuel consumption while ecological reasons, mainly due to international regulations, is the drive behind cleaner and quieter engines. Both aims, however, will contribute to the introduction of more efficient aircraft with modern engines. In the next two sections, firstly fuel costs, and then pollution and noise will be discussed and the relationship between these and an increase in engine thermal efficiency assessed.

1.1.1. Economic Reasons

Fuel costs oscillate according to global economic development and are also a function of the world production largely governed by the Organization of Petroleum Exporting Countries (OPEC). Since production of fossil fuels can go up or down, so do the fuel costs associated with running an airliner. Whether there is a glut or shortfall in the market, this can represent a decrease or sometimes as much as a twofold or threefold increase in the price of crude, the basis for gasoline, diesel, and jet fuel.

A fuel conservation programme has always interested the scientific community involved in the aircraft industry and fuel reduction has been a major aim sought for most of the history of this industry. It follows, therefore, that conserving fuel or minimising fuel costs is of the utmost importance both currently and in the foreseeable future. The importance of this is because it affects the economics of engine operation (Demaray et al., 1981; Duvall and Ruckle, 1982; Meier et al., 1991a; Meier and Gupta, 1994; Schmitt-Thomas et al., 1996; Boeing[1], 1997; Howse, 1998).

The scientific community is also addressing the development in gas turbines for power generation, marine applications, and military aircraft propulsion. This distinction is important because different types of fuel and different operating temperatures are used for the various gas turbines. A low-grade fuel contains higher levels of sulphur, vanadium and salt particles (Jones and Reidy, 1994), which attack the components reducing their lives. However, they are cheaper than clean fuel.

In the 1960s jet fuel was a mere 12 cents a gallon in the United States. This represented about 15 percent of an aeroplane's direct operating cost and very few people worried about reducing fuel costs (Boeing, 1997). In the 1970s, however, there was an interruption in the supply of petroleum (Duvall and Ruckle, 1982) responsible for an approximate fourfold increase in fuel prices (Boeing, 1997). During this period, fuel

[1] Boeing Commercial Airplane Group, hereafter referred to as Boeing

costs represented between 40 to 50 percent of the direct operating cost of an aeroplane. In the early 1980s there was again an increase of jet fuel emphasising the need for development in fuel efficiency (Duvall and Ruckle, 1982). Using 1997's fuel prices (85 cents a gallon), the total cost saved by conserving one percent of fuel for a fleet of 25 747s was $2,125,000 (Boeing, 1997). In other words, minimising fuel costs was vital for a company to stay in business.

More recently, and while this thesis was being written, airlines have shown a renewed interest (or maybe renewed worries) in fuel conservation programmes. This is due to fresh increases in fuel price. In the latter part of 1999, fuel costs had again suffered a dramatic increase. On August 16th 1999 the Financial Times reported, in their web page, a two-year high in fuel costs to around $21 a barrel. In February of the same year, i.e. six months before, that figure was only half of that (around $10 a barrel). Some experts in this area predicted that the crude price could increase to as much as $25 a barrel before prices started coming down[2].

All the above rises in fuel costs, however, have been paralleled by an increase in fuel cost awareness. There can be few enterprises where complacency is so damaging as the aircraft industry and unless an organisation is aware of all the issues affecting the economic viability of this industry it does not stand a chance in this highly competitive market.

To sum up, with fuel prices at the current level and due to the highly competitive market (brought about partially because of the so-called "low cost" airline companies) the importance of a programme to reduce fuel usage becomes obvious. Fuel costs are described as being one of the highest expenditures, second only to the expenditure on personnel, in the cost index of an airline company, representing between 8 to 10% of the total cost[3]. Moreover, reducing fuel usage also reduces fuel emissions, which are harmful to the environment. This is also a significant factor but less easily quantified financially. It will be discussed in the next section.

1.1.2. Ecological Reasons

Air pollution and noise are two negative issues of the impact brought about by the aircraft industry. Gas turbines, whether for aircraft propulsion, marine or land-based applications, that produce power by burning fossil fuels, release nitrogen oxides, carbon monoxide and other harmful gases into the air which can adversely affect the weather, the health of people, animals and plants (Rolls-Royce, 1986; Howse, 1998).

Growing pressures on polluters by both governmental and non-governmental organisations means that environmental problems should decline as a United Nations air pollution protocol comes into force. Other European regulations aimed at achieving lower pollution levels will force engine manufacturers to improve engine efficiency thus minimising harmful gases released during combustion.

---

[2] CNN.com "Gasoline Prices Soar as Labor Day Travelers Hit the Road" September 3rd 1999
BBC 2 Ceefax p.202 September 22nd 1999

[3] Spanish newspaper El País (http://www.elpais.es) September 7th 1999

From the above, it follows, therefore, that there is a growing interest in more efficient aircraft with modern engines. Not only is it fundamental to reduce fuel usage but also to use fuel more efficiently in order to lower exhaust emissions, which adversely affect the environment (Jones and Reidy, 1994; Brown, 1996; Nicholls, 1997a; Nicholls, 1997b). As widely discussed by the scientific community, the hotter the exhaust gases the more efficient is the operation of the jet engine. By increasing the combustion temperatures, the engine produces cleaner exhaust gases (less pollutants), and there is also a decrease in fuel usage. As reported earlier, increases in turbine operating temperatures, which have been achieved on average at 5°C per year for the last few decades, generate big payoffs in turbine performance, efficiency, and pollution reduction (Brown, 1996).

Howse (1998) demonstrated how a predicted twofold increase in air traffic over the next 15 years is likely to be the drive behind the development of more efficient aircraft in order to negate the environmental impact brought about by such growth. He discussed how major improvements in emissions and noise have been achieved in the last 20 years. Conner and Connor (1994) described the suppression of emissions (nitrous oxide) as being one of the terms that govern the hot-section components in a gas turbine. Mukherjee (1997) discussed industrial gas turbines with particular reference to the processes involved in order to optimise production. A list of the demands made on the gas turbine suppliers in terms of goals for future developments focused on clean combustion as one of the core technologies.

In conclusion, jet engine noise suppression has become one of the most important fields of research due to airport regulations and aircraft noise certification requirements (Rolls-Royce, 1986). It is foreseeable that cleaner and quieter engines will continue to be pursued, if not increased, in order to reduce the negative impact and to comply with international regulations.

1.2. Techniques to Increase Engine Efficiency

Engine efficiency is directly linked to the temperature at which the gases are burnt in the combustion. Hence there is a strong incentive to raise this temperature. As observed by many materials engineers, turbine aerofoil alloys used in modern gas turbines, whether for power generation, marine applications, or aircraft propulsion have typically a lower melting point than the current temperature of the gases leaving the combustion chamber (Sheffler, 1988; Meier et al., 1991a). As a result, hot section engine component development is being addressed by tackling different aspects. These aspects include developments in alloy composition and manufacturing processes, cooling techniques, and coatings. Maximum allowable surface temperature is a function of all these aspects. Current temperatures, with a maximum of around 1200 to 1400°C (depending upon the type of gas turbine) are only possible through a combination of advances brought forward in all these areas. Since engine components already operate at up to 90% of their melting point, further major increases in operating temperature are not possible with the current class of superalloy materials if structural damage is to be avoided. Alternatively, material development strategies therefore have to be used.

The next sections discuss the techniques that have enabled aircraft engines to operate with such fuel efficiency, namely controlling the composition and processing of materials, cooling techniques, and protective coatings.

1.2.1. Composition and Processing of Materials

In order to withstand the extreme service conditions typical of gas turbines (GT), components subject to high stress, high temperature applications are manufactured from alloys known as superalloys. Superalloys are heat-resistant alloys having superior strength at high temperatures (Sims et al., 1987). Moreover, they exhibit high temperature mechanical integrity with an unusual degree of oxidation and creep resistance[4] (Leverant, 1996). In order to improve their performance over a wide range of applications, they are divided into three classes: nickel-based, cobalt-based and iron-based superalloys. A partial list of nickel- and cobalt-based superalloys used in land-based and aircraft gas turbines is given elsewhere (Sims et al., 1987; NMAB, 1996). Today's best turbine blade materials are single-crystal nickel-based superalloys containing additions of twelve or more other elements. CMSX-4 and RENE N5 are typical examples.

Superalloys used in GT aerofoils are among the most complex and costly alloys known to man. They have undergone several "generations" of development at enormous expense, with modern GT blades costing as much as $5000 each (Jones and Reidy, 1994). The early materials used were high temperature steel forging, but these were rapidly replaced by cast nickel-based alloys which give better creep and fatigue properties (Rolls-Royce, 1986, p56). Improved service life can be obtained by aligning the crystals to form columns along the blade length, produced by a method known as "Directional Solidification" (DS). This technique provided the first major advance in alloy temperature capability (Gell et al., 1987). However, the greatest advance in metal temperature capability has been provided by single-crystal superalloys (SC). Figure 1-1 shows the improvement in commercial engine fuel efficiency that has come with each new engine model, as well as the contributions made by turbine materials and processes (data cited is for Pratt and Whitney engines but similar performance can be observed for GE and Rolls-Royce engines).

Within one of the harshest environments ever created by man, GT alloys have to maintain their structural integrity over a long period. Several decades of developing the material used in today's GT engines have enabled modern jets to operate with such high fuel efficiency. Progress in investment-casting technology, which allowed engineers to cast DS and SC aerofoils, ranks as the single most important process development for nickel-based superalloys (NMAB, 1996). However, advanced DS and SC alloys are currently operating near their strength limits, and it appears that a point of diminishing returns in alloy development has been reached (Srinivasan, 1994; Brown, 1996; NMAB, 1996; Howse, 1998). Similarly, Nissley (1995) argued that cost-effective superalloy advances have virtually become exhausted.

[4] See "TBC Failure" on page 43 for more information about oxidation and creep.

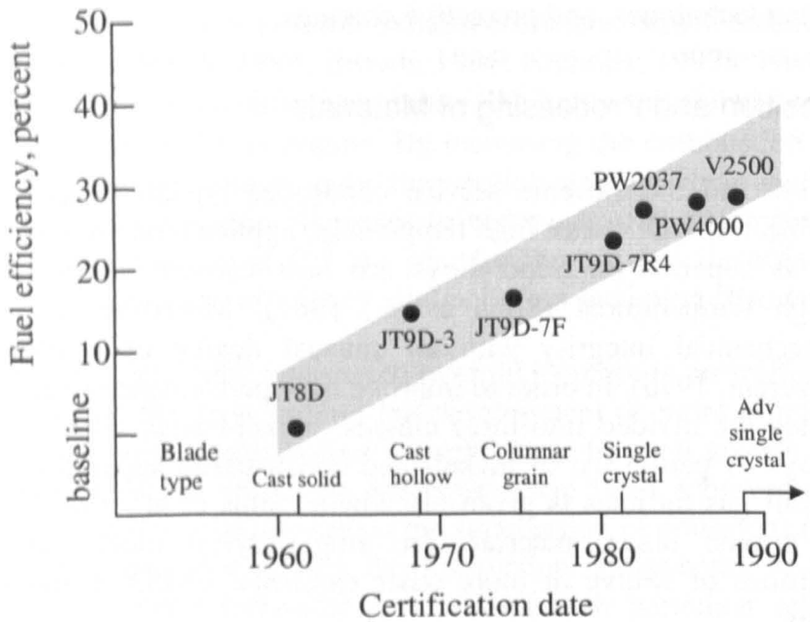

Figure 1-1: The improvements in fuel efficiency with engine model and the contributions made by cast superalloys technology (Source: Gell et al., 1987).

Design trends are, however, toward ever-increasing thermal efficiency, thus dictating that the turbine inlet temperature be significantly increased. This means that the targeted temperatures will inevitably exceed the capabilities of current superalloys. Therefore, higher thermal efficiency needs to be accomplished without structural failure of components by various degradation mechanisms such as melting, creep, and oxidation. In other words, reliability is now a critical factor that drives future materials development prior to increasing the TIT further, so that superalloys do not fail prematurely.

Furthermore, since current superalloys operate at around 90% of their melting point and as temperatures continue to increase, it becomes clear that in order to take the next step in engine efficiency the scientific community will have to find alternative materials or ways to protect superalloy surfaces from the ravages of high-temperatures and oxidation attack. One technique, which offers this potential, is physical cooling and this is discussed next.

1.2.2. Blade Cooling

For the last three decades, cooling technology has allowed turbine entry temperature to increase by roughly 370°C (NMAB, 1996 p.4). In other words, cooling methods have arguably accounted for more than 75 percent of the increased temperature capability and are still the "first line of defence" in new turbine designs (NMAB, 1996 p.8).

As noted by some scientists, and reported earlier, engine components in the hot section (combustion chamber and turbine) routinely operate at more than 90% of their melting point with some localised regions actually operating above their melting point (Gell et al., 1987; NMAB, 1996; Brown, 1996). However, continuous cooling of these

components allows their environmental operating temperature to exceed the material's melting point without affecting the blade or vane integrity (Rolls-Royce, 1986).

Turbine blade cooling methods include convection cooling, impingement cooling, film cooling, full-coverage film cooling, and transpiration cooling. Turbine blade components are made hollow and air is injected through the hollow channels during engine operation. Air cooling lowers the metal surface temperature and therefore avoids structural failure by melting, creep, oxidation, thermal fatigue, and other mechanisms.

All cooling methods, without exception, have drawbacks that partly offset the benefits of reduced fuel consumption and increased engine efficiency expected with increased TIT. Firstly, internal cooling channels add to the complexity of the turbine blade or vane, thus increasing both the potential failure modes and the manufacturing costs associated with the component. Secondly, the air extracted from the compressor for cooling purposes and which bypasses the combustion process can amount to as much as 20% of the compressor capacity, hence resulting in a significant efficiency penalty (Parks et al., 1997). Finally, for certain cooling methods such as film cooling and transpiration cooling, air flowing out through small holes results in a change in the aerodynamic profile of the component in addition to disturbing the main flow of the hot gases.

It is acknowledged that even though cooling schemes have become more complex in order to enhance cooling of the gas path surface, they will eventually reach a limit where it will not be possible to keep the superalloy cool enough to avoid structural damage (Durham et al., 1994). According to Nissley (1995), cost effective intricate cooling methods have virtually become exhausted. As a result, other alternative methods of protecting the components will be required. As this cooling technology matures, however, the technical community is searching for innovative technologies to increase engine efficiency further (Duvall and Ruckle, 1982) while maintaining the structural efficiency of components. Environmentally protective coatings provide one such solution. Only by protecting these components is it possible to operate at even higher temperatures and still avoid component failure.

1.2.3. Protective Coatings

A protective layer applied over a component is termed a coating. A coating for use at high temperature can be defined as a layer of material, usually ceramic or metallic or both, that is capable of inhibiting direct interaction between the substrate and the potentially damaging environment (Wood and Goldman, 1987). In fact, many materials used in high technology applications are composites, i.e. they combine the properties of both the underlying material and the coating. This is needed because quite often the properties of a substrate do not provide adequate protection against the many degradation modes at high temperature. Hence, the substrate/coating combination is a way of benefiting from the usually conflicting properties required from the bulk and the surface of a component. In high technology applications it is often desirable to provide a combination of such properties, for example, resistance to corrosion/oxidation and high temperature strength, as is the case for the first stage blades and vanes in a gas turbine.

Coatings have been known for many decades and have been applied in the hot section of aircraft engines for over four decades (Talboom and Grafwallner, 1970; Talboom et al., 1970; Goward, 1974). According to Wolfe and co-workers (1997), nearly 75% of all engine components are now coated with different materials. This acknowledges that coatings have gained an impressive reputation to enhance the life and performance of the components.

The most promising and exciting development in superalloy coatings research in recent years is the use of thermal barrier coatings (Wood and Goldman, 1987). A thermal barrier coating (TBC) is a multilayer coating system consisting of a thermal insulating ceramic outer layer, usually applied over a metallic "bond coat". TBCs insulate the underlying substrate from the ravages of high-temperature attack and have been extensively developed since the early 1970s by agencies such as NASA and the US Army, within the USA (Dapkunas, 1974; Liebert et al., 1976; Stecura, 1976), with similar initiatives within Europe, funded by the CEC (BriteEuram and COST) (Liège, 1978).

The importance of TBCs is described by the fact that the potential temperature reduction is greater than the cumulative gains made in temperature capability of the superalloys over the past 25 years (Meier et al., 1991a) which thus allows a significant increase in thermal efficiency and/or increase in component durability.

However, it is not yet known to what extent TBCs will provide for the next generation of advanced gas turbines. This is a major challenge. Nevertheless, full exploitation of the benefits brought about by TBCs requires further research in order to understand both TBC failure modes and to overcome some technological barriers.

1.2.4. Conclusion

The thermal efficiency of a gas turbine has steadily improved over the last few decades. Many approaches have been used to increase the operating temperature limit such as advances in superalloy composition and processes, sophisticated cooling techniques, and by using protective coatings. The need for greater performance from advanced turbine engines will continue, requiring even higher operating efficiencies, longer operating lifetimes, and reduced emissions (NMAB, 1996 p.1).

With the potential temperature capability of both superalloy composition and cooling techniques regarded as being at or close to their ultimate service temperature, materials engineers have realised that coatings, mainly TBCs, have become an enabling technology for advanced engines. There is general agreement within the scientific community that for a further increase in turbine inlet temperature, the most advanced high temperature superalloys have to be thermally insulated from the hot combustion gases (Schmitt-Thomas et al., 1996).

This study is concerned with the development of a computer-based model to predict vapour deposition around components with complex geometry, typically turbine blades. The application of these models to the deposition of TBCs is examined and this should permit the controlled deposition to tailor the TBC performance and durability.

CHAPTER

2

2. Coatings

Coatings are becoming increasingly important: firstly to protect components against several degradation mechanisms such as oxidation, corrosion, and erosion, and secondly to work as thermal insulators. Both of these objectives are being met by diffusing various elements into the component (diffusion coating), by depositing a layer of specific composition to the surface to be protected (overlay coating), or by a combination of these.

2.1. Diffusion Coating

Diffusion coatings are formed by diffusing one or more elements into the surface of the component to be protected (Bunshah, 1982; Conner and Connor, 1994). They provide the necessary protection only by the interdiffusion between the substrate and the initial deposition coating materials (Goward, 1974). In other words, the coating and the surface of the metal are actually mixed together to form a "new" material. Diffusion coatings were the first protective coatings to be applied to gas-turbine aerofoils when it was first realised that there was a need, and the potential, for this surface engineering technique on components in the hot section of aircraft engines in the 1950s (Goward, 1986, NMAB, 1996). Nevertheless, diffusion coatings are much older. According to Goward (1998) they were first used around 1911, as described in a US patent by Van Aller, where metals were embedded in a powder mixture of aluminium.

The depth at which the coating interdiffuses into the component is an important parameter when considering this type of coating and is a function of the protection required for each specific application, coating process (the method for applying the coating), and component and coating composition, amongst other parameters. Also worth noting is that diffusion coatings, by their mode of formation, cannot have the same concentration on the surface and the interior of the component. Instead, there is a gradient as defined by diffusion laws from a coating rich in the diffused element at the surface of the alloy to the alloy composition deeper down from the surface as can be seen schematically in Figure 2-1.

Figure 2-1: Schematic of a component a) uncoated and b) with a diffusion coating.

Typical diffusion coatings elements include aluminium, chromium, silicon, and platinum, among others (Mévrel et al., 1986; Goward, 1998; Nicholls, 2000).

Many conference proceedings (Marine, 1974; NACE, 1981; EPRI, 1981; Royal Society, 1986) have highlighted the importance of such coatings in providing protection to components in the hot gas path section of the gas turbine, with many investigators reporting how well aluminide diffusion coatings had performed and on their importance in future coating systems. These coatings produce a thermally grown alumina (Al_2O_3) surface layer in service. As pointed out by many investigators, alumina is known for its low rate of diffusion of oxygen. It follows, therefore, that alumina diffusion barriers provide the component with resistance against oxidation attack thereby extending component life. The relationship between diffusion barrier thickness and oxidation attack has been studied and it has been proved that a thin alumina diffusion barrier can provide an extended resistance to thermal cycles.

Many investigators studied the use of coatings (including diffusion coatings) in the hot section of a gas turbine, which are required to operate at constantly high temperatures. Diffusion coatings have provided protection against the harsh environment found in gas turbines since the 1960s and, have therefore, extended the component life (Pichoir, 1978; Restall et al., 1986; Telama et al., 1986). This improvement is achieved by the diffusion of aluminium, chromium, silicon, or a combination of these, for example (Bürgel, 1986).

In a recent review, Goward (1998) described not only the history of turbine aerofoil coatings from simple aluminides, through modified diffusion aluminides, but also highlighted several decades of research in an attempt to predict future advances in the science and technology of superalloy coatings. Chan (1999) also recently reported the use of diffusion coatings applied to land-based combustion turbine blades to improve the oxidation and corrosion resistance.

Diffusion coatings may be classified as inward diffusion and outward diffusion. The first pertains to the diffusion of the deposited coating element into the component, whereas the latter relates to the diffusion of one, or more, of the substrate elements out into the deposited coating. Whether inward or outward diffusion occurs depends on the local chemical concentration gradients (surface activity). Duret and Pichoir (1983), Wood and Goldman (1987) and Nicholls (2000) for example, qualified this for aluminide coatings with the former type known as 'high activity' and the latter as 'low activity'. This difference in diffusion is due to the different microstructural variations in coating and to the component composition.

Coating processes to apply diffusion coatings such as the pack cementation process, over pack, vapour deposition, and chemical vapour deposition (CVD) are discussed in detail elsewhere (Vossen and Kern, 1978; Mévrel et al., 1986; McMinn, 1987; Smith, 1995; Nicholls, 2000). Both a brief and a more detailed discussion of coating processes is given in "Introduction to Coating Processes" on page 16 and in the section on "Coating Processes" on page 55, respectively.

All the above investigations were directed at determining the benefits brought about by the introduction of diffusion coatings or to ascertain their potential in future more-demanding applications to provide oxidation and corrosion protection.

2.2. Overlay Coating

An overlay coating differs from diffusion coatings in the sense that it is not formed by diffusion into the substrate. Instead, it functions as an independent layer applied to the surface of the component (Talboom et al., 1970; Talboom and Grafwallner, 1970; Goward, 1974; Bunshah, 1982). Figure 2-2 shows a schematic representation of an uncoated component and one with an overlay coating.

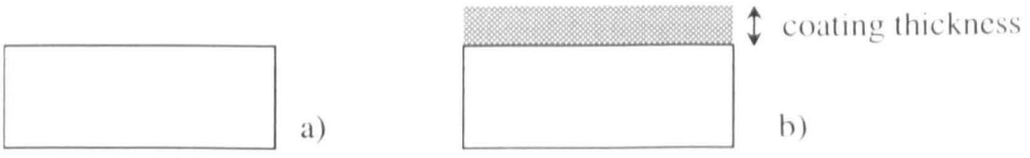

Figure 2-2: Schematic of a component a) uncoated and b) with an overlay coating.

An example of a widely used overlay coating is known as MCrAlY coating (where M is usually nickel (Ni) or cobalt (Co); Cr is chromium, Al is aluminium and Y is yttrium). This type of coating is important because it provides oxidation and corrosion resistance. One of the first overlay coatings to be used in gas turbines was a coating alloy with a composition based on cobalt, chromium, aluminium and yttrium (known as CoCrAlY), with a composition Co25Cr12Al0.6Y (in wt%), to protect nickel-based alloys as explained by Talboom and co-workers (1970). A typical overlay coating is also thicker than a diffusion coating. Overlay coatings as thick as 7 mm have been reported in the literature (Litchfield et al., 1981) although the current state of the art for protection of gas turbine components deposit coatings in the order of a few hundred micrometers.

Overlay coatings provide a higher degree of resistance and use, therefore, more advanced compositions including some rare-earth elements. A drawback of overlay coatings is that they are usually more expensive than diffusion coatings. The cost of applying an overlay coating is typically 2× – 4× that of a conventional aluminide (Nicholls, 2000). In addition, vacuum processes such as plasma spraying (PS) and physical vapour deposition (see "Coating Processes" on page 55) used to deposit overlay coatings are 'line-of-sight', hence the entire surface of the component cannot be uniformly coated, unless the component is moved or rotated. These mechanisms together with vacuum pumps make this equipment expensive. On the other hand, the pack cementation process, which is a very well known process for applying diffusion coatings, is not a 'line-of-sight' process and uses relatively cheap equipment and, therefore, renders lower unit costs.

It should be emphasised that diffusion and overlay coatings are not mutually exclusive. None, one or both may be desirable for a particular application. In addition, when depositing an overlay coating and depending upon the coating process and process

parameters used, an interdiffusion layer may be formed between the substrate and the overlay coating (Bunshah, 1982). Overlay coatings will be discussed further in the section "Metallic and Ceramic Coatings" on page 12.

2.3. Duplex Coatings

A duplex coating is the combination usually of a diffusion coating and an overlay coating. For instance, an aluminide diffusion coating applied over an MCrAlY overlay coating. In some cases two overlay coatings may be sequentially deposited, e.g. a thermal insulating ceramic layer applied over an oxidation/corrosion resistant metallic layer. This is also called a duplex system.

Rairden (1976) patented a protective coating for superalloys by combining an aluminium rich coating (for oxidation resistance) over a high chromium diffusion barrier (for corrosion resistance). More recently, Taylor et al. (1995) patented a coating composition for oxidation and corrosion protection where the coating can be a duplex coating. In this case the coating composition comprised an alloy having the formula RCrAlR'R" (R is nickel, cobalt), R' is yttrium or hafnium and R" is tantalum, rhenium and/or platinum, preferably mixed with an oxide dispersion such as alumina. Since duplex coatings are a combination of the two previous types of coatings, they are also more expensive than overlay coatings.

2.4. Metallic and Ceramic Coatings

The previous sections described how a coating could be applied to a component. This section explains what materials are currently being used for both diffusion and overlay coatings. Broadly speaking there are two types of materials, namely metallic or ceramic coatings. Metallic coatings are more adequate for protection against failure mechanisms such as oxidation and corrosion. Ceramic coatings, on the other hand, are designed to act as a thermal insulator and therefore provide thermal protection. Both types are used throughout gas turbines to protect components not only against oxidation, corrosion, and thermal fatigue, but also erosion, wear, creep and other degradation mechanisms.

Four elements are currently the most widely used in diffusion coatings. They are aluminium, chromium, silicon and platinum (Mévrel et al., 1986; Goward, 1998; Nicholls, 2000). Diffusion of aluminium, which is one of the most widely used metallic elements in diffusion coatings, into nickel-based alloys form various aluminides that protect superalloy substrates against oxidation (Bunshah, 1982). In addition, for many systems the above elements are employed in combination, for instance, chrome-aluminised (Mévrel et al., 1986; Nicholls, 2000), silicon-aluminised (Nicholls, 2000) or platinum-aluminised (Mévrel et al., 1986; Baxter et al., 1997; Wright, 1998; Nicholls, 2000). Strangman (1996b) gave a more detailed description of the variety of beneficial elements that can be incorporated into diffusion aluminide coatings. The elements include platinum (Pt), palladium (Pd), silicon (Si), hafnium (Hf), yttrium (Y) and oxide particles such as alumina, yttria, hafnia, for enhancement of alumina scale adhesion; chromium (Cr) and manganese (Mn) for hot corrosion resistance; rhenium (Rh),

tantalum (Ta), and niobium (Nb) for diffusion stability and/or oxidation resistance, and nickel (Ni) and cobalt (Co) for increasing ductility or incipient melting limits.

Overlay coatings are more advanced, more expensive coatings. Therefore, more complex alloy composition is used to fabricate these coatings and the coating deposition technologies are more capital intensive. A metallic layer known as MCrAlY (where M is usually nickel or cobalt; Cr is chromium, Al is aluminium and Y is yttrium) provides oxidation and/or corrosion protection and is a major source of interest among the coating community. These coatings can be tailored readily to specific applications and can usually provide better protection than diffusion coatings (Talboom et al., 1970; Talboom and Grafwallner, 1970; Restall et al., 1986; Mévrel et al., 1986).

Baxter et al. (1997) described developments in coating composition applied to industrial gas turbines. In his work, the use of CoCrAlY coatings applied to both nickel-based and cobalt-based superalloys was addressed with the aim of decreasing the corrosive attack. Another type of coating, silicon-aluminised (Al-Si) was described as able to support the formation and maintenance of very protective surface oxides. This type of coating is also of interest as a diffusion coating. In a similar report, to prevent corrosion in oil firing gas turbines, Nakamori et al. (1997) considered the use of CoNiCrAlY coatings. The use of CoCrAlY and NiCrAlY coatings with useful hot corrosion and oxidation resistance in some applications led to the introduction of a NiCoCrAlY coating with exceptional ductility within a useful range of compositions (Goward, 1998).

It is important to emphasise that different elements provide resistance against different failure modes. As a rule, nickel-based alloys provide better oxidation resistance than cobalt-based alloys, while chromium confers corrosion resistance. Depending upon application requirements, the contents of nickel, cobalt and chromium are varied in order to provide resistance against both of these two degradation modes. Figure 2-3, schematically shows the compromise when selecting a coating composition for an environment that requires resistance to both oxidation and corrosion.

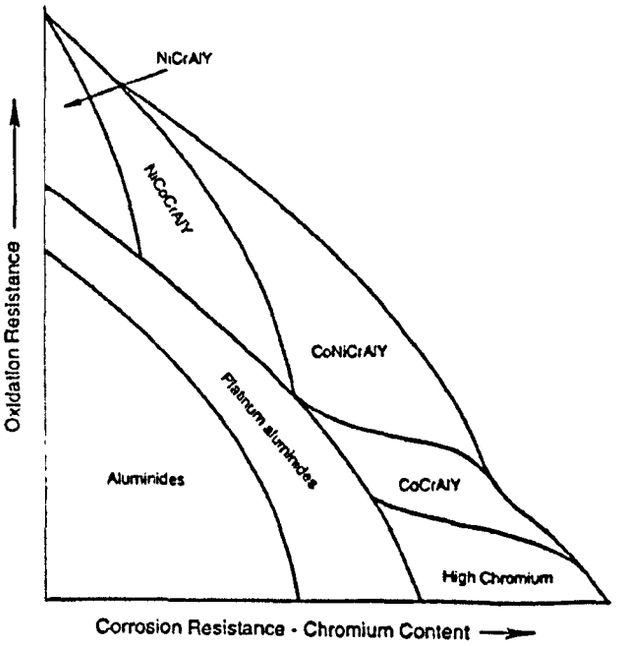

Figure 2-3: Coating compositions as related to oxidation and corrosion resistance (Source: Novak, 1994).

An understanding of the interactions between the coating and the substrate, which have an important effect on coating degradation, is far from complete but initial models to study the interdiffusion between these two layers have been formulated. Mazars et al. (1986) investigated NiCrAlY, CoCrAlY and FeCrAlY coatings deposited by PS on nickel-, cobalt-, and iron-based alloys. After diffusion treatment it was possible to identify which systems had considerable and limited diffusion. The systems with interest for high temperature applications appeared to be NiCrAlY on Ni-based alloys, NiCrAlY on Fe-based alloys, and CoCrAlY on Fe-based alloys.

In a more recent report, Itoh and Tamura (1999) also studied MCrAlY coatings applied by vacuum plasma spray (VPS) to three kinds of nickel-based substrates with various crystal structures (equi-axed, directional solidified and single crystal). Four kinds of metallic coatings, namely CoCrAlY, NiCrAlY, NiCoCrAlY and CoNiCrAlY were selected for the experiments. These authors investigated a computer-aided interactive system aimed at analysing the order of reaction diffusion behaviour at the coating/substrate interface. It was found that a two-layer structure formed at this interface: an Al depleted zone and a reaction interdiffusion zone below the depleted zone. The NiCoCrAlY coating was found to be the most stable, this result being independent of the substrate used.

More complex NiCoCrAlY compositions containing other reactive and rare earth elements have been used. In his review on protective coatings Goward (1986) explained the usefulness of metallic elements for use in high-temperature turbine aerofoil coatings. In recent studies, additions of tantalum, tungsten, titanium, niobium, rhenium and zirconium have been reported (Goward, 1998). Similarly, Nicholls (2000) described a Pratt and Whitney patented overlay coating containing oxygen active alloys such as hafnium and silicon making up a NiCrAlHfSiY coating. These more complex alloy systems are known as MCrAlX or MCrAlXY, where X refers to oxygen active elements other than yttrium.

Overall, MCrAlY type overlay coatings provide protection for service temperatures between 815-1150°C (NMAB, 1996). Metallic coatings can, thus, be used in service at temperatures up to the incipient melting point of the metallic elements that form the metallic coating. It follows, therefore, that with growing pressures to further increase the operating temperatures of gas turbines, metallic coatings will inevitably reach a point where they will no longer provide adequate protection. This is being addressed by the scientific community by using a top layer of low thermal conductivity ceramic material. Ceramic layers are used because of their beneficial properties: at high temperatures there are chemical, mechanical, physical, thermal, electrical, magnetic, and optical properties that distinguish them from metals. Some properties of ceramics such as strength, stiffness or hardness decrease as temperature is increased. Conversely, some others like thermal expansion coefficient, fracture toughness, plasticity or creep increase with temperature. Ceramic materials are known to possess many of the properties desired for higher-temperature replacements of superalloys: very high melting points, high-temperature strength, low density, and some increased resistance to aggressive environments (NMAB, 1996. p15). They hold considerable promise and are

therefore objects of interest within the scientific community; their major failing is their low damage tolerance (resistance to cracking).

2.5. Background to Zirconia Ceramics

From the vast range of possible ceramic candidates, zirconia-based systems have gained by far the most attention and have been used since the early 1970s for thermal protection. The characteristics that make zirconia (ZrO_2) the leading material for use as a thermal insulator include:

- good mechanical integrity when subjected to thermal shock and thermal cycling;
- relatively high coefficient of thermal expansion (CTE) ($8\text{-}10\times10^{-6}$ K^{-1}) close to that of the superalloy substrates;
- high thermodynamic stability;
- high melting point (2710°C);
- low thermal conductivity (~ 2.2 W/mK depending on morphology).

(Wortmann, 1990; Ohring, 1992; Bose, 1995; Wolfe et al., 1997)

Ceramic coatings of engineering materials such as zirconia-based coatings for advanced gas turbines and diesel engines are among the most studied and developed applications for surface protection (Strangman, 1982; AGARD, 1997).

The stabilised zirconia ceramics (stabilising elements are explained in the following paragraph) have a thermal conductivity approximately 3% that of gas turbine alloys (Levine and Clark, 1977) and can thus reduce the metal temperature of air-cooled gas turbine components. For example, the thermal conductivity of both a substrate (410 stainless steel) and a TBC (APS 8wt%YSZ) is around 20 and 0.8 W/m.K, respectively (Slifka et al., 1998).

Even though ZrO_2-based systems possess a combination of desirable properties, pure zirconia, however, undergoes phase transformation in the temperature range of gas turbine engine operation (Stecura, 1976; Wolfe et al., 1997). The stable form at room temperature is monoclinic, but it transforms to tetragonal at around 1200°C which in turn transforms to cubic at 2370°C (Sohn, 1993; Nazeri and Qadri, 1996; Immarigeon et al., 1997). In addition, associated with the phase transformation from monoclinic to tetragonal there is a volume change in the order of 3 to 12% (Ohring, 1992) which creates high stresses causing even strain tolerant structures of ceramic to crack (Kaysser et al., 1997; Schulz et al., 1997a). To minimise this phase transformation, various elements are added to zirconia to produce a cubic or tetragonal form that does not undergo a transformation and is thus suitable over the range of engine operation. Some of the stabilising agents include calcia (CaO), ceria (CeO_2), magnesia (MgO), and yttria (Y_2O_3). Other stabilisers, which could be used for engine operating on marine fuel, have been discussed elsewhere (Jones, 1996).

It is noteworthy that, from the foregoing, the use of the term "zirconia," includes zirconia-based ceramic materials which may be either pure zirconia or zirconia plus the addition of one or more additives, of which the above are examples.

In 1976 the introduction of a zirconia ceramic coating proved to be a major breakthrough since it provided a thermal insulation reduction of as much as 200°C in the substrate's surface temperature (Demaray et al., 1982; Gell et al., 1987). Previous ceramic compositions only provided half that reduction and then only locally. Therefore, after considerable research into the extensive range of coating materials, the most suitable system for use as a thermal barrier is generally accepted to be yttria partially stabilised zirconia (YPSZ) with an yttria content between 6-8wt% (Demaray et al., 1982; Alpérine and Lelait, 1994; Sohn et al., 1994b; Unal et al., 1994; Rybnikov et al., 1995; Schulz et al., 1997a; An et al., 1999).

YPSZ has good fracture toughness, good chemical stability, good adhesion, high CTE, and the lowest thermal conductivity of any ceramic material, the latter leading to a lower metal surface temperature (Rybnikov et al., 1994; Unal et al., 1994; Pint et al., 1996; Wolfe et al., 1997). A critical factor in the success of the ceramic is its adherence to the underlying alloy. Zirconia adhesion directly to the substrate is poor, so there is a need for an intermediate coat – the bond coat. The evolution of ceramic coating has been paralleled by the evolution of the bond coat. The combination of a ceramic coat using YPSZ with an oxidation resistant MCrAlY bond coat, or a platinum-aluminide diffusion coating, is currently employed, and further improvements are expected from both the top coat and the bond coat. This bilayer system is known as a thermal barrier coating (TBC). This was first applied in 1976 and is still in use today, but in much improved forms particularly with respect to strain tolerance (See "Thermal Barrier Coatings (TBCs)" on page 19).

2.6. Introduction to Coating Processes

Only a brief characterisation of the issues concerning coating processes, as related to the advantages/limitations of the process and the coating properties that result, is discussed in this section. A more detailed explanation of these processes will be dealt with in the section "Coating Processes" (page 55).

A number of coating processes, which can be used to deposit protective coatings, are commercially available. All coating processes, without exception, have limitations or drawbacks of one form or another. These limitations can be, for example, technical, economic, commercial, or concerning the logistics of manufacture (Restall and Wood, 1986). Process issues are, therefore, important because they affect both the economics and coating microstructure, the latter affecting coating properties. Some of the features which vary with process include, but are not limited to, deposition rate (from angstroms to millimetres), microstructure, properties (density, etc.), substrate temperature during deposition, and efficiency of coating complex shapes (Bunshah, 1982).

Coating processes can be classified as those based on a chemical reaction (chemical vapour deposition or CVD), spraying (thermal spray or TS) and physical vapour deposition (PVD). Worth noting is that different authors categorise coating processes differently, according to various schemes. These coating processes produce diffusion (CVD) and overlay (TS and PVD) types of coating. The literature indicates that, from the vast range of coating processes, two seem to appear the most promising for

depositing high-temperature resistant overlay coatings: plasma spraying (PS) and electron beam-physical vapour deposition (EB-PVD) (NMAB, 1996; AGARD, 1997).

In the CVD process the substrate is reacted with other substances thereby converting its surface into different compounds having different properties from the uncoated component. It allows the formation of thin layers on shapes with complex geometry and there is invariably a good adhesion between the substrate and the coating. However, low deposition rates are typical and the process also produces chemical wastes.

Plasma spraying uses a high-temperature arc plasma to melt powder particles and accelerate them towards the substrate. It is a process involving the transfer of molten droplets capable of coating large components at very high deposition rates. Notwithstanding, in addition to the fact that it produces various coating defects because not all powder particles are melted by the plasma gun, it is speculated that droplet deposits have a negative effect on the properties of the substrate.

The EB-PVD coating process is a relatively new coating process which was first used for the application of MCrAlY overlay type coatings in the late 1960s (Goward, 1974). Evaporation is carried out in a vacuum chamber at low pressures and involves an atom by atom transfer from the source to the component. It has many advantages for the gas turbine industry although the cost of the capital equipment hinders the widespread participation of scientific centres in the development of the EB-PVD technology for this industry.

From the foregoing it can be seen that coating process compatibility is an important factor. Given that a coating system for a particular application has been identified it is important to analyse which coating process is capable of achieving the desired coating properties. Moreover, process issues affect coating properties such as thermal conductivity, thermal shock resistance, creep, and oxidation and corrosion resistance, thus affecting the durability and performance of the coating. In addition, coefficient of thermal expansion, surface roughness, adhesive strength, erosion resistance and other mechanical and physical properties also affect both coating durability and performance.

Many published studies have concentrated on further developing process control and process capabilities in order to overcome the limitations associated with each particular process. The two most important parameters of any commercial coating process are flexibility and reproducibility. That is, on the one hand, it is important that the process allows various configurations or process variation, and, on the other, for the same set of parameters the process should produce similar coatings as far as their properties are concerned. It is evident, therefore, that an important area of research is process control in order to produce coatings with increased durability and performance.

2.7. Conclusion

The development of coatings for superalloys has progressed from the simple diffusion aluminides of the early 1950s through the MCrAlY to the TBCs of the present (Wood and Goldman, 1987). As TIT continues to increase, coatings more resistant to oxidation and thermal fatigue will be required. Currently, efforts to develop more durable TBCs

for turbine blades and vanes are likely to intensify. To sum up, coatings must be integrated into the total component design taking into full consideration the alloy composition, casting process, and cooling scheme (NMAB, 1996).

CHAPTER

3

3. Thermal Barrier Coatings (TBCs)

3.1. Background to TBCs

3.1.1. Introduction

A thermal barrier coating (TBC) is the name given to an insulating layer of usually low thermal conductivity material, such as ceramic or metal/ceramic, which is deposited onto the surface of the components used in the hottest regions of the engine for thermal protection. The current ceramic TBCs used in gas turbines, whether for airborne, marine or land-based propulsion systems, have a long and costly development behind them. They have been extensively developed for the past 30 years or more by agencies such as NASA (Liebert et al., 1976; Stecura, 1976; Liebert and Stepka, 1976 and 1979; Meitner, 1978; Gladden and Liebert, 1980; Stecura, 1985), the US Army (MARINE, 1974) and others worldwide (AGARD, 1997).

Ceramic materials are good thermal insulators (Wolfe et al., 1997; Nied, 1998) but they do not adhere well to the underlying substrate (Skelly et al., 1995) because, for example, the coefficient of thermal expansion (CTE) mismatch between the ceramic and metal can be high and this generates thermally induced strains on heating and cooling (Duderstadt, 1996). It follows, therefore, that in order to improve adhesion of the ceramic coating to the superalloy, a metallic bond coat is employed. This metallic layer has a CTE higher than the ceramic layer but intermediate between the ceramic and superalloy substrate, hence minimising the stresses induced by the expansion of the component. The combination of the ceramic layer for thermal protection (which is usually around 250 μm thick) overlying a metallic coating (approximately 100 μm thick) applied over the substrate is known as a TBC system.

Wolfe et al. (1997) indicated that, based on engineering applications, ceramic TBCs can be classified into three groups: oxides (Al_2O_3, ZrO_2, SiO_2, etc.), nitrides (TiN, SiN, AlN, etc.), and carbides (TiC, SiC, AlC, ZrC, HfC, etc.). The first group, the oxides, is the preferred ceramic composition for protecting gas turbine hot section components because of their high-temperature stability and lower thermal conductivity in the oxygen-enriched environments.

As pointed out by Siegel and Spuckler (1998), TBCs are important, and in some instances a necessity, for protecting highly stressed parts in high-temperature applications for current and advanced turbine engines. According to various reports (Toriz et al., 1988; Wortmann, 1990; Ulion and Anderson 1993; Brown, 1996; Goward,

1998; Nied, 1998; Siegel and Spuckler, 1998), TBCs are typically used to protect elements in the combustion chamber walls, burner cans, transition ducts, shrouds, nozzle guide vane platforms, vane aerofoils, and rotating blades.

As is made clear in the literature (Liebert and Stepka, 1976; Duderstadt, 1996), a TBC must possess certain properties in order to do the job of reducing metal surface temperature. To start with, it must protect the superalloy components from the ravages of the hot environment gas. Secondly it must be adherent to the superalloy and lastly, it must remain adherent during thermal cycling, i.e. the cycles of heating to the operating temperature and then cooling back to ambient temperature when the engine is turned off (Duderstadt, 1996).

The most important feature of thermal barrier systems is their thermal insulating properties, since the temperature reduction in base metal and thermal stresses are related to both the thermal conductivity of the zirconia ceramic and the thickness of the coatings. According to Goward and co-workers (1981), Rhys-Jones and Toriz (1989), and Strangman and Schienle (1990) the desired properties of a practical thermal barrier coating can be summarised as follows:

- Low thermal conductivity;
- High melting point;
- Closest possible coefficient of thermal expansion to the substrate alloy;
- Durability (ability to withstand all strain-temperature conditions in addition to oxidation and hot corrosion resistance);
- Adequate adherence for resistance to thermal stress spalling, i.e. good interparticle and substrate bonding is required;
- Adequate stabilisation of the desired (tetragonal or cubic zirconia) crystal structure to minimise effects of the non-linear thermal expansion caused by structural transformation;
- Repairability during manufacturing and after field service;
- Maintain the required component aerodynamics.

In conclusion, TBCs have many advantages which interest materials engineers, including superalloy surface temperature reduction and/or extending component life, thereby increasing component durability and/or engine efficiency.

As reviewed recently by Goward (1998), major programmes were initiated in the last two decades to further understand TBC/superalloy interactions and develop TBC coating composition and coating processes, hence increasing TBC durability. The next sections explain in some detail the milestones in TBC development, and characterise typical TBC systems examining both the bond coat and top coat. Finally, a consideration of the issues concerning the advantages brought about by the introduction of TBCs as well as some drawbacks to TBC incorporation on gas turbine components is given.

3.1.2. TBC History

Since the introduction of TBCs in the 1960s (Bose and DeMasi-Marcin, 1995), many developments have been performed in order to increase engine efficiency further. The same authors also described in detail the historical background of TBC use in the Pratt and Whitney engines. The first TBC system consisted of zirconia stabilised with calcia (CaO) or magnesia (MgO) in order to avoid the detrimental tetragonal to monoclinic phase transformation of zirconia, the latter being the preferred stabiliser used in Pratt and Whitney engines according to the previous report (see "Background to Zirconia Ceramics" on page 15 for more information about stabilising zirconia to avoid phase transformation). For around 20 years, from the early 1960s to the early 1980s, these ceramic compositions were broadly accepted until they were replaced by yttria-stabilised zirconia (YSZ) with an yttrium content of between 6 to 20wt%. In 1976, NASA was already studying PS zirconia stabilised with 12wt% yttria (Liebert et al., 1976), in addition to CaO and MgO-stabilised zirconia. At this time, a TBC system consisted of a duplex coating with both layers being applied by air-plasma spray (APS): an YSZ top coat overlying an MCrAlY bond coat (called generation I or Gen I TBC). By replacing the 22wt% MgO with the 6-8wt% yttria composition the life of the TBC was increased fourfold at temperatures above 1094°C (Meier et al., 1991a; Meier and Gupta, 1994).

According to a report by the National Materials Advisory Board (NMAB, 1996), E. Muehlberger developed a coating process known as low pressure plasma spray (LPPS) in the early 1970s (see "Coating Processes" on page 55). This process found widespread commercial use in the mid-1980s and was and still is capable of producing high-quality metallic MCrAlY coatings for certain applications, the reason being twofold: flexible coating composition and high coating rates. From the above, it can be seen that the LPPS process was adopted in place of the APS process for depositing the bond coat. Hence, a new generation of TBC systems entered service which comprised such a process for applying the bond coat (LPPS) whilst the deposition of the top layer was by APS. This is known as second generation TBCs (Gen II) and it took place in mid-1980s. The benefit of this Gen II TBC is that it allowed TBCs to be introduced on highly thermally loaded parts like vane platforms and vane aerofoils (Schulz et al., 1997a).

However, the search for increased engine efficiency led to the investigation of new processes which would allow TBCs to be applied to blade platforms and aerofoils, these being one of the most stressed components in the hot section turbine part of the engine. Rotating turbine blades, for instance, although not subjected so much to thermal fatigue as other engine components (in the combustion part, for example) still endure not only high fatigue and thermal shock but also high centrifugal loads which translates into needing protection against creep resistance. Gen I and Gen II TBCs do not perform well under these severe conditions and were, therefore, not applied to high stress components. The application of TBCs to high intensity components (rotating aerofoils) was achieved with the introduction of the more strain tolerant electron beam-physical vapour deposition (EB-PVD) coating process (Strangman, 1982). However, only in the mid-1990s did TBCs enter service on the most demanding components (Brown, 1996). TBC systems consisting of a ceramic layer (YSZ) applied by the strain tolerant EB-PVD over an LPPS MCrAlY bond coat, designated Gen III TBC, appeared very

attractive based on burner rig tests and exhibited a tenfold increase in durability relative to the Gen II TBC, which translated approximately into a threefold improvement in blade life (Bose and DeMasi-Marcin, 1995). According to the literature, one of the characteristics which make EB-PVD so interesting is the fact that it produces a columnar microstructure which is tightly bonded to the underlying bond coat "but essentially free to separate from adjacent columns as the substrate thermally expands relative to the ceramic" (Meier and Gupta, 1994). It is this structure that makes the EB-PVD process strain tolerant and simultaneously so promising for demanding applications (Movchan, 1996a; PennState, 1996 and 1998; Singh, 1997; Schulz et al., 1997a; Wolfe et al., 1997). These generations of TBCs and the year of their introduction are summarised in Table 3-1.

Table 3-1: TBC Development at Pratt and Whitney (Source: Bose and DeMasi-Marcin, 1995).

TBC System	Year of Introduction	Bond Coat	Ceramic Coat	Design of Layers
Early Combustion TBC	1963	Flame sprayed Ni-Al	APS 22MSZ	Ceramic/Bond Coat
"	1973	APS Ni-Cr/Al	APS 22MSZ	Ceramic/Cermet/ Bond Coat
"	1974	APS CoCrAlY	APS 22MSZ	Graded
"	1980	APS NiCoCrAlY	APS 22MSZ	Ceramic/Bond Coat
Gen I	1982	APS NiCoCrAlY	APS 7YSZ	Ceramic/Bond Coat
Gen II	1984	LPPS NiCoCrAlY	APS 7YSZ	Ceramic/Bond Coat
Gen II	1987	LPPS NiCoCrAlY	EB-PVD 7YSZ	Ceramic/Bond Coat

In addition to developments in TBC generations, developments in coating processes and/or coating composition, amongst others, are responsible for an increase in the maximum surface temperature allowable on superalloy surfaces. Nicholls (1999) listed the development of manufacturing processes as related to maximum metal service temperature. His data is included in Table 3-2 for reference.

From the above, it can be seen that TBCs are of interest to coating engineers with many economical and ecological advantages if they are applied to components in the hot parts of the engine.

Table 3-2: Development of Manufacturing Processes of High Temperature Coatings (Source: Nicholls, 1999).

Approximate Year of Introduction	Coating Development	Maximum Metal Service Temperature (°C)
1957	Hot dip aluminium: first practical use of a diffusion coating on a turbine aerofoil.	900
1960	Pack Cementation: diffusion aluminides widely introduced into service.	930
1970	Modified aluminide coatings introduced into service.	960
1970	Process developed for depositing overlay coatings.	960
1970	Plasma sprayed TBC introduced into service on combustion chamber components.	960
1975	MCrAlY overlay coatings introduced into service on turbine hardware.	975
1985	Processes developed for the deposition of EB-PVD TBCs.	
1987	EB-PVD TBCs introduced into service to solve hot spot problems.	1035
1993	EB-PVD TBCs commercially available for advanced engine designs.	1050
1995	EB-PVD TBCs in service on several engines including the GE CF6-80C2, GE CFM 45-5a and Pratt and Whitney's PW2000 and PW4000 series.	

3.1.3. Three- or more layer systems and graded coatings

As referenced by Maricocchi (1993), a TBC system is formed of one, two or more layers, one on top of the other in the multilayer cases. It follows, therefore, that although TBCs are typically assumed to have two layers, sometimes described as a bilayer system (Bose, 1995) or duplex coating (Schmitt-Thomas et al., 1995), strictly speaking the number of layers is not inherent to the term TBC, i.e. a two-layer system cannot be assumed. In addition, even though many coating systems have a metallic bond coat of usually the MCrAlY type, overlying the substrate, and an outer layer of a thermal resistant ceramic coating, this cannot again be generalised. In the early 1980s, Duvall and Ruckle (1982) described that an outer layer is selected by its reduced thermal conductivity and may be a ceramic or a metal/ceramic layer.

The earliest systems were bilayer and comprised of an alumina or zirconia ceramic layer applied over a metallic coating (Duvall and Ruckle, 1982). However, the stresses in this system were high due in part to the different coefficients or thermal expansion (the rate at which the components expand when heated) which was responsible for the failure of

the coating. It became necessary, therefore, to develop a new TBC that would accommodate the differential thermal expansion between coating and substrate more adequately. This was important because with thermal stresses induced by different coefficient of thermal expansion, the TBC coating looses adherence and fails by a failure mechanism known as spallation. Without the TBC coating and with increasing severe conditions observed in the hot section of gas turbines, the component could melt.

A three-layer system started to be employed which used an intermediate layer of metal and ceramic mixture (Duvall and Ruckle, 1982) or a metallic layer (Schmitt-Thomas et al., 1995) between the metallic bond-coat and the ceramic layer. Tchizhik and co-workers (1995) investigated the durability of a three-layer coating with different thicknesses. Similarly, Movchan and co-workers (1994) proposed a three-layer coating, which could increase considerably the life of alloys, by successive deposition of two different layers of metallic composition, and finally the external ceramic layer.

Strangman (1996b) investigated lower thermal conductivity TBC systems by EB-PVD. It was argued that a ceramic layer with a first portion of unstabilised porosity, a second portion, on top of the first, with stabilised porosity, and an outer portion with the pores coated with a noble metal renders a TBC system with relatively low thermal conductivity. Duderstadt (1996) contended that a three-layer system, comprised of a hardenable metallic bond coat, a layer of nickel aluminide intermetallic compound, and a ceramic top coat, resulted in improved thermal cycling performance.

Kokini and Takeuchi (1994) investigated failure mechanisms of PS TBCs using multilayer systems. Other parameters affecting coating durability were also studied, namely yttria content, oxidation resistance of the bond coat, manufacturing parameters and coating geometry. Their work examined a four-layer TBC comprising of a "normal" bond-coat and top ceramic layers, and two intermediate layers composed of metal and ceramic mixtures. The lowest layer, which was applied over the bond coat, was 40wt% ceramic and 60wt% bond coat. Overlying this one was another layer composed of 85wt% of ceramic and 15wt% of bond coat as shown schematically in Figure 3-1. The use of a four-layer TBC system aimed at gradually changing the properties of the material, hence reducing the stresses due to different coefficients of thermal expansion.

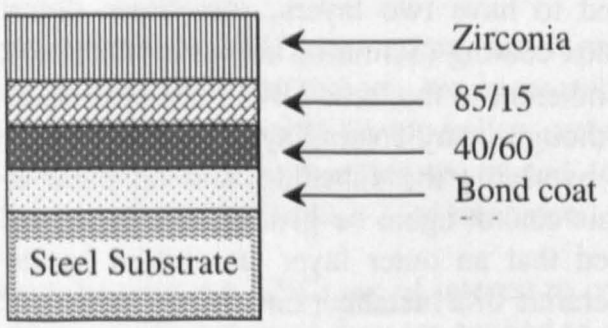

Figure 3-1: Four-layer system studied by Kokini and Takeuchi (1994).

Another basic mixed system consists of a layer of graded metal/ceramic material from all metal at the metallic/graded coating interface to all ceramic at the outermost surface.

Graded coatings increased thermal barrier durability when they were first introduced (Goward et al., 1981; Duvall and Ruckle, 1982). Two distinct descriptions for a graded coating exist: one according to Duvall and Ruckle (1982) and the other as reported by Strangman (1982). These two systems are explained schematically next, in Figure 3-2.

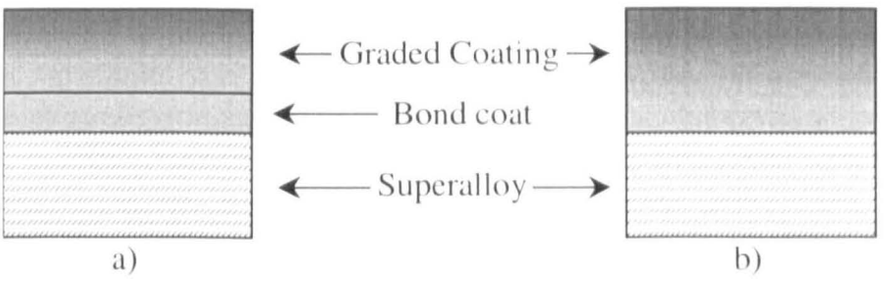

Figure 3-2: Graded system according to a) Duvall and Ruckle (1982) and b) Strangman (1982).

As far as the two previous graded systems are concerned, two possible interpretations are possible. The first one is that both systems are identical and therefore both studies discuss the same type of coating, that is, both use a single or two processes to deposit the graded layer from all metal to all ceramic. The other possible interpretation is that they are actually distinct. It is possible that the graded system according to Duvall and Ruckle is actually a two-layer coating in the sense that two distinct steps are used: firstly, the deposition of the metallic layer and then the graded metal/ceramic coating. In this interpretation, the TBC system according to Strangman is not composed of a bond coat, albeit both systems have a 100% metallic/0% ceramic mixture at the substrate/coating interface. Goward (1981) unveiled a TBC system that was adherent and resistant to thermal shock composed of a thin metallic bond coat applied to the substrate and a continuously graded mixture of metal and ceramic.

As reported by Duvall and Ruckle (1982), with increased temperature in the combustion chamber and turbine inlet temperature, graded coatings would fail because isolated metallic particles would oxidise owing to their high surface-to-volume ratio and the oxygen transport through zirconia.

The above TBC systems were used for several years in GT components and further research into different TBC systems with improved properties is still under development. However, there is general agreement that the typical bilayer systems, comprised of a bond coat and a YSZ layer, are the most promising for the gas turbine industry (Schmitt-Thomas et al., 1995, for example).

3.1.4. TBC Applications

For almost the whole history of TBCs, ceramic coatings were used mostly on stationary components (Toriz et al., 1988). Due to their static condition, stationary components do not endure the same stresses as rotating parts. Until recently, TBCs were not adequate for demanding applications because they would fail prematurely. Wortmann (1990) argued that TBCs had not yet evolved for use on vane aerofoils and rotating turbine

blades. Similarly, Ulion and Anderson (1993) noted that ceramic TBCs were widely used in the gas turbine industry, their most common use being in the combustion section of the engine, applied to stationary metal alloy components which define the combustion chamber.

A breakthrough came in the early 1980s when Strangman (1982) patented a coating application method that produces a columnar grain ceramic TBC. In the 1980s and early 1990s this strain tolerant physical vapour deposition process improved coatings significantly, thereby the use of TBCs was extended to vane platforms and/or vane aerofoils. Nevertheless, application on rotating turbine blades proved problematic due to the centrifugal stresses experienced by these components (Goward, 1998).

More recently, Alpérine and Lelait (1994) noted that the current challenge was the application of TBCs on rotating parts. Ulion and Anderson (1993) confirmed this by noting that efforts have been directed towards developing TBCs which can be applied to components other than in the combustion chamber, i.e. on blades and vanes in the turbine section of the engine. This is important because it is estimated that efficiency gains resulting from the application of TBCs to all high-temperature turbine aerofoils in a typical modern gas turbine engine could result in considerable annual fuel savings (Meier et al., 1991a). More recently, some investigators have already reported the use of TBCs on both the combustion chamber walls and the more demanding rotating turbine blades. Brown (1996) reported that TBCs have been used on rotating components in Pratt and Whitney's PW2000 and PW4000 and General Electric's CF6-80C2 and CFM56-5a series since 1994.

With recent improvements to the columnar grain process proposed by Strangman (1982), the literature indicates that the EB-PVD coating process is the only process capable of developing TBCs for use in the most demanding applications (Gell et al., 1987; Durham et al., 1994; Schmitt-Thomas et al., 1994; Bose and DeMasi-Marcin, 1995; Movchan, 1996a; NMAB, 1996; Morrell and Rickerby, 1997; Schulz et al., 1997a; Singh, 1998). EB-PVD TBCs have significantly enhanced TBC reliability and promise to realise the full potential of thermally insulating coatings.

All of the above acknowledges that the importance of TBCs, especially those produced by the EB-PVD technology, is too great to be ignored, as recently review by Goward (1998).

3.1.5. Bond Coat

Because zirconia is permeable to oxygen and does not adhere well to the underlying substrate the bond coat performs three functions:

- To provide oxidation and corrosion resistance;
- To reduce stresses induced by differences in thermal expansion (CTE);
- To adhere the ceramic physically and chemically to the substrate.

(Grünling and MannsMann, 1993; Jaslier and Alpérine, 1997)

Oxidation of the bond coat is a major factor contributing to ceramic spallation (Schmitt-Thomas et al., 1996; Freborg et al., 1997; Kaysser et al., 1997; Parks et al., 1997; Wolfe et al., 1997). Oxidation resistance in superalloys is usually achieved by growing a thin (submicron/micron) adherent film of alumina (Al_2O_3), which acts as a barrier to the diffusion of oxygen (Pettit and Goward, 1983b). The literature indicates that by allowing the metallic bond coat layer to react with oxygen, a thin dense alumina layer is formed, which significantly increases coating bonding as well as reducing the rate of bond coat oxidation. This layer is usually formed by bleeding oxygen inside the EB-PVD chamber prior to deposition, hence oxidising the bond coat and forming a submicron alumina oxide layer to which the ceramic adheres well, this layer becoming effectively a bonding layer (Strangman, 1982; Ulion and Ruckle, 1983; Ulion and Anderson, 1993; Rickerby et al., 1995; Jaslier and Alpérine, 1997; Gell et al., 1999). The continuous alumina layer forms an oxygen barrier and reduces further oxidation of the substrate (Demaray, 1987). In the case of YPSZ top coat, deposited over a metallic bond coat, the alumina layer is responsible for increased strength (Alpérine and Lelait, 1994).

In addition, the success of a coating system is critically linked to the presence of a reactive element like yttrium or zirconium in the bond coat. These elements further enhance alloy oxidation resistance by making spallation of the TBC system more difficult. Small amounts of yttrium in the bond coat greatly increase system life, often shifting the failure of the TBC to the bond coat/ceramic interface (Jordan, 1994; Kaysser et al., 1997).

From the above, it is evident that a major concern associated with the longer design life for future gas turbines is the stability of the bond coat. Thus, there is currently considerable research into more adherent bond coats with improved durability. Some methods which have been shown to improved TBC durability by improving alumina oxide scale adhesion include using superalloys with certain compositions, using a diffusion aluminide coating, or by reducing the sulphur levels, as explained in the following paragraphs.

Ulion and Anderson (1993) described a TBC system for a "new" class of oxidation resistant superalloys. Certain superalloy composition can produce an adherent alumina oxide scale on the substrate surface. The most preferred coating process for applying the ceramic is by EB-PVD. The same authors stated that a combination of certain superalloy compositions plus the alumina scale, which should be at least about 0.25 μm thick, renders an improved TBC system.

Strangman (1996c) contended that an MCrAlY layer was not necessary to grow an adherent alumina scale. Instead, a diffusion aluminide layer could grow an oxide layer with sufficient adhesion for a good bonding. This method significantly reduces TBC cost by eliminating the need for an MCrAlY bond coat. This was confirmed by Rickerby et al. (1995); their work investigated an improved TBC coating which according to one aspect of the invention could comprise a platinum-aluminide layer, then an alumina scale layer (thermally grown oxide) and finally the low thermal conductivity ceramic layer.

Schaffer et al. (1996) showed another approach in which a TBC system works without the bond coat. Their technique relied on the fact that low sulphur levels increase the alumina scale adhesion to the superalloy and to the ceramic YSZ layer (Andritschky et al., 1995). The level of sulphur, which enables the deposition of a ceramic layer directly over the superalloy, is 1 ppm (part per million). A method for removing sulphur from superalloys is described. Worth noting is that by maintaining a sufficiently low sulphur level the alumina layer and ceramic TBC do not debond from the substrate. Advantages of this invention include reductions in weight and manufacturing costs, the latter being achieved through the elimination of the expensive MCrAlY bond coat (even though there is a need for a method of reducing sulphur content). In addition, rare earth elements such as yttrium and zirconium which are added in small amounts to the superalloy for oxide scale adhesion can be reduced or eliminated, hence making manufacturing less complex and expensive. Worth noting is that the improvements of this invention only occur if the ceramic layer is applied by a PVD method such as EB-PVD and not by other processes such as plasma spraying.

Smialek (1998) has recently described the effect of sulphur level and yttrium additions to the superalloy on the oxidation resistance and alumina adhesion. According to the report, single crystal (SC) superalloys have a typical impurity level of around 5 ppm and their cyclic oxidation resistance would be greatly increased if the sulphur content was reduced to below 0.5 ppm. It should be emphasised that while Schaffer et al. (1996) opted for reducing sulphur levels instead of controlling the additions of rare earth elements to increase alumina scale adhesion, Smialek noted that for many commercial systems the direct addition of yttrium is more practical than removing ppm levels of sulphur. Notwithstanding this, excellent improvements are possible from desulphurization by hydrogen annealing. However, the preferred content of yttrium, which is between 0.01 and 0.1wt%, is difficult to achieve in advanced SC superalloys. Hafnium was also reported to be in use but with less success than yttrium in imparting scale adhesion.

From the aforementioned, it can be seen that the critical concentration of sulphur as related to alumina scale adhesion is an important quantity which need to be defined (Schaffer et al., 1996; Smialek, 1998). In order to reduce costs the maximum tolerable sulphur level without degrading scale adhesion should be used. Therefore, further research is required to understand microstructural variations in order to minimise the negative impact of sulphur levels on the rate of scale growth and on adhesion of TBCs (Parks et al., 1997).

3.1.6. Top coat

The importance of zirconia ceramics to act as thermal insulators has already been discussed in the section "Background to Zirconia Ceramics" (page 15). Therefore, their properties, advantages and limitations are only going to be discussed briefly in this section.

Some of the properties which make zirconia the preferred ceramic for use in TBCs include low thermal conductivity, high melting point, relatively high CTE, and high thermodynamic stability. Zirconia is usually stabilised with yttria in order to avoid a

detrimental phase transformation, which occurs at around 1200°C, responsible for a volume change causing the ceramic to spall. Yttria partially stabilised zirconia (YPSZ) has good fracture toughness, good chemical stability, good adhesion, high corrosion resistance, and the lowest thermal conductivity of any ceramic material, the latter leading to a lower metal surface temperature (Unal et al., 1994; Rybnikov et al., 1994; Pint et al., 1996; Wolfe et al., 1997).

Table 3-3 indicates the extensive research performed in the last few decades into the most durable YPSZ composition for use as thermal insulators. After comprehensive research into coating materials, the most suitable system for use as a thermal barrier is generally accepted to be YPSZ with an yttria content between 6-8wt% (according to around 75% of the studies). A higher yttria content corresponds to the fully stabilised zirconia cubic phase and the thermomechanical resistance of the coating drops significantly (Stecura, 1985) (see "Yttria Additions" on page 41).

Table 3-3: Yttria content as reported in the literature for use in a TBC system (Source: compiled by the author).

Year	Author	Yttria Content	Comments
1976	Liebert et al.	12	Also other stabilisers (MgO and CaO).
1976	Stecura	12	Also other stabilisers (MgO and CaO).
1977	Levine and Clark	12	Studies for industrial gas turbines.
1978	Stecura	6.2, 7.9	Effects of compositional changes on the performance of a TBC.
1979	Liebert and Stepka	12	Value used in various engine applications.
1979	Stecura	6.2, 7.8	Effects of compositional changes on the performance of a TBC.
1981	Demaray et al.	8-10	
1981	Gedwill	12	A study of a Mach 0.3 burner rig test with a 380 μm thick TBC.
1981	Taylor et al.	6.6	Studies on a TBC for use in utility gas turbines (applied by PS).
1982	Duvall and Ruckle	6 and 20	21 MSZ was also studied.
1982	Strangman	20 or 35	Referring to the experimental work done to date.
1985	Stecura	6.1 and 8	Optimisation of the YSZ/NiCrAlY thermal barrier system.
1986	Goward	8	Most durable TBC.
1987	Gell	7	Improved content for more demanding application with increase resistance to failure mechanisms.
1988	Cruse et al.	7	Value used in a physical experiment.
1988	Toriz et al.	6-8, 20	Studies of coating properties related to coating composition with applied with either APS or PVD processes.

Year	Author	Yttria Content	Comments
1989	Harmsworth and Stevens	6-12	Deduced largely from empirical tests. Referencing another work.
1989	Kvernes et al.	8	The most spall-resistant zirconia composition is attained with around 8wt%.
1989	Stecura	6.1 and 8	Studies of bond coat and ceramic composition on TBC durability.
1989	Toriz et al.	20, 6-8	Evolution from 20YSZ to 6-8YSZ.
1990	DeMasi-Marcin et al.	7	TBC system investigated was an APS 250 μm 7YSZ/LPPS 130 μm bond coat.
1990	Nagaraj and Wortman	8	Experiments of coatings applied by APS and EB-PVD with vanadium-contaminated fuels.
1990	Strangman and Schienle	8-20	YSZ applied by EB-PVD is about 5 times more resistant to molten sulphate salt attack than alumina scale layers.
1990	Wortman et al.	6-8	Typical PS TBC. 8YSZ APS was used for a physical experiment.
1990	Wortmann	6-20	
1991a	Meier et al.	7	Comparison between the EB-PVD and PS coating processes.
1991b	Meier et al.	7	Value used in a physical experiment applied by APS and EB-PVD. Composition is an improvement over the 22wt% MgO (22MSZ).
1992	Gruninger and Borls	7	Eight references on the history of 7YSZ.
1993	Miller et al.	6-9	Studies of thermal diffusivity and durability of PS TBCs. Also PS hafnia-yttria TBC characterisation.
1993	Robson et al.	8	Value used in a physical experiment.
1993	Ulion and Anderson	7	Most preferred ceramic.
1994	Alpérine and Lelait	6-8	8.5wt% was used in an experimental procedure. Above 8wt% corresponds to the fully stabilised zirconia and thermomechanical resistance drops significantly.
1994	Bertamini and Di Gianfrancesco	7	Value used in a physical experiment.
1994	Cosack et al.	7	Value used in a physical experiment.
1994	Durham	7	Evolution from 22MSZ.
1994	Jordan	8	Explains why the 8wt% yttria is desirable.

Year	Author	Yttria Content	Comments
1994	Kokini and Takeuchi	20	Value used in a physical experiment.
1994	Meier and Gupta	7	Value used in a physical experiment applied by APS and EB-PVD. Composition is an improvement over the 22wt% MgO (22MSZ).
1994	Movchan et al.	6.5-8	Properties of such content.
1994	Rybnikov et al.	8-12	Lists the advantages of this content. 8YSZ used in experiments.
1994a	Sohn et al.	8	Value used in a physical experiment.
1994b	Sohn et al.	8	Value used in a physical experiment.
1994	Srinivasan	8	
1994	Unal et al.	20	Value used in a physical experiment.
1995	Andritschky	7	Value used in a physical experiment.
1995	Bose	7	Deposited by APS, then LPPS and now EB-PVD.
1995	Chen et al.	8	Value used in a physical experiment.
1995	Crostack and Beller	7	Value was used in an experimental test. Thickness of the coating was varied from 0.5 mm up to 2 mm.
1995	Jue et al.	2.6, 3, 4.5, 6 and 8	Value used in a physical experiment. Other rare earth-oxide doped zirconia materials were studied.
1995	Nissley	7	
1995	Rigney et al.	7	Initial applications include the combustion chamber and afterburner.
1995	Rybnikov et al.	8	From references.
1995	Tchizhik et al.	8	Value used in a physical experiment.
1995	Teixeira and Andritschky	7	Value used in a physical experiment.
1996	Duderstadt	6-20	Top coat is zirconia with yttrium oxide or with cerium oxide (15-40wt%). YSZ is preferable 8wt% Y_2O_3.
1996	Gaudenzi et al.	8	Value used in a physical experiment.
1996b	Movchan	8	
1996	Pint at al.	7-8	Value used in a physical experiment.
1996	Schaffer et al.	6-20	Desirable composition.
1996	Schmitt-Thomas et al.	6-8	6YSZ used in a physical experiment. 6-8YSZ shows superior thermal cycling resistance.
1997	Alpérine et al.	6-8	For high temperature applications.
1997	Chevillard et al.	5-20	Applied by plasma assisted CVD.
1997	Dorvaux et al.	6-8	Typical TBC top coat composition. 8wt% was used in tests.
1997	Fauchais et al.	8	Studies of PS TBCs.

Year	Author	Yttria Content	Comments
1997	Fritscher et al.	7	Value used in a physical experiment.
1997	Haubold et al.	7-8	7wt%YSZ was used in tests.
1997	Immarigeon et al.	8	A stabiliser which performs well in aero engines.
1997	Jaslier and Alpérine	6-8	Typical composition for both EB-PVD and PS TBCs. 7wt% used in tests.
1997	Kaysser et al.	6.5, 20	Investigation of different stabilisers.
1997	Mogro-Campero et al.	7-8	Studied thermal conductivity of an APS TBC using the laser flash method.
1997	Morrell and Rickerby	8	Value used in physical experiments.
1997a	Nicholls et al.	8, 12, 20	Studies on erosion and damage of TBCs applied by APS and EB-PVD.
1997b	Nicholls et al.	8	Typical composition of a TBC
1997	Ravichandran et al.	8	Thermal conductivity studies for PS and EB-PVD TBCs.
1997	Tamarin et al.	8 Y_2O_3-MO 8-10 Y_2O_3	Thermal conductivity and thermal diffusivity studies.
1998	Goward	8	Work at P&W as an advance on MSZ.
1998	Slifka et al.	8	Investigated the thermal conductivity of a TBC applied by APS.
1998	Smialek	8	Value used in a physical experiment.
1998	Wright	7	Value used in a physical experiment.
1998	Zhu et al.	8	Lists the properties of 8YSZ as well as other TBC systems.
1999	An et al.	8	Experiments with single and multilayer coatings.
1999	Cernuschi et al.	7-8	The best compromise to meet TBC requirements applied either by APS or EB-PVD.
1999	Gell et al.	7	Studied the spallation failure of a TBC system applied by EB-PVD.
1999	Lima and Da Exaltação Trevisan	8	Value used in a physical experiment (applied by APS).
1999	Shillington and Clarke	9	Value used in a physical experiment applied by PS.
1999	Stiger et al.	7	Value used in a physical experiment.
1999	Tamura et al.	8	Value used for multilayered TBCs in a physical experiment.
1999	Trice et al.	7	Studied the role of additions of a member of the zirconium phosphate in PS YSZ.

3.1.7. Advantages of TBCs

According to Bose and DeMasi-Marcin (1995) the main advantage of using TBCs is concerned with the fact that superalloy surfaces are kept at a temperature lower than without a TBC due to the fact that ceramics have a low thermal conductivity. This is important because it helps to maintain the component surface properties within acceptable bounds, thus extending component durability and enhancing its capabilities.

According to the literature (Liebert et al., 1976; Liebert and Stepka, 1976 and 1979; Stecura, 1976; Goward, 1986; Bennett, 1986; Toriz et al., 1989; Rhys-Jones and Toriz, 1989; Wortmann, 1990; Cosack et al., 1994; Meier and Gupta, 1994; Bruce et al., 1995; Nagaraj et al., 1995; Skelly et al., 1995; Itoh and Tamura, 1999) the advantages and improvements of TBC on engine components can be summarised as follows:

- Enhanced component performance by decreasing its temperature at constant gas operating temperatures, thus increasing component life and engine reliability due to a decreased thermal fatigue load;
- Reduced cooling air at constant gas and component temperatures, thus increasing compressor efficiency;
- Increased turbine entry temperature, thus increasing engine efficiency;
- Reduction in maintenance requirements;
- Possibility of using lower grade fuels, hence decreasing operating costs, or decreasing exhaust emissions, which adversely affect the environment;
- Reduced component weight (particularly important on turbine blades);
- Decreased strains;
- Reduced fuel usage;
- Cheaper than new alloy development.

By developing more efficient aircraft with modern engines, the aircraft produces cleaner exhaust and burns less fuel. It is estimated that efficiency gains resulting from the application of TBCs to all high-temperature turbine aerofoils in a typical modern gas turbine engine could result in annual fuel savings as high as 38 million litres for a 250-aircraft fleet (Meier et al., 1991a). This is confirmed by the work of Gell (1994). Gell has estimated that fuel costs can amount to as much as 40% of airline operating cost, hence there are continuing competitive pressures to further improve fuel efficiency.

Moreover, work by Srinivasan (1994) showed that TBCs have been used primarily to extend component life but utilisation of TBC continues to grow for reasons beyond thermal protection, as seen previously. In addition, TBCs, particularly YSZ, are currently regarded as having the potential for at least "the same impact as major recent advances in engine materials such as directional solidification and single crystal technology on the efficiency and durability of turbine engines" (cited in Demaray et al., 1982).

Although discrepancies do exist in the literature regarding the temperature reduction contributed by TBCs, they are capable of significantly lowering metal surface temperature thereby providing significant advantages, as seen previously. Rhys-Jones

and Toriz (1989), and Toriz and co-workers (1989) reported that this life improvement can be traded off for 1) higher inlet temperatures and increased thrust or for 2) reduced cooling air usage and reduced fuel consumption. Table 3-4 lists many of the works available in the literature and the temperature reduction achieved by a TBC compared to an uncoated substrate (some deduced by empirical tests, others the result of experimental data). It is noteworthy that temperature reduction achieved by a TBC system compared to an uncoated aerofoil depends on ceramic thickness, ceramic microstructure and the degree of cooling, but is also influenced by surface roughness, ceramic density and ceramic composition.

Table 3-4: Temperature reduction achieved by a TBC system (Source: compiled by the author).

Year	Author	Temperature Reduction	Comments
1976	Liebert and Stepka	190°C	Measurement of the mid-span leading-edge vane with a 280 μm thick coating.
1976	Liebert et al.	135°C	Investigation on the durability of a PS TBC.
1976	Stecura	140-190°C	Data for an APS 12wt%YSZ J-75 turbine blade in a Mach 0.3 burner rig test.
1977	Levine and Clark	110°C	Tests for industrial gas turbines.
1978	Meitner	83-228°C	Various values for PS TBCs depending on coating thickness and coolant flow (on both section and pressure surfaces).
1979	Liebert and Stepka	30-100°C	Results of other references for various engine components.
1980	Gladden and Liebert	122 and 212°C	For a ceramic thickness of 250 μm and 500 μm, respectively.
1981	Bratton et al.	50-220°C	TBCs applied by the PS process. Various ceramic compositions were discussed.
1981b	Levine et al.	100-300°C	TBCs applied by Plasma Spray. Temperature reduction is for a 250 μm thick TBC.
1982	Demaray et al.	93.3°C (200° F) or more	Also 10% reduction in specific fuel consumption (sfc) or as much as 30% increase in engine power.
1982	Duvall and Ruckle	38 - 149°C	Depending on thickness (0.005 in - 0.010 in.) and on local heat flux conditions. Reference to other work.
1986b	Meetham	200°C (estimated)	2-layer system: MCrAlY bond coat + 8wt%YPSZ. Much improved thermal fatigue resistance compared with the 3-layer system.

Year	Author	Temperature Reduction	Comments
1986b	Meetham	50°C or more	Results for combustion chambers. Combustion chamber life has been at least doubled. 3-layer system: Ni-Cr bond coat, ceramic/metallic interlayer and a ZrO_2-20wt% Mg (375 μm thick).
1986	Spengler and Whitlow	38-93°C (100-200° F)	Land and marine combustion turbines. Typical coating is 500-750 μm thick
1987	Gell	93.3 - 205°C (200-400° F)	Full potential of TBC implied removal of cooling air.
1988	Sheffler	170°C	Calculation for a 250 μm thick zirconia coating.
1990	DeMasi-Marcin et al.	170°C	Maximum reduction but depends on local heat flux.
1990	Wortman et al.	150°C	Depending on coating thickness. Benefits include increase in gas temperature, life extensions or reductions in coolant flow.
1991a	Meier et al.	167°C	Also fuel savings (1%) and improved durability.
1991b	Meier et al.	149°C (300F)	Comparison between the EB-PVD and PS coating processes.
1994	Bertamini and Gianfrancesco	120°C	Applied by the Atmosphere and Temperature Controlled Spraying (ATCS) process; 7wt%YPSZ; 300 μm thick coating.
1994	Durham et al.	167°C	
1994	Jones and Reidy	100°C or more	Thickness between 125 μm and 250 μm.
1994	Jordan	170°C	
1994	Meier and Gupta	167°C	A typical TBC is a 254 μm thick ceramic layer over a 127 μm thick bond coat.
1994	Srinivasan	167°C	6-8wt%YPSZ, 300 μm thick.
1995	Bartz et al.	56-83°C	Engine test results with a 125 μm PVD TBC.
1995	Bose and DeMasi-Marcin	165-170°C	
1995	Nissley	17-33°C (each 25 μm)	Reduction is for each 25 μm of TBC and depending upon ceramic structure and level of convective cooling. According to Sheffler, 1988.
1996	Brown	110°C	According to NMAB.
1996	Jones	100°C or more	Thickness between 125 μm and 250 μm.

Year	Author	Temperature Reduction	Comments
1996	National Materials Advisory Board (NMAB)	40°C or 110°C or more	Limited to 40°C for critical applications since components must not fail before next inspection.
1997	Alpérine et al.	50, 82, 113°C	50 and 82°C for a thermal conductivity of 1.9 and 1.1 W/m.K, respectively. Maximum gain considering the whole leading edge reaches 113°C.
1997	Dorvaux et al.	200°C	For a ceramic coating 250 μm thick.
1997	Fauchais et al.	50-170°C	50-80°C average reduction. 139°C blade hot-spot reduction. 170°C capability.
1997	Haubold et al.	150°C	Benefits result in reduced cooling airflow requirements and/or component durability improvement.
1997	Kaysser et al.	150°C	EB-PVD top coat overlying a LPPS bond coat (Generation III TBC).
1997	Morrell and Rickerby	70-150°C	
1997	Mutasim	55°C	Experimental data using EB-PVD.
1997b	Nicholls et al.	150°C	
1997	Tamarin et al.	40-100°C	Reduction is equal to a 3 to 4 times increase of service life.
1997	Tsantrizos et al.	120°C (350°C)	120°C for a conventional TBC. Studies of TBC systems that could achieve a temperature drop of 350°C.
1998	Goward	170°C	Simultaneously reduces cyclic thermal strains.
1999	Stiger et al.	up to 200°C	
2000	Nicholls	150°C	150°C surface temperature reduction in conjunction with component cooling.

According to the reports by Schulz et al. (1997a) and Kaysser et al. (1997), an earlier report by Harrison in 1993 in a conference on "European Propulsion Forum" explained the necessity of close control of the materials' surface by the simple rule that blade life in creep (a degradation mechanism which affects high temperature components) is halved for each 10-15°C increase in temperature.

From the foregoing, it can be seen that TBCs are a vital part of gas turbine technology and have the potential to enable gas turbines to reach new heights in performance and efficiency. However, as with all high performance technological developments, drawbacks do exist in the application of TBCs to high stressed components. In addition, manufacturing a TBC suitable for a particular application is a complex and arduous task due to the fact that TBCs have to resist the various degradation mechanisms existent in one of the harshest environments ever created by man. The next section discusses some

of the disadvantages of using TBCs and what is being done to reduce or even eliminate their negative impact on engine performance.

3.1.8. Disadvantages of TBCs: a reason for reticence

This section discusses some of the technological barriers to TBC incorporation on gas turbine components. Although TBC failure modes (oxidation, spallation, corrosion, etc.) do affect TBC life, thus limiting TBC application to all high stressed parts, they are not discussed in this section. These failure modes are discussed in "TBC Failure" on page 43.

Investigations to study both coated and uncoated superalloys have been performed in order to understand further the interactions between a TBC and the underlying superalloy (Liebert and Stepka, 1976; Meitner, 1978; Gladden and Liebert, 1980; Stecura, 1985; Sheffler and Gupta, 1988; Watt et al., 1988; Morrell and Rickerby, 1997). According to these published investigations, the disadvantages of using TBCs can be summarised as follows:

- Increased surface roughness (particularly for plasma sprayed TBCs);
- Potential alteration of cooling hole geometry and flow as a result of ceramic deposition;
- Alteration of turbine aerodynamics as a result of increased aerofoil thickness;
- Increased centrifugal loading of rotating aerofoils;
- Potential alteration of superalloy composition and/or mechanical properties;
- Increased manufacturing complexity.

In addition, a report by McMinn (1987) on coatings technology for hot components of industrial turbines discussed other means in which a coating may be detrimental to the resistance of the substrate. Although it was acknowledged that TBCs offer a significantly lower superalloy surface temperature, TBCs may affect superalloy properties because of:

- Heat treatment due to the coating process;
- Long range residual stresses in the substrate;
- Crack initiation due to the coating;
- Interdiffusion between the coating and substrate.

Moreover, with the exception of the first factor, the detrimental effects of all the other measures increase with increasing coating thickness. Stecura (1985) and Tchizhik et al. (1995) investigated and described the influence of coating thickness on TBC durability. Varying both the bond coat and the YSZ thickness affects thermal barrier system lives.

Sheffler and Gupta (1988) argued quite correctly that while all of the above technological barriers have technological solutions, some of these solutions increase coating cost. For example, a post-treatment using an abrasive material may be used to reduce surface roughness to within an acceptable level; laser drilling of holes after TBC

deposition is another method that has been considered in order to overcome TBC limitations. In another technique, Meier and co-workers (1991a), for example, suggested the use of lower density ceramic coatings to reduce overall component weight. This is desirable for rotating aerofoil applications to reduce the centrifugal loading from the added weight of the structural parasitic coating.

The magnitude of the negative impact of both increased surface roughness and hole plugging problems are closely linked to the various coating processes. In addition, for each coating process, the careful control of the many process parameters also affects these problems. A more detailed discussion of the differences between both EB-PVD and PS coating processes as related to surface roughness and hole closure will be dealt with in the section "Coating Processes" on page 55.

Several investigators (Liebert and Stepka, 1976; Jordan, 1994; Watt et al., 1988; Morrell and Rickerby, 1997) indicated and described aerodynamic performance as being adversely affected by both the surface roughness and the increased aerofoil thickness. This is important because surface roughness and the alteration of the component aerofoil design leads to alteration of the airflow, which significantly affects performance. Watt and co-workers (1988) characterised aerodynamic performance for a profile typical of first-stage nozzle guide vane in a cascade test as related to surface roughness. The same authors stated that surface finish is important in terms of its effect on cascade efficiency. In addition, performance penalties vary depending on Reynolds number, due to the TBC in its as-sprayed state; there appears to be a critical low Reynolds number below which the range of roughness tested has no effect on cascade efficiency.

Also, Gradden and Liebert (1980) showed that at low gas Reynolds number, where an apparent laminar boundary layer developed on the uncoated-vane suction surface, the ceramic layer trapped the boundary layer resulting in higher metal temperatures because of the higher heat flux. However, it is believed that this test condition is not considered similar to the conditions encountered in the gas turbine service.

Coating thickness is of particular relevance because while increased ceramic thickness provides additional thermal insulation (thus cooler components), it adds to component weight, which is critical for rotating components, (Bose and DeMasi-Marcin, 1995) and accelerates TBC failure (Stecura, 1985). As reported by Stecura (1985), an increase in coating thickness from about 250 to 850 μm renders a twofold decrease in life for a PS 6.1YSZ and 8YSZ. In addition, thinner coatings have the advantage of contributing to a lighter engine, thus increasing efficiency.

The composition of the MCrAlY bond coat is usually selected to match that of the underlying superalloy. Nevertheless, during repeated engine cycles both the bond coat and the superalloy composition interdiffuse after which each composition is substantially changed. It follows, therefore, that the bond coat composition may alter the mechanical properties of the substrate. Moreover, the bond coat may also affect the mechanical properties of the substrate due to the way in which it is applied. Special care should therefore be taken since the coating may sufficiently change the conditions at the surface of the component resulting in easier coating failure (McMinn, 1987).

In conclusion, in order to decrease the negative impact of some of the technological barriers existent in the application of TBCs, the many finishing steps or post-treatment processes developed increase not only manufacturing complexity but also manufacturing costs. In addition, the more complex the manufacturing processes the more potential failure modes and possibilities for manufacturing errors exist (Schaffer et al, 1996).

3.2. TBC Properties

3.2.1. Thermal Conductivity

Thermal conductivity is one of the most important properties in the design of thermal barrier coatings for high-temperature gas-turbine components (Voyer et al., 1995; Alpérine et al., 1997; Siegel and Spuckler, 1998; An et al., 1999).

Ceramic materials have a low thermal conductivity (Demaray et al., 1982; Jordan, 1994; An et al., 1999) and are therefore a good candidate for use not only as coatings (Demaray et al., 1982; Duvall and Ruckle, 1982; Crostack and Beller, 1995; Nicholls, 1997b), but also as a replacement of superalloys (NMAB, 1996; Rolls-Royce, 1996). The initial production application for ceramic materials is likely to be for small high-speed turbines, which have very high turbine entry temperatures (Rolls-Royce, 1996).

Thermal conductivity varies with coating thickness (Jordan, 1994; Bose, 1995; Lawson, 1996), coating composition (Tamarin, 1997), coating process (Nicholls, 1997b) and with coating microstructure (Harmsworth, 1989; Alpérine and Lelait, 1994; Tamarin, 1997). For each coating process, the parameters used to deposit the coating also affect the properties of the coatings, for instance, the density and porosity of the coating, hence affecting coating thermal conductivity. Some processes such as physical vapour deposition (PVD) and chemical vapour deposition (CVD) for example, create coatings that have a finer grain structure with many more boundaries at the substrate/coating interface than at the coating/outer surface interface (Lawson et al, 1996).

Work recently developed at Cranfield University in collaboration with Rolls-Royce Plc (Derby, UK) showed that thermal conductivity of zirconia coatings varies with coating microstructure and coating thickness. Lawson et al. (1996) demonstrated the feasibility of modelling the zirconia thermal conductivity applied by physical vapour deposition throughout the deposition process. An accuracy of about 0.1 W/m.K between predicted and measured was achieved. The model uses a rule of mixtures, which was formulated based on a two-layer model which in turn, is related to the number of column boundaries in the microstructure. More recently, Nicholls and co-workers (1997b) compared the thermal conductivity of different coating processes and described methods for reducing the thermal conductivity of EB-PVD TBCs by using layers. The initial microstructure that characterises PVD ceramics is desirable since there is a higher number of column boundaries at the substrate/coating interface thereby scattering the thermal waves (Nicholls et al., 1997b). Methods for reducing thermal conductivity in this type of coating include colouring, addition of dopants, and layering.

Worth noting is that ceramic layer composition is selected based not only on thermal conductivity, but also on high temperature stability and thermal expansion compatibility with the substrate (Jordan, 1994; Bose, 1995). In addition, TBC application efficiency depends on ceramic layer thermal conductivity and coating thickness, both factors determining the temperature drop across the TBC (Tamarin, 1997).

A TBC system with reduced thermal conductivity helps to maintain the component surface at a temperature low enough to retain its properties within acceptable bounds. Mechanical failure from high temperature oxidation and melting would quickly occur if the hot section components were not protected using TBCs with low thermal conductivity.

3.2.2. Thermal Shock Resistance

Next to thermal conductivity, thermal shock resistance ranks high among selection criteria for insulating capacity (Wortmann, 1990). Gupta et al. (1996) disclosed a TBC having grooves, which was then tested for thermal shock resistance. They determined that such TBC exhibited improved properties that were evident from a thermal shock resistance test. Land-based and marine combustion turbines have also been investigated as related to thermal shock. Spengler and Whitlow (1986) described a plasma sprayed TBC for land and marine gas turbines with improved properties against failure modes. The same authors also stated that the best thermal shock resistance was achieved with a coating containing about 20% by volume porosity in order not to shorten thermal stress lifetime.

3.2.3. Coefficient of Thermal Expansion (CTE)

During thermal cycling, coating and superalloy expand and contract according to the various power levels. Because ceramics and nickel-based alloys have different CTE (~10×10^{-6} and 15×10^{-6} K^{-1}, respectively) (Wortmann, 1990), cycles of heating and cooling tend to cause the ceramic coating to crack and spall off, which results in the superalloy being overheated in the area of the defect (Duvall and Ruckle, 1982; Duderstadt and Nagaraj, 1983). Coating lifetime generally increases as the thermal expansion mismatch between the coating and the substrate decreases (Jordan, 1994). For instance, additions of elements such as tantalum and niobium to the bond coat have been reported to increase coating strength and increase CTE approximating it to a value closer to that of the substrate (Strangman and Vonk, 1988).

The current thermal barrier coating for engine hot section components have an outer ceramic layer that has a columnar grained microstructure tightly bonded to the substrate but essentially free to separate from adjacent columns as the substrate thermally expands relative to the ceramic (Meier and Gupta, 1994). Gaps between the individual columns allow the columnar grains to expand and contract without developing stresses that could cause spalling (Strangman, 1982). These stresses are responsible for the initiation of cracks that develop at the bond coat/alumina layer interface. With increasing number of thermal cycles the crack then propagates (usually parallel to the surface of the substrate) and eventually a small portion of the alumina layer (including

the ceramic layer overlying it) is liberated from the substrate leading to failure of the thermal barrier coating system (Skelly et al., 1995).

A problem with columnar grained ceramic layers is that when exposed to temperatures over 1100°C (2012°F) for substantial periods of time, sintering of the columnar grains occurs. The gaps close as adjacent columnar grains bond together. Once the gaps become closed, the ceramic layer can no longer accommodate the thermal expansion and may crack and spall (Strangman, 1996a).

3.2.4. Yttria Additions

In most applications, TBCs contain yttria-stabilised zirconia. However, it should be emphasised that there is no universal agreement in the literature regarding the best possible ceramic material and their composition. To start with, yttria additions vary greatly. The minimum and maximum amount was found to be 2.6wt% (Jue et al., 1995) and 35wt%YSZ (Strangman, 1982), respectively. Some investigators reported the use of 20wt% (Duvall and Ruckle, 1982; Toriz et al., 1988 and 1989; Kokini and Takeuchi, 1994; Unal et al., 1994; Schaffer et al., 1996; Kaysser et al., 1997) but the majority investigated a content between 6 and 8wt%. However, a higher yttria content results in a lower thermal conductivity as shown in Figure 3-3.

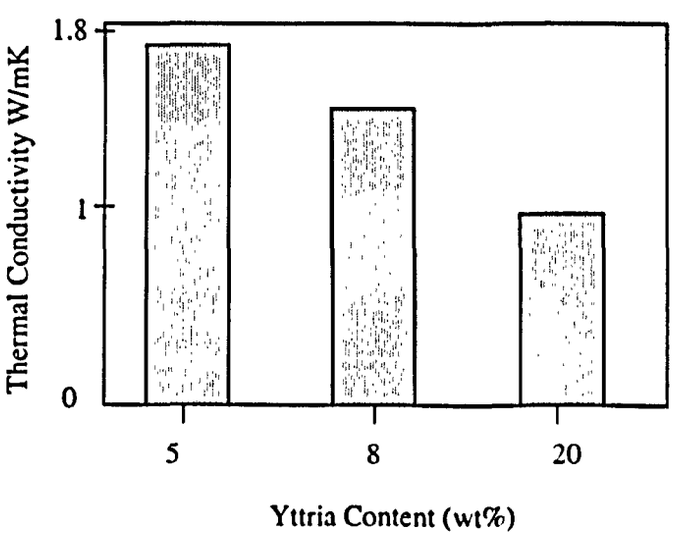

Figure 3-3: Theoretical conductivity of EB-PVD zirconia ceramic as a function of yttria content (Source: Nicholls et al., 1997b).

Although the 20wt% yttria content has the lower conductivity of the three compositions studied, many published studies agree that the best composition is when zirconia is stabilised with between 6-8wt% of yttria (see Table 3-3 on page 29). This is due to the fact that thermal conductivity is only one of many properties desirable for TBCs. As reported first by Stecura (1985) and then by Alpérine and Lelait (1994), an yttria content above 8wt% corresponds to the fully stabilised zirconia cubic phase and the thermomechanical resistance of the coating drops significantly as can be seen from Figure 3-4.

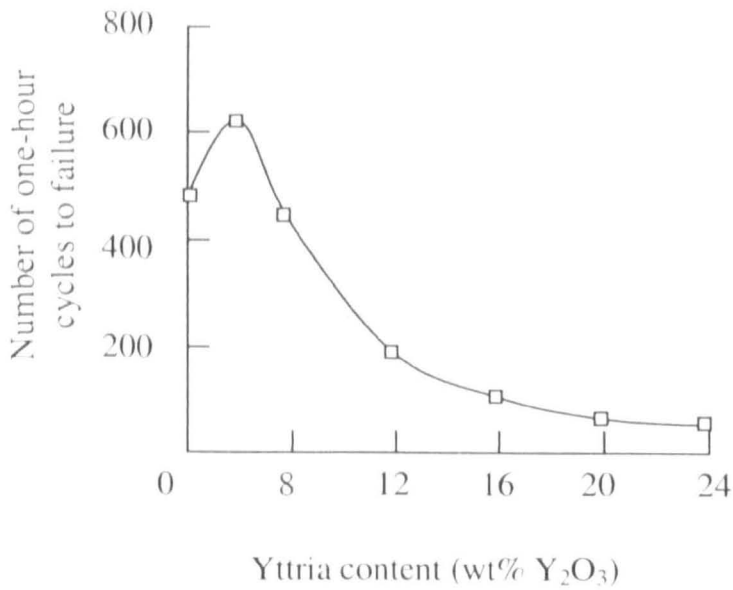

Figure 3-4: Influence of yttria content on the life of a plasma sprayed barrier system (Source: Stecura, 1985 and Alpérine and Lelait, 1994).

Jue and co-workers (1995) characterised yttria-, erbia-, ceria-, and lanthana-based zirconia as related to phase content and density, microstructure, low and high temperature phase stability, and mechanical properties. They found out that zirconia strength and toughness decreased with increasing yttria content as shown in Figure 3-5.

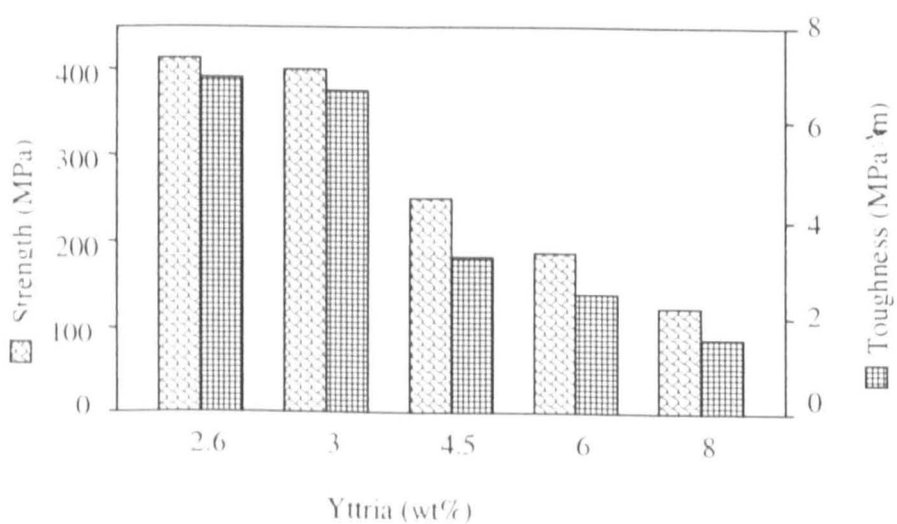

Figure 3-5: Fracture strength and toughness as a function of yttria content (Source: derived from Jue et al., 1995)

The above figures demonstrate the compromise required between thermal and mechanical properties when choosing the ceramic composition. Designing a TBC system is thus a compromise between the mechanical, chemical, and thermal properties that characterise a TBC, and the best yttria content depends on the required resistance against the many degradation mechanisms.

Tamarin (1997) studied the thermophysical properties of the ceramic layers and disclosed a ceramic composition, ZrO_2-8wt%Y_2O_3-MO with a lower thermal conductivity than the "traditional" ZrO_2-8wt%Y_2O_3.

All of the above investigations emphasise the importance of improving the knowledge of the relationship between coating composition and thermal conductivity. Nevertheless, as previously mentioned, thermal conductivity also varies with coating thickness, coating process, and coating microstructure making the definition of the coating composition with the lowest thermal conductivity more difficult. To sum up, ceramic composition greatly influences thermal conductivity and the choice of the exact composition should always be application-specific.

3.3. TBC Failure

Hot section components in gas turbine engines are required to retain mechanical and surface integrity for thousands of hours within a harsh environment under conditions of very high stresses (Pettit and Goward, 1983a). Therefore, there are a number of alloy/environment interactions that take place, highlighting the need to minimise the negative impact that this aggressive environment may impart on component properties.

The life of an engine component is limited by degradation mechanisms such as creep, low cycle fatigue (due to variation of stress with engine power), high cycle fatigue (due to vibration), thermal fatigue, oxidation and corrosion, and erosion. Those strongly influenced by temperature, especially after an extended period of high temperature service, are creep, thermal fatigue, and corrosion (Rolls-Royce, 1986; Maricocchi, 1993). For instance, higher firing temperatures exacerbate oxidation and corrosion problems (Srinivasan, 1994).

TBC development has not been so rapid as engineers would like even though potential TBC payoffs are large in terms of overall improved engine efficiency and/or durability (Sheffler and Gupta, 1988). To start with, all ceramic systems have poor damage tolerance (resistance to cracking). Moreover, at higher gas temperatures a failure in the coating system quickly leads to a failure in the substrate emphasising the need to prevent structural damage by, for example, melting and thermal fatigue cracking (Gell et al., 1987; Brown, 1996; NMAB, 1996).

Given that a coating system has been identified to provide environmental protection, the techniques used to reduce structural failure vary with engine component. For example, a combustor element primarily needs thermal shock and oxidation resistance; a turbine rotor blade also needs creep and fatigue strength; a bearing demands special tribological properties (Wortmann, 1990).

From the above, it is clear that a thorough understanding of all TBC failure mechanisms is key to increasing as well as predicting TBC durability (Freborg et al., 1998). Problem areas that need to be addressed include prevention of coating failure due to thermal cycling, oxidation of the bond coat, and erosion due to gas stream solid particles. Some of the techniques that contribute to increased TBC durability include optimisation of process parameters to achieve both smoother surfaces and ensure consistent high quality

coatings. In addition, resistance to wear, erosion, oxidation, and improved thermal resistance have been partly met with the introduction of nanostructured materials (Gell, 1994 and 1995). Although progress has been made, the problems associated with the many failure modes of TBC systems remain.

3.3.1. Spallation

One of the most important and studied degradation mechanisms, which hinder full exploitation of the TBC benefits to all high stress/high temperature engine components, is spallation (Andritschky et al., 1995; Skelly et al., 1995). TBC spallation occurs, with varying degrees of importance, at the different coating interface layers.

Because metal superalloys and ceramic TBCs have different coefficient of thermal expansion (CTE), repeated thermal cycles cause stresses to build up at the metal/ceramic interface (Durham et al., 1994; Freborg et al., 1998). In addition, the ceramic layer cannot usually be deposited directly on the metal superalloy in part because adhesion between current ceramic coatings and superalloy compositions is poor (Duderstadt, 1996). However, it is possible to pretreat the superalloy to form an alumina scale with a corresponding increase in adhesion (Rickerby et al., 1995). Adherence of the ceramic both physically and chemically to the substrate is important because insufficient adhesion may result in the ceramic spalling. As pointed out by Andritschky et al. (1995) loss of adherence and spalling of the ceramic coat is due to the oxidation of the metallic bond coat at the bond coat/top coat interface. To sum up, failure by spallation occurs primarily due to the difference in CTE, phase and volume changes due to oxidation (Movchan, 1996a), and poor adhesion (Andritschky, 1995). Adherent, spallation-resistant coatings have, therefore, been the object of considerable research during the past decades (Rairden, 1976; Strangman, 1982; Duderstadt and Nagaraj, 1993; Schaffer et al., 1996; Gupta et al., 1996). As was seen previously, a typical TBC is composed of a thin alumina layer (produced by oxidation of the MCrAlY layer) between the MCrAlY layer and the outer insulation layer. This is the result of studies that show that a thin alumina layer provides both adhesion and oxidation-resistance to the TBC system. Unfortunately, jet fuel contains impurities, such as sulphur, which diffuse into the coating and instigate loss of TBC adhesion and as a consequence the TBC spalls.

There has been considerable research in order to increase coating durability and to further understand the methods that instigate TBC failure by spallation (Spengler and Whitlow, 1986; Kokini and Takeuchi, 1994; Shillington and Clarke, 1999). Therefore, before TBCs can be used in more demanding applications, more reliable life prediction models must be developed to help engine designers to predict coating spallation life with reasonable confidence (Cruse et al. 1988). Chan (1999) developed a coating life model to predict the useful life of combustion turbine coatings. Nissley (1995) investigated and proposed analytical models based on observations of TBC spalling to predict TBC spalling life. Because TBC spallation is not fully understood, TBCs have only recently been applied to turbine rotating aerofoils due to their lack of resistance to spalling (Duvall and Ruckle, 1982; Durham et al., 1994). When developing a TBC system it is important, therefore, to create a system with adequate adherence for resistance to thermal stress spalling (Goward et al., 1981). Delamination or spalling of

the ceramic or of the bond coat leads to the exposure of the underlying component to the hot-gas environment (Cruse et al., 1988). Without the thermal protection needed to oppose the hot gases, the failure region rapidly deteriorates leading to component failure, i.e. even a "small" failure in the TBC may lead to the whole blade being put out of service.

Skelly and co-workers (1995) listed some techniques employed to reduce TBC spallation failure as described next:

- Coating composition optimisation;
- Coating process improvement;
- Adding new layers to the TBC system;
- Changes of the metal superalloy.

Meier and Gupta (1994) also describe some of the approaches used to improve spallation life. Not only ceramic composition (as suggested by Skelly et al.), but also residual stress control, and most importantly careful control of ceramic microstructure. In addition, post-processing treatments may also be used in order to optimise residual stresses that may lead to TBC spallation (Johnson et al., 1998).

Also, as is made clear in the Skelly et al. patent (1995), although the various techniques suggested above have been successful to varying degrees, there are also disadvantages in using these methods, namely:

- Increased weight;
- Constraints on design;
- Manufacturing complexity.

Moreover, other drawbacks may include increased manufacturing costs and increased coating thickness. Coating thickness is of particular relevance because while increased ceramic thickness provides a higher temperature drop across the TBC system (thus cooler components), it adds to component weight (critical for rotating components) and accelerates TBC spallation (Stecura, 1985; Bose and DeMasi-Marcin, 1995). In addition, increased coating thickness also modifies the aerodynamic performance of the gas turbine (Watt et al., 1988; Morrell and Rickerby, 1997).

Other work developed aiming at increasing the spallation resistance of TBC has been reported. As pointed out by Duderstadt (1996), reducing the aluminium content of the bond coat to preferably 6-7wt% allows it to be hardened by heat treatment by the gamma/gamma prime precipitation method. This increases the spallation resistance and prolongs component life. Schaffer et al. (1996) discussed an adherent TBC system having low sulphur content and excellent spallation resistance to thermal cycles. According to Gupta and co-workers (1996) a new method of improving ceramic adherence and resistance to spalling was considered. They described the use of selectively located grooves which enhance the strain tolerance of the TBC such that it resists spalling even when exposed to high stress conditions created by a combination of thermal, mechanical and dynamic stresses.

As far as bond coat composition is concerned, several rare-earth reactive elements have been included in small percentages, which have been found to increase the durability of the coating. Small additions, typically between 0.3 and 0.5wt%, of the rare element yttrium and the formation of yttrium oxides within the alumina scale, for instance, are known to greatly improve coating adherence to the substrate and minimising spallation (Ulion and Ruckle, 1982; Goward, 1986; Kvernes et al., 1989). As reported by Kvernes (1989), yttrium increases bond coat durability by reducing the oxygen diffusion rate; it is also more practical than reducing levels of sulphur (Smialek, 1998). Other elements used to reduce the negative impact of TBC spall include silicon or hafnium (Movchan, 1996a).

In addition to bond coat optimisation, the optimum composition of the ceramic top layer has also been a theme of considerable research. Yttria content in the zirconia-yttria system has been proved to be a critical parameter in developing a durable TBC system (Alpérine and Lelait, 1994). Kvernes et al. (1989) found that the most spall-resistant zirconia composition is obtained with around 8wt% yttria. Coating process also affects coating spallation life. The literature indicates that different failure mechanisms pertain to different coating processes (Jordan, 1994).

3.3.2. Oxidation

As noted by Pettit and Goward (1983b), most engineering alloys in today's advanced applications are used in environments that contain oxygen. It follows, therefore, that oxide scales are developed on the surfaces exposed to oxygen. Hence, oxidation of these alloys is inevitable and a very important form of high temperature corrosion. Though not of sole importance, oxidation of the bond coat is a primary failure mechanism of commercial TBCs (Quadakkers et al., 1999). Unfortunately, the understanding of the mechanisms by which oxidation induce TBC failure is far from complete. It is recognised that there is a critical oxide thickness at which oxides spall, and this varies when coated with a TBC. In addition, it is unclear how oxidation may interact with other potential degradation mechanisms (Freborg et al., 1998). Nevertheless, inability to provide sufficient oxidation protection of the bond coat has been repeatedly identified as one of the important factors affecting the ceramic top coat durability during service (Freborg et al., 1998).

Investigations to study the oxidation behaviour in an environment at temperatures that can be considered relevant to gas turbine service have been formulated.

Conner and Connor (1994) showed a method for performing both static and cyclic oxidation tests. In the static test, substrates were firstly exposed isothermally in static air. Secondly, testing was stopped at set intervals for specimen review. Lastly, visual observations, weight loss measurement and destructive evaluation were used to characterise coating performance. Typical test temperature was around 1000°C. In the cyclic test an emphasis on thermal shock was effected by using cool air on the test specimens.

Freborg and co-workers (1998) have recently described the importance of understanding oxidation attack in order for TBCs to achieve their full potential against the harsh

environment in gas turbines. They argued that TBC life might be influenced by other factors through interactions with the mechanism of oxidation, namely bond coat coefficient of thermal expansion, bond coat roughness and creep behaviour of both the ceramic and bond coat layers. A finite element model to identify the oxidation effects on the stresses within the TBC system and their interaction with other factors was proposed.

In a recent review, Nicholls (2000) described the historical developments of oxidation and corrosion resistant coatings. Progress is being made by including multiple active elements in the metallic bond coat and by developing "smart coatings". These coatings are resistant to both oxidation and corrosion by including a high chromium enriched region that reduces Type II corrosion attack and a β aluminide rich zone for oxidation and Type I hot corrosion protection.

Coating composition of both the bond coat and top coat plays an important role in protecting the component against oxidation. Current compositions are the culmination of a long and costly development in order to meet requirements from various industries. As pointed out by Bruce et al. (1995) many ceramics are resistant to degradation mechanisms such as oxidation to which metals are usually more prone. Nevertheless, ceramic composition is usually selected for thermal protection whereas the bond coat composition is selected to for the ceramic to adhere physically and chemically to the substrate and provide oxidation resistance.

Grünling and Mannsmann (1993) reported that one of the tasks of the bond coat is to provide good oxidation resistance to the TBC system; this is a direct result of lowering the component's metal surface temperature. Progress in bond coat composition is being made not only by varying the high content elements such as aluminium (Gupta et al., 1995; Duderstadt, 1996), but also by including small amounts of elements such as tantalum, rhenium, and platinum (Taylor et al., 1995), or others including the oxygen active elements hafnium and silicon (Movchan, 1996a; Nicholls, 2000). For many MCrAlY alloys, the Al level lies between 7-12wt% (Gupta et al., 1995). Duderstadt (1996) claimed that the aluminium content of the bond coat should be kept even lower, preferably between 6-7wt% so that the bond coat may be hardened by gamma/gamma prime precipitation. A higher content of Al is undesirable since it would render a soft bond coat. However, if this level of Al compromises oxidation resistance, then an extra layer of nickel aluminide can be used. The loss of Al from the coating can take place by the following three means: oxidation, spallation, and inward diffusion (Chan, 1999).

If the TBC system includes an MCrAlY bond coat, resistance to oxidation is met by oxidising the metallic bond coat hence growing a thin aluminium oxide diffusion layer (Al_2O_3 or alumina) on top of the bond coat. Several investigators have acknowledged the importance of this layer not only to provide adhesion between the bond coat and the ceramic coat, but also to resist oxidation of the metallic bond coat (Stragman and Vonk, 1988; Taylor et al., 1995).

Even though the most common method to create the alumina layer is through oxidation of the bond coat, other work investigated the deposition using a chemical vapour deposition process (CVD). Strangman and Solfest (1989 and 1991) reported a TBC system that provided about four times the life of prior systems applied by EB-PVD: the

coating was applied by EB-PVD but the alumina layer was applied by a CVD process. According to the same authors, the relative absence of impure oxides in the CVD alumina might contribute to a slower alumina scale growth, which renders increased oxidation resistance. In addition, other elements may be included in the alumina diffusion coating in order to increase coating stability and/or oxidation resistance such as rhenium, tantalum and niobium (Strangman and Solfest, 1989 and 1991; Strangman, 1996a, 1996b, 1996c).

Despite these advances, there is still much room for improvement not only as far as substrate/bond coat/ceramic composition is concerned, but also understanding how oxidation interacts with other failure modes.

3.3.3. Corrosion

With increasing combustion temperatures to achieve more efficient engines with greater fuel economy, insulation coatings have become more vital than ever to protect engine aerofoils against corrosion and other failure mechanisms. It is therefore critical to maintain surface components within acceptable limits in order to minimise corrosion attack. According to the literature (Hancock, 1974; Stringer and El Dashshan, 1974; Pettit and Goward, 1983b; McMinn, 1987; Conner and Connor, 1994), there are two forms of hot corrosion: high-temperature hot corrosion and low-temperature hot corrosion (also known as Type I and Type II hot corrosion, respectively). Type I hot corrosion is a high-temperature surface reaction between a metal or coating, a molten deposit of Na_2SO_4 and/or NaCl, and a combustion gas containing sulphur. This type of attack is also referred to as sulphidation due to the presence of metal sulphides under the corrosion scale. Type II hot corrosion is a lower-temperature surface reaction between a metal or coating, a molten deposit containing base metal sulphates and Na_2SO_4 and/or NaCl, and a combustion gas containing sulphur. Which type of hot corrosion is predominant depends upon the operating temperature: Type I is common at temperatures between 800 and 1000°C and Type II between 650 and 850°C.

Worth noting is that corrosion attack is not specific to aircraft engines. In the field of utility gas turbines and marine gas turbines hot corrosion has been defined as a form of accelerated oxidation induced by certain impurities in the combustion gases (Hancock, 1974; Stringer and El Dashshan, 1974; Stringer, 1981; McMinn et al., 1988). Mutasim and Brentnall (1997) reported studies of the effects of coating properties by varying fuel quality. Even though clean fuel does little to degrade coatings properties, low-grade fuel can be very detrimental.

Gas turbine fuels are known to contain, even in small percentages, particles of contaminant elements such as sodium (and sodium chloride or salt) and sulphur (Movchan et al., 1994; Rybnikov et al., 1994; Strangman, May 1996) and others including vanadium and potassium (Nakamori et al, 1997). Even traces of these impurities are responsible for instigating corrosion problems (Nakamori et al., 1997), thus introducing TBC failure. In addition, some studies have also shown that the presence of the element molybdenum is also recognised to induce TBC corrosion (McMinn, 1987). These impurities bring about hot corrosion and vanadate corrosion, which significantly reduce the life of coated hot-section components (Srinivasan, 1994).

In addition, cheaper, less purified fuels contain higher percentages of these impurities. With the recent increase in price of petroleum derivatives the use of less pure fuels is a tempting area of research although it would intensify corrosion problems (Movchan et al., 1994; Ryknikov et al., 1994).

The dominant cause of TBC degradation by hot corrosion in low-grade fuels appears to be "destabilisation" of the zirconia structure (Jones and Reidy, 1994; Mutasim and Brentnall, 1997). Low-grade fuel contains harmful impurities, which react with yttria and form compounds that deplete the zirconia matrix of stabiliser, causing TBC failure (Jones and Reidy, 1994). In order to limit TBC failure, Jones (1996) investigated possible candidates for stabilising zirconia in TBCs for use in marine applications. Among the oxides investigated were titanium oxide (TiO_2), cerium oxide (CeO_2), yttrium oxide (Y_2O_3), magnesium oxide (MgO), scandium oxide (Sc_2O_3), indium oxide (In_2O_3) and tin oxide (SnO_2). From the possible candidates, Sc_2O_3 and especially Sc_2O_3 with yttria mixtures are the most worthy to be studied and developed as a stabiliser for hot corrosion-resistant TBCs. McMinn (1987) noted that the use of calcium oxide (CaO) for stabilising zirconia was also known in the literature.

Apart from the field of aircraft gas turbines, the issue of low-grade fuels is more acute. Marine and industrial GT fuels can contain 1-5% sulphur and up to several hundred parts per million (ppm) of vanadium. High-purity aviation fuel, on the contrary, contains less than 0.05% of sulphur and no vanadium (Jones and Reidy, 1994). As is made clear in the Spengler and Whitlow (1986) patent, research and progress is being made in turbines designed to be operable with low-grade fuels. In addition, military fuel is of intermediate quality but fuel quality cannot be guaranteed in wartime. It follows, therefore, that TBCs should maintain integrity regardless of fuel purity, although this value must obviously be kept within certain limits.

Several studies concentrated on developing corrosion-resistant bond coats in the field of gas turbine components (Itoh, 1999). Due to the differences in fuel impurities, when designing a system substrate/bond coat/top coat, materials and coatings engineers should develop them taking into consideration the properties for each specific application. As pointed out by Conner and Connor (1994) an aero-derivative turbine for pumping oil on an offshore platform with low-grade fuels requires a significantly different turbine blade/coating solution than do the same components operating in a flight engine on clean jet fuel.

Air also contains harmful impurities that increase the corrosion effect on high-temperature coatings. Impurities in the air and fuel can lead to the deposition of alkali metal sulphates in turbine components resulting in hot corrosion attack (McMinn, 1987). Therefore, corrosion problems are associated not only with too high a temperature during thermal cycling, but also with low graded fuel and air which contain impurities.

For decades, investigators have questioned and studied corrosive attack on TBCs and simultaneously the potential of these coatings to resist this type of degradation mechanism (Nakamori et al., 1997). Hot corrosion attack has been investigated in the following US patents (Table 3-5):

Table 3-5: US Patents where hot corrosion attack is discussed (Source: compiled by the author).

Inventor	Patent No.	Year	Comments
Ulion and Ruckle	4,321,310	1982	TBC system which provides oxidation and corrosion resistance.
Strangman	4,321,311	1982	TBC system which provides oxidation and corrosion resistance.
Spengler and Whitlow	4,576,874	1986	Patent title "Spalling and corrosion resistant ceramic coating for land and marine combustion turbines".
Duderstadt and Nagaraj	5,238,752	1993	TBC system which provides oxidation and corrosion resistance.
Maricocchi	5,254,413	1993	Developed surface treatments to resist damage.
Taylor et al.	5,455,119	1995	A coating composition with good corrosion and oxidation resistance is disclosed.
Strangman	5,514,482	1996c	Thin ceramic coating applied on top of diffusion aluminides resist hot corrosion attack of the component by fuel and air impurities.

In addition, Strangman and Solfest (1989), Solfest and Strangman (1990), and Strangman (1991, 1996a, 1996b) reported that chromium and manganese elements can be incorporated into diffusion aluminides for hot corrosion resistance.

Since information pertaining to bond coat composition is often considered proprietary, the field performance of the many commercially available coating compositions in different environments has not been adequately documented (McMinn et al., 1988). Notwithstanding this, various studies have investigated the relative resistance of different coatings for aircraft gas turbines. Staia et al. (1995) studied the relative corrosion resistance of three aluminide coatings applied by pack cementation onto a nickel-based superalloy used for turbine blades. The three aluminide coatings included an unmodified aluminide, a platinum-aluminide, and a silicon-aluminide which were tested at various temperatures and the microstructure of the coatings before and after the corrosion tests were carried out by SEM analysis. Similarly, Gaudenzi and co-workers (1996) investigated the resistance to high temperature corrosion of four coatings (PtAl, two CoNiCrAlY, and a TBC system) applied over various superalloy components. Worth noting is that the alumina oxide layer, which is formed by oxidation of the bond coat, can contain chromium and silicon oxides.

MCrAlY bond coats and in particular CoCrAlY coatings have performed well in protecting components against corrosion at medium temperatures (around 700 to 930) (Srinivasan, 1994; Movchan, 1996a; Itoh and Tamura, 1999).

3.3.4. Erosion

Erosive attack by air impurities such as sand particles is a common degradation problem in GT components and in realising the full potential of TBCs (Pettit and Goward, 1983b). At the combustion temperatures and air velocities typical of today's jet engines, the kinetic energy of small solid particles present in the air stream may have a negative effect on the normal functioning of the engine. A component with a damaged TBC by erosion does not protect the component in the same way as a TBC without damage and this leads to an increase in component temperature (Bartz et al., 1995). In the commercial aircraft gas industry the use of clean fuel with relatively small number of foreign particles is common but in the field of land and marine-based gas turbines erosion can become a serious problem. Nevertheless, the aircraft gas turbine industry does not encompass solely commercial aircraft. Gas turbines for use in military aircraft may also suffer from the use of lower-grade fuels or by particle ingestion in less pure environments. As pointed out by Srinivasan (1994), in normal operating conditions erosion takes a secondary position but in special situations such as the Operation Desert Storm in the Persian Gulf War, erosion can become a major degradation process. Gas turbine compressor blades and vanes suffer severe erosion by the ingestion of airborne particles in desert environments. Particle size, which can be up to 1 mm, plays an important role in the severity of degradation of the component.

In a recent report by Stiger et al. (1999), one of the failure modes that needs to be understood in order to realise the full potential of TBCs is erosion both by small particles that wear away the coating and by larger ones causing cracks in the TBC system. A significant deterioration in engine performance results from these particles impacting engine components. The origin of these solid particles varies with the field of gas turbines (Tabakoff et al., 1995). This is explained in the next table:

Application	Origin of solid particles
Industrial and power generation	Produced during the combustion of heavy oils, synthetic fuels and pulverised coal.
Commercial and military aircraft	Vortices generated during landing/takeoff, sand storms, volcanic ash and thrust reverser efflux at low speed.
Steam turbines	Mainly iron oxide from boiler scale that break off and enter the stream flux.

It follows, therefore, that the presence of solid particles in the gas stream, although undesirable, is inevitable. With air speeds approaching the speed of sound the impact of even small particles of debris crashing against the component surfaces causes considerable damage (Tabakoff et al., 1995; Walsh et al., 1995). As was pointed out by Toriz et al. (1989) erosion of TBCs is a potential problem that will have to be dealt with on aerofoils subject to high stream speed and where high angles of impingement occur.

Accordingly, there is a need for a thermal barrier coating, and production method, that has increased erosion resistance. There is, therefore, currently considerable research into

materials, compositions, coatings and coating processes with increased erosion resistance. This is important because erosion can lead to loss of efficiency due to reduction in blade chord width and tip recession, and surface roughening accompanied by a change in blade geometry (uneven surfaces affect aerodynamics) (Walsh et al., 1995; Tabakoff et al, 1995; Watt et al., 1988). In addition it can also lead to reduced service life, increased down time, cause unscheduled shut downs, and increase replacement or repair costs (Walsh et al., 1995).

Beele (1996) discussed a TBC system and process for high-temperature components, resistant to both erosion and corrosion attack. Due to the inherent brittleness of the ceramic coating (as opposed to the ductility of the metallic bond coat), a silicide coating (preferably $MoSi_2$) is much more suited to withstand erosive attack than ceramic. A TBC layer that includes such coating as the outer layer can provide a threefold increased protection against corrosion, erosion, and excessive thermal load.

According to two reports by Gell (1994a and 1994b), a further increase in erosion-resistant TBCs can be achieved with the use of nanostructured materials. Although these materials are likely to be costly and limited in supply in the near future, their initial production is likely to be for high-payoff applications.

Two works by Toriz and co-workers (1988, 1989) and another one by Nicholls et al. (1997a) investigated the erosion behaviour of various TBC systems by varying parameters such as temperature, particle size, particle velocity and impact angle. Another very important parameter when considering erosion degradation is effected by the coating process. It is widely known that the coating process greatly affects the erosion rate of TBCs and therefore a comparison between the two preferred coating processes as regards to erosion behaviour has also been the object of these studies. Toriz et al. (1988) showed a normalised erosion rate for nine plasma sprayed coatings, one applied by PVD (8wt%YSZ) and two nickel superalloy substrates. The PVD coating was the most erosion resistant of all coatings only having a higher erosion rate than the two superalloys. Moreover, the higher the impingement angles the better the PVD coating outperformed all the other PS coatings. However, PVD is only two times more erosion resistant than PS at low angles of attack, such as on the combustion chamber and vane platforms, but these improvements can be as high as 1000% at a 90° impingement angle. This makes PVD coatings particularly important for turbine blades and NGVs where high angles of impact occur. In fact, the PVD process is the only process suitable for such demanding applications, one of the reasons being that they approximately replicate the surface finish of the component applied to. PS coatings produce a surface roughness, typically 10 μm (Nicholls et al., 1997b), which conflict with the aerodynamic needs of aerofoil components. Contrary to PS-deposited coatings, PVD coatings do not induce high loss of aerodynamic performance for they have a surface roughness of around one to two micrometers. Nicholls et al. (1997a) reviewed erosion damage to PS and PVD coatings, their work being concurrent with the work by Toriz et al. (1989). Using a high velocity gun rig at Cranfield University, Nicholls et al. (1997a) concluded that EB-PVD TBCs provide a tenfold improvement in erosion resistance over PS TBCs.

In conclusion, more life prediction models are necessary in order to determine the erosion rate induced by solid particles entering the aircraft gas turbine in order to further

understand the behaviour and relationship between various parameters such as component temperature, particle velocity, particle size, and impact angle. As far as the coating process is concerned it is widely accepted that only the PVD process is suitable for demanding applications such as turbine aerofoils. EB-PVD TBCs provide a smoother surface finish and a better surface finish retention, this being responsible for a tenfold erosion resistance when compared to PS TBCs.

3.3.5. Creep

Over a period of operational time the turbine blades slowly grow in length. This phenomenon is known as creep and there is a finite useful life limit before failure occurs (Rolls-Royce, 1986). Similarly, coatings also expand and contract according to the different thermal cycling powers of a gas turbine.

Sheffler and Gupta (1988), Meier and Gupta (1994), and Bose and DeMasi-Marcin (1995) related creep resistance to component surface temperature. With increased combustion temperatures, degradation mechanisms become exacerbated. To avoid structural failure by creep and other degradation modes, an important factor in the design stage of a gas turbine engine is the need to ensure that certain parts of the engine do not absorb heat to the extent that it is detrimental to their safe operation (Rolls-Royce, 1986). According to the reports by Schulz (1997a) and Kaysser (1997), an earlier report by Harrison in 1993 in a conference on "European Propulsion Forum" explained the necessity of close control of the materials' surface by the simple rule that blade life in creep is halved for each 10-15°C increase in temperature.

From the above, it is, therefore, important to develop materials and coatings to protect them against creep, thus increasing substrate durability. One way of extending TBC life has been achieved by the development of a creep resistant bond coat (Sohn et al., 1994b). Bennett (1986) in his appraisal of TBC properties noted that the bond coat is probably the least creep resistant portion of the coating system. Improvements in the bond coat can be achieved by lowering the aluminium (Al) content from 8-10wt% to preferably 6-7wt%, but this would be at the expense of oxidation life (Duderstadt, 1996). Similarly, Gupta et al. (1995) reported the influence of aluminium content on creep and oxidation resistance. MCrAlY bond coats with less than 12wt%Al have better high temperature creep and stress rupture resistance but lower oxidation resistance. Moreover, because of its weight, the bond coat can be detrimental to the creep life of the component, particularly in the case of rotating parts (NMAB, 1996). Furthermore, as seen previously, oxidation of the bond coat is one of the most important degradation mechanisms that can contribute to reduced TBC durability. It follows, therefore, that creep resistance is important because creep behaviour of the TBC system and other factors may influence TBC thermal fatigue life both separately and through interactions with the mechanism of oxidation (Freborg et al., 1998).

In the field of industrial gas turbines (IGT), the use of TBCs is also related to improvements in creep life. Amagasa et al. (1994) investigated the benefits in creep life while Mutasim and Brentnall (1995) reported a tenfold increase in creep resistance and twice the corrosion life brought about with the introduction of TBCs applied to turbine blades. As part of an experiment, TBCs accounted for a metal surface temperature

reduction of 55°C compared to uncoated turbine aerofoils and are, therefore, responsible for considerable increases in coating life. This is important in the field of IGT because the time before overhaul is approximately fivefold that of aircraft engines (Mutasim and Brentnall, 1995).

Although the application of TBCs is beneficial in reducing metal surface temperature thus increasing creep resistance, the deposition of a coating can be detrimental to the creep resistance of the substrate. The application of a coating can affect the creep properties of hot components of industrial turbines by the following means:

- Heat treatment due to coating process;
- Long range residual stresses in the substrate;
- Crack initiation due to the coating;
- Interdiffusion between the coating and substrate.

(McMinn, 1987)

With the exception of the first factor, all of the other measures are more noticeable with increasing coating thickness and decreasing substrate thickness. This report is concurrent with the study by Tchizhik (1995) as far as the influence of the coating thickness on creep resistance is concerned.

Creep strength also varies with coating thickness (Tchizhik et al., 1995). When the coating thickness increases after a certain critical value, the time to failure begins to decrease. The experimental procedure examined a three-layer CoCrAlY/ZrO_2 coating. Advances in creep life have also been addressed by improving coating processes. Bose and DeMasi-Marcin (1995) explained the benefits associated with different coating processes as related to blade creep. Several "generations" of coating processes rendered turbine aerofoils more creep resistant.

CHAPTER

4

4. Coating Processes

Industrial coating processes can be broadly classified into three groups depending upon the method they use to apply the coating. These are chemical vapour deposition (CVD), thermal spray (TS), and physical vapour deposition (PVD) (Hancock, 1986; Nicoll et al., 1986; NMAB, 1996; Singh, 1997). Each process can again be subclassified based on various schemes (for instance, the source of energy) used for the deposition of the coating. No manufacturing technique or industrial coating process that in any way offers an advantage or improvement to the gas turbine coating industry is ignored, and often a combination of coating processes are used in order to take advantage of the benefits of the various existent processes. Table 4-1 lists the classification of the major coating processes used in surface engineering.

Table 4-1: Coating Deposition Techniques.

Chemical Vapour Deposition (CVD)

- Pack Cementation
- Over Pack CVD
- CVD
- Low-Pressure CVD
- Plasma enhanced (or assisted) CVD (PECVD or PACVD)

Thermal Spray (TS)

- Flame Spraying
- Arc Spraying
- High Velocity Oxy-Fuel (HVOF)
- High Velocity Air Fuel (HVAF)
- Detonation gun (D gun)
- Atmosphere and Temperature Controlled Spraying (ATCS)
- Shrouded Plasma Spray (SPS) (Toriz et al., 1989)
- Air Plasma Spray (APS)
- Low-Pressure Plasma Spray (LPPS; also known as Vacuum Plasma Spray or VPS)
- High Pressure Plasma Spray (Andritschky et al., 1995)

Physical Vapour Deposition (PVD)

- Thermal Evaporation
  - Radio Frequency Plasma Assisted PVD (PAPVD)
  - Electron Beam PVD (EB-PVD)
  - Reactive Evaporation
  - Biased Activated Reactive Evaporation (BARE)
- Ion Plating
- Sputtering
- Sputter Ion Plating
- Reactive Sputtering

It is noteworthy that even though various schemes do exist to classify coating processes, different authors categorise them differently, the reason being that processes overlap different categories or may even use more than one method to deposit the coating. For example, the versatility of the PVD process led to the development of processes that involve chemical reactions (Teer, 1983; Boone, 1986), such as reactive evaporation and reactive sputtering, rendering the distinction between PVD and CVD processes more difficult. Process classification issues are discussed in more detail in the classic text by Bunshah (1982) or more recently in the report by NMAB (1996).

The coating processes listed previously produce diffusion (CVD) and overlay (PVD and TS) types of coating and the thickness of the coating can vary from angstroms to millimetres. Diffusion coatings adhere well to the substrate although they have limited compositional flexibility. In addition, their usefulness is strongly dependent on substrate/coating interaction as defined by diffusion laws. Overlay coatings are thicker, reasonably well bonded with a higher degree of resistance than diffusion coatings (Talboom et al., 1970). Also, they have a broader compositional flexibility although coating composition and manufacturing process render a higher unit cost.

Aside from the process, the challenges presented in applying gas turbine coatings are:

- To apply thin, uniform, dense, clean, and well bonded coatings;
- To achieve this on geometry parts which involve small radii and re-entrant angles;
- To achieve this without affecting blade cooling passages;
- To achieve this with a surface finish that is aerodynamically acceptable.

(Gill and Tucker, 1986)

Superalloy components used in today's aircraft gas turbines are among the most complex and costly alloys known to man. Therefore, to apply a coating which protects superalloys and simultaneously meets the above challenges is clearly also a complex, costly, and time-consuming process. In this harsh environment, a failure in one (either the coating or the substrate) quickly leads to a failure in the other (NMAB, 1996). In fact, there are some examples in the literature of coatings that actually reduced component life by leading to a more rapid deterioration of the component as compared to the uncoated component. Such reduced lives can for example be due to an unstable

coating (coating chemically incompatible with the substrate) leading to a lower melting point or lower creep resistance.

Of utmost importance when selecting a coating system is determining whether the coating actually protects the component against the environmental degradation mechanisms which negatively affect component life. Some of the most important failure modes include spallation, oxidation, corrosion, erosion, and creep; these were discussed in the section "TBC Failure".

Process issues are important because they affect economics and coating microstructure, hence affecting coating properties such as thermal conductivity, CTE, bonding, coating durability, and other important coating properties. Some of the features that vary with process include, but are not limited to deposition rate, properties of coating microstructure, substrate temperature during deposition, efficiency of coating complex shapes, and deposition species (atoms or droplets) (Bunshah, 1982). In some cases, during the production of coatings, in particular TBCs, the process or processes used may appear by some standards to be elaborate, complex, time consuming or expensive, but they are only adopted after careful consideration of rig test studies that show them to produce increased component lives. Notwithstanding this, all coating processes, without exception, suffer from shortcomings or limitations of one form or another. Gill and Tucker (1986) described the origin of these limitations as follows:

- Technical (e.g. the ability to deposit a particular type of coating);
- Economic (cost per item for a given output);
- Geographical and commercial (e.g. a rival company having exclusive rights on a particular process);
- Logistics of manufacture (e.g. whether or not it can be automated).

Once a coating system required for a particular application has been identified, several important engineering factors much be evaluated (NMAB, 1996):

1. Chemical compatibility. Coating and substrate usually have similar compositions; however, differences do exist and interaction between these may affect the properties of both the coating and the substrate (Cooper and Strang, 1986). An unstable coating can lead to premature failure by altering the mechanical properties of superalloys at elevated temperatures.

2. Coating process compatibility. Although a suitable coating composition may have been developed, this may not be compatible with the coating process due, for instance, to high temperatures or special pre-coating surface treatment.

3. Mechanical compatibility. In order to protect the component against failure modes the coating must remain adherent throughout the component's life. It follows, therefore, that important factors include the difference in the coefficient of thermal expansion (CTE) of the coating and the substrate and strain tolerance of the coating.

4. Component coatability. Some coating processes do not coat internal passages (known as line-of-sight processes) and others are done inside a chamber that

limits component size. In addition, coating some "difficult" areas such as edges, inside corners, and irregular part contours, must also be evaluated.

Other important engineering factors that need evaluation include contaminants in air and fuel (e.g. sodium, sulphur, and vanadium) and their impact, acceptable turbine emission levels, availability of coating databases, and coating standardisation for optimum performance for a specific application.

4.1. Chemical Vapour Deposition (CVD)

Chemical vapour deposition, as the name implies, involves a chemical reaction between the gaseous phase and the heated surface of the substrate in order usually to produce a thin coating at the substrate surface. The parts to be coated are mounted in a retort and placed in the CVD vacuum chamber (NMAB, 1996). A wide range of metallic and ceramic (oxides, carbides, nitrides) coatings can be produced by this technique at a rate of 5-10 μm/hour (Singh, 1997). Nevertheless, a deposition rate of 100 μm/hour has recently been reported by Chevillard et al. (1997) although around 55 μm/hour was measured in the experimental procedure. In addition to metallic and ceramic coatings, semiconductors, alloys, and refractory compounds can also be deposited by this process (Bunshah, 1982). According to the works of Duret and Pichoir (1983) and Singh (1997) the CVD reaction takes place frequently between temperatures of 500 and 1100°C. CVD coatings are used in semiconductors and optical films, or in industries for decorative purposes and in the area of corrosion (e.g. Ta) and wear resistance (e.g. TiC) in aircraft engines (Duret and Pichoir, 1983). In addition, the CVD process is also a forming technique whereby complex-shaped components can be obtained in materials difficult to machine by conventional processes.

A well established CVD technique which has been widely used for nearly fifty years to apply diffusion coatings to aircraft hot section components (superalloys) is known as pack cementation. CVD and pack cementation processes are discussed further elsewhere (Blocher, 1982; Duret and Pichoir, 1983; Bettridge and Ubank, 1986; Mévrel et al., 1986; Restall and Wood, 1986; Wood and Goldman, 1987; NMAB, 1996; Chevillard et al., 1997).

As with all processes there are some advantages and disadvantages and/or limitations which can be categorised as follows (Bunshah, 1982; Duret and Pichoir, 1983; NMAB, 1996; Wadley and Groves, 1996; Singh, 1997; Wood and Goldman, 1987):

Advantages

- High throwing power (i.e. not line-of-sight);
- Possibility to form very thin layers on shapes with complex geometry;
- Good adhesion to the substrate;
- Good compositional flexibility;
- High quality deposits;
- PECVD allows the growth of columnar morphologies (Chevillard et al., 1997).

Disadvantages

- The steps to form a deposit occur simultaneously and cannot be independently controlled preventing the control of structure properties and deposition rate (Bunshah, 1982, p85);
- Production of chemical wastes leading to recycling/disposal problems;
- Low deposition rate;
- Requires high temperatures;
- Heating of the substrate itself sometimes difficult;
- Difficult to accommodate large components.

From the foregoing, it is evident that the CVD coating process, although with some applicability to the aircraft engine industry (diffusion coatings), is not currently capable of depositing overlay TBCs, although work is underway on the PECVD process (Chevillard et al., 1997) which yields a columnar microstructure. In order to deposit thick thermal insulating layers two processes are currently considered the most popular, namely plasma spray and physical vapour deposition processes (Goward, 1974; NMAB, 1996; Schulz et al., 1997a).

4.2. Plasma Spray (PS)

Plasma spraying is the most widely used thermal spray technique for depositing overlay coatings onto gas-turbine components (NMAB, 1996). PS is a "line-of-sight" process in which raw powder (ceramic or metal, for instance) is fed into a high-temperature, high-velocity arc plasma by which the powder particles are almost instantaneously melted and accelerated towards the substrate (Goward, 1974; Rhys-Jones and Toriz, 1989; Jordan, 1994; Schmitt-Thomas et al., 1995). A schematic view of plasma spray equipment is shown in Figure 4-1.

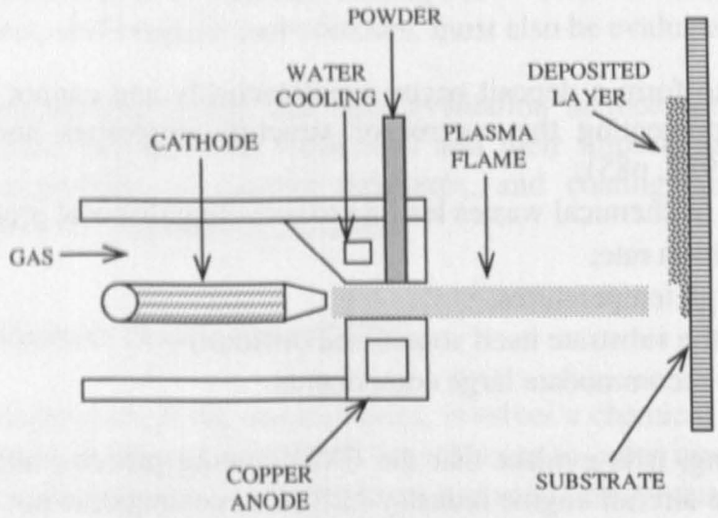

Figure 4-1: Schematic view of plasma spray equipment (Source: Derived from Gill and Tucker, 1986 and Schmitt-Thomas et al., 1995).

Prior to deposition, the substrate is usually degreased and grit blasted to improve adherence of the bond coat (Liebert et al., 1976; Gill and Tucker, 1986; Jordan, 1994). As can be seen in Figure 4-1, the growth of the coating is achieved by the building up of the molten droplets in a direction parallel to the substrate surface (Wood and Goldman, 1987). The inert plasma gas is generally argon with a few percent of hydrogen to minimise surface oxide formation (Goward, 1974; NMAB, 1996). Very high temperatures are achieved, in the order of 15,000°C, for the typical torch operating at 40 kW. The powder particle size varies from about 10 to 100 microns in diameter (Liebert et al., 1976) while the particle velocity can range from 100 to several hundred metres per second depending on spray parameters and the ambient atmosphere (NMAB, 1996). Due to the fact that the deposition species are droplets, not atoms, and also that some of the droplets are not melted completely by the plasma flame, the PS process produces an inhomogeneous microstructure containing defects; not only unmelted particles but also oxide layers and voids (Singh, 1997). These factors render a rough surface finish (around 10 microns, Liebert et al., 1976; Nicholls et al., 1997b) which affects blade aerodynamics. It follows, therefore, that PS coatings usually necessitate a post-process treatment to bring the surface roughness to within acceptable limits (Stabe and Liebert, 1975).

Air plasma spray (APS) TBCs have been employed since the early 1960s as thermal barriers on combustors and afterburners in aircraft gas turbines to reduce metal temperature and thermal fatigue cracking. Compositional control by this process is good since at the typical temperatures of the plasma gas, virtually all elements of practical importance can be incorporated in the pre-alloyed powder and will be easily deposited in the coating.

PS yttria-stabilised-zirconia coatings usually contain a high level of porosity and microcracking (between 10 to 15% according to Jordan, 1994) which are thought to increase the ceramic strain tolerance (Meier et al., 1991). However, Bunshah (1982) argued that the main disadvantage of the droplet transfer process is the porosity in the

final deposit, which affects the properties of the coating. In addition, this porosity allows the penetration of molten sodium particles, which can lead to coating failure.

Relative to EB-PVD process, PS offers a significant advantage in terms of compositional flexibility because the vapour pressures of the coating elements are not a concern. Any material that can be produced as a powder of appropriate size fraction can be sprayed through the plasma gun, although variations in the melting temperature of the starting powder may require modifications to gun design for optimum particle melting (Wood and Goldman, 1987).

4.2.1. Low-Pressure Plasma Spray (LPPS)

A typical PS coating takes place under atmospheric conditions (air plasma spray, APS) but a further development of this process has increased adhesion strength to very high values by carrying out the spray in a reduced-pressure inert gas chamber (Schmitt-Thomas et al., 1995; NMAB, 1996). According to the NMAB report (1996) this reduced pressure spray (argon, between 50 to 200 mbar but typically 100 mbar), known as low-pressure plasma spray (LPPS), was developed in the early 1970s by Muehlberger; however, it was only in the mid-1980s that it gained widespread commercial use for high-performance applications. The introduction of the LPPS process was driven in the late 1980s mainly by two reasons. Firstly, due to the unsatisfactory protection provided by APS to protect MCrAlY bond coats applied to highly thermally loaded parts like stationary vane platforms and vane aerofoil components in the turbine (Leverant, 1996; Schulz et al., 1997a). Secondly, by the need to protect these components against oxidation and to extend their lives (Rigney, et al., 1995). The LPPS process possesses a highly compositional flexibility, a very high deposition rate, as characteristic of PS processes, a virtually oxide free, dense coating, with a better oxidation resistance than APS metallic coating (Meier et al., 1991; NMAB, 1996). Unfortunately, the major disadvantages of this process are equipment costs and a reduction in productivity due to the use of a partial vacuum chamber; for each chamber load, the vacuum chamber must be refilled with the reduced pressure inert gas, then spray coating is conducted, followed by cool down in vacuum and unloading (Gupta et al., 1995). Nevertheless, the manufacture of overlay metallic coatings by the LPPS process are currently favoured for more complex formulations, as indicated in a recent review by Goward (1998).

4.2.2. Plasma Spray Properties

Many published studies have focused on the influence of process parameters on coating properties. Important parameters such as spray parameters (e.g. gas plasma temperature) or powder variables, amongst others, have a crucial effect on the microstructure of the coating. As an example, depending on the powder production process, powder variables include chemical composition, particle size, density, shape and distribution, surface morphology and phase composition (Schmitt-Thomas et al., 1995). As can be seen in Figure 4-2, different process parameters can produce various degrees of melting, which may render differing values for thermal conductivity and erosion resistance, for instance.

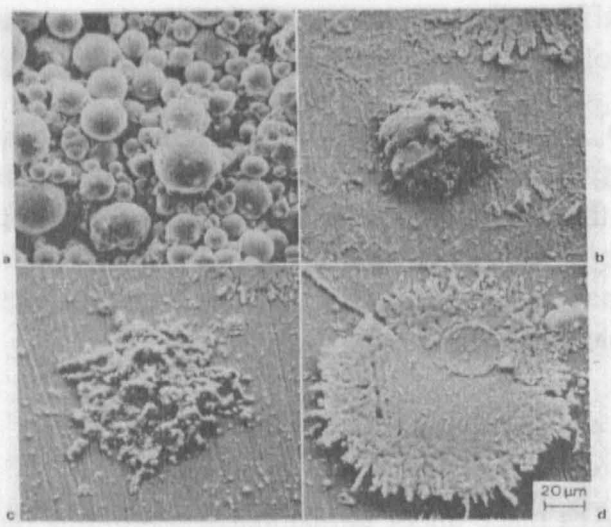

Figure 4-2: SEM micrograph of NiCoCrAlY powder particles (a) initial condition and (b)-(d) with various degrees of melting (Source: Gruner, 1984).

One of the most important properties in the design of a TBC system is thermal conductivity. Several investigators have evaluated thermal conductivity as a function of coating process in order to optimise coating parameters to achieve the lowest possible thermal conductivity (thus reducing even further metal temperature or increasing engine efficiency). Thermal conductivity issues were discussed previously, in the section on "TBC Properties".

The works of Lawson et al. (1996), Mogro-Campero et al. (1997), Taylor (1998), and An et al. (1999) evaluated and measured thermal conductivity for one or more of the three major coating processes: CVD, PS and EB-PVD. In the AGARD (1997) meeting on "Thermal Barrier Coatings" several other researchers also studied and characterised thermal conductivity issues (Alpérine et al., Dorvaux, Nicholls et al. (1997b), Ravichandran et al., for example).

Slifka et al. (1998) have also recently measured thermal conductivity for a PS 8YSZ coating. The thermal conductivity of the coating was 0.62 W/m.K; this measurement has been shown to be temperature independent. Even though PS coatings have a low thermal conductivity value, the recent work by Trice et al. (1999) investigated the possibility of further reducing this value by the addition of a member of the zirconium phosphate or NZP family to the YSZ.

All of the above investigations were directed to determining the state of current coating processes with regard to thermal conductivity. They have shown that thermal conductivity values can be relatively low for a PS coating, between 0.5 to 2 W/m.K (this is close to the value for bulk ZrO_2 at 2.2 W/m.K) but typically between 0.7 and 1.0 W/m.K (Liebert and Stepka, 1979).

Another important characteristic of a TBC system is its erosion resistance. PS coatings have a low erosion resistance, which limit their application on critical components such as rotating turbines (Liebert and Stepka, 1976; Stecura, 1976; Rhys-Jones and Toriz, 1989; Tabakoff, 1989; Tabakoff et al., 1995; Walsh et al., 1995). Nicholls et al. (1997a) reviewed erosion damage to PS and PVD coatings, their work being concurrent with

previous works. Using a high velocity gun rig at Cranfield University, EB-PVD TBCs provided a tenfold erosion resistance improvement over PS TBCs. A separate section on "Erosion" under "TBC Properties" discusses this property in a more detailed way.

Still another characteristic of PS processes is the tendency to build up coating material at the opening of cooling holes, used in most high-pressure turbine aerofoils in advanced aircraft engines (Meitner, 1978; Parks et al., 1997; Schulz et al., 1997a). This build-up of the molten particles, which can be a few tens of micrometres in diameter, considerably reduces cooling effectiveness. Laser drilling of holes to open them to within reasonable limits, in addition to filling holes with wires during spraying or over sizing holes have been considered but none have proven to be acceptable (Rigney et al., 1995).

As far as cost is concerned, studies have shown PS equipment to be very competitive since it requires only a plasma gun and a robot arm as opposed to e-beams and vacuum chambers as in the EB-PVD process (Goward, 1974; Brown, 1996). Furthermore, it can accommodate large components such as aircraft combustion chambers and afterburners or modern large power generation machines (Fauchais et al., 1997).

4.2.3. Advantages and Limitations

From the foregoing, it can be seen that the advantages of the plasma spray process can be summarised as follows:

- Flexible coating composition - virtually all elements can be deposited;
- Produces homogeneous coatings which do not change in composition with thickness (length of deposition time);
- Ability to achieve high deposition rates (>4 kg/hr);
- Very low thermal conductivity;
- Allows the coating of large components since it does not use vacuum chambers;
- Lower cost than EB-PVD because it only requires a plasma gun and robot arm rather than expensive e-beams and vacuum chambers;
- Ability to process materials in virtually any environment (e.g. air, low-pressure, high-pressure, under water).

while the drawbacks include:

- Line-of-sight process, i.e. internal passages cannot be coated;
- Droplet deposits affect the properties;
- Rough surface finish (around 10 microns) which has a detrimental effect on the aerodynamics of the component especially if it is an aerofoil section;
- Poor surface finish retention (erosion is an important degradation mechanism);
- Various coating defects including unmelted particles, oxide layers and voids;
- Significant interference with blade cooling holes.

(Goward, 1974; Meier et al., 1991a; Brown, 1996; NMAB, 1996; Parks et al., 1997; Jaslier and Alpérine, 1997)

4.2.4. Conclusion

Goward (1974) argued that plasma spraying could prove to be an important near term production method and this was demonstrated by innumerable studies (Liebert and Stepka, 1976 and 1979; Stecura, 1976; Levine and Clark, 1977; Gladden and Liebert, 1980; Miller et al., 1993). However, he also envisaged this process to have long-term limitations with regard to good coating thickness control and optimum coating structure. In the last two decades many published studies reported a growing interest in a more strain compliant process which can produce a columnar structure thus preventing the build up of long range stresses. This is achieved by evaporating the material to be deposited in an atomistic manner involving the nucleation and growth of the coating from a vapour phase. Physical vapour deposition processes will be discussed next with particular emphasis on the "revolutionary" electron beam PVD process (EB-PVD).

4.3. Physical Vapour Deposition (PVD)

According to Teer (1983) the term "physical vapour deposition" was first described by Auwarter in 1961 (US patent 2,920,002). It was originally intended to describe the deposition of metals by the transport of vapour (atoms) in vacuum, without involving a chemical reaction. However, as described previously, advances in the PVD process led to it being more versatile involving, for the deposition of some compounds, a chemical reaction, such as reactive evaporation and reactive sputtering (Teer, 1983; Boone, 1986). The coating forms as a result of the atomistic processes involved in the nucleation and growth of the coating from the vapour phase. It is evident, then, that one of the features of the PVD process is that it is an atomistic process as opposed to PS processes, which involve the deposition of molten droplets onto the substrate.

Notwithstanding the fact that PVD processes have only recently (in the last few decades) been the aim of major studies, the process is not new. Historically the first thin films were probably prepared in 1852 by Faraday by exploding wires in vacuum (Bunshah, 1982).

PVD technology consists of three techniques: evaporation, ion plating and sputtering (Bunshah, 1982). It is a very versatile process and virtually any metal, ceramic, or compounds can be deposited. The deposition rates vary considerably with process. Sputtering has one of the lowest deposition rates (a few nanometres per minute) while at the other end of the scale depositions of 150 $\mu m/min^{-1}$ or more (Bunshah, 1974; Shaw et al., 1997) have been achieved, mainly since the introduction of electron beam sources. Sputtering is a popular and versatile process for depositing thin films (typically up to 1 μm thick). However, typical TBCs used in turbine-powered aircraft are between 150 and 300 μm thick and, therefore, only by using electron beam sources is it possible to deposit these layers effectively and economically. Sputtering is not attractive economically when a thickness greater than 25 μm is involved (Bunshah, 1974). Today, the electron beam evaporation process is the most popular coating process for depositing TBCs onto the turbine section of the engine.

A major disadvantage of PS and PVD relative to CVD coating is that they are both line-of-sight, though each has its strengths and weaknesses. With the complex shapes common in turbine blade and vane designs, this limitation inevitable causes problems with coating thickness control due to "shadowing" (Wood and Goldman, 1987). On the other hand, unlike the CVD process, PVD processes are clean and do not produce chemical wastes (Singh, 1997).

In PVD processes a very important consideration is that the steps in the formation of any deposit can be independently controlled with much greater degree of flexibility in controlling the structure and properties and deposition rate (Bunshah, 1982).

EB-PVD is believed to be the most promising coating process, not only for non-critical applications as the alternative PS, but also to the most demanding rotating aerofoil sections, due to the improved mechanical and physical properties as compared to plasma spraying.

CHAPTER

5

5. Electron Beam-Physical Vapour Deposition (EB-PVD)

5.1. Introduction

Today, the electron beam evaporation process is the most popular coating process for critical applications, typically on rotating turbine blades. Many published studies indicate that EB-PVD is the only cost-effective technique that can meet the turbine industry requirements for the most demanding of stationary and rotating components (Meier et al., 1991; Wolfe et al., 1997; Stiger et al., 1999). Schulz et al. (1997a) argued that only through uneconomical advanced cooling techniques or by the introduction of EB-PVD TBCs is it possible to maintain and increase turbine inlet temperature.

Process issues are important because they affect not only economics but also coating mechanical and physical properties. Considerable enhanced performance of current TBCs is possible by process development (i.e. control of process parameters). Coating processes will enable a higher degree of control in the future in order to process the materials required to meet these demands.

In a typical EB-PVD system two contradictory deposition process objectives must be met: reproducibility and stability, on the one hand, and process variability, i.e. flexible process variation from sample to sample, on the other (Demaray et al., 1982). The EB-PVD is a highly automated process consisting of a vacuum chamber, an electron gun (EB-gun), a substrate jigging for holding the components to coat, and a source with the evaporator material. The electron beam is focused onto the surface of the material to be evaporated (usually a solid ingot), the material melts and then evaporates in a vapour of atomic proportions. The atoms deposit onto the substrate thereby growing the coating.

The next sections discuss the EB-PVD process in some detail. Firstly, the EB-PVD is characterised with particular attention to the parts that make up the equipment, the steps needed to achieve a coating and the typical applications where EB-PVD is being used. Secondly, a description of EB-PVD TBCs is given by describing the microstructure that can be achieved with this process and its properties especially those related to TBCs on hot section aircraft components. Thirdly, process development issues are identified, and typical characteristics of EB evaporators are discussed from what is reported in the literature. Lastly, a compilation of the advantages and drawbacks or limitations of the process are listed.

5.2. Deposition of EB-PVD Coatings

The deposition of a thermal barrier coating involves the following process stages. Firstly, the component is coated with a bond coat; this can be via a CVD route (e.g. a platinum aluminide bond coat), plasma spraying (usually LPPS), EB-PVD, or electroplating to deposit an MCrAlY oxidation resistant overlay coating. One of the roles of the bond coat is to grow a surface alumina layer, which acts to chemically bond the YSZ TBC to the metallic substrate.

As stated before, the deposition of the EB-PVD coating does not significantly alter the surface roughness of the substrate, and therefore does not introduce an additional aerodynamic performance loss as observed for the rougher plasma sprayed counterpart (Morrell and Rickerby, 1997).

Once bond coated and surface finished, the components are introduced into the vacuum deposition chamber to be coated with usually ZrO_2-8%Y_2O_3 ceramic. Depending on the machine, it is possible to have an independent preheat chamber, an oversource heater, controls for rod feed and a multicomponent fixture for the simultaneous coating of parts. With the exception of the last feature, the others, whilst enabling a higher degree of reproducibility, increase unit cost. Figure 5-1 illustrates a schematic diagram of a commercial EB-PVD coater.

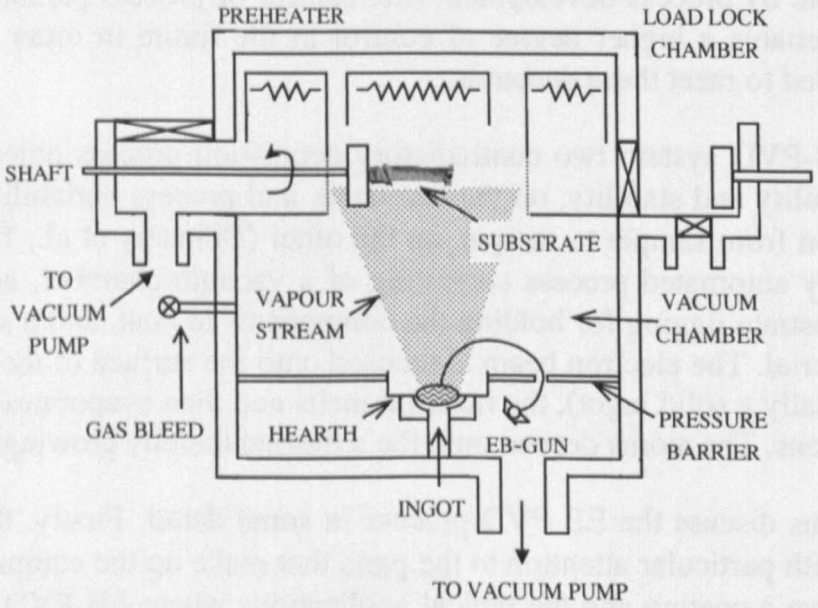

Figure 5-1: Schematic diagram of a commercial EB-PVD coater system (Source: Bunshah, 1982; Schiller et al., 1982; McMinn, 1987, amongst others)

To maximise the throughput of coated parts, most commercial coaters utilise a load lock system. The EB-PVD coating cycle to deposit the ceramic involves the following steps (Nicholls et al., 1998):

1. Load the components to be coated onto a manipulator, which allows typically two or three axis of planetary motion of the component to be coated.

2. Pump the load lock chamber to vacuum and load the components to be coated into the preheater. Commercial coaters are fitted with multiple load locks to ensure that the process is virtually continuous (Goward, 1974).

3. Heat the components to the deposition temperature, usually circa 1000°C, prior to loading in the main coater chamber.

4. Load into the main coater chamber and commence evaporation of the ceramic onto the component. The component to be coated is continuously rotated about its axis, while being moved, rotated or oscillated about a second axis. This ensures that all surfaces of the component are coated with ceramic. At the vacuum levels used within a commercial coater the vapour deposition of ceramic is effectively a line-of-sight process. Thus, this planetary motion is necessary to ensure all surfaces are adequately coated. Additional heating may be required to maintain the components being coated at the desired temperature.

   As can be seen in the detailed view of an EB-PVD hearth (Figure 5-2), a molten pool, usually a few millimetres deep depending on the EB-gun power, is formed. In the course of melting and evaporating in vacuum, the YSZ ceramic becomes dissociated, or oxygen deficient (Demaray et al., 1981; Tamarin et al., 1997). The loss of oxygen by zirconia dioxide is accompanied by a change of the melt pool from white to black. It follows, therefore, that during evaporation a small but controlled amount of gas is bled into the system to achieve a coating composition with the same properties as the source (ingot rod) (Bunshah, 1974). In addition, oxygen is also bled into the system prior to vaporisation in order to grow a thin, adherent alumina to which the ceramic adheres well, the former becoming effectively a bonding layer scale (Strangman, 1982; Ulion and Ruckle, 1983; Ulion and Anderson, 1993; Rickerby et al., 1995; Jaslier and Alpérine, 1997). The continuous alumina layer forms an oxygen barrier and stops further oxidation of the substrate (Demaray, 1987).

5. Once coated the component is removed through the preheater and load lock system and the procedure is repeated for other components via a second load lock. Systems with up to four load locks are commercially available to ensure a continual throughput of parts.

In theory, various arrangements of EB-guns exist in order to produce an electron beam but they all have a cathode, an anode, and usually a tungsten filament (Figure 5-2). Together the cathode, at high negative voltage and the anode, at earth potential provide an accelerating electric field for electrons emitted from the hot tungsten filament. EB-guns are typically classified according to the angle between the beam direction upon entry into the beam-deflecting field and the normal plane of the crucible (known as angle of turn). EB-guns with angles of deflection of 0°, 90°, 180° or 270° are common (Schiller et al., 1982). The most common and convenient have a magnetic deflection of

270°, which means that the filament is remote from vapour flux and, therefore, less prone to damage from "spits" of molten material from the melt pool (Teer, 1983). Moreover, EB-guns usually require lower pressures than the main coating chamber. This is achieved by keeping the gun in a different part of the coater separated from the main chamber by a pressure barrier (See Figure 5-1). Beam positioning and scanning of the source is achieved with a coil, which produces a magnetic field, by varying the current (See Figure 5-2). The magnets, which are strategically positioned in order for the beam of electrons to enter the melt, are responsible for the deflection or circular path of the beam. Beam power is increased by increasing the filament heating current, hence increasing the density of electrons emitted by the process (Baghurst, 1987).

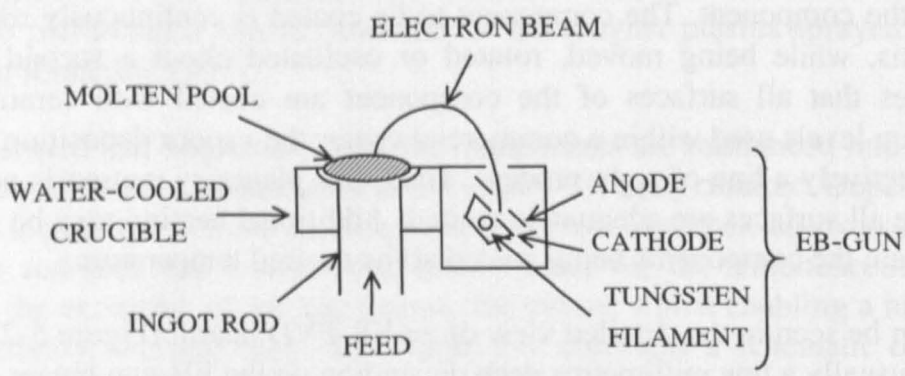

Figure 5-2: Detailed diagram of an EB-PVD hearth, source and EB-gun (Source: compiled by the author).

An EB-PVD system typically includes one or more shutters in order to protect certain areas from undesired vapour. One shutter is positioned just above the evaporation source and provision is made to move the shutter between two positions: the closed position over the source and the open position in which the source can see the substrate. This is important because it is unusual to increase power to the source from zero in full view of the substrate because the substrate would then receive a varying deposition rate. Thus, it is normal to use the shutter in the closed position during power increase, open at the desired power level in order to achieve the optimum deposition rate, and close again during power ramp-down.

An important interaction between the user and the evaporation process is the visual one. Even though the process may have been set up to run completely automatically, it is usual to inspect the source (or sources) and other contents at regular intervals through a window (sometimes using a mirror, Graper, 1971) that is protected by another shutter. If the melt could see the window the latter would become coated and useless. The importance of the window is best described by way of an example. Because the ceramic evaporates as a result of the high temperatures, and in order to maintain a constant source to substrate distance, the rod is usually pushed up from time to time. This is usually done manually although computerised systems with a melt view camera have been reported (Anklam, 1998). Maintaining a constant source to substrate distance, i.e. keeping the rod at the same height, contributes to a higher degree of process control since the electron beam erodes the rod in a uniform way (depending on the rod being rotated and the EB scanning pattern). Moreover, it avoids a change in the vapour plume

or preferential direction of evaporation by keeping the top of the rod flat. Neither the shutter above the source nor the shutter protecting the window are shown in the schematic of an EB-PVD coater (Figure 5-1).

5.3. Applications

PVD processes in general, and EB-PVD in particular, are very versatile processes enabling the deposition of virtually any metal, alloy or compound. The deposition rate ranges from a mere 1 Å per second (Shaw et al., 1997) to as much as 150 μm min^{-1} (Schiller et al., 1983; Wolfe et al., 1997). Deposition rates for rotated substrates of >25 μm min^{-1} have been reported (Boone, 1986). Both the possibility to deposit any material and high deposition rates, associated with other advantages, make the versatility of this process to appear unlimited. Coating technologies like EB-PVD are important in many industries, from microchips to aeroplane engines. Coatings alter the surface properties of materials, providing qualities needed for a particular application: not only thermal insulation but increased hardness, resistance to oxidation, electrical conductivity, and many others. Marynsky (1998) enumerated many of the coating types produced by EB-PVD as being corrosion-resistant, heat resistant, super hard, wear resistant and with special electrical, magnetic and chemical properties. Several other investigators pointed out some of the applications of the EB-PVD process.

Bunshah (1982) described PVD applications in general. The characteristic of the coatings produced by the PVD method were enumerated as follows:

- Decorative: toys, cosmetics, pens, pencils, eyeglass frames, home hardware;
- Optically functional: home mirrors, eyeglass lenses, binoculars, telescopes;
- Electrically functional: semiconductor devices, integrated circuits, memories, solar cells, magnetic tape;
- Mechanically functional: aircraft engine parts, tool bit hard coatings;
- Chemically functional: corrosion resistant fasteners, gas turbine engine blades and vanes, marine use equipment.

The same author also listed future areas for the application of the products of deposition technology. Similarly, Teer (1983) illustrated some examples of PVD application techniques. Coating industries include the electronics field, semiconductors, solar energy, optics and for decorative purposes. A wide range of applications are found in the area of tribology (wear-resistant coatings) and in corrosion protection.

Singh (1997 and 1998) explained in some detail some known successful applications of both the EB-PVD and ion-assisted EB-PVD processes. They included:

- Optics industries. Thin oxide films for optics, solar cells, i.e. solar thermal electricity (Smilgys, 1996), and sensors;
- Microelectronics. Multilayer oxide films in order to obtain good quality, superconducting thin films (from about 100 Å to 1 μm);
- Tools and die industry. Wear-resistant coating such as titanium carbide (TiC), titanium nitride (TiN), or others;

- Corrosion-resistant coatings. The flexibility of the EB-PVD process allows the deposition of tailor-made dense coatings for specific applications, which is especially useful when corrosion is a problem;
- Gas turbine industries. Whether for airborne, land-based or marine applications, the life of thermal insulating, oxidation and wear-resistant coatings made by the EB-PVD process and applied to components such as turbine blades, was reported to increase by a twofold factor when compared to PS coatings.

The work of Schiller et al. (1983) concentrated on high rate electron beam evaporation and described the coating of paper and plastic films as a very promising application, in addition to the already well-established technology for TBCs onto turbine components. Wood and Goldman (1987) described protective coatings applied for use at high temperature. They also reviewed coating processes and indicated current and future applications of TBCs in turbine engines. A very high potential payoff exists if TBCs can be used successfully on stationary and rotating turbine aerofoils especially if an increase in turbine entry temperature is preferred (as opposed to extending component life). In this manner, aerofoil surface temperature would be above the components' melting point in which case the durability of the ceramic coat is critical. In the same way, Mutasim and Brentnall (1997) suggested an identical approach to industrial gas-turbine applications. Again, EB-PVD is expected to play an important part in the development of TBCs in order to protect components from the harsh environment.

5.4. Microstructure of EB-PVD TBCs

The processing parameters of any PVD coating process affect the microstructure and properties of the ceramic coating (Jacobson, 1982). Substrate temperature, and chamber pressure are two of the most important parameters affecting the microstructure of PVD layers. The first systematic work to study the influence of process parameters on the structure of the resulting coatings appeared in 1969 when Movchan and Demchishin (M&D) observed that the condensation of EB-PVD coatings could be roughly classified intro three zones, each with its own characteristic structure and physical properties. These zones were based on the relationship or ratio (T/T_m) where T is the substrate temperature during evaporation and T_m is the coating material's melting point (in Kelvin) as shown in Figure 5-3. This model was subsequently improved by Thornton (1974 and 1977) to include a transition zone, Zone T, which is not conspicuous when depositing pure metals, as was the case in M&D's work (Figure 5-4). It should be noted that while M&D's model was derived from data collected over 10 years on evaporated films, that of Thornton was based on sputtered thin films (Shaw et al., 1997).

Bunshah (1974 and 1982) described in detail many published studies that have focused on understanding microstructure evolution as a function of process parameters. Other work aimed at developing the knowledge of varying coating morphology that might occur at various substrate temperatures has been described in detail elsewhere (Lardon et al., 1978; Teer and Delcea, 1978; Grovenor et al., 1984; Boone, 1986; Ohring, 1992; Smith, 1995).

The evolution of the structural morphology is as follows:

At low temperatures (Zone 1, $T/T_m < 0.3$) the atoms have limited mobility since their kinetic energy is low producing a columnar structure of tapered crystals with domed tops and weak open boundaries. As the substrate temperature increases, the surface mobility increases (Bunshah, 1982). In Zone 2 ($0.3 < T/T_m < 0.5$), the structure remains in the shape of columnar grains but with a finer structure, parallel boundaries and with a smooth appearance. These boundaries are stronger than in Zone 1 and contain no porosity. Above about 0.5 of the melting point of the coating material (Zone 3) the structure consists of equiaxed grains with a bright surface. Teer (1983) pointed out that chamber pressure also influences columnar growth. High gas pressures during deposition inhibit surface mobility and hence can be the cause of columnar structures, even at elevated temperatures. The same author also showed schematically the effect of temperature on coating structure as shown in Figure 5-5.

Schulz et al. (1997a) contended that although substrate rotation during deposition affects coating morphology it is not yet regarded as an essential contribution factor to the growth process. Nevertheless, coating microstructure can be widely varied by substrate rotation. In addition to the most important factors affecting coating microstructure (substrate temperature and chamber pressure) other parameters which influence columnar growth of EB-PVD TBCs are deposition rate, vapour incidence angle, and substrates' surface roughness. Similarly, Rigney et al. (1995) reported the effects of line-of-sight and substrate rotation on coating microstructure. Results with a stationary cylinder showed a difference in coating density on the backside, at the tangency of the vapour flux, and at head-on position of the cylinder. It follows, then, that in a line-of-sight process the open columnar structure is the result of shadowing effects (Boone et al., 1974).

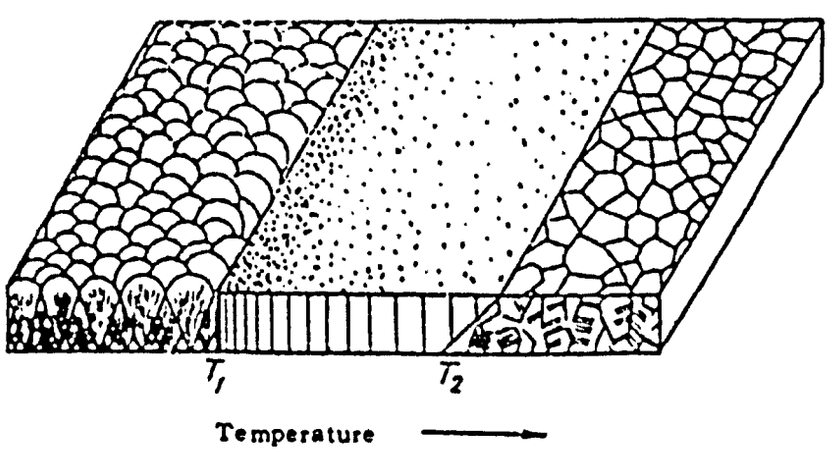

Figure 5-3: Diagram of structural zones of condensates at various substrate temperatures (Source: Movchan and Demchishin, 1969).

The structure of EB-PVD coatings is characterised by distinct stages of growth. In the early stages, the microcrystallites being formed occur at discrete nuclei, until they form a continuous film (Teer, 1983). Outward growth then proceeds and some regions of condensation will act as preferential nuclei formation from which, in many cases, columns of textured material will grow (Thornton, 1974 and 1977; Lawson et al., 1996). Growth will continue and, with time, surface shadowing becomes effective, leading to some columns to prevent the continuing formation of others (Teer, 1983; Unal et al., 1994). This is illustrated schematically in Figure 5-5a.

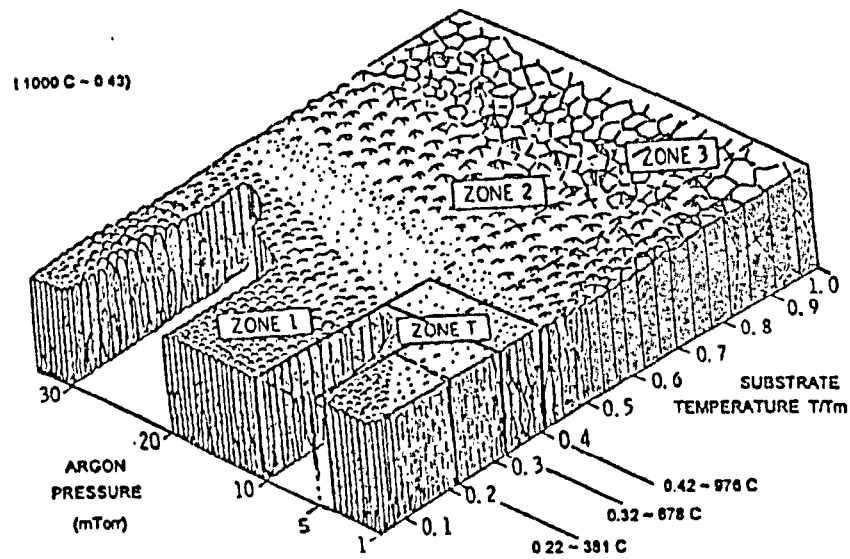

Figure 5-4: Structural zone models for coating growth for sputtered metal coatings (Source: Thornton, 1974).

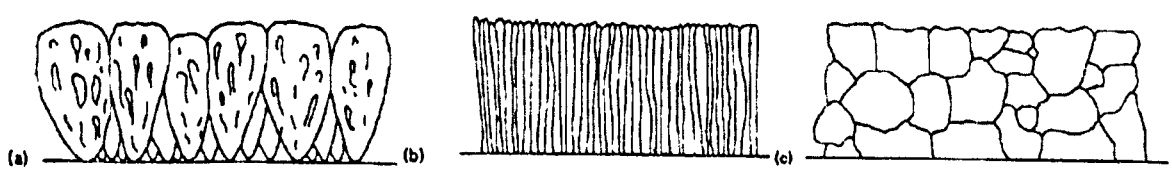

Figure 5-5: Effect of temperature on coating structure (a) Zone 1 (T/Tm < 0.3); (b) Zone 2 (0.3 < T/Tm < 0.5); (c) Zone 3 (T/Tm > 0.5) (Source: Teer, 1983).

Boone (1986), in a review of the EB-PVD process, described the steps in the PVD process unique to EB-PVD coatings of gas turbine components. These steps accounted for some of the misunderstanding and for some of the problems encountered in experiments on processing components. His work discussed heated substrates, rotated substrates, deposition of multi-element coatings and deposition rate. More recently, Sohn et al. (1994b) also determined the effects of processing parameters on the microstructure of 8YSZ deposited by a dual source EB-PVD coater. Their study observed differing coating structures by varying chamber temperature, substrate thickness and substrate rotation. In addition, the orientation of the columns was seen to vary when the vapour incidence angle was varied.

All of the above investigations were directed at further understanding coating microstructure and properties as a function of substrate temperature and chamber pressure, in addition to other coating parameters. Various coating properties, such as thermal conductivity, adhesion, and hardness are strongly dependent on substrate temperature and chamber pressure (Chow and Bunshah, 1971; Demaray et al., 1982; Nicholls et al., 1997b)

5.5. Properties of EB-PVD TBCs

Each coating process has its intrinsic characteristics. It follows, therefore, that not only each process produces different coating microstructures, but also the nature of the material transfer varies with process (EB-PVD is an atom by atom transfer process as compared to droplet transfer for PS), both factors affecting coating properties.

Many published studies have focussed on the influence of coating process and control of process parameters on the coating microstructure and mechanical and physical properties such as, but not limited to, thermal conductivity, CTE, thermal shock resistance, surface roughness, adhesive strength, Young's Modulus, and erosion rate (Durham et al., 1994).

One of the major characteristics of the EB-PVD process is that it generates a highly columnar ceramic microstructure which possesses a superior strain tolerance and cyclic thermal spallation life, as compared to earlier coating systems (Strangman, 1982). These columns are tightly bonded to the underlying substrate but essentially free to separate from adjacent columns as the substrate thermally expands relative to the ceramic (Meier and Gupta, 1994). It is this structure that makes the EB-PVD process simultaneously strain tolerant and so promising for demanding applications.

Nevertheless, the columnar microstructure which gives EB-PVD TBCs its high strain compliance and good erosion resistance leads to a relatively high thermal conductivity when compared to PS coatings (Meier et al., 1992; Strangman, 1996b; Alpérine et al., 1997; Lawson et al., 1996; Nicholls et al., 1997b). EB-PVD TBCs typically have a thermal conductivity which is about two times higher than the thermal conductivity of TBCs produced by PS. Several methods for reducing EB-PVD thermal conductivity have been reported in the literature (Strangman, 1996b; Nicholls et al., 1997b). The difference between the conductivity of EB-PVD and PS TBCs is attributed to the anisotropy of the EB-PVD ceramic as compared to the isotropic plasma structure (Meier et al., 1992).

Many published studies have focused on the properties of EB-PVD TBCs such as thermophysical properties, mechanical properties and cyclic strain life (Bunshah, 1982; Meier et al., 1992; Movchan et al., 1994; Bose and DeMasi-Marcin, 1995; Fritscher et al. 1997; Tamarin et al. 1997; Johnson et al. 1998; Wright, 1998).

Contrary to PS-deposited coatings, PVD coatings do not induce high loss of aerodynamic performance for they have a surface roughness of around one to two microns (Brown, 1996; Nicholls et al., 1997a; Morrell and Rickerby, 1997). Several investigators have measured and discussed erosion damage to PS and PVD coatings (Rhys-Jones and Toriz, 1989; Toriz et al., 1989; Tabakoff, 1995; Nicholls et al., 1997a). Their work concluded that EB-PVD TBCs provide a tenfold improvement in erosion resistance over PS TBCs.

Another important feature is the coating effect on hole closure as a result of the deposited material. Bettridge and Ubank (1986), Brown (1996), and Rigney et al. (1995) argued that the atom by atom nature of the EB-PVD process results in a rapidly,

smoothly tapered coating at the hole entrance. This is important because if the coating interferes with blade cooling holes then there is a penalty in cooling efficiency.

From the various mechanical and physical properties of TBCs, the thermal conductivity of EB-PVD coatings is probably the one which the scientific community is more interested in reducing to the value of PS-deposited coatings. Virtually all other properties of interest in high temperature materials have been improved with the introduction of the EB-PVD process. For example, improved thermal shock life means higher temperature capability than other processes, while smoother surface finish and better surface finish retention prevents the loss of aerodynamic efficiency caused by rough surfaces.

5.6. Advances in EB-PVD processing

The performance of EB-PVD TBCs is governed by many complex and interrelated factors. The mechanisms by which process parameters influence the quality of the coating are poorly understood. However, results of coating microstructure and process development are correlated. Many of the recent advancements in coating technology have been achieved through improved process control rather than coating composition development (Duvall, 1981; NMAB, 1996). Nevertheless, much of the processing details of EB-PVD are largely proprietary (NMAB, 1996). Process modelling, process monitoring, and real-time control have become more common in the last 20 years mainly from developments in coating equipment in the former Soviet Union, United States and Europe.

In order to qualify the EB-PVD process for a specific application, it is not uncommon for the use of empirical data to adjust the several operating conditions until a set of acceptable parameters are achieved. Nevertheless, work is being done to improve process control and the following paragraphs explain some of the work contributing to this aim.

Many published studies (Tin et al., 1996; Senf et al., 1996; Marinski, 1996; Lankin, 1996; Youchison, 1996; Anklam, 1998; Marynsky, 1998; Chang et al., 1998) concentrated quite correctly on process modelling, process control and/or real-time control of the deposition process. Simpson (1998) evaluated future EB-PVD requirements for naval applications by concentrating on equipment costs. The single most expensive factor in utilising EB-PVD technology is the capital equipment cost. Other costs such as coating process costs (gases, electricity, etc.), labour costs and other costs (cleaning, masking, etc.) are not necessarily higher than PS technology. In fact, PS technology requires extensive substrate preparation and post-processing treatments, contrary to most PVD processes, resulting in higher labour costs.

Lankin (1996) described a functional diagram that demonstrates the connection between input and output parameters. It showed which sensors as well as controllers are required for the EB-PVD process. Moreover, means to stabilise melt pool level, control coating thickness, and to design electron beam scan patterns was discussed. This work also pinpointed some of the tasks that will need further development in order to modernise EB-PVD equipment.

Hague et al. (1996) developed, tested and implemented an intelligent process control system that led to a reduced coating life variability. Major process parameters studied included chamber pressure, electron beam adjustments, ingot feed rate, melt pool level, electron beam current, part motion and preheat temperatures. While some of these parameters were under the control of the operator, others were in closed-loop control. Various sensors improved control of temperatures, coating thickness, and vapour flux. Anklam (1998) developed a closed-loop control to adjust ingot feed velocity to maintain constant pool height (pool height was measured by a low-angle camera view and image processor).

In a patent by Azad et al. (1997) a method was described for an EB-PVD equipment with two electron beams, one to melt and vaporise the ingot and the second beam superimposed across the ingot top surface in order to increase deposition rate of the melt pool. By controlling beam focus and melt pool stability, coating defects can be minimised (Goward, 1974).

An understanding of all process interactions is far from complete but initial models have been formulated. Process control aims at decreasing variability whilst increasing process flexibility is of utmost importance to produce coatings with enhanced performance. In conclusion, metallic or TBC coatings would significantly benefit from advances in process control. Further research is required to explore the process control of EB-PVD equipment.

5.7. EB Evaporators

Various EB evaporators with different apparatus have been built for the deposition of EB-PVD TBCs (Marynsky, 1998). EB-guns have also been the focus of parallel development to meet the requirements for EB systems (Senf et al., 1996; Wadley et al., 1996).

As stated before, EB-PVD deposition is produced in a vacuum chamber to promote ceramic evaporation and to minimise oxidation of the substrate (Meier et al., 1991). The quality of vacuum must, therefore, be controlled since the vapour flux being evaporated has atomic proportions. At the pressures used in commercial coaters, the EB-PVD process is a line-of-sight process thus interior surfaces are not coated. With the aim of tailoring coating profiles and as a result of the geometry of most components, it is necessary to rotate and translate the substrates during deposition in order to achieve the intended coating profile.

Figure 5-1 (Page 68) shows a schematic diagram of a commercial EB-PVD system. Depending on the machine, it is possible to have an independent preheat chamber, an oversource heater, load-lock, controls for rod feed and a multicomponent fixture for the simultaneous coating of parts. These features, whilst enabling a higher degree of reproducibility increase unit cost to varying degrees. The cost of this machine is, nowadays, described as "very large" (Boone, 1986) thus rendering unit costs very high. This is one of the major disadvantages of using EB-PVD. Equipment cost is described in detail elsewhere (Simpson, 1998).

Unit cost can be reduced by coating multiple components simultaneously, a solution which is possible with this process. In addition, it is possible to build a more versatile system with more than one source (usually two or three) (Sohn et al., 1994b; Movchan, 1996a). This contributes to a higher deposition rate and also reduces unit cost. In fact, EB-PVD equipment with a single source and single EB-gun are not used commercially because they do not have the necessary process flexibility.

A multiple source system usually allows each source to be evaporated either sequentially, thus producing multilayered coating, or simultaneously. When evaporating simultaneously from independent sources of different materials it is possible to produce an alloy coating (the material combines in the vapour cloud) or by varying the EB-gun power to produce a gradient coating. Lastly, simultaneous evaporation from independent sources of equal materials is also possible, this being a popular method to increase deposition rate. A system with multiple sources, whether for alloy deposition, gradient TBCs, or for increased deposition rate, is much more versatile than a single-source system. In addition, gradient TBCs are also possible with single source evaporators (Movchan, 1996b and 1998). Evaporation from single sources and/or multiple sources is discussed in more detail elsewhere (Bunshah, 1974 and 1982; Schiller et al., 1982; Schulz et al., 1997a; Schulz and Peters, 1998)

Singh (1997) reported the use of a six-gun, three-source general coater. The highest EB-PVD deposition rates are achieved with equipment like this. However, Bunshah (1982) noted quite correctly that multiple source evaporation is more complex than evaporation from single source systems since the evaporation rate from each source has to be monitored and controlled separately. In addition, the source to substrate distance would have to be significantly large (depending on the separation of the sources) to have complete blending of the vapour flux prior to deposition, which decreases deposition rate (See Figure 5-6). Notwithstanding this, evaporation from multiple sources can be made simpler if the sources are of equal material and the substrate(s) are rotated and translated. This configuration is of considerable interest to the coating industry.

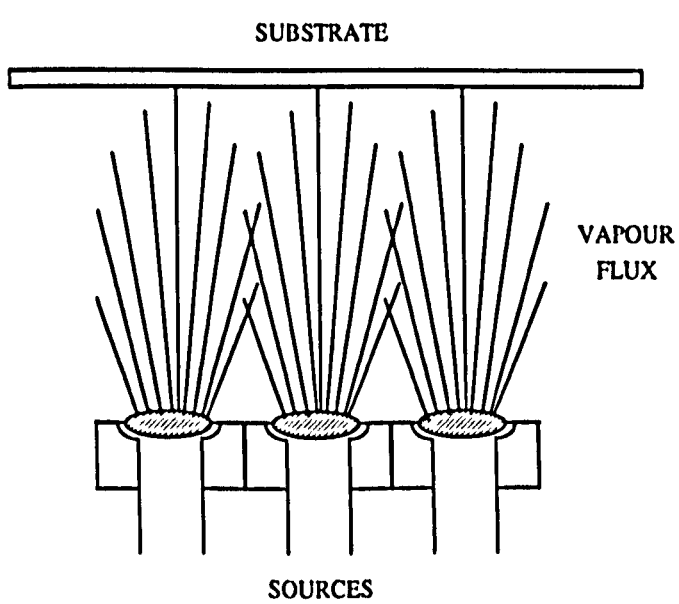

Figure 5-6: Schematic of a three-source evaporation.

Several works outlined the features of EB-PVD equipment and typical process conditions during experimental procedures (Schiller et al., 1983; Movchan, 1996a; Shaw et al., 1997; Singh, 1997; Wolfe et al., 1997; Reinhold et al., 1999). Movchan (1996a) discussed in detail the importance of lowering EB equipment cost in order for universities and scientific centres to participate in the development of the EB-PVD technology.

Teer (1983) reviewed and discussed other issues of vacuum evaporation such as substrate jigging, evaporation sources, electron beam gun sources, deposition rate, thickness control, quality of pressure, and preferred orientation.

To sum up, some of the characteristics of evaporators which should be considered when deciding the most appropriate equipment for a particular application are as follows:

- Chamber size (the bigger the chamber the more parts can be coated concurrently);
- Number of EB-guns and power (for substrate heating and evaporation);
- EB-guns with independent programmable scan pattern;
- Power source power and working voltage;
- Independent preheat chamber;
- Load-Lock;
- Automatic feed mechanism in case of continuous feed ingot;
- Rotation mechanisms (vertical/horizontal) and/or translation;
- Number of hearths/sources;
- Multicomponent fixture for the simultaneous coating of parts.

While the simpler evaporator may consist of a small coating chamber with a single source, single EB-gun and a simple stationary holder for substrate jigging, only the most advanced EB-PVD equipment will have, for example, a 1.6 m^3 chamber, two load locks, six guns, 3 sources, a power source power of 250 kW and working voltage between 20-25 kV measuring 9 m in length as described by Movchan (1996a and 1996b).

Sensors are also in widespread use to control many of the parameters during deposition (Lankin, 1996). The use of sensors to control substrate temperature, thickness, and vapour flux has been reported (Hague et al., 1996). Also, a low-angle camera and image processor to measure pool height and adjust ingot feed velocity to maintain constant pool height, has also been developed (Anklam, 1998). Additional on-line control must be developed to help ensure the resultant mechanical and physical properties of the coating are within limits for the service requirements (NMAB, 1996).

Coating processes are changing and will continue to change to meet the increased demands of aircraft hot section components for fuel efficiency, cost and weight reductions. The more complex the system is the more likely for the equipment to meet the two main requirements of any evaporator: reproducibility and stability, on the one hand, and process variability, i.e. flexible process variation from sample to sample, on the other.

5.8. Advantages and Limitations

From the foregoing it can be seen that there are many advantages of the EB-PVD process over competitive processes such as APS or even LPPS. They are:

- Robust, highly reproducible process;
- Columnar structure with superior tolerance against thermal shock, erosion and cyclic fatigue;
- Flexible deposition rates (from a few angstroms per minute to >25 μm min^{-1} onto rotated substrates);
- Good metallurgical bonding to the substrate;
- Smoother surface finish and better surface finish retention than the PS counterpart;
- Limited cooling holes plugging problems;
- Multiple (small) parts can be coated simultaneously;
- Elimination of pollutants and effluents which is a very important ecological factor.

However, there are also limitations and disadvantages by using this process, as follows:

- Capital intensive (the cost of EB-guns increases geometrically as the power increases arithmetically) rendering a high unit cost;
- Line-of-sight process; as with PS internal surfaces cannot be coated;
- Relatively high thermal conductivity of TBCs compared to PS TBCs;
- Use of vacuum (as with LPPS) which renders a decrease in productivity as well as adding to equipment cost.

5.9. Conclusion

From the aforementioned it is apparent that the performance of a thermal barrier coated aerofoil section is critically dependent on, for instance, the ceramic coating thickness, structure morphology and surface roughness of the zirconia thermal barrier layer. A TBC system with enhanced performance is likely to come about from further advances in process control.

EB-PVD is the only cost-effective technique that can meet the turbine industry requirements for the most demanding of stationary and rotating components (Meier et al., 1991; Wolfe et al., 1997; Stiger et al., 1999). In the future coating processes will enable a higher degree of control in order to process the materials required to meet these demands.

The typical ceramic layer thickness profile is around 200 μm on the leading edge and between 100 and 150 μm on both the pressure and suction surfaces, although a much thinner coating is required on the trailing edge for good aerodynamic performance. Thus, the ability to predict coating thickness, morphology, inclination and surface roughness both around a component, or from component to component is key to ensuring the reproducible manufacture of TBC coated hardware.

To sum up, reproducibility and flexibility (the two objectives of the EB-PVD system) although contradictory are being met by advances in computer control, in an intensive process control environment.

The remainder of this study addresses the development of a computer based process model, capable of predicting the thickness, and inclination of the TBC microstructure on substrates with complex geometry, typical of aerofoil components.

CHAPTER

6

6. Modelling Vacuum Evaporation

6.1. Controlling Thickness Distribution

For many applications of coatings it is often undesirable to have a uniform thickness distribution around a component. Instead, it is usually required that the deposit should follow a specified thickness distribution over the substrate surface. Thermal barrier coatings on aerofoil components are a particular example where a uniform coating distribution around the blade or vane would degrade aerodynamic performance. Other applications may require more uniform coatings, on substrates with either a simple or complex geometry. Catalyst support is an example of this, where it is required to produce uniform coatings down a geometry with re-entrant holes, while limiting the coating build up on component connection hardware.

Both of these applications, indicative of widely different markets, have the same basic underlying problem. That is to say, the design of tooling and masks for use in a PVD coating system capable of limiting the undesirable deposition of coatings on parts of a component. Currently, such masks are designed ad-hoc, on a trial and error basis. From the knowledge of the thickness distributions as a function of deposition parameters (evaporation rate and distribution, substrate's position, for example) it should be possible to develop computer based models capable of predicting mask performance, once the basic deposition behaviour, as modified by non contact masks, has been established.

In addition to the two applications cited above, other coating industries could benefit from tailoring the structure of PVD-deposited coatings such as cutting tools, optical surfaces, and other applications of vacuum deposited coatings.

When depositing a TBC system two conflicting properties must be met: firstly, the layer must be sufficiently thick for adequate thermal protection (temperature drop across the ceramic layer increases with increasing coating thickness), and secondly, not too thick a layer that would degrade aerodynamic performance. A typical ceramic layer thickness profile for a turbine blade is around 200 μm on the leading edge and between 100 to 150 μm on both the pressure and suction surfaces, although it is desirable to deposit a much thinner coating on the trailing edge of these components for good aerodynamic performance. Thus, the ability to predict coating thickness distribution and morphology, both around a component and from component to component is key to ensuring the reproducible manufacture of TBC coated hardware.

Moreover, other properties such as inclination of the ceramic columns and surface roughness are closely linked to the durability and performance of a TBC system. The more inclined the columns are to the aerofoil surface the less likely it is for them to remain intact throughout the life of the turbine. It is desirable, therefore, to grow ceramic columns perpendicular to the aerofoil surface in order for the columns to withstand erosion and foreign object damage.

From the foregoing, it follows that modelling (i.e. predicting) coating morphology and thickness distribution would significantly enhance TBC performance and increase TBC durability. TBCs with improved properties would, as previously mentioned, contribute to engines using less fuel, making less noise, producing less harmful emissions and delivering greater performance. The next paragraphs discuss the theory and mechanisms of evaporation and some of the initial models that have been proposed to study thickness distribution.

6.2. Theory of Evaporation and Deposition

In the scientific literature, the deposition of thin films by Joule heating was proposed as early as 1887, when Nahrwold used joule heating of platinum in vacuum to deposit thin metal films (Bunshah, 1982).

The transition of solids or liquids into the gaseous state can be explained with the laws of thermodynamics, based in an understanding of the evaporation rates, source reactions, changes in composition during evaporation, and stability of compounds. Historically, well-known scientists such as Hertz, Knudsen and Langnuir were the first researchers to investigate the behaviour of such vapour streams. A detailed explanation of the thermodynamic and kinetic bases of evaporation processes is given by Knudsen (1934), Kennard (1938), and Holland (1966). More recently, the same subject was covered in an excellent review by Glang (1970) and in other chapters of the classic book by Maissel and Glang (1970).

The first systematic investigation of evaporation rates was conducted by Hertz in 1882. He measured the evaporation rate of mercury in high vacuum and found that the evaporation rate, based on the equilibrium vapour pressure is given by:

$$\frac{dN_e}{A_e dt} = \sqrt{2\pi\, mkT}\,(p^* - p) \qquad [1]$$

where $\frac{dN_e}{dt}$ is the rate of evaporation of a number of molecules from a surface area A_e; m is the molecular weight, k is the Boltzmann's constant, T is the temperature in °K, and $(p^* - p)$ is the difference between the equilibrium pressure of mercury at the surface temperature of the reservoir and the hydrostatic pressure acting on that surface.

Furthermore, Knudsen argued that some of the molecules impinging on the surface might be reflected back into the gas phase rather than incorporated into the liquid. There is thus a certain fraction $(1 - \alpha_v)$ of vapour molecules which contribute to the evaporant

pressure but not to the net molecular flux from the condensed phase into the vapour phase. Accordingly, he suggested the evaporation coefficient α_v, defined as the ratio of the real evaporation rate in vacuum to the theoretically possible value, as defined in equation [1]. This then results in the equation:

$$\frac{dN_e}{A_e dt} = \alpha_v \sqrt{2\pi\, mkT}\,(p^* - p) \qquad [2]$$

which is commonly referred to as the Hertz-Knudsen equation.

In addition, it is well established that the directionality of evaporation molecules in vacuum at low rates from a small area source leads to a thickness distribution on a flat surface which follows a well known cosine law (Bunshah, 1982; Teer, 1983). This law states that the mass per unit area deposited on an element of surface is equal to:

$$\frac{dM}{dA} = \frac{M_e}{\pi h^2}\cos^n\theta\cos\alpha \qquad [3]$$

where M_e is the total mass evaporated, θ is the angular displacement of the substrate relative to the normal to the source, n is a coefficient that defines the focus of the source, α is the inclination of the substrate to the line of vapour flux, measured normal to the substrate, and h is the source to substrate distance, as shown in Figure 6-1.

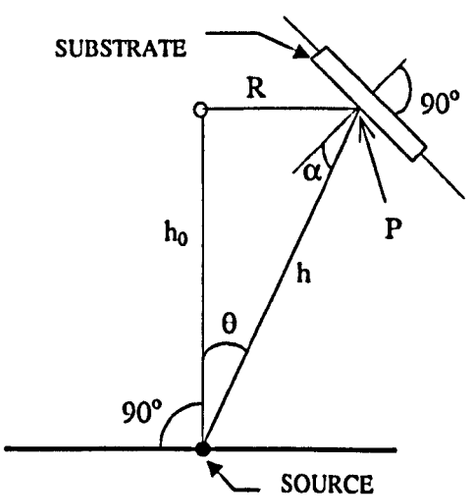

Figure 6-1: Schematic representation of geometry of evaporation.

However, this simple rule is characteristic only when the source behaves as a single-point evaporator, or in other words, when the vapour-emitting surface is a small area compared to the source-to-substrate distance. For the more general case, the thickness deposited is related to the rate of deposition from all sources and the time of the deposition. Thus, at P in Figure 6-1,

$$\text{thickness} \propto \frac{1}{h^2}$$

and $$\text{thickness} \propto \cos^n \theta$$

and $$\text{thickness} \propto \cos \alpha$$

From the foregoing, the thickness distribution of a thermally evaporated coating, deposited from an ideal point source evaporator follows an inverse square law governed by an equation of the form (Maisell and Glang, 1970; Vossen and Kern, 1978; Bunshah, 1982):

$$\frac{d}{d_0} = \frac{h_0^2}{h^2} \cos^n \theta \cos \alpha \qquad [4]$$

where d is the coating thickness at a distance h from the vapour source, d_o is the thickness directly over the vapour flux at a distance h_o from the source, and α, θ and n define the source to substrate geometry and the evaporation characteristics of the source.

In practice, a real evaporation source, typically a ceramic rod between 3 and 7 cm in diameter with the diametrical surface molten, can be envisaged as multiple point source evaporators, evaporating in parallel. Furthermore, during high rate deposition a virtual omni-directional source will be generated in the vapour cloud immediately above the source due to the localised high vapour pressure and atom-atom collisions within this vapour cloud. Thickness distribution is, therefore, affected by the virtual source, which appears to emanate from a position higher than the real source. Thus the deposition rate at any point on a substrate (component) surface will follow a general equation of the form:

$$\frac{d}{d_0} = \sum_{j=1}^{k} A(j) . \frac{h_{0_j}^2}{h_j^2} \cos^{n(j)} \theta_j . \cos \alpha_j \qquad [5]$$

where $\sum_{j=1}^{k} A(j) = 1$. Thus, the aggregate flux arriving at any point on a substrate surface reflects the summation of the flux, from an array of 3-dimensional point sources, which model the molten surface of the evaporant directly above this rod.

Values of α, θ, h and h_o are set by systems geometry, whereas $n(j)$ and $A(j)$ are dependent on the performance of the evaporation source. It is known that as the evaporation rate increases, $n(j)$ increases, i.e. the evaporation process is more focused the higher the deposition rate (Bunshah, 1982; Schiller et al., 1983). Equally $n(j)$ may vary with angular displacement around the source, i.e. the source may have an asymmetric deposition profile. Similarly, changes in operating conditions, for example chamber pressure, can modify both $n(j)$ and $A(j)$. Hence the performance of the source

depends on source geometry, deposition rate and the operating conditions within the coating chamber.

The rate of coating growth and direction of growth, at any point on a component surface, depends on integrating the complex vapour flux field from all sources, both virtual and real, onto an inclined surface element. However, the simple mathematical formula does not describe the real source where, for instance, the source is not a point source evaporator and may be asymmetrical due to electron beam asymmetry or magnetic field effects.

Bunshah (1982) and Schiller and co-workers (1982 and 1983) also stated that during high power (a characteristic of high rate evaporation), the electron beam impact area on the surface of the molten pool is not flat but forms an inward bulge into an approximate concave spherical segment on the heated area. This bulge becomes more pronounced the greater the evaporation rate. As the bulge grows inwards instability increases.

From Equation [4] the effect of both the angular displacement of the substrate relative to the normal to the source (0) and the inclination of the substrate to the line of vapour flux (α) on the variation in thickness distribution is evident. To start with, $\cos^n\theta$ (or $\cos\alpha$) has its minimum and maximum values at zero and one, respectively, or when 0 (or α) is 90 and zero degrees (0 and α are never greater than 90 as that would mean a substrate below the source or a point on the back of the substrate, respectively). Therefore, in theory, the maximum deposition is achieved when both the following conditions are met ($0=\alpha=0$) i.e. the substrate is directly above the source ($0=0$) and placed horizontally (not inclined to the line of vapour flux) ($\alpha=0$). For a given plane above the source the deposition drops gradually as the substrate moves away from the centreline of the vapour flux. In addition, for a given position in the half-space above the source the deposition drops gradually as the inclination of the substrate to the line of vapour flux increases (i.e. the flux arrives at a shallower angle relative to the substrate's surface). Figure 6-2 is a schematic of a typical deposition profile for a plane 20 cm above the source.

As stated before, the cosine law is only applicable in theory, for a small-area evaporator, and for low rate evaporation. In addition, even if the evaporation source behaves as a small area evaporator, there are a series of effects that are likely to change the vapour flux distribution (Schiller et al., 1982). Figure 6-3 illustrates the effects that cause the evaporator characteristics to deviate from a simple cosine distribution.

Notwithstanding the factors that affect the vapour flux distribution, various models have been proposed for calculating the deposit temperature and thickness distribution of PVD films (Chow and Bunshah, 1971; Nimmagadda and Bunshah, 1971; Musset, 1990; Bosch, 1993; Pereira, 1996). In addition to the factors already discussed, which may affect thickness distribution, it has been speculated that the gas pressure that leads to collisions between particles as in, for example, a high rate evaporation, is one of the most important factors which hinder further developments in this area. Therefore, the next section concentrates on the interactions of the residual gas, the electron beam and the vapour stream, and the collisions between particles during high rate deposition.

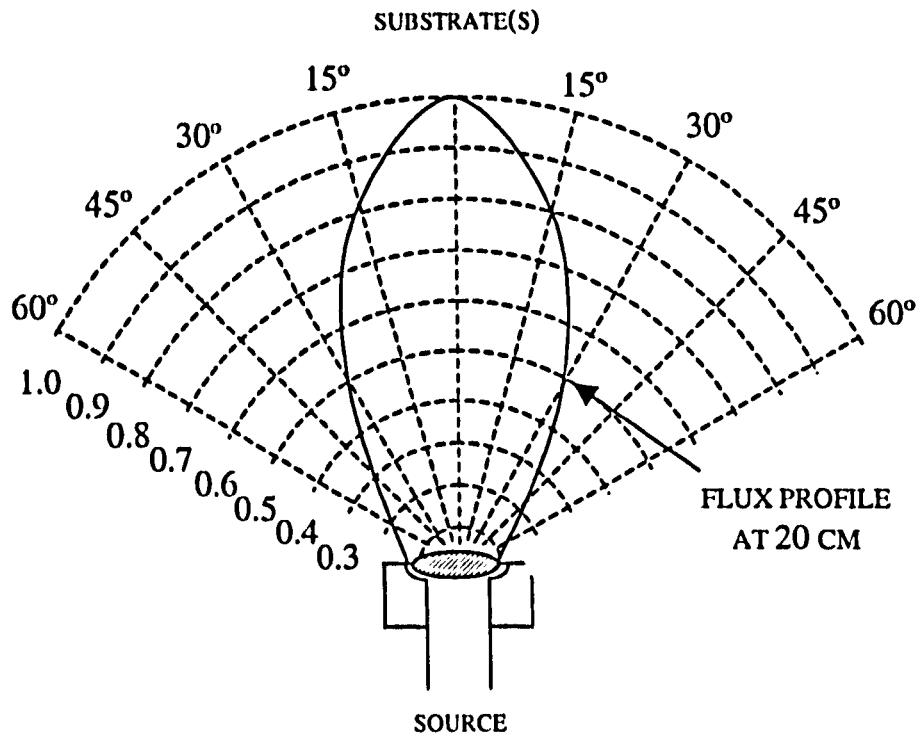

Figure 6-2: Deposition profile for a plane 20 cm above the source (Source: Bunshah, 1982).

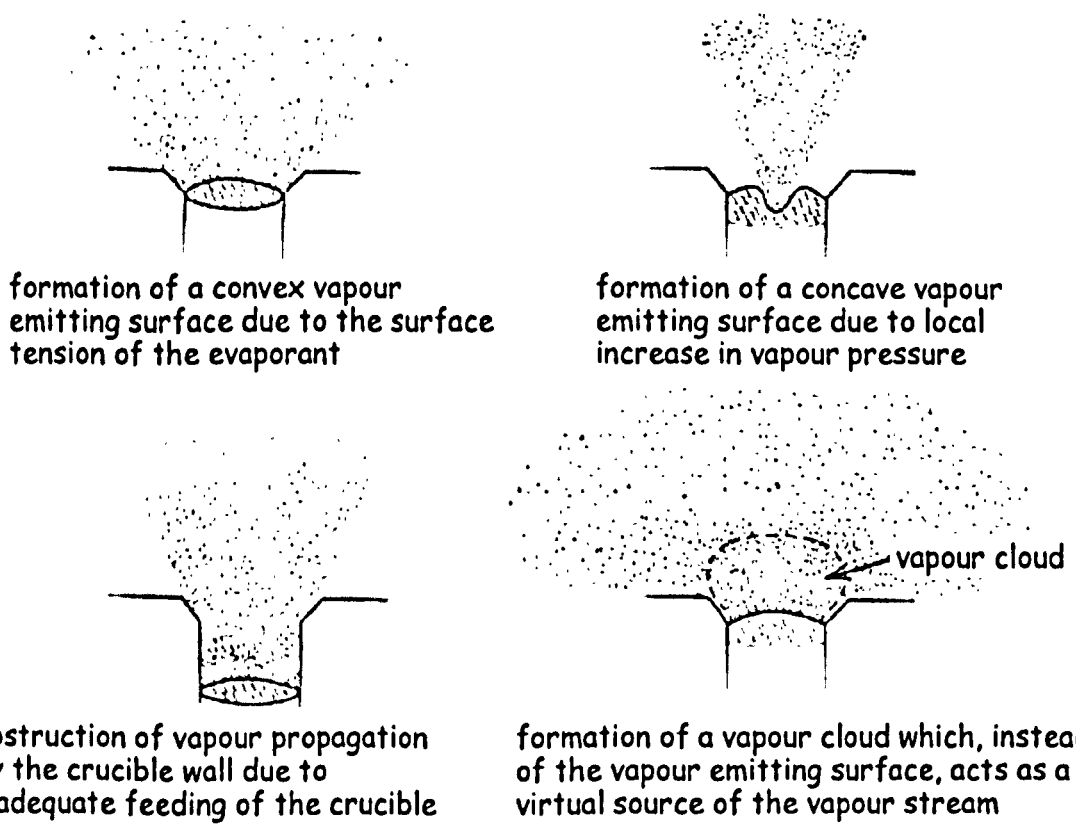

Figure 6-3: Effects of the source surfaces of actual small-area evaporators on the distribution of vapour stream density (Source: Schiller et al., 1982).

6.3. Evaluation of the Evaporation Parameter for the Cranfield Coater

Recently, Pereira (1996) developed a computer model to assist in the prediction of the thickness distribution of EB-PVD TBCs. The coating thickness for horizontal substrates coated at five heights (15, 16.88, 18.75, 20.6, and 22.5 cm) and distributed along and parallel to the centreline was measured. The thickness distribution showed an almost circular symmetrical contour plot for the two lowest heights considered (15 and 16.88 cm); at higher working heights, particularly for 20.6 and 22.5 cm above the source, the measured results indicated a slightly asymmetrical source. Asymmetric issues are discussed later in the chapter on the "Evaporation Model". Results from both the computer model and physical experiments were presented and discussed.

When evaporating from a 3.8 cm diameter rod, as was the case in the previous work, the n value was calculated to be 4.5. In other words, the differences between the predicted coating thickness and that measured for the Cranfield coating equipment were minimum for the n value just cited (in the modelling work the n value was varied from 1 to 9). Computer generated values of the coating thickness, using an ideal single point source, agreed reasonably well with the experimentally measured values for the Cranfield EB-PVD coater.

Even though the model and assumptions made appeared to be valid, further work is required in order to investigate the feasibility of predicting coating profile and column inclination by combining the evaporation and deposition effects. This current work used thus an n value of 4.5 for all calculations of coating thicknesses.

6.4. Degree of Vacuum

The mechanisms of evaporation and deposition are affected by the degree of vacuum. That is, both the deposition rate and thickness distribution may be affected by the amount of residual gas that collides with the vapour flux. Therefore, an adequate low pressure must be maintained in order to ensure that the gas particles in the chamber do not hinder or deflect the vapour flux from the intended trajectory.

Even though evaporation in a PVD process takes place in a vacuum chamber (usually at pressures lower than 10^{-3} Pa), two factors account for a deviation of the vapour stream from the cosine law, in addition to the residual gas in the chamber. Firstly, the vapour pressure above the vapour-emitting source is usually higher than 10^{-1} Pa (Schiller et al., 1982) or even as high as 400 Pa (Schiller et al., 1983). At these vapour pressures the effect of the interactions between electron beam and the vapour stream plays a substantial role and cannot, therefore, be neglected. The other factor inducing deviation of the vapour flux from the cosine law is the already described high rate deposition, whereby the high atom-atom collisions account for a deviation between theory and practice of evaporation (Bunshah, 1982; Teer, 1983).

The ideal situation is when the amount of gas is kept low enough so that the interactions or collisions between vapour particles and gas particles can be neglected. However, this situation is sometimes difficult or even impossible to achieve since it conflicts with high rate deposition. For instance, even if a high vacuum is achieved prior to deposition, it

has already been shown that a controlled amount of usually argon or oxygen is bled into the chamber in order to achieve a coating composition with the same properties as the source ingot. In addition, during high evaporation rate conditions a vapour cloud is formed just above the melt pool with a high particle density which contributes to a higher number of collisions between the vapour particles. Therefore, the interactions between the vapour particles cause the thickness distribution to deviate from the cosine law. High evaporation rates are linked with a high vapour density and therefore with a "high" number of collisions between the vapour particles (Schiller et al., 1983). The *mean free path* of the particles between collision is, therefore, short.

As the gas pressure is lowered the average distance traversed by a vapour molecule before colliding with a gas molecule increases, i.e. the *mean free path* of the vapour molecule in the residual gas increases (Holland, 1966). The number of collisions per unit volume is thus decisive in the interactions between vapour particles, or electrons, and the gas (Schiller et al., 1982).

Schiller and co-workers (1982 and 1983) described in some detail the effect of gas pressure on the mean free path of the vapour particles. Firstly, a description of the kinetic theory of gases and the probability of a collision with a neighbouring gas atom or vapour particle can explain how the distance travelled by a particle varies as a function of the gas pressure. The mean free path was shown to vary as follows:

Pressure	Mean Free Path (m)
1 Pa	5×10^{-3}
10^{-2} Pa	5×10^{-1}
10^{-4} Pa	5×10^{1}

In addition, Schiller et al. (1983) also demonstrated that in each region of the vapour cloud there must be particles moving in the direction of the substrate as well as towards the source. The density distribution of the particle flow at a point within the vapour cloud was represented showing flow distribution to the substrate and back to the crucible as a percentage. This is important because particle interactions (or gas scattering, Bunshah, 1982) may account for a deviation from the cosine law and cannot, therefore, be neglected especially the high-pressure region immediately above the source (virtual source).

6.5. Modelling the Evaporation and Deposition

From the foregoing, it is possible to pinpoint one of the problems with evaporation technology, that is, the variation in thickness distribution on a flat substrate. Investigations to study possible solutions for this problem have been proposed (Nicholls et al., 1998). With the aim of predicting the thickness profile of coatings, the early deposition theory discussed previously has been re-examined and a computer-based model developed capable of integrating the vapour flux from multiple sources to predict the distribution of coating thickness on a component.

The rate of coating growth and direction of growth, at any point on a component surface, depends on integrating the complex vapour flux field from all sources, both virtual and real, onto an inclined surface element. A computer model was recently proposed for predicting the distribution of vapour flux (thickness profile) for EB-PVD TBCs (Pereira, 1996).

The surface of the substrate can be modelled using a small-area surface, such that each surface element can be approximated to a flat plate of known geometry and orientation. The influence of substrate rotation about a component axis and the effect of varying the inclination of the component, or rotation about a second axis, can then be accommodated by moving this substrate element within the 3-dimensional coating space to match the expected substrate movement. In addition, the evaporation behaviour of real sources (termed wide area sources in this study) can also be modelled as an array of point sources evaporating in parallel. It follows, therefore, that the distribution from multiple sources (typically 3 sources) can also be determined by the summation of either the individual point sources or wide source geometries.

An understanding of all these interactions is far from complete but initial models capable of predicting vapour deposition have been formulated (Nimmagadda and Bunshah, 1971; Musset, 1990; Bosch, 1993; Pereira, 1996).

Nimmagadda and Bunshah (1971) discussed a method for calculating the temperature and thickness distribution for the deposition of yttrium and yttria. Their work aimed at optimising the deposition temperature in order to obtain fine grain size fully dense deposits. Many important variables were enumerated and their effect investigated, with particular recognition to the following: temperature of the source, diameter of the source (2.5 and 3.8 cm), source-to-substrate distance (10, 15, 25, and 50 cm), substrate material, and thickness of the substrate. The same authors have made the following observations. As the temperature of the source increases, the evaporation and the deposition rates increase, in addition to increasing substrate temperature. As the source-to-substrate distance increases, the deposition rate and the temperature at each point on the substrate decrease and the deposit becomes more uniform in temperature and thickness. In addition, with increasing source diameter the thickness and temperature at each point on the deposit increase.

Musset (1990) concentrated on achieving uniformity of coating thickness using multiple pairs of omni-directional sources ($n = 0$) by varying their position, charge, and number of source pairs. Uniformity inside a cylinder 80 cm high and 40 cm in diameter was achieved by optimising the above parameters. In one proposed solution two pairs of sources were positioned at ±16 cm and ±48 cm relative to the mid-height position, with a 2 and 3 g charge, respectively. The uniformity achieved was fairly good, with a variance of 0.97.

Bosch (1993) proposed a computer-aided procedure to optimise the layer thickness distribution on lenses, based on the cosine law. The coating of ophthalmic lenses is an example where it is required to produce uniform coatings, in this case over the convex side of the coated substrate. Optimisation of the dome-shaped substrate holder taking into account the geometry of the substrate was performed for a PVD unit.

This study aims at completing the computational procedures related to the modelling of the source, i.e. symmetrical and asymmetrical large area sources, multiple source configuration, and virtual sources, and also related to the deposition process of the substrate characteristics/behaviour, namely inclination of the substrate, the use of shadow masks, and substrate rotation.

CHAPTER

7

7. The Concept of the Computer Model

A computer program has been developed in C++ to simulate the behaviour and characterise the emissive properties of an EB-PVD source. C++ was adopted because it is a powerful, flexible, and portable general-purpose object-oriented language in widespread use. The computer program was intended to be an experimental development tool and it has been created using the incremental development concept, i.e. the different functions or procedures needed for the various theories were included as the necessity arose. In order to allow for incremental development, the analysis, design, and programming were all object-oriented. Object-oriented analysis, design, and programming (OOA, OOD and OOP, respectively) are now widely used as they address a large number of problems that arise during complex software development providing viable and practical solutions.

From the previous chapter it is evident that there is a need to manipulate the details of points and angles, for example. All the details of these two entities (points and angles) were encapsulated or hidden from a potential programmer who may be responsible for maintenance and future upgrades. In the C++ language, the description of an encapsulated data/function set is called a Class. For instance, from the geometry of evaporation and derived cosine inverse square law, the need to define the substrate using the Cartesian coordinate system and the retrieval of the equivalent in Polar coordinates is apparent, since the cosine equation requires the source-to-substrate distance and the angular displacement of the substrate to calculate the coating thickness. Moreover, angular measurements may suggest the need to handle angles in radians and degrees. All these variations can be encapsulated in a Class contributing to increased ruggedness while simultaneously hiding the complexity of the details.

With the aim of predicting profiled thickness coatings, the deposition theory described in the previous chapter has been re-examined and a computer-based model developed capable of integrating the vapour flux for various source geometries. These source variations were encapsulated in a Class and are termed "evaporation model" in this study (See "Evaporation Model" on page 99 for more information about the evaporation model). In the early stages of the development, the surface of the substrate was modelled using a small-area surface, such that it could be approximated to a flat plate of known geometry and orientation. However, this does not describe the real case where, for instance, the substrate has a complex aerofoil section, and may be masked and rotated within the vapour cloud. It is clear, therefore, that various other concepts pertain to another aspect of the EB-PVD process, i.e. the deposition model (See "Deposition Model" on page 127 for more information about the deposition model).

In conclusion, the modelling of the EB-PVD process can be seen as a two-phase operation: the evaporation and the deposition. These two models are discussed in more detail in the next sections and then each model and the various concepts that characterise them are analysed in detail in different chapters.

7.1. Evaporation

Theoretically, the inverse square law, which is based on the Knudsen equation, predicts the thickness distribution deposited from an ideal point source evaporator. However, this equation does not describe the real case where, for instance, the source is not a point source evaporator and may be asymmetrical. In order to model a real source several source variations have been accommodated in the computer model by developing a generalised point source evaporation model with directional properties. These are described in the next paragraphs.

In practice, a real evaporation source, typically a ceramic rod 3 to 7 cm in diameter with the diametrical surface molten, can be envisaged as multiple of point source evaporators, evaporating in parallel. Thus, it is possible to combine arrays of point sources to predict the evaporation behaviour of a large diameter ceramic ingot (termed 'wide' sources).

Furthermore, it is not necessary for each point source in a wide source configuration to have identical evaporation characteristics. Hence, it is possible to model asymmetric evaporation behaviour due to the fact that the electron beam impact area on the surface of the molten pool is not flat but forms an inward bulge on the heated area. This is important because one part of the source may behave in a highly focused manner while other areas may give a more dispersed distribution of vapour flux.

As mentioned previously, a typical commercial coater has a multiple source arrangement with all sources usually evaporating the same material for increased evaporation rate. Therefore, it is possible to combine the effects of multiple sources evaporating in parallel. Also, one can envisage models where each individual source in a multiple source evaporation configuration is represented with 'wide' source clusters to ensure an extremely wide and uniform vapour flux.

Many published studies indicate that the EB-PVD process is not a true line-of-sight process (Rigney et al., 1995, for example). For instance, during high-rate evaporation the vapour pressure above the vapour-emitting source is relatively high (10^{-1} Pa according to Schiller et al., 1982) and a virtual omni-directional source will be generated in the vapour cloud due to the localised high vapour pressure and atom-atom collisions. Therefore, the virtual source concept has been both re-examined and characterised based on an understanding of the physics of evaporation. This virtual source concept accounts for the deposition of material on surfaces hidden from the real source.

The rate of coating growth and direction of growth, at any point on a component surface depends on integrating this complex vapour flux field from all sources, both virtual and real, onto an inclined surface element.

7.2. Deposition

As reported earlier, during the development stages of the evaporation model, the substrate was stationary and was modelled as a predefined, small-area element. It is clear, therefore, that this early model does not describe the real case where, for instance, the substrate has a complex aerofoil section and is rotated within the vapour cloud. Accordingly, the issues that characterise the EB-PVD coating of gas turbine components were analysed and identified as follows.

Gas turbine components that are to be coated with a TBC have a complex aerofoil shape and are "twisted" from root to tip. They are designed using complex analytical surfaces within sophisticated CAD packages. Therefore, the need to predict the coating thickness on substrates with complex geometry is apparent. In addition, the coating of a cluster or groups of blades is being pursued by the coating industry as an approach to decrease the unit coating cost. The geometric information of the substrate is thus available and could be exported to a file from within the CAD package.

Deposition onto aerofoil components is usually limited or prevented with the use of shadow-masks. For example, good aerodynamic performance is desirable and this requires the build-up of coating on the trailing edge of aerofoil components to be limited to a few tens of microns (coating on the leading edge is around 250 μm thick). It follows, therefore, that the modelling of the deposition should allow shadow-masks to be positioned relative to the substrate and the coating thickness calculated for the combined arrangement, based on the influence of the shadow-mask. These fixtures could be defined by a CAD package similarly to the substrate.

Another issue typical of the EB-PVD process is substrate rotation (or more generally substrate manipulation). Turbine blades, for example, are usually rotated around their main axis while being translated or tilted around a second axis. This planetary motion is necessary to ensure that all surfaces of the component are adequately coated with ceramic. Programming of the planetary motion of the simulated parts manipulator is, therefore, required for suitable accuracy of the computer model to be achieved.

From the above, it cán be seen that deposition modelling requires an accurate representation of the model (substrate, and shadow-mask, if used) and a suite of procedures to accommodate substrate manipulation. In addition, the importance of being able to visualise the predicted results within a user-friendly environment capable of allowing the user to select both the evaporation and deposition parameters, is apparent.

7.3. Choice of environment

Various programming languages on different platforms exist capable of modelling the EB-PVD coating process. However, the development of the computer model within an environment capable of generating a simple user-interface with relative ease, to be operated by both casual and advanced users, was desired. For instance, Windows® is a popular and flexible operating system with many available packages for development of software. Similarly, Visual C++ is a powerful widely-used programming environment

that can generate fast and compact code using a high-level language. In addition, there appears to be many libraries with functions for various applications, which indicates that a relatively short time for development is possible without requiring the coding of functions that might have been previously developed for similar applications. For example, "standard" functions such as rotation and visualisation of a solid are common within various areas. Therefore, the computer model could use available libraries of graphical functions to both optimise and make the final tool more robust. A detailed discussion of the user interface of the computer model in addition to an explanation of how it is used to predict the thickness profile around any component is given in chapter 10 (page 139).

An important aspect of the modelling is concerned with the visualisation of the results. In order for the software tool to have applicability in the modelling of the coating distribution, it was important to define a relatively simple method to visualise the results predicted using the computer model. The thickness distribution was thus represented with different colours, similar to the colour gradients used by a CAD or finite element analysis tool to represent, for instance, stress distribution or surface temperature.

7.4. Programming for the Windows environment

The use of Visual C++ within the Windows operating system (OS) is characterised by various tools designed to make the programming simpler. For instance, the *ClassWizard* manages the various Classes related to the user interface, their objects, and messages. A typical Windows application has two important classes: a *document* (any information to be handled, for example, the geometric information of a turbine blade) and a *view* (an area to visualise an image of the *document* on the screen or printer and interpret user inputs such as operations upon the *document*). From the above, it is evident that both the *document* and the *view* Classes have properties and events. The location and dimension of the *view* is an example of a property while an event could be opening a new *document* or the user clicking on the *view*. To handle all of the above, Classes have *member variables*, which hold the state of the object, and *member functions*, which are called when a certain event is triggered. A list of the main Classes and principal procedures that have been written and their function is given in APPENDIX A.

Due to the characteristics of the Visual C++ programming environment, which is based on the hierarchy of the Windows OS classes, many of the events that occur within an application are handled by the code generated automatically by Visual C++, allowing the programmer to concentrate on writing code for the events specific to the application being developed. Typical examples that do not need to be programmed are the move, size, minimise and maximise commands available from the control box (which are standard to any Windows application). On the other hand, commands such as opening or saving of a *document* are application-specific and the programmer needs to write code for that object (since the *document* can be in any file format, only the programmer knows what "open" or "save" means).

For ease of understanding and increased ruggedness, all of the Classes of the software tool have two separate files: one is the header file and the other the application source file. While the header file (.h) declares the Class and includes project-specific headers

(such as structures to hold the geometric information of the turbine blade), the application source file (.cpp) contains the application class (the actual code for the functions defined in the header file).

From the above, it is evident that programming for the Windows environment can be described as follows: coding of the application-specific base Classes (in the case of this study, Classes to handle angles, points, and the evaporation and deposition aspect of the model) and then adding code to handle Windows events, such as menu commands, button clicks, etc. Some examples of the functions to handle the evaporation aspect of the model include, defining a substrate, defining its position and orientation, calculating the coating thickness for the theoretical single point source, 'wide' source and multiple source arrangement, and the virtual source concept. As far as the deposition model is concerned it requires functions to define a substrate with complex geometry, which may include shadow-masks, substrate rotation, and the visualisation of the coating thickness around the component. Windows events may include menu commands such as File/Open, visualisation of the model to represent various features, commands to move and rotate the substrate within the coater space, and the calculation of the coating thickness (a detailed description of the computer model is given on page 139).

7.5. Validation of the results

The software tool proposed was aimed at comparing the results from both theory and practice (or the calculated and measured, respectively), in order to investigate the variation of coating thickness distribution around components. Thus, this study proceeded to verify the computer model by first measuring the coating thickness for experimental trial runs and then compared the calculated coating thickness to that measured using a laboratory coater.

Various case-studies were analysed and the measured coating thickness was compared to that predicted in order to increase the control of the EB-PVD process and permit the controlled deposition to tailor the TBCs performance and durability. Predicted thickness distributions are in good agreement even for the simplified evaporation model, but can be improved further by increasing the complexity of the source model. This is discussed in detail in chapter "Validation of the Computer Model" on page 157.

CHAPTER

8

8. Evaporation Model

8.1. Introduction

The computer program that has been developed is intended to be an experimental development tool for process control and an aid to understanding and successfully using the EB-PVD coating process. It has been created using the "incremental development" concept, i.e. the different functions or procedures needed for the various concepts were included as the necessity arose. For example, the procedure for calculating the evaporation from a small-area evaporator (single point source) was included before the one for a wide area source (a wide source is a "large" diameter ceramic ingot that cannot be adequately modelled using a single point source). In fact, a wide source can (and was) represented as the summation of various single point sources.

The initial versions of the software tool (Pereira, 1996) had limited user interaction mainly because in early stages of development little or no information from potential users was available. All the major program parameters were included in the code as constants. For example, if the source-to-substrate distance needed to be changed then the line of code that contained this parameter would have to be modified and the program compiled to produce the desired results. Furthermore, little was known regarding the best, or at least the ideal way of presenting the information or results from the computer model. Therefore all results were displayed on the screen, or written to a text file, which could then be read into a spreadsheet tool for analysis. Subsequent versions of the program enabled a higher degree of flexibility by allowing the major process parameters to be modified without the need to change the code. As the program evolved from "static" to parametric, user interaction was easier to accomplish and the major process parameters could be specified using dialog boxes.

8.2. Simplifying Assumptions

Several modelling assumptions were made, especially in the first stages of the development, in order to simplify the complexity inherent in the EB-PVD process.

Firstly, the source was modelled as a single point source operating in a 3D half space above the melt. Generally speaking, it is characteristic of a point source evaporator that the dimensions of the vapour-emitting surface are small compared to the source-to-substrate distance (Schiller et al., 1982). This assumption aimed at understanding whether the theory of a single point source evaporator could adequately model the

experimental coater available at Cranfield University. Further developments of the computer model investigated the more complex sources by combining arrays of single point sources to predict the evaporation behaviour of a large ceramic ingot.

Secondly, it was assumed that the particles undergo a line-of-sight process. The effects of a virtual source usually generated during high-rate evaporation by the atom-atom collisions or by the interaction between the electron beam and the vapour stream, both factors causing the vapour particles to deviate from their initial trajectories, were assumed to be non-existent (see "Modelling Vacuum Evaporation" on page 83 for more information about virtual sources). In addition, every vapour molecule arriving at the substrate's surface condenses on first impact (i.e. there are no particles flowing in the direction of the source). These assumptions are necessary for Knudsen's cosine law to be applicable.

Thirdly, the surface of the substrate was modelled using a small-area surface, such that each surface element can be approximated to a flat plate of known geometry and orientation. The minimum number of sides needed to model a surface is three; therefore, the substrate was modelled by using a three-sided polygon, which defines a triangle in 3D space. In addition, it was also important to control how front-facing substrates were determined (define which side of the triangle was the front and which one was the back). In a completely enclosed surface constructed from a set of triangles, none of the back-facing triangles are ever visible – they are always obscured by the front-facing triangles. One way of solving this is by using a normal vector. A normal vector is a vector that points in a direction that is perpendicular to a surface. For a flat surface, one perpendicular direction is the same for every point on the surface. Therefore, a substrate's normal vector defines the orientation of its surface in space. However, for a given point on a surface, two vectors are perpendicular to the surface, but they point in opposite directions. Hence, by convention, the substrate's front side is defined by the normal pointing to the outside of the surface being modelled. Figure 8-1 shows a substrate (triangle) with its front side, which is defined by the normal n_1, visible by the source. If the backside of the surface was the one visible by the source (n_1 pointing in the opposite direction) then no deposition would arrive on the substrate's surface.

In addition, if each triangle is part of a more complex shape, then each triangle shares its vertices with other triangles. Therefore, calculating the coating thickness for each vertex would be confusing since, depending on the surface analysed, the same vertex may have two or more different normal vectors. For example, in Figure 8-2 vertex P is shared by four triangles having three distinct normal vectors (the top two triangles are on the same plane having, thus, the same normal). For this reason, the coating thickness was calculated not for each vertex but for the centroid of each triangle (Figure 8-2). The centroid (centre of mass) of the vertices of a triangle is defined as the point G which is the intersection of the triangle's three medians (Figure 8-3).

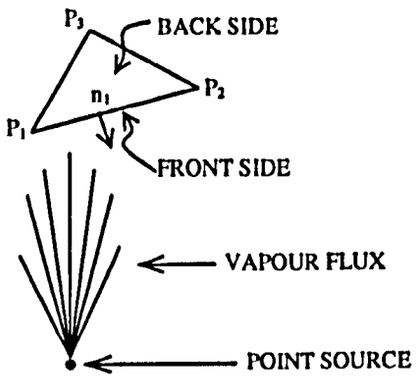

Figure 8-1: Substrate modelling using a three-sided polygon and a normal vector to define the front side of the surface.

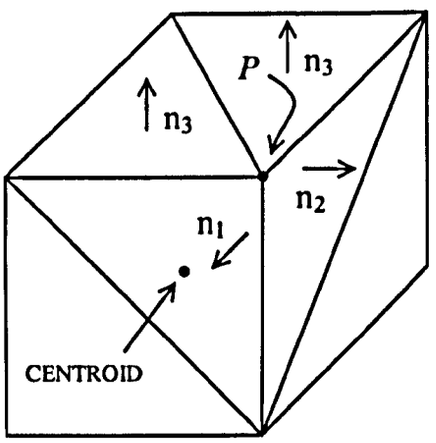

Figure 8-2: A vertex is shared by two or more triangles, as is the case in a cube.

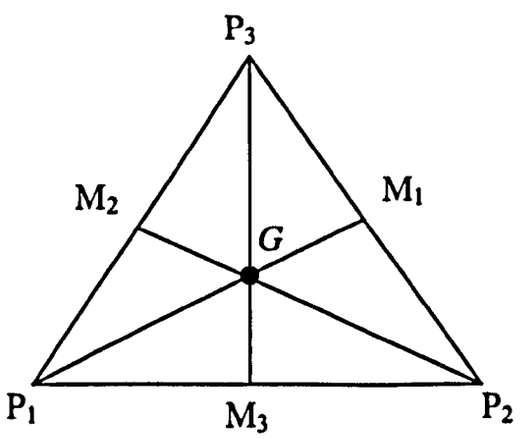

Figure 8-3: The centroid, *G*, of a triangle defined by vertices P_1, P_2 and P_3 is the intersection of the triangle's three medians.

Still another assumption is related to the fact that even though the ceramic rod is being evaporated, the model assumed a constant source-to-substrate distance. On the one hand, it is well established that the rod needs to be pushed up from time to time, either manually or by a computerised system, in order to maintain a constant source-to-substrate distance. On the other hand, it was thought that the effect of increasing the source-to-substrate distance by a few millimetres on the deposition profile could be

neglected for the typical source-to-substrate distances, which are in excess of 20 cm. Other parameters such as electron beam focusing, scanning pattern, and inclination of the substrate are more important and if not controlled adequately may contribute to the modelling being less accurate.

All of the above assumptions aimed at developing the simplest model capable of predicting the thickness distribution within acceptable bounds.

8.3. Parameters Controlling the Deposition

Table 8-1 defines all parameters controlling the deposition from the cosine equation discussed previously ($\frac{d}{d_0} = \frac{h_0^2}{h^2}\cos^n\theta\cos\alpha$).

Table 8-1: Parameters controlling the deposition of vapour flux onto a substrate.

Parameter	Definition
d	Unknown deposition rate (coating thickness) on the substrate (calculated for the centroid of the substrate).
d_0	Reference deposition rate at a distance h_0 directly above the source for a horizontal substrate.
h	Source-to-substrate distance.
h_0 (also z)	Height of substrate plane, measured directly above the source.
α	Inclination of the substrate to the line of vapour flux measured normal to the substrate. Also known as the vapour incidence angle (VIA).
0	Angular displacement of the substrate, measured relative to the normal to the source.
n	Index defining the focus of the vapour flux from the evaporation source. A value of zero is an omnidirectional evaporator.

From the foregoing it is evident that some parameters are set by the system geometry (h, h_0, α, 0); others have to be estimated (d_0 and n); while d is the parameter which needs to be calculated.

The use of d_0 as a reference point was important because the thickness on the substrate's centroid, at any distance away from the normal to the source (0), could be compared with this value. The value of d_0 was set to 100 for a position 10 cm above the source. By using the inverse square law it was possible to calculate the decrease in deposition rate for a point directly above the source at any height relative to the 10 cm reference. The

thickness for any point on the plane h_0 above the source was thus a percentage of the deposition directly above the source (d_0).

The value of n is an index reflecting the evaporation characteristics (focus) of the source (typically between 1 and 9). A more detailed discussion of the influence of the n value on the thickness distribution is given in the next section.

It is proposed that with this model one can set up evaporation experiments whereby a measure of the thickness distribution around a substrate with complex geometry can be obtained. The next sections discuss the model for calculating the thickness of the deposit and then proceeds to verify the model by calculating the thickness for experimental conditions and comparing it to those measured from physical experiments.

8.4. The effect of varying the n *value on the thickness distribution*

By solving the family of equations implicit in the cosine equation it is possible to predict the deposition profile expected for a classic single point source evaporator. Results for horizontally positioned substrates are illustrated in Figure 8-4. Firstly, the deposition profile exhibits the classic bell shaped curve with a peak rate of deposition directly above the source, i.e. x = y = 0 (the z-axis represents the deposition rate, which directly above the source is d_0 = 100). Secondly, the deposition decreases as the substrate is positioned further away from the point directly above the source. Also, it is evident that the when the substrate's distance from the point directly above the source is big enough, then the deposition is almost zero. The exact deposition profile for substrates positioned horizontally is a function of the height of the substrate, measured directly above the source (h_0) and also the angular displacement of the substrate, but in all cases it can be represented as a bell-shape.

One important factor that frequently varies with coating equipment is the rate at which the deposition decreases as the substrate is moved further away from the point directly above the source. This is defined by the n value. It can be seen from Figure 8-5 that as the value of n increases, the evaporant plume is more focused. The implication of this is that substrates have to be directly over the source, or rotated through the evaporant flux, if an acceptable deposition rate and coating uniformity is to be achieved.

Worth noting is that for a source with a low n value, not only is the deposition rate higher, but also the evaporant plume larger, enabling multiple parts to be coated simultaneously. Factors affecting the n value include the material being evaporated, the scanning pattern produced by the electron beam, and some effects on the source surfaces which alter the vapour stream distribution (see Figure 6-3 on page 88).

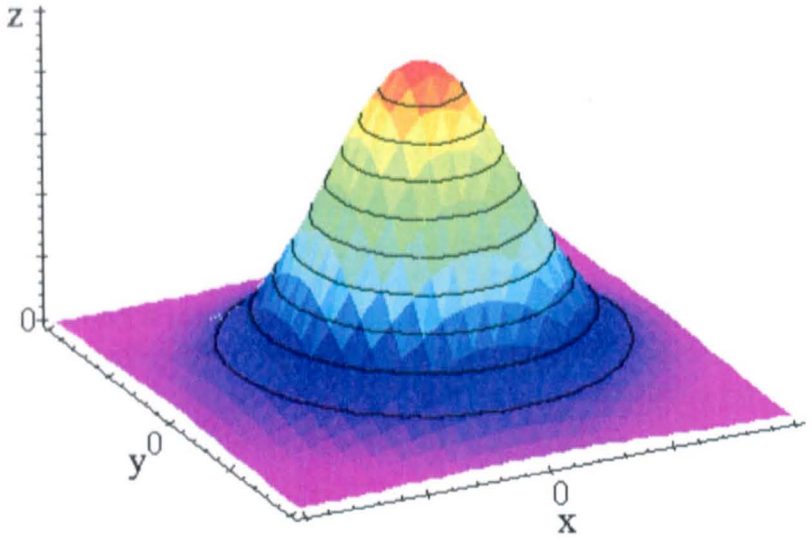

Figure 8-4: 3D profile generated for a typical plane above the source with horizontal substrates.

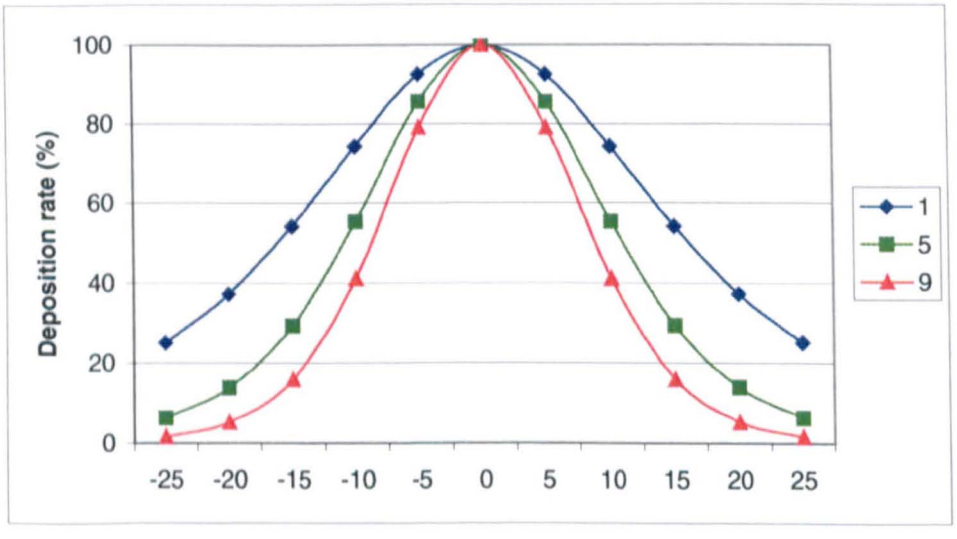

Figure 8-5: Predicted deposition profile for a point source evaporator with index *n* = 1, 5 and 9 along the centreline (y = 0; height of the substrate, measured directly above the source, *z* = 25). (See also Figure 8-9)

8.5. Inclined Substrates

A systematic investigation of the effects of the inclination of the substrate on the thickness distribution was addressed for inclined substrates at 0, 30, 45, 60 and 90 degrees. The angles investigated refer to the inclination of the substrate surface to the horizontal plane of the substrate's centroid as shown in Figure 8-6.

It should be noted that all units of measurement are typically expressed in centimetres. However, this does not necessarily have to be assumed; any other unit of length can be used providing it is used consistently, i.e. if, for instance, inches are preferred then inches have to be used for all measurements.

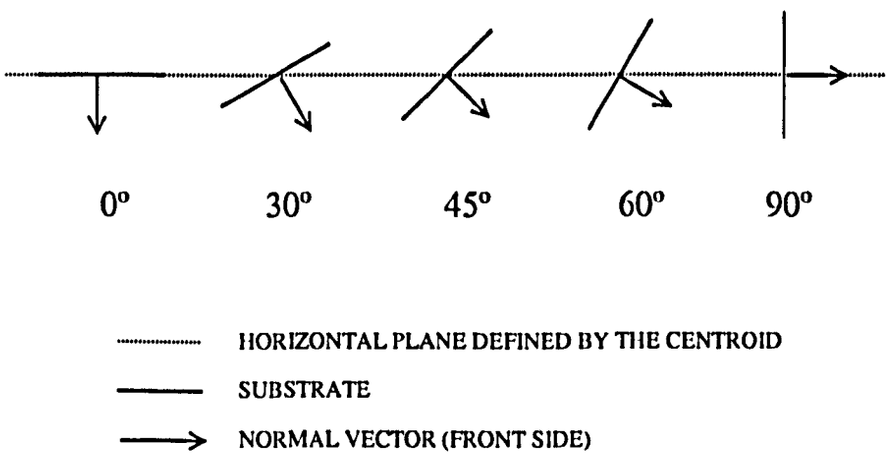

Figure 8-6: Configuration of the inclined substrates studied.

To fully understand the effect of inclined substrates, a series of results were calculated by simulating a square matrix of substrates on the same plane within the range –15 to 15 units (for both the x and y-axis) separated 3 units apart. Figure 8-7 shows this arrangement whereby each substrate was positioned on the intersection between each column and row, with the source in the centre of the coordinate system (0,0). The matrix is 11×11 and, therefore, the deposition thickness for a total of 121 substrates (for each angle studied) was calculated.

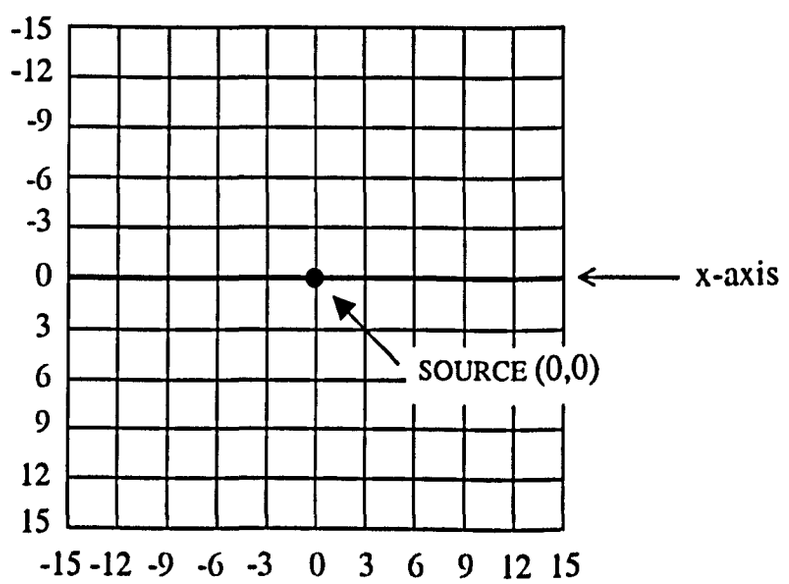

Figure 8-7: Matrix representing the location of each substrate measured using the source as the centre of the coordinate system (intersection between each column and row).

For each set of results (each angle of inclination) a contour plot was generated in order to study the varying distribution profile.

8.5.1. Substrates inclined at 0 degrees

At 0 degrees of inclination (0 = α, i.e. horizontal substrates) it is possible to detect a perfect circular symmetric plot in relation to the origin of the coordinate system (symmetric along both the x and y-axis, Figure 8-8). The deposition profile exhibits the classic bell shaped curve with the peak rate of deposition directly above the source (d_0 = 100).

An important parameter that controls the deposition rate is the separation between the centre of the source, projected onto the substrate plane, and the substrate's centroid (defined as r for radius, which is a function of the parameter 0), to the height of the substrate's plane, measured directly above the source (h_0). This aspect ratio is important because it describes the decrease in thickness as the distance of the substrate from the line directly above the source varies. By choosing various aspect ratios it is possible to devise a table of calculated results to describe uniformity as shown in Table 8-2:

Table 8-2: Calculated deposition rate for various aspect ratios (r/h_0).

Aspect Ratio $\frac{r}{h_0}$	0	Deposition rate (d_0) for $n = 4$	% decrease in thickness
0	0°	100	0.0
0.05	2.86°	99.01	0.99
0.0625	3.58°	98.45	1.55
0.0833	4.76°	97.27	2.73
0.125	7.13°	93.99	6.01
0.25	14.04°	78.47	21.53

The above results show that to obtain a uniform deposition h_0 should be made as large as possible compared to r. However, increasing h_0 decreases the deposition rate by the inverse of the distance squared. For example, increasing the source-to-substrate distance by a factor of two will result in the deposition rate being reduced by a factor of four. Figure 8-9 encapsulates the effects of simultaneously varying h_0 (z), r, and n. It is evident that when considering the deposition rate relative to d_0, the profile with the less focused plume is when $z = 25$, $n = 1$. Conversely the most focused evaporation plume is when $z = 15$ and $n = 9$ (Figure 8-9a). Worth noting is that two profiles $z = 25$ and $n = 9$, and $z = 20$ and $n = 5$ produce an almost identical relative deposition profile, with a maximum difference of around just 1%, closely followed by $z = 15$ and $n = 5$, and $z = 20$ and $n = 9$. However, when considering the effects of the inverse square law on the deposition rate, $z = 25$ clearly has the lowest deposition rate of the three heights. It follows, therefore, that the focus of the evaporation plume can be reduced by increasing z but at the expense of decreasing the evaporation rate. This study allows, therefore, much closer working distances, while still achieving the desired deposition profile.

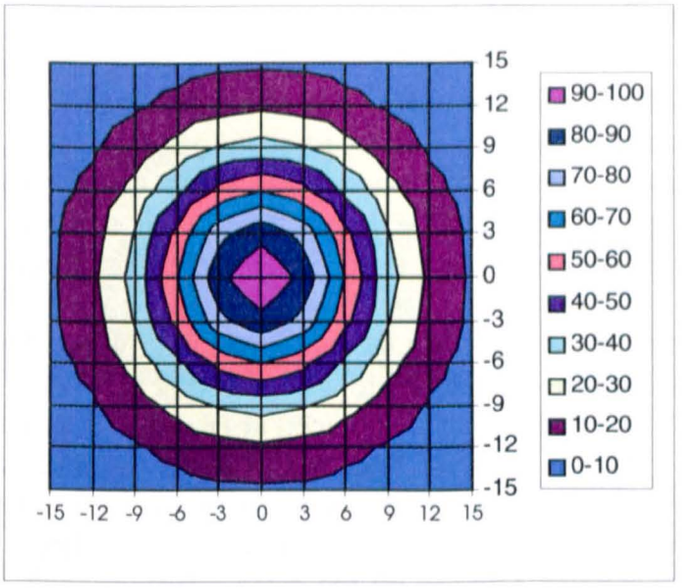

Figure 8-8: Contour plot of the predicted thickness distribution for substrates inclined at 0 (zero) degrees.

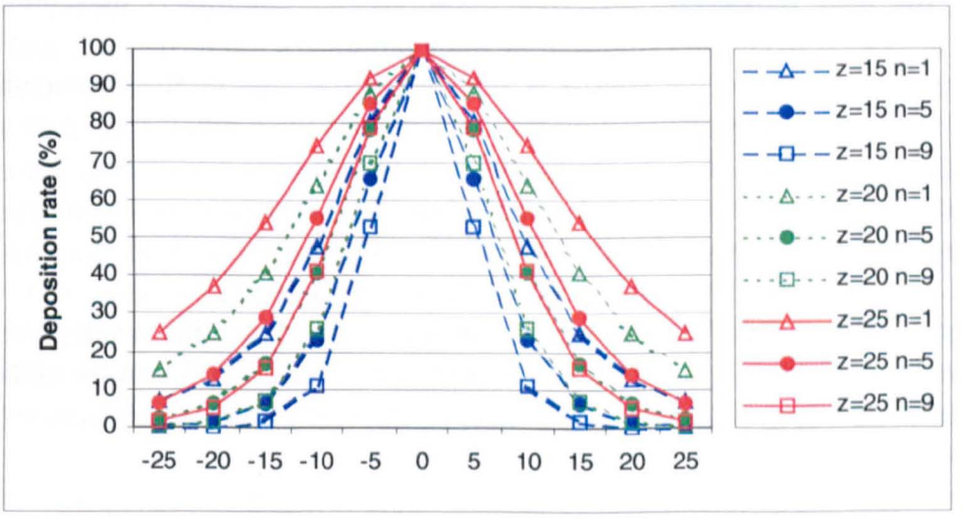

a)

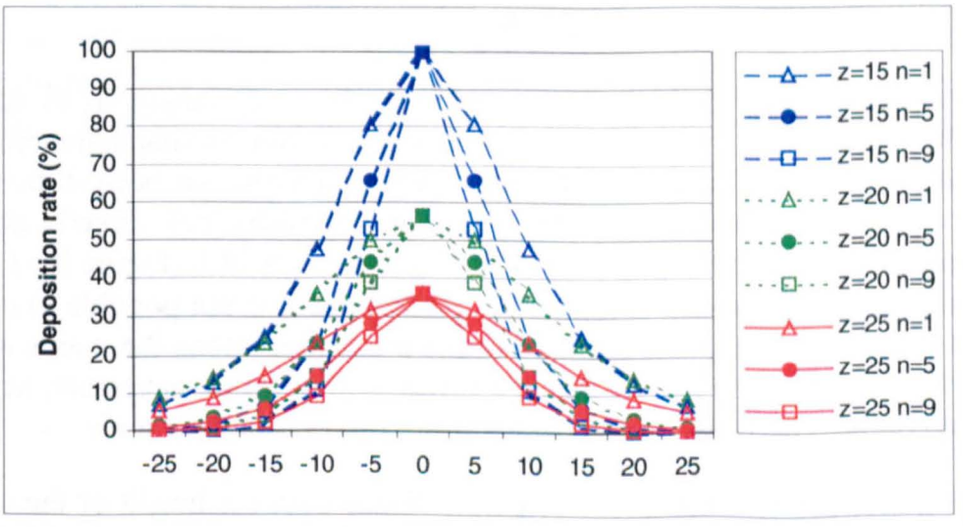

b)

Figure 8-9: Predicted deposition rate for three working heights (z = 15, 20, 25) for n=1, 5 and 9; (a) d_0=100 for all three planes; (b) d_0 varies by the inverse distance squared (z = 15, d_0 = 100; z = 20, d_0 = 56.25; z = 25, d_0 = 36).

8.5.2. Substrates inclined at 30 degrees

When an inclined substrate is held over the vapour source, the maximum coating thickness measured on the substrate is reduced as the vapour flux arrives at an oblique incidence resulting in an asymmetric coating thickness distribution on the substrate (Figure 8-10). Even though the profile is asymmetric in relation to the origin it is evident that an axis of symmetry does exist along the x-axis. Because the substrate is tilted relative to this axis, when the substrate is placed to the right of the origin (when x is positive), the vapour flux arrives at a steeper angle than when the substrate is to the left of the y-axis. For instance, if a substrate was placed at ($x = -3$, $y = 0$) the deposition rate would be 84.21%; if another one was placed at ($x = 3$, $y = 0$) the deposition would drop to 66.78% even though they are both at the same distance from the source. In conclusion, it is the angle of incidence that is affecting the deposition rate for this case and not the source-to-substrate distance, which has already been studied. A similar effect occurs with the sunrays arriving on the earth's surface with different intensities depending on the inclination of the surface.

In addition, the peak deposition rate (maximum coating thickness) measured on the substrate is displaced from the centreline of the evaporant source. Instead, and because the substrate directly above the source is not facing the vapour flux perpendicularly, which is when the maximum deposition rate is achieved for a given source-to-substrate distance, the deposition on this substrate drops to the 80-90% band ($\alpha = 30$; $cos\ 30 = 0.866$). Even though the contour plot does not show the region around the origin (0,0) in sufficient detail, a much more detailed calculation was performed which showed that the highest deposition rate (around 88.6%) occurred when ($x = -1.2$, $y = 0$). This acknowledges that for a constant source-to-substrate distance, the steeper the vapour incidence angle (VIA) the less deposit arrives on the surface. This can be modelled by the cosine function which returns a lower value as the α angle increases from 0 (zero) to 90 degrees.

8.5.3. Substrates inclined at 45 degrees

For substrates inclined at 45 degrees the profile predicted is analogous to substrates inclined at 30 degrees. It is evident that the contour plot is not circular symmetrical (but symmetric along the x-axis) and that the highest deposition rate has been shifted further to the left of the source than for the 30° case. The deposition rate directly above the source is around 70% while for ($x = -3$, $y = 0$) it is just under 74% (Figure 8-11). Worth noting is that due to the discrete nature of the predictions it is not possible to comment on the exact point of peak deposition rate. Further predictions along the x-axis would be needed, particularly between $x = -6$ and $x = 0$ (i.e. with a lower increment, say 0.5 or lower, instead of the 3 used) but this accuracy is not relevant for this study.

An interesting fact occurs when ($x = 15$, $y = 0$). Since both the height of the substrate and its displacement relative to the line directly above the source is equal to 15 (i.e. $h_0 = r = 15$), the vapour flux is parallel to the substrate's surface. In other words, the substrate is edge on with the vapour rays and, therefore, the predicted deposition is zero (the column corresponding to $x = 15$ has a deposition rate of zero). If the substrate had

been moved a little more to the right, the back of the substrate would be coated. This is better explained when the inclination is set to 60 degrees.

8.5.4. Substrates inclined at 60 degrees

One interesting feature of substrates inclined at 60 degrees is that the deposition rate directly above the source is exactly 50% of that had the substrate not been inclined (α = 60, thus *cos* 60 = 0.5). Most of the predicted results are similar to the previous two contour plots studied (displaced peak deposition rate and circular asymmetric). However, an interesting feature happens, which occurs for the first time, for $x = 12$ and $x = 15$. Because the substrate has crossed the limit explained previously for substrates at 45° (when $x = 15$), the model predicts a "negative" deposition rate (Figure 8-12). As mentioned previously, if the visible surface is the backside then no deposition is predicted for the front side. In addition, the model predicts the deposition rate for the back of the substrate. Therefore, a negative deposition rate not only means that the side we are interested in is invisible, but also that the deposition on the back of the substrate would be the absolute value of that predicted by the model.

8.5.5. Substrates inclined at 90 degrees

For substrates inclined at 90 degrees to the horizontal plane, a combination of various effects from previous angles of inclination occurs (Figure 8-13). Along the y-axis (x = 0) the deposition is null because the vapour flux is edge on with the substrate's surface (as for 45° when $x = 15$). The maximum deposition rate is low (less than 25%) due to the steep vapour incidence angle – only three colour bands were used to represent the positive deposition. The peak deposition rate, for the values studied, is when ($x = -6$, y = 0) (around 24%). While for $x < 0$ the deposition rate is positive, as soon as the substrate crosses the y-axis, the front side of the substrate becomes shadowed or hidden. This results in a negative deposition rate for all points with an x value greater than zero (as observed for 60° deposition at both $x = 12$ and $x = 15$). On the whole, what is true for the front side of the substrate when $x < 0$ is true for the backside when $x > 0$. Therefore, if the absolute values are considered, the predicted deposition rate is mirrored about the y-axis (the y-axis appears as a mirror plane for this 90° inclination deposition).

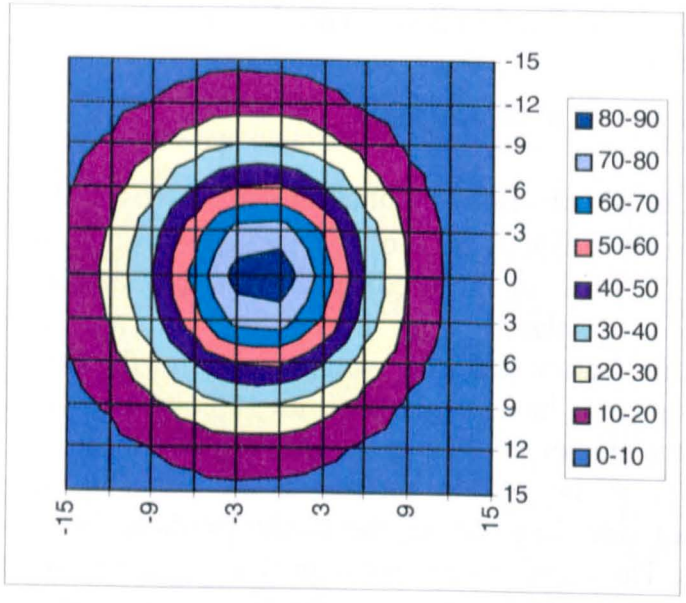

Figure 8-10: Contour plot of the predicted thickness distribution for substrates inclined at 30 degrees.

Figure 8-11: Contour plot of the predicted thickness distribution for substrates inclined at 45 degrees.

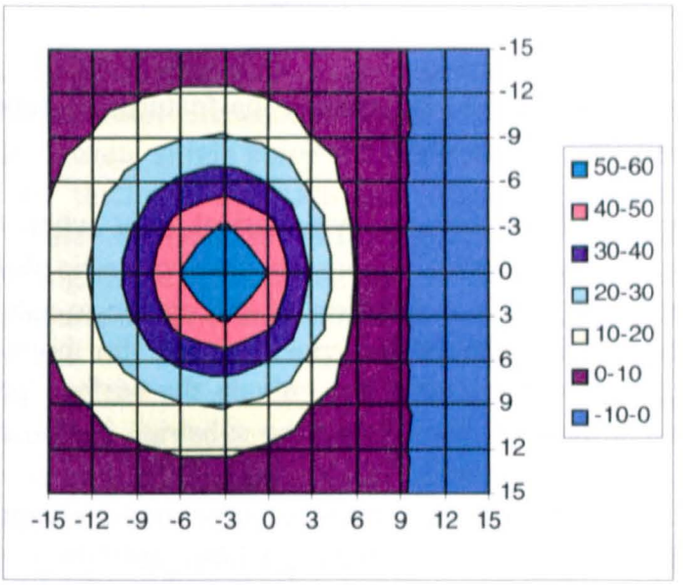

Figure 8-12: Contour plot of the predicted thickness distribution for substrates inclined at 60 degrees (negative thicknesses indicate a deposition on the backside of the sample; the actual coating thickness is its absolute value).

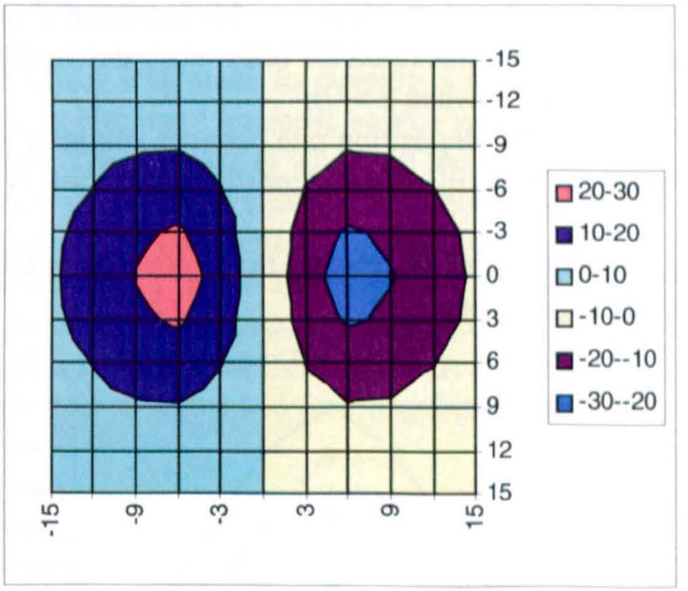

Figure 8-13: Contour plot of the predicted thickness distribution for substrates inclined at 90 degrees (negative thicknesses indicate a deposition on the backside of the sample; the actual coating thickness is its absolute value).

8.5.6. Conclusion

From the foregoing, it is possible to summarise the features of deposition rate for the various angles of inclination studied as follows:

- The deposition profile is circular symmetrical only when $\theta = \alpha$ (horizontal substrates); circular asymmetrical otherwise, but symmetric along the x-axis;
- The peak deposition rate is a function of the source-to-substrate distance and vapour incidence angle. The peak deposition rate for horizontal substrates is directly above the source because not only is the surface perpendicular to the vapour flux ($\theta = 0$ thus $\cos\theta = 1$), but the substrate is also at its closest to the source for any given height;
- For a constant source-to-substrate distance, increasing the vapour incidence angle (increasing α) renders a decrease in the deposition rate;
- When the vapour flux is edge on with the substrate's surface (i.e. the vapour flux is perpendicular to the substrate's normal vector) the deposition is null (as illustrated in previous figures for both substrates inclined at 45° when $x = 15$ and at 90° when $x = 0$);
- The deposition rate that the model predicts on the back side (invisible surface) of a substrate is negative; the deposition on the substrate's back surface is the absolute value predicted (as illustrated for both substrates inclined at 60° when $x > 9$ (approximately) and at 90° when $x > 0$);
- For a vertical substrate, the deposition rate behaves similarly to the odd function. If `f` is the function which calculates the deposition rate, then `f(–x, y) = –f(x, y)`.

Figure 8-14 shows the above features by plotting the deposition rate for the centreline ($y = 0$) for the five angles of inclination.

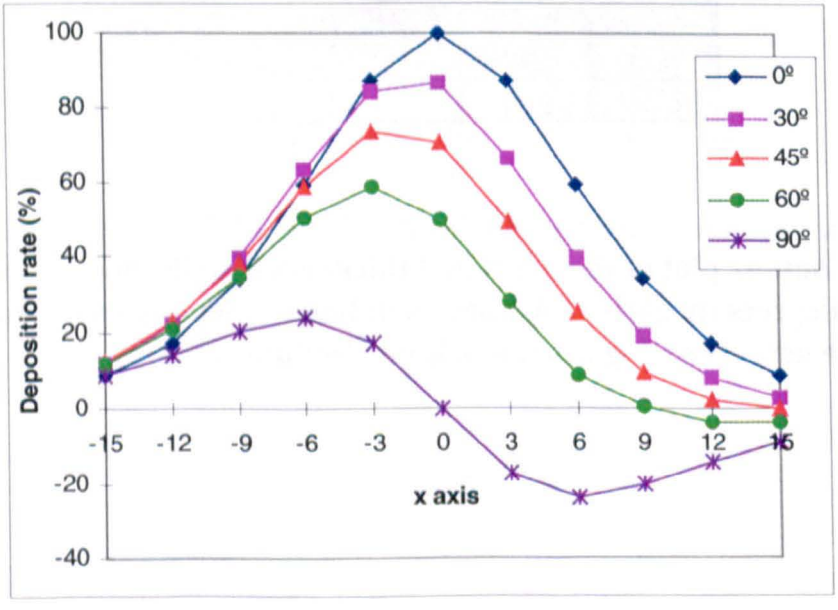

Figure 8-14: Deposition rate along the centreline ($y = 0$) for the five angles of inclination studied (negative thicknesses indicate a deposition on the backside of the sample; the actual coating thickness is its absolute value).

8.6. Modelling Sources with Large Dimension, termed 'Wide' Sources

A wide source is a 'large' diameter ingot that cannot be adequately modelled using a single point source evaporator. Instead, a 'wide' source is modelled by combining an array of circular symmetrical single point sources with the total coating thickness being the summation of the thickness for each individual single point source. While the typical evaporation source diameter varies from around 2.5 cm to around 7 cm for a rod fed evaporator (Nimmagadda and Bunshah, 1971; Movchan, 1996b), the term 'large' is not necessarily a comparison between source diameters. Instead, it is a function of both the source diameter and the source-to-substrate distance. For example, a single point source may adequately model a 3 cm source rod for a substrate height of 25 cm but may not be sufficiently accurate for the same substrate at 10 cm above the source. However, the latter situation may be modelled by a 'wide' source geometry.

In practice, the vapour atoms evaporate not from a single point but from an area on the top surface of the rod (depending on the temperature of the melt pool). The size and format of the area varies depending upon the EB scan pattern, EB source power, and source rotation speed. While experimental coaters may not allow the EB scan pattern to be programmed, a typical commercial coater usually has a preselected library of different scan patterns producing various temperature gradients across the melt pool (Senf et al., 1996; Youchison, 1996).

For ease of use, an effort was made to develop a wide source model in a simple yet efficient way. Firstly, a circular symmetric source geometry was proposed, made up of multiple point sources. The distance at which all the sources, or the first row of sources for a very large source geometry, are from a common centre (r for radius) is a variable. Secondly, the number of point sources (s) that will make up a wide source is a natural number variable greater than 1. If $s = 1$ then we have the single point source case. In all other situations we have a wide source. For instance, if $s = 7$ there is one source on the centre of the circle plus six others at a distance r from the centre. Figure 8-15 shows all seven sources represented as ingots and their angular distance on a circle with radius r.

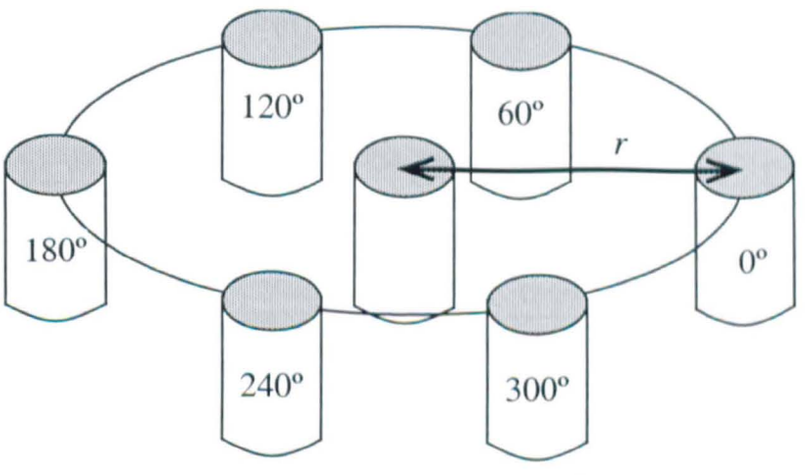

Figure 8-15: Schematic of a wide source represented by the combined effects of 7 single point sources (equally radially spaced).

The modelling assumptions for the wide source were as follows:

- Two wide sources were studied (a seven-point and a thirteen-point source). The angular separation was 60° and 30°, respectively;
- Three radii, namely 1.2, 1.5 and 1.8 cm;
- All substrates were horizontally positioned (0 = α);
- The height of the substrate plane, measured directly above the source, was 15 cm.

8.6.1. Symmetric Wide Source

A symmetric wide source is a wide source with each point source having the same evaporation characteristics (*n* value). For predicting the deposition rate for the symmetric wide source the *n* value of four was considered for each point source.

For ease of analysis and because the predicted graphs for wide sources look similar to the single point source analogue, the differences in deposition rate between a single point source and the wide source case was examined, rather than plotting the deposition rate for each set of results. In order for this to be possible, the wide source results were normalised, i.e. the relative deposition rate to the point directly above the source (point with the highest deposition) was calculated. It follows, therefore, that both the single source and the wide source results had a deposition rate above the source of 100 and all the other values are the predicted deposition relative to this reference.

Table 8-3 illustrates the maximum differences found in the deposition rate for each case between the single point and wide source. The results from the wide source are less focused (higher deposition rate) than the single point source evaporator, the difference thus being positive. The minimum difference is zero, which occurs for the reference point (point directly above the source).

Table 8-3: Normalised maximum difference (%) between a single point source and a wide source.

Number of Sources (*s*)	Wide source radius (*r*)	Maximum difference of deposition (%)
7	1.2	0.81
	1.5	1.26
	1.8	1.81
13	1.2	0.87
	1.5	1.36
	1.8	1.96

The table above indicates how minimal the differences are between a single point source and the wide source geometry for the cases studied. The maximum difference predicted between these two geometries was just under 2% for the case when $s = 13$ and $r = 1.8$. A possible explanation is that the radius of the source (r) was too small when compared to the height of the substrate plane making the wide source behave similar to a point source. Also, minor changes to the source diameter (from 2.4 to 3.6) rendered a small variation in the overall deposition rate (around 1%).

To sum up, both the 7-point and the 13-point wide sources with a diameter up to 3.6 cm can be approximated to within 2% to a centrally positioned single point source. If the difference is higher than 2% the reasons may be because a bigger radius (r), a lower substrate plane, or more sources were used.

8.6.2. Asymmetric Wide Source

A wide source is asymmetric if at least one point source has a different evaporation characteristic (n value). With a computer model it is not necessary that each point source has an identical n value. Thus, it is also possible to model asymmetric evaporation behaviour, where due to the scanning pattern of the electron beam one part of the rod source behaves in a highly focused manner (say $n = 9$), while other areas give a more dispersed distribution of the vapour flux (say $n = 1$) (Figure 8-16).

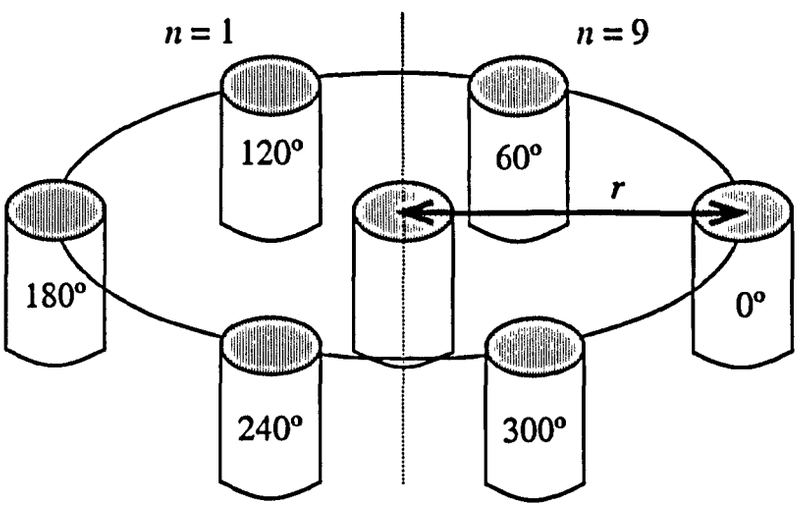

Figure 8-16: Schematic of an asymmetric wide source for $s = 7$.

It is widely accepted that the cosine formula does not describe the real case where, for instance, the source may be asymmetrical. In fact, theory predicts a constant thickness distribution in a horizontal plane above the source at any position swept out by the angle 0. However, the distribution of evaporant for an EB source is not constant over such a circle. Baghurst (1987) measured a higher deposition rate in a direction away from the position of the electron beam (Figure 8-17). A polar distribution of such profile in a plane above the source would be egg-shaped. Such an effect can clearly be accommodated and accurately modelled using an asymmetric wide source.

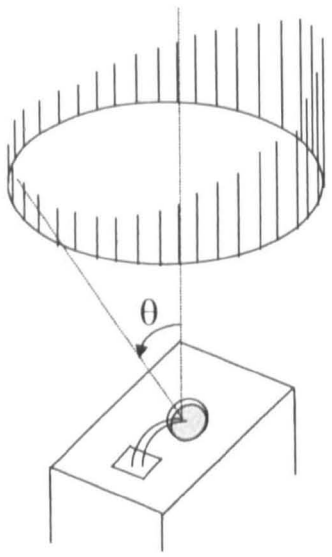

Figure 8-17: Diagram representing the distribution rate on a circle above the source (Source: Baghurst, 1987).

The model parameters studied were similar to the symmetric wide source (two wide sources, three radii, horizontal substrates, and height of the substrate plane, z = 15). However, as illustrated in Figure 8-16, the n value was not the same for all sources. The source in the centre of the wide source had an n value of 4 (as in the symmetric wide source). For s = 13 there are two point sources on the imaginary dotted line shown in Figure 8-17. One point source at 90° and the other one at 270° and their n values were 1 and 9, respectively.

All results were normalised and the differences between the asymmetric wide source and the symmetric analogue with all sources with n = 4 calculated. It is evident from Table 8-4 that the differences of deposition rate between asymmetric and symmetric wide sources can be higher than the differences between a symmetric wide source and a single point source.

Table 8-4: Normalised minimum and maximum differences (%) between asymmetric and symmetric wide sources.

Number of Sources (s)	Wide source radius (r)	Minimum difference of deposition (%)	Maximum difference of deposition (%)
7	1.2	–3.6	4.8
	1.5	–3.9	5.1
	1.8	–4.3	5.4
13	1.2	–3.8	5.1
	1.5	–4.1	5.4
	1.8	–4.4	5.7

Moreover, for some results the difference is negative which means that the asymmetric deposition rate is not always higher than the symmetric analogue. Figure 8-18, shows that the positive difference is mostly when $x < 0$ ("c" shaped contour, 4-6% band) which was expected since the less focused sources (with $n = 1$) were to the left of the centreline of the wide source (See Figure 8-16). In addition, the values with a negative difference are a small region (just 5 values) slightly to the left of the centre of the wide source (around $x = -5$, $y = 0$).

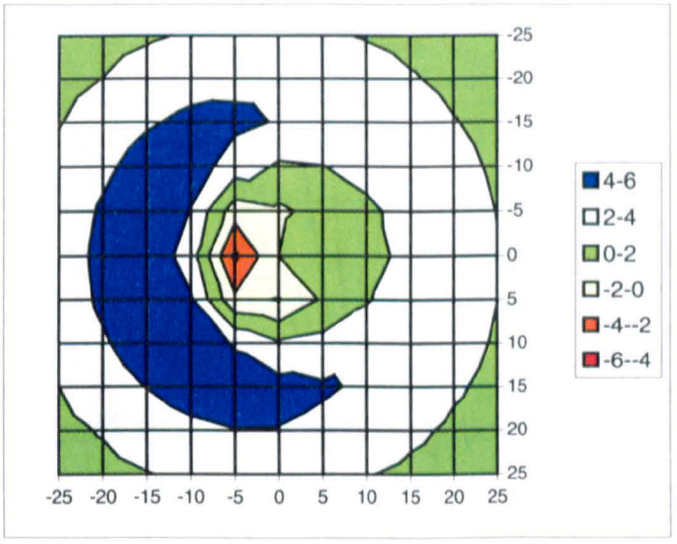

Figure 8-18: Differences in deposition rate between the asymmetric and symmetric wide source ($s = 13$, $r = 1.8$).

On the whole, if the difference between the maximum and minimum differences is considered, then a maximum difference between asymmetric and symmetric wide sources was around 10% for $s = 13$ and $r = 1.8$ (5.7 – (–4.4)). From the above, it can be seen that asymmetric wide sources may play an important role in the computer model in order to predict the deposition rate from substrates with complex geometry.

8.7. Multiple Sources

As discussed previously (See "EB Evaporators", page 77), a typical commercial coater has a multiple source arrangement usually linearly spaced as shown in Figure 8-19. The configuration is such that in order to have a higher degree of process control, the sources are equidistant. This configuration allows not only the deposition of alloys (the sources evaporate different materials), but also the evaporation of the same material from all sources thus increasing the evaporation rate (i.e. the component throughput).

Calculating the predicted deposition profile from such a configuration is seen as vital since most industrial coaters used for the aerospace coating industry have this configuration. However, in the open literature there are EB-PVD coaters with different configurations, such as a dual source coater (Sohn et al., 1994b) and a three-source coater (Movchan, 1996a). Notwithstanding this, the computerised model was used to

investigate a three-source evaporator. It is thought that the results from both the dual source and three-source coaters can be correlated.

In order to simplify the computer procedure, and because the symmetric wide source geometry investigated had little effect on the overall deposition rate, the multiple sources were modelled as single point sources (as opposed to wide sources). However, this multiple source arrangement can be modelled using both symmetric and asymmetric wide sources if the single point source is not accurate enough.

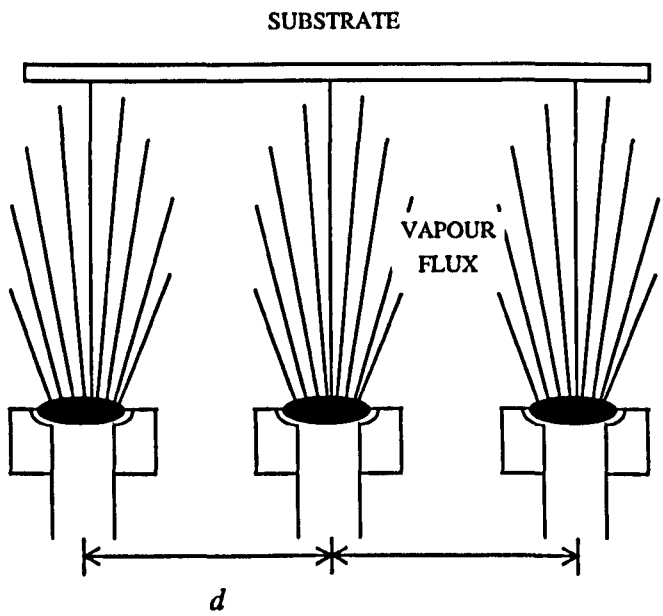

Figure 8-19: Schematic of a three-source evaporator (*d* = source separation).

The critical parameter that controls uniformity under multiple source evaporation conditions is the relative separation of the source (*d*) to the height of the substrate plane above the source (z). However, this is only true when the *n* value is known. Therefore, varying the *n* value was also important because it defines the focus of the evaporation plume hence affecting the overall uniformity for this type of geometry. The analysis was analogous to that used to predict the deposition rate for both the point source and wide-area source models. The model investigated a three-source evaporator at various distances (from 10 to 20) and for several heights (from 10 to 30). In addition, the effects of both horizontal substrates and inclined at 45° were also determined. For all configurations the *n* value was 5. In order to investigate the influence of the configuration on the distribution profile, various ratios were selected as shown in Table 8-5.

Table 8-5: Height of the plane and source separation used for the various ratios investigated.

Height of the plane (z)	Source separation (d)	Ratio ($\frac{z}{d}$)
10	20	0.5
15	20	0.75
20	20	1.0
25	20	1.25
15	10	1.5

Figure 8-20 summarises the uniformity distributions predicted, using the computer model, for the above aspect ratios. The stages of predicted deposition rate are as follows (for $n = 5$):

A ratio equal to or less than 0.5 produces a "W"-shaped profile typical of a configuration without or at least with little interaction between the sources. The sources are too far apart relative to the height of the plane not enabling thus the blending of the vapour flux prior to deposition (See also Figure 8-22a).

For a ratio of 0.75 and 1.0 there is clearly some interaction between the sources and the "W"-shaped profile is less noticeable, particularly for a ratio of 1.0.

A ratio of 1.25 produces a smooth profile with little variation in the deposition along the centreline. For the case studied ($z = 25$, $d = 20$) the difference between the maximum and minimum deposition rate was around 10% for x between –20 and +20 (See also Figure 8-22b).

Finally, for a ratio of 1.5 or higher the configuration behaves more like a single point source (or a 3-point wide source in this case) than as a multiple source arrangement. A ratio above 1.5 will allow even more blending of the vapour flux but at the expense of reduced deposition rate and reduced envelope size.

Various other ratios were analysed, for example 2.0 ($z = 30$, $d = 15$) and 1.33 ($z = 20$, $d = 15$) and, therefore, could have been included in order to explain the transition stages of the predicted deposition rate. Moreover, for a ratio of 1.0 two other configurations could have been used, z=d=10 and z=d=15 but with little difference from the results obtained.

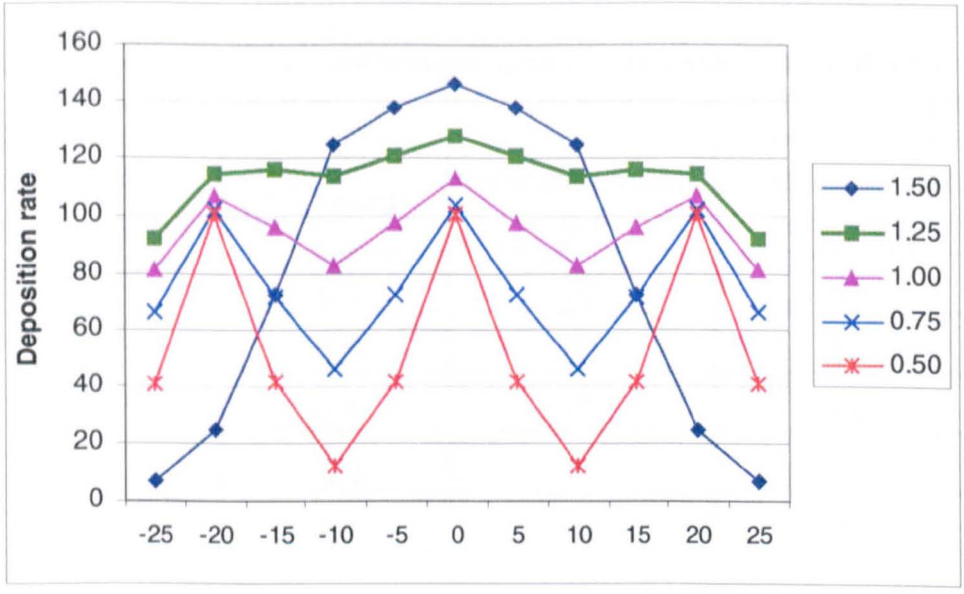

Figure 8-20: Deposition rate for various z/d ratios along the centreline (y = 0).

Worth noting is that all of the above applies only for horizontal substrates and for an n value of 5. From Figure 8-21, it is apparent that for constant z and d values, varying n yields differing stages of predicted deposition rate.

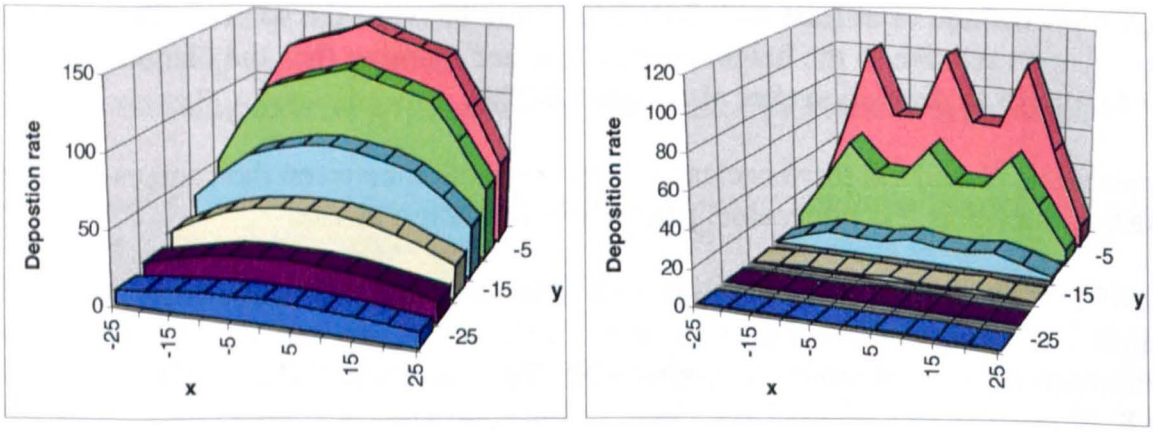

a) b)

Figure 8-21: Predicted deposition rate for a multiple source configuration both along and parallel to the centreline for z = 15 and d = 15 (a) n = 1 (b) n = 9.

In addition, the results of the effects of inclined substrates at 45° are correlated to the predicted deposition rate for the single point source already discussed. The peak deposition rate is displaced from the centreline of the evaporant sources. Moreover, the maximum coating thickness is reduced and the profile is not symmetrical in relation to the centre source.

In conclusion, Figure 8-22 illustrates the uniformity distributions predicted for $\frac{z}{d} = 0.5$ (Figure 8-22a) and $\frac{z}{d} = 1.25$ (Figure 8-22b) both along the centreline and parallel to the

centreline. Clearly, a ratio of 1.25, i.e. spacing three multiple sources apart, each by just less than the working distance, gives a much more uniform deposition profile, both directly above the source and parallel to the three evaporation sources.

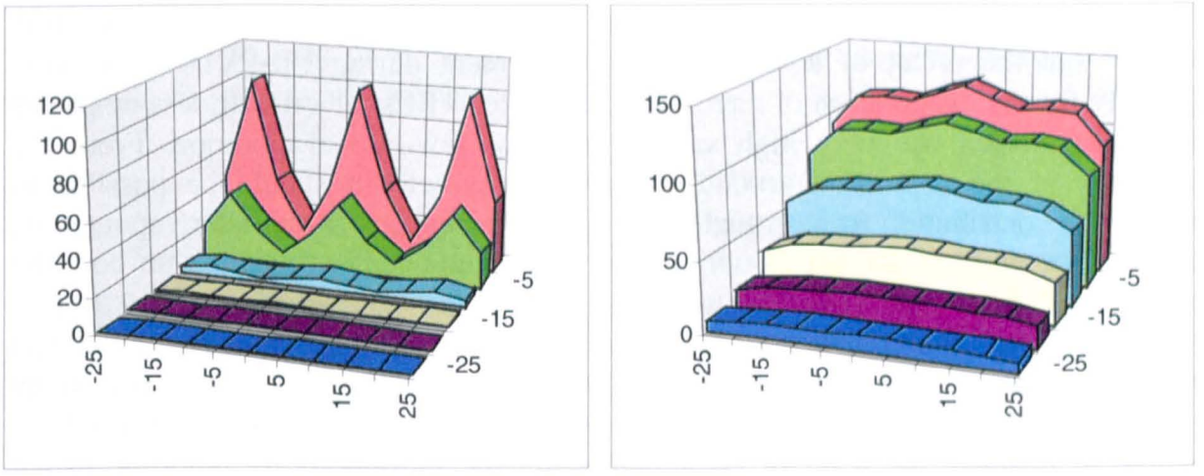

a) b)

Figure 8-22: Variations in deposition rate for a multiple source configuration both along and parallel to the centreline (a) $z/d = 0.5$ (b) $z/d = 1.25$.

This approach allows much closer working distances, while achieving uniform deposition, and thus permits greater component throughput, better yields and more simple planetary motion designs.

8.8. Virtual Sources

As was shown in the section "Theory of Evaporation and Deposition" (page 84), during high rate deposition a virtual omni-directional source will be generated in the vapour cloud immediately above the source due to the localised high vapour pressure. The associated pressure rise is due to the soft vacuum generated by the vapour stream and results in a lower mean free path. Graper (1971) showed that at deposition rates above 3 µm/min the chamber pressure may increase by one order of magnitude. Because the EB-PVD process can achieve deposition rates well above this value, it is necessary to consider the effect these virtual sources have on the deposition profile.

In addition, even though the EB-PVD evaporation source can be considered as a Knudsen point source evaporator, source characteristics vary with the material being evaporated, the shape of the source, and the geometry of the electron beam scan pattern. Schiller et al. (1982) (See Figure 6-3, page 88) described some of the effects that are likely to change the vapour distribution and which explain why the vapour flux deviates from the simple cosine distribution. These effects include the formation of a vapour cloud above the molten pool, which instead of the source surface, acts as a virtual source of the vapour stream. The "source" under these circumstances becomes an undefined region above the melt; evaporant appears to emanate from it, not from the melt itself. Moreover, the interaction between the electron beam and the vapour flux may also highlight the formation of a virtual vapour source generated above the melt pool.

In an appraisal of EB-PVD TBCs, Rigney and co-workers (1995) investigated the line-of-sight effects on a stationary cylinder. They demonstrated that even though theory does not predict a deposition on the hidden side of a stationary substrate, both a very thin fine-grained coating and a thicker porous coating was measured on the backside and at the tangency point of the stationary cylinder, respectively. From the above, it is apparent that the effect of a virtual source is present during EB-PVD evaporation especially for the evaporation of zirconia ceramics for TBCs, albeit with less emphasis for systems which use very high vacuum and for low-rate evaporation. From the knowledge of the deposition around a stationary cylinder it should be possible to estimate the contribution from virtual sources as a percentage of the main vapour flux. However, the work of Rigney is only descriptive – the coating thickness on both the backside and front side positions was less than 12 μm and greater than 230 μm, respectively, but other information such as the thickness at the tangency point and source-to-substrate distance were not specified. Notwithstanding this fact, this study aims at coating a stationary cylinder in a laboratory evaporator from which it will be possible to estimate the level of error that would be introduced by ignoring virtual sources. This is discussed in detail in section "Validation of the Computer Model" on page 157.

The soft vacuum present in certain localised regions is responsible for gas scattering (atom-atom collisions), hence particles deviate from their original trajectory. Moreover, theory would predict a constant thickness in a horizontal plane above the source at any position swept out by the angle θ. In fact, the distribution of evaporant for an EB source is not constant over such a circle. Baghurst (1987) measured a higher deposition rate in a direction away from the position of the electron beam. A polar distribution of such profile in a plane above the source would be egg-shaped. Even though this effect may be represented using an asymmetric wide source, more complex effects, such as the deposition on the backside of substrates, can only be accommodated by using a virtual source, which can be positioned anywhere in the vacuum chamber.

These source variations can be accommodated in the computer model by developing a generalised point source evaporation model that involves real and virtual sources operating in a 3D half space above the melt. It follows, therefore, that a computerised model not capable of predicting the deposition from virtual sources is only applicable, in theory, for a small-area evaporator and for low-rate deposition. For ease of use, no attempt was made to compensate for the atom-atom collisions. However, if the Knudsen point source model (and source characteristics studied, e.g. wide source and asymmetric effects) proved to be inadequate to model EB-PVD deposition, then the virtual source effects could be included in the model. In conclusion, the rate of coating deposition, and the direction of growth, at any point on a component surface depends on integrating the complex vapour flux distributions from all sources, both virtual and real, onto a predefined, surface element.

8.9. Validation of the Evaporation Model

The previous sections discussed the model for calculating the predicted thickness. This section discusses the equipment used to deposit a coating onto substrates and then

proceed to verify the model by calculating the thickness for experimental conditions and comparing it to those measured from physical experiments. Therefore, to validate the predictive capability of this computerised evaporation model a number of deposition trials using a laboratory EB-PVD evaporator were compared to the model predictions.

A detailed description of the specifications of the EB-PVD coater used for the physical experiments is given in Table 8-6.

Table 8-6: Specifications of the laboratory EB-PVD coater.

Volume	$\approx 0.3\ m^3$
Number of Sources	1
Source Diameter	38 mm
Source Height	20 cm
Pressure (upper chamber)	1×10^{-2} mbar
Pressure (lower chamber)	5×10^{-4} mbar
Gun Acceleration Voltage	10 kV
Current	0.6 A
Power	6 kW
Substrate Temperature	1000°C
Gas Flow	Ar-10%O_2 (50 cc/min^{-1})

A partially stabilised zirconia (ZrO_2-8 wt.% Y_2O_3) coating was deposited from ceramic ingots onto Nimonic 75 (N75) flat plates. The N75 substrates – an alloy of nickel, 20wt% chromium and 4wt% iron – were positioned in the chamber by using a 3D frame in order to allow the arrangement of the substrates at different heights and various angles of inclination. This allowed the vapour incidence angle (VIA) to be investigated. The value of VIA varies as the location of the substrate changes within the PVD chamber or the angle between the vapour flux and the substrate surface is varied.

All substrates were stationary and were coated at three heights within the chamber, distributed with inclinations of 0°, 30°, and 60° to the horizontal plane. Seven strips of N75 material were used: three at 0°, two at 30° and two at 60°. A total of 27 specimens were cut, mounted and polished to a few microns of roughness. In addition, a small reference sample was always placed directly above the source at the same height in all runs at 10 cm. This sample allowed the comparison of the deposition rate between runs regardless of the coating time allowed for each run. This was achieved by normalising all of the coating thickness samples using the reference sample.

For all specimens, the thickness was measured using the Leica Q500 MC Image Analysis system. This system comprises an optical microscope, a computer, a motorised stage, and a video camera.

All reasonable steps have been taken to ensure that all processing parameters were kept as stable as realistically possible. For example, the rod was raised from time to time in order to maintain a constant source-to-substrate distance. Deposition rates between 0.3 and 8 $\mu m/min^{-1}$ were achieved depending on source-to-substrate distance. The fractograph illustrated in Figure 8-23 is typical of the coating microstructures obtained in these coating trials for substrates directly above the evaporation source, showing the vertically oriented columnar microstructure expected for an EB-PVD TBC.

Figure 8-24 presents a comparison between the predicted and measured results. Agreement is exceedingly good over the range of deposition trials undertaken for the three working heights and three angles considered. From Figure 8-24 it is evident that within the Cranfield coater the evaporation source can be modelled using a point source evaporator to an accuracy of ±10%. Further improvements, of the order of around 2%, were possible by assuming a wide source geometry.

A measure of the 'goodness of fit' of these predictions is apparent from Figure 8-25. This figure plots a direct comparison between predicted and measured coating thicknesses irrespective of source-to-substrate separation or substrate inclination. The fit of the model to experiment is extremely good for the EB evaporation source used within this coater at Cranfield University for an n value between 4 and 5. A perfect fit would be the diagonal straight line, included in Figure 8-25.

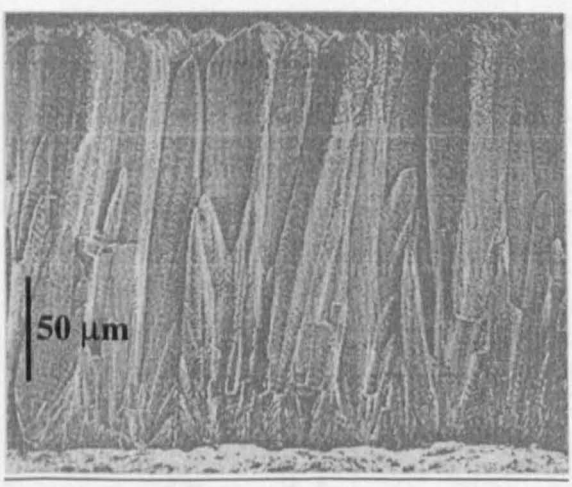

Figure 8-23: Fracture micrograph of an EB-PVD thermal barrier coating.

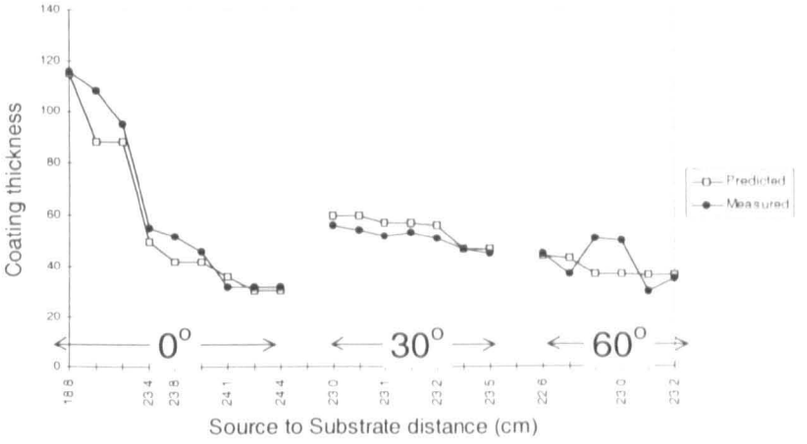

Figure 8-24: Comparison between measured and predicted deposition profiles.

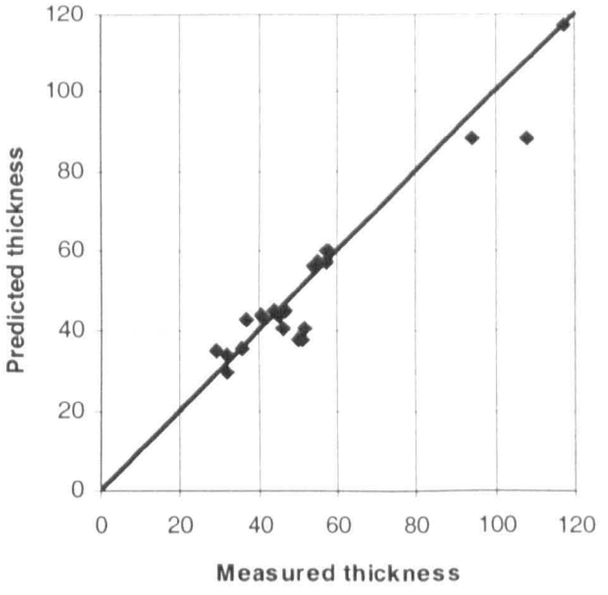

Figure 8-25: Scatter diagram demonstrating the "goodness of fit" of the computer model predictions and experimental results.

8.10. Conclusion

It has been shown that it is possible, using computer methods and a model for an ideal point source evaporator, to model the rate of deposition, and hence coating thickness, on any substrate positioned, and inclined, within a coater chamber. Substrate complexity does not invalidate the model assumptions, although calculations on very complex geometry would be computer intensive.

The model allows the characteristics of the evaporation source to be determined and permits the prediction of the thickness distribution for EB-PVD deposited ceramics on substrates with more complex geometry. Ultimately it should be possible to predict the

coating thickness profiles around aerofoil sections, as a function of the planetary motion of the component, although this has not yet been demonstrated.

One can foresee computer models, similar to that proposed, being used to design mask geometry and component planetary motion, allowing the custom profiling of EB-PVD TBCs onto aerofoil sections to achieve optimal thermal resistance and good erosion behaviour without compromising the aerodynamic performance of the turbine blade or vane. Other applications, where coating uniformity is critical to component performance, would benefit from the use of this software if the coatings are deposited by EB-PVD methods, for example, optical coatings on lenses and mirrors, and multilayered wear resistant coatings on cutting tools.

CHAPTER

9

9. Deposition Model

9.1. Introduction

As discussed in the section on the "Evaporation Model" on page 99, the computer model can simulate the behaviour of, and accommodate various source configurations. These include the theoretical point source evaporator, real source geometries including asymmetric evaporation behaviour that depends on the electron beam scan pattern, and the inclusion of multiple sources within a vacuum coating system. However, at this stage of the development the substrate was stationary and was always modelled as a predefined (its position was known and was specified in the code), small-area element (represented by a small triangle such that the coating thickness predicted for its centroid was representative of the whole area). It is clear, then, that this early model does not describe the real case where, for instance, the substrate has a complex aerofoil section, is rotated within the vapour cloud, and may additionally include fixtures specifically added to limit the vapour deposition on selected areas (shadow-masks).

From the above, it is evident that for application within the coating industry it is important that both the modelling of the source (evaporation model) and the modelling of the deposition onto rotated substrates with complex geometry is included. In order to understand the deposition process, the issues that characterise the EB-PVD coating of gas turbine components were analysed and identified as described in the next sections.

9.1.1. Substrates with complex geometry

The components that are to be coated with a TBC, either for increased component durability or for operation at even higher temperatures, vary in size and shape depending upon the application they are used for (aircraft, industrial, or marine gas turbines) and exactly where in the engine they are located. Due to their location, both the nozzle guide vanes (NGV) and rotating turbine blades of the first stage of the turbine part of the engine (immediately after the combustor), endure the highest stresses and are, therefore, more prone to damage from the degradation mechanisms of this harsh environment (creep, oxidation, thermal fatigue, etc.). The need to increase both the aerodynamic performance and strength of a blade is a continuing challenge for the turbine blade designers in the development of the engine. For instance, for increased performance both NGVs and blades have an aerofoil shape, and are "twisted" from root to tip with the blade stagger angle greater at the tip than at the root (Figure 9-1). The reason for this twist is to make the gas flow from the combustion system to do equal work at all positions along the length of the blade (Rolls-Royce, 1986).

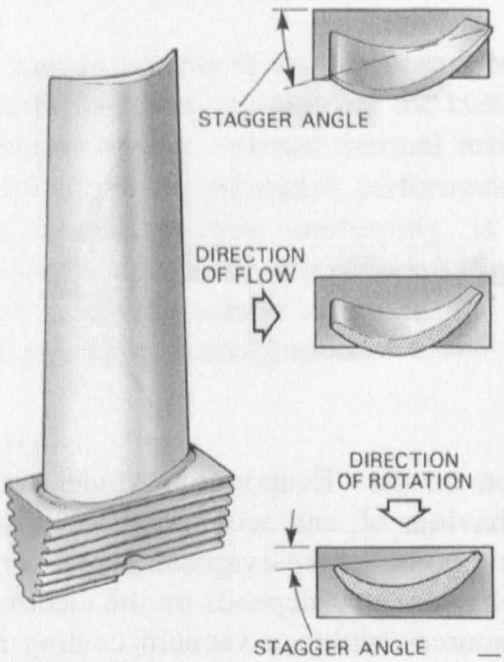

Figure 9-1: A typical turbine blade showing twisted contour (Source: Rolls-Royce, 1986).

The aerofoils used in advanced aircraft engines are made from some of the most complex and costly alloys known to man. They have a complex shape, with most turbine aerofoils having many small holes with a diameter between 250 μm and 1 mm. Therefore, predicting the thickness distribution across the whole surface is vital to reduce the large sums of money which could be wasted in scrap components.

9.1.2. The effect of shadow-masks

During deposition some areas of certain components are usually masked with fixtures specifically added either to limit the vapour deposition, or even to prevent the build up of coating. Therefore, attention must be paid not only to areas where coating is required, but also to areas that must be kept free of coating. For example, for aerodynamic purposes it is desirable to limit the thickness of these coatings on the trailing edge of the aerofoil components. According to Gill and Tucker (1986) in most cases prevention of coating deposition by masking is preferable to removal by, for instance, grinding. Currently, such masks are designed *ad hoc*, on a trial and error basis.

The ceramic layer thickness for a turbine blade varies typically between 150 and 350μm. However, coating thickness profile depends on various parameters and for a specific blade varies both longitudinally (along the surface) and transversely (across the blade). The coating at the trailing edge is usually the thinnest on the component while at the leading edge, due to the high temperatures of the impinging hot gas, the coating is at its thickness. Both the pressure and suction surfaces typically have thicknesses which are within this range (usually the suction surface requires a slightly thicker layer than the pressure surface).

From the above, it is clear that further research is required in the design of masks for use in an EB-PVD coating system, capable of limiting the undesirable deposition of coating on parts of a component. Good masking design can have a significant effect on the cost and efficiency of a coating operation. In conclusion, from the knowledge of the coating distribution, which may occur below non contact masks as a function of deposition conditions (evaporation rate and distribution, chamber pressure, etc.), it should be possible to design both the mask geometry and manipulation to produce any desired coating distribution. Equally, it should be possible to develop computer-based models capable of predicting mask performance, once the basic deposition behaviour, as modified by non contact masking, has been established. This programme of work aims to address these two issues.

9.1.3. Substrate Manipulation

In a line-of-sight process such as EB-PVD it is usually necessary to rotate, but is also common to tilt and/or translate the components within the vapour cloud in order for all surfaces to be exposed to the vapour flux. This can be achieved by using complex rotating carousels performing complicated movements to ensure a specified thickness distribution on all substrate surfaces is obtained (Teer, 1983). Several studies have investigated the influence of substrate rotation during deposition on the coating morphology and TBC performance. There is general agreement that, during coating deposition, defects are produced by shadowing resulting from the complex shape of the engine components being rotated in the vapour cloud (Boone et al., 1974; Boone, 1996). In addition, the columnar TBC microstructure can be widely varied by substrate rotation (Demaray et al., 1974; Rigney et al., 1995; Schulz et al., 1997a).

Even though substrate rotation is necessary to coat virtually all components, to the author's knowledge, there has been no published work to date on the predicted thickness distribution as a function of substrate geometry and speed of rotation, for example.

9.1.4. Cooling Holes Blockage

The EB-PVD coating process cannot coat internal cooling passages, as it is a line-of-sight process. However, small-diameter holes are partly blocked by the building up of coating at their entrance. Schulz and co-workers (1997a) argued that cooling hole closure is avoided with the EB-PVD coating process. Notwithstanding the fact that deposition by this process does not greatly interfere with hole closure, cooling air flow will be reduced, which may have a detrimental effect on the lives of the component.

An understanding of the deposition down cooling holes is far from complete but initial models to predict hole closure have been formulated. Several investigators have shown that the atom by atom nature of the EB-PVD process results in a rapidly, smoothly tapered coating at the hole entrance (Bettridge and Ubank, 1986; Rigney et al., 1995; Brown, 1996). Various approaches have been attempted to overcome this problem including drilling holes after coating, filling holes with wires during deposition, and over sizing holes but none have proven to be universally acceptable. More recently,

Thilloy (1999) has proposed a model to predict the thickness profile down the entrance of the cooling holes based on the Knudsen cosine law.

From the above, it is evident that an understanding of the EB-PVD deposition process onto turbine components must include the prediction of hole closure and the thickness profile down the hole as a function of hole diameter, inclination of the hole, source-to-substrate distance, and substrate rotation.

9.1.5. Inclination of the Columns

The growth direction of the columns influences the thermal conductivity of the TBC, but is a major factor in determining the erosion performance of the ceramic. The more inclined the columns are to the substrate's surface the less likely is it for them to remain intact against erosion and foreign object damage (FOD). Figure 9-2 shows the relationship between angle of inclination of the columns with respect to the substrate normal and erosion rate.

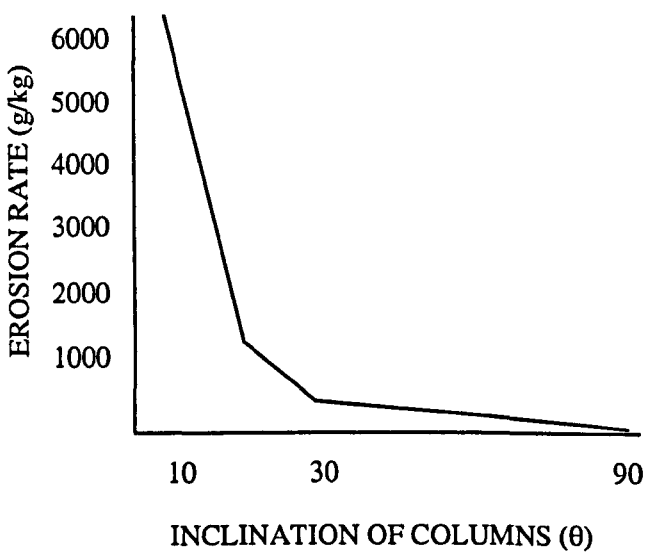

Figure 9-2: Influence of column inclination on the erosion resistance (Source: Nicholls and Deakin, 2000).

From Figure 9-2 it is clear that the ceramic columns should grow perpendicular to the substrate's surface for optimum performance. However, for rotated substrates a "beaded" or "c"-shaped structure of the columns is formed due to the continuous change in the vapour incidence angle, and the amount of vapour particles that arrive on the surface during each revolution (Demaray et al., 1981; Rigney et al., 1995; Schulz et al., 1997a). Nonetheless, the macro growth pattern should be perpendicular to the substrate's surface.

9.1.6. Cluster of Blades

To be economic, the coating industry must coat multiple blades per coating session. One approach is to coat clusters of blades and this is actively being pursued by coating

usually two, three, or four blades as a group. This is important because it not only increases the throughput of the coating equipment, but also reduces unit coating cost. The ideal arrangement of the cluster is such that the blades limit the deposition on the trailing edge of other blades (act as a shadow-mask) whilst not masking the leading edge of the component. One solution is the position of, for instance, identical blades in a circle each at 120° (for the cluster of three blades) with their trailing edges pointing to the centre of the circle and their leading edges pointing away from the centre of the imaginary circle (Figure 9-3).

The computer model should allow for this arrangement to be investigated by predicting the modification in coating thickness as a function of the distance of blades from the centre of rotation and speed of rotation.

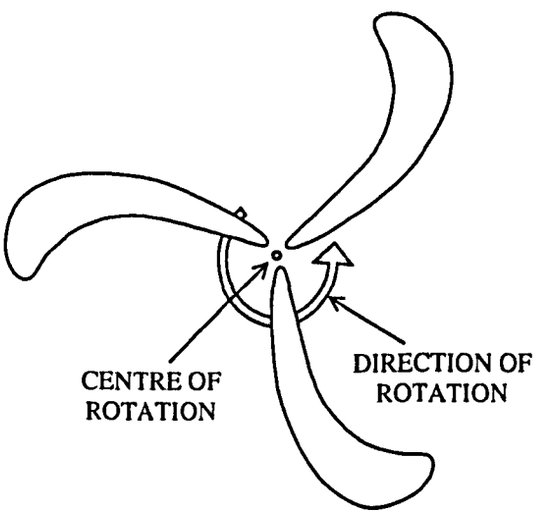

Figure 9-3: Schematic representation of a cluster of blades (Source: Compiled by the author).

9.1.7. Conclusion

From the above, it can be seen that modelling the deposition requires, firstly, an accurate representation of the component, and secondly, a suite of procedures to accommodate substrate rotation, which may have shadow-masks, and to visualise the predicted results, for instance.

Since the development and understanding of the coating process was defined as an integral part of this project and in order for the computer model to accommodate the modelling of the substrate, the development of procedures capable of achieving the requirements described above were investigated as explained below.

9.2. *Modelling Substrates with Complex Geometry*

9.2.1. CAD-dependent Application

Substrates with complex geometry such as engine components, in general, or turbine blades, in particular, are designed using CAD packages. However, there appears to be no dominant standard CAD package currently in use by the industry for the design of turbine blades. All CAD packages have advantages and disadvantages of one form or another and engine manufacturers may even use more than one CAD system during the various stages of designing and manufacturing a component. Some of the most well known CAD systems include, but are not limited to: AutoCAD (www.autodesk.com), CATIA (www.catia.com), SDRC IDEAS (www.sdrc.com), EDS Unigraphics (www.ugsolutions.com), and MicroStation Modeler (www.bentley.com).

CAD systems are becoming increasingly sophisticated and comprehensive tools covering the whole of the manufacturing process. For example, some CAD systems may allow the interaction between the many available tools (sometimes known as modules) and user-defined procedures. This is important when CAD engineers require to calculate or analyse certain aspects of the part for which the CAD system does not provide tools or modules. This usually occurs in very specific areas when the aim is to tailor a CAD system to the specifics of a particular application. For instance, AutoCAD uses a programming language called AutoLisp, which is part of the CAD system.

From the above, it is evident that one way of modelling substrates with complex geometry was to use a CAD package that allowed user-defined procedures (created using a programming language or a script language) to interact with the CAD system. On the one hand, procedures to "read" the geometric information of the part would be developed, in addition to modelling the asymmetric behaviour of the source, and the multiple-source configuration, for example. On the other hand, the CAD system would determine the visibility of each "point" from the source, which could be altered by a shadow-mask, and also perform the rotation and translation of the substrate. This solution has the advantage of not only using the CAD system to visualise the results, but also of using procedures that already have been written to move and/or rotate the substrate, and to determine the visibility for any position of the substrate based on code that has been tested and optimised. However, there are also drawbacks of using a specific CAD system to develop the computer model. The biggest disadvantage of such solution is the fact that because there is no dominant CAD system anyone interested in using the computer model would have to have that specific CAD system. In addition, the programming languages provided by the CAD packages are not as mature as other general purpose programming languages, e.g AutoLisp is not an object-oriented programming (OOP) language.

Despite the fact that some CAD packages have their own programming language to enable an interface between the user-defined needs and the package's modules, a solution which would be CAD-independent would be more useful. One approach to achieving this could be to develop a self-contained software tool by creating all the necessary procedures, e.g. substrate rotation, evaluation of whether the point is visible, prediction of the thickness distribution, and visualisation of the results. In conclusion,

this tool would read the part's geometry stored in a file, which could be created using a CAD system, and rely upon the developed procedures in order to manipulate the part and simulate the coating process. However, because all procedures would have to be created, i.e. the software tool would have to be developed from scratch, encompassed a twofold disadvantage. First, the fact that having to develop procedures such as substrate rotation, which have already been developed for other applications may be regarded as "reinventing the wheel". Not only would the procedures be slower than those that have been optimised; they would also have to be carefully tested. Moreover, developing such a project from scratch, i.e. planning, designing, coding and testing all procedures to model the substrate, was not a viable solution within the time allocated for this project.

A far-reaching solution, in addition to contributing to a faster development, was thus the upgrade of the evaporation model to include graphics capability by using a suite of functions already developed which could be embedded in the existing computer program. If these procedures did all the necessary graphical operations (visualising, rotating, etc.) then this solution would be a self-contained tool (CAD-independent). Two possible solutions have been considered and their advantages and limitations are discussed below.

9.2.2. Developing a CAD-independent Application

One way of developing a CAD-independent application was to use a standard computer graphics package (suite of graphics commands) such as PHIGS (programmer's hierarchical interactive graphics system) or OpenGL (GL stands for Graphics Library).

PHIGS is a system of routines for creating graphical structures, which was popular at the beginning of 1990s for Unix-based applications (Wisskirchen, 1990; Howard et al., 1991; Hopgood et al., 1992; Blake, 1993). The use of PHIGS is usually associated with the use of X-Windows and MOTIF. X-Windows is a suite of routines that provide the underlying functions that can be incorporated in any program requiring the use of windows, menus, icons, and mouse control. However, X is a set of low-level routines that are difficult to use for creating an application. One example of a higher-level windowing system based on X is OSF/MOTIF (Open Systems Foundation). MOTIF is a proprietary windowing system that provides the user with the functionality needed to create a graphical user interface. The major disadvantages of using X, MOTIF and PHIGS include:

- Both the Unix operating system and workstations are relatively expensive;
- Developing an application using X-Windows is difficult;
- MOTIF is only one of many available windowing systems based on X (although one of the most commonly used);
- PHIGS is not popular in the PC domain. In addition, it is not maintained and is not as mature as other graphical interfaces.

OpenGL is a "software interface to graphics hardware" (Wright and Sweet, 1996; Woo et al., 1997). It is a relatively new industry standard for high-quality 3D graphics applications. It is designed, maintained, and enhanced by the OpenGL Architecture Review Board (ARB) and is available on a variety of hardware platforms and operating

systems, including Microsoft Windows 98 and Windows NT, IBM's OS/2, DEC's AXP and OpenVMS, and X Windows (Fosner, 1997).

OpenGL is a 3D graphics and modelling library, which consists of about 150 distinct commands, that programmers use to specify the objects and operations needed to produce interactive 3D applications. Some of the advantages of OpenGL include, but are not limited to the following:

- Widely used and supported across different platforms (hardware-independent);
- Orders of magnitude faster than ray-tracing since it uses carefully developed and optimised algorithms;
- Can be used with other graphics interface such as the Windows GDI;
- Possibility of using shading, lighting, hidden surface removal, and texturing (similarly to PHIGS);
- Maintained by an independent group which includes representatives of the major software companies (DEC, IBM, Intel, Microsoft and Silicon Graphics).

If a program is OpenGL-based it means that it was written in some programming language (such as C or C++) that makes calls to one or more OpenGL libraries. It does not mean that the program uses OpenGL exclusively to do drawing. It may combine the best features of two different graphics packages. Therefore, it is possible to use OpenGL for only a few specific tasks and environment-specific graphics (such as the Windows GDI) for others.

The advantages of using OpenGL as far as this project is concerned can be summarised as follows (many are also available in PHIGS):

- All models, or objects, are constructed from a small set of geometric primitives - points, lines, and polygons – that are specified by their vertices;
- Provides routines for modelling transformations (moving and rotation);
- The possibility of combining the "depth buffer" and lighting functions to test for hidden surface removal and vertices' visibility;
- The use of "display lists" which allow to record OpenGL functions calls (and their results) and play them back at a later time thus improving performance;
- The use of the "feedback mode" to extract information from OpenGL about how a scene would have been rendered;
- The use of the "selection mode", which enables interaction with the scene.

From the above, it is evident that the use of OpenGL provides the preferred solution. In addition, using OpenGL allowed the possibility to start modelling straight away using software that had already been extensively tested. Shadow masking can easily be accommodated if the CAD system generates a file with the geometric information of both the substrate and the shadow-mask.

In conclusion, the design of the software tool was based on the following steps:

1. Read the geometric information of the part from a file, which can be created by a CAD package;
2. Manipulate the part using OpenGL commands. The graphical functions provided by OpenGL allows the specification of the objects and operations needed to produce interactive 3D application;
3. Calculate the coating thickness;
4. Visualise the results.

From the above, one last aspect which needs to be investigated concerns the evaluation of the best file format (data file) that can be used to store the geometric information of the part and then be read by the computer program in order for all the modelling to be performed.

9.2.3. On the Best File Format for Data Exchange

CAD packages usually have a proprietary method of storing data (saving the part). However, different CAD systems can share data by using what is known as a neutral file format. According to Eastman (1988) and Wix (1989), from the many available file formats, two are considered to be the common standards for data exchange between CAD packages. They are IGES (initial graphics exchange specification) and STEP (standard for the exchange of product model data). There are, however, some disadvantages of using these formats as far as the scope of this work is concerned. The main problem is that they are far more comprehensive, and therefore complex, than what is needed, including layers, symbols and attribute data, which are not necessary for the computer model. In addition, understanding either file format, in order to extract the geometric information of the part, is both arduous and time-consuming.

Since the modelling of the evaporation (source characteristics) represented substrates with simple geometry as a small triangular surface, it was found that a file format already exists which uses triangular facets to represent a 3D model. This file format is widely used by the Rapid Prototyping (RP) industry. RP is the fabrication of a physical 3D part from a numerical description by a highly automated and flexible process. These 3D models contribute to greater knowledge of both the product performance and specifications earlier in the development cycle. A discussion of the RP industry and the various existing systems, and the technology and equipment is given elsewhere (Lart, 1991; Nathanael, 1993; Ribeiro, 1995).

The file format used by the RP industry is known as STL (Stereolithography) and represents the part entirely as a mesh of triangles and their surface normal. It complies with the 3D Systems Company requirements, as well as other companies in the rapid prototyping industry (Unigraphics, 2000). However, differences do exist in the STL generators (known as CAD/STL translator) i.e. CAD vendors have implemented variations to the standard STL file. Nonetheless, due to the importance of the RP industry most CAD packages have a CAD/STL translator, including, but not limited to:

AutoCAD (www.autodesk.com), CATIA[5], PTC CADDS5 and PTC Pro/ENGINEER (www.pct.com), SDRC IDEAS (www.sdrc.com), Microstation Modeler (www.bentley.com), EDS Unigraphics (www.ugsolutions.com), SolidWorks (www.solidworks.com, www.solid-works.com), and SolidDesigner (www.cocreate.com).

Worth noting is that while both the IGES and STEP file formats try to handle the data without any information loss, STL does not, as this file format is an approximation of the solid. The parameter controlling this approximation is known as tolerance. Tolerance determines how close the straight-line sections of the model can deviate from the actual curves of the part itself. In other words, it represents the maximum distance from the facet to the part's surface. The smaller the deviation, the more accurate the prototype. However, there is one drawback when decreasing the tolerance (i.e. when making the triangles approximate the solid closer), that is, as the deviation is decreased, the size of the STL file increases exponentially, and all calculations require much more time. Therefore, to obtain the best performance possible, the largest triangulation tolerance possible to meet the application needs should be used. The possibility to specify a tolerance value was confirmed to be available in both EDS Unigraphics and SDRC IDEAS but it is thought that all CAD packages have this parameter to generate an STL file. The lowest tolerance possible for EDS Unigraphics was found to be 0.0025 mm (0.0001 in).

When creating an STL file it is usually possible to specify either a text file (ASCII file) or a binary file, the latter being a more compact and efficient form but which requires more translation in order to understand it. For simplicity, the ASCII file was adopted since the data is in text format. During the creation of the STL file, the CAD package triangulates the surface of the component with all the edge vertices matching, and creates the file with the following information (for each triangle):

- The surface normal, which points to the outside of the surface, represented by the vector components X, Y, Z;
- The surface itself represented by the three vertices of the triangle (X, Y and Z co-ordinates).

Table 9-1 is the STL text file representation of a 25 cm^2 square flat plate, 20 cm above the origin. The STL file represents all numbers in scientific notation, as follows: each value has the form "[–]d.dddde[sign]ddd" where *d* is a single decimal digit, *dddd* is one or more decimal digits, *ddd* is exactly three decimal digits, and *sign* is + or –. For example, the number 25 is represented as 2.500000e+001. From Table 9-1 it is evident that a flat plate is represented by two triangles, with their "front sides" visible by the source, for this example (the surface normal, which points towards the outside of the surface, is the vector (0,0,-1)).

[5] www.catia.com, www.catiasolutions.com, www.catia.ibm.com

Table 9-1: STL file of a 25 cm^2 flat plate, 20 cm above the origin (source).

```
solid flatplate
  facet normal 0.000000e+000 0.000000e+000 -1.000000e+000
    outer loop
      vertex    -2.500000e+001   2.500000e+001   2.000000e+001
      vertex     2.500000e+001   2.500000e+001   2.000000e+001
      vertex     2.500000e+001  -2.500000e+001   2.000000e+001
    endloop
  endfacet
  facet normal 0.000000e+000 0.000000e+000 -1.000000e+000
    outer loop
      vertex     2.500000e+001  -2.500000e+001   2.000000e+001
      vertex    -2.500000e+001  -2.500000e+001   2.000000e+001
      vertex    -2.500000e+001   2.500000e+001   2.000000e+001
    endloop
  endfacet
end solid
```

The CAD/STL translator creates the minimum number of triangles for a given tolerance. Therefore, a rectangular surface, regardless of size, is always represented by two triangles. This is important because, for example, the suction surface of a turbine blade is nearly flat, particularly the area near the trailing edge, and may, therefore, be represented with too few triangles in order to represent the coating thickness distribution accurately. However, using computer functions, it is possible to overcome this limitation by using a triangle interpolation routine (see "Tessellation Menu" on page 143 for more information about producing a finer mesh, i.e. subdividing the triangles into groups of smaller triangles).

In conclusion, the biggest advantage of the STL file format is that it contains the minimum information necessary to accomplish the objectives of this study, i.e. the surface normal, which is important to determine the visibility of each facet, and the surface of the component, represented by triangles. In addition, STL text files do not require translation in order to understand the data. This made the problem simpler allowing the programmer to concentrate on the information that was really necessary.

9.2.4. Putting everything together

Several new concepts "emerged" when moving from modelling a source (or evaporation) to modelling a substrate (or deposition). One very important feature, as seen previously, is that the "new version" of the computer model should have graphics capability. For example, visualising the component, although not relevant to the modelling capabilities since all calculations can be performed without anything being shown, can be in fact of great significance as it allows the user to control the position and inclination of the component. Another noteworthy aspect is visually rotating the component as it is being coated. This aspect can show the point and vector along which

the model is being rotated enabling the user to fully understand the whole process. These two examples explain the usefulness of having graphics capabilities.

From the description of the EB-PVD process applied to gas turbine components, seen previously, the following goals of the computer model were identified:

- A simple user-interface to allow casual users to operate the software;
- The possibility of defining the geometry of the substrate with ease (STL file);
- Routines to allow the positioning and/or rotation of the substrate to the desired location within the coater space;
- Interactively show the configuration (position and inclination of the substrate relative to the source);
- Allow the study of both stationary as well as rotating components;
- Easy-to-understand method of plotting the deposition rate for showing the predicted results.

In order to provide the software with a simple user-interface, easily operated by both casual and advanced users, the flexibility, availability of related packages, and the use of the Windows operating system for development and deployment was dictated. At this stage it was important to decide on the programming language and the necessary routines to use to accommodate extensions (i.e. upgrades) in order to tackle the geometric information of substrates such as turbine blades.

Visual C++ was (and still is) a widely used programming environment which can make full use of the Windows graphics device interface (GDI) and which allows the manipulation of graphics routines. Moreover, it is a highly portable, resilient and robust language, with translators available in many different systems and on many platforms. Object-oriented analysis and programming (OOA, OOP) is now widely used as it addresses a large number of problems that arise during software development providing viable and practical solutions. In addition, by using OpenGL functions within the computer model, the simulation of all the issues that characterise the deposition of EB-PVD TBCs could potentially be modelled. Other programming languages such as JAVA were not sufficiently developed, albeit having solid foundations, especially concerning the object-oriented issues.

The next section discusses the software tool developed, how it is used to predict the thickness profile around any component, and its advantages and limitations.

CHAPTER

10

10. Description of the Computer Program

10.1. Introduction

As mentioned previously, a stand-alone computer program was developed for experimental evaluation. This section describes what the computer program does and how it is used to predict the thickness distribution around a stationary or rotated substrate. An example using a turbine blade illustrates the steps necessary to use the program.

The computer program was developed using Microsoft Visual C++ 5.0. It is compatible with both the Windows 98 and Windows NT operating systems. There are no requirements concerning the hard disk; however, even though the screen display can be of any resolution (800×600 or above preferred), only a high colour palette (16-bit, 65536 colours) or a true colour palette (24-bit, 16 million colours) will display the substrate adequately. This is important because lighting effects and thickness distribution are represented as a colour gradient, which cannot be adequately represented using, for instance, 256 colours. For ease of use, an effort was made to retain the look of the typical Windows application, i.e. similar menu bar structure, toolbar with commands most used, dialog boxes, buttons, etc. with similar behaviour to the "standard" Windows program.

The computer program comprises a single executable file and when the program is launched the geometric information of a substrate can be opened using the File/Open command. After opening a file, the substrate can be subdivided into smaller triangles to achieve a finer mesh, moved and/or rotated to anywhere in the "vacuum chamber" and then the thickness profile calculated either for a stationary or rotated substrate. In order to study the effects of shadow masks, both the geometric information of the substrate and the shadow masks should be included in the same STL file. Figure 10-1 shows the menu bar and toolbar of the software tool. The following sections explain in detail the computer program.

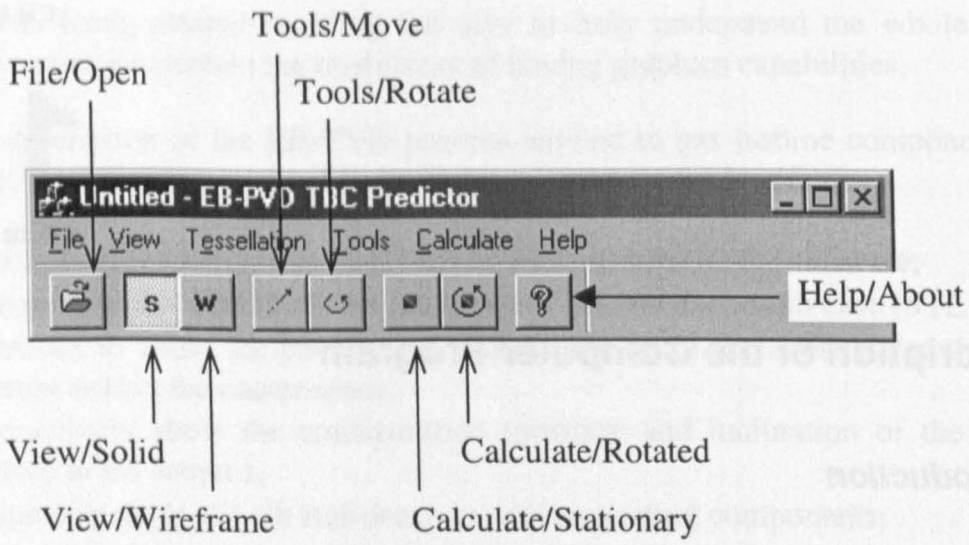

Figure 10-1: Menu bar and toolbar of the computer program.

10.2. File Menu

When the program is launched only the File menu is active. This is because the first step must be opening an STL text file, using the Open command. The selection of text format is performed within the CAD package, when generating the STL file. The STL text file can have any extension (but usually "stl" or "txt") and contains the geometric information of the substrate (and the shadow mask if used).

When opening a file a typical Windows open dialog box similar to the one shown in Figure 10-2 appears. By default, the dialog box shows files with extensions "stl" and "txt". This can be changed to display only "stl" files, only "txt" files, or all types of files.

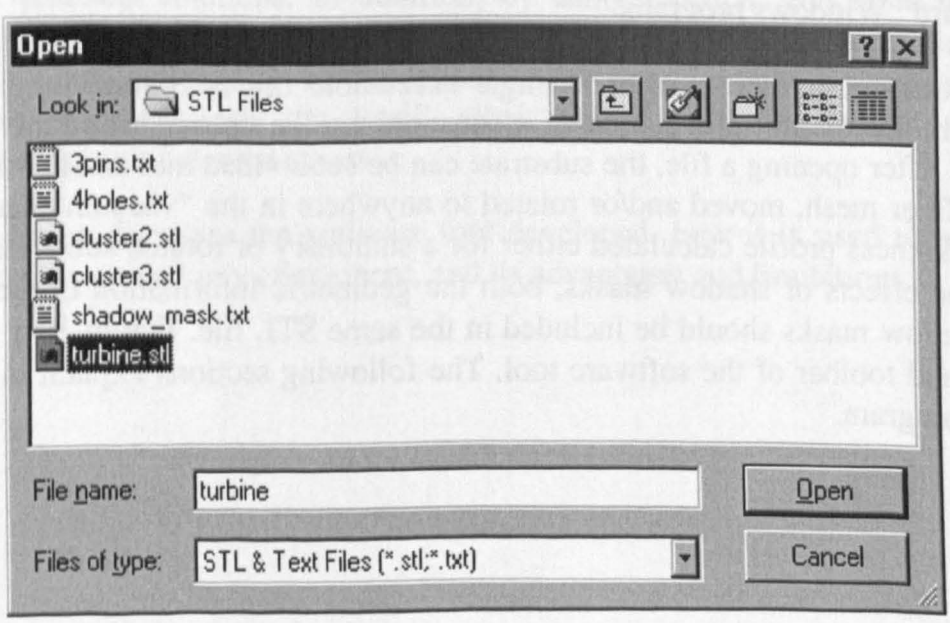

Figure 10-2: Open dialog box

Once the file has been selected the data is read and stored in memory and a solid representation of the model will automatically be displayed in the display area. The file "turbine.stl" contains the geometric information of a turbine blade. Therefore, a solid representation of this file is shown in the display area, as can be seen in Figure 10-3.

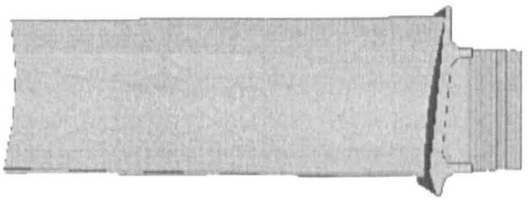

Figure 10-3: Geometric information of a turbine blade (file "turbine.stl").

Worth noting is that the centre of the 3D coordinate system (0,0,0) is the reference for all vapour source arrangements. For a single source the source is actually in the centre of the coordinate system; for a wide source it is the source in the centre of the wide source, and for a multiple source arrangement it is the middle source which is in the centre of the coordinate system. For this reason, the substrate in the modelling process should be located above this position prior to creating the STL file or, by using the Tools menu explained later, moved or rotated to the desired location, above the source within the coater space.

Consequently, in order to assess the position of the substrate relative to the origin of the coordinate system, it is possible to view the substrate from various angles by manually changing the location from which the model is viewed, using the mouse. By clicking with the left mouse button anywhere on the display area and dragging the mouse horizontally or vertically, the substrate is rotated around the y-axis (vertical axis) or the x-axis (horizontal axis), respectively. In addition, it is also possible to rotate the substrate around the z-axis, which points towards the viewer, by pressing the "Ctrl" key and then clicking and dragging the mouse horizontally (Figure 10-4). From Figure 10-5 it is possible to see the effect of rotating the substrate around the x, y and z axes by approximately 90°. All these rotations do not move the substrate relative to the origin: what is being rotated is the location from which the model is viewed. Moving and rotating the substrate relative to the source is discussed in the section "Tools Menu" on page 145.

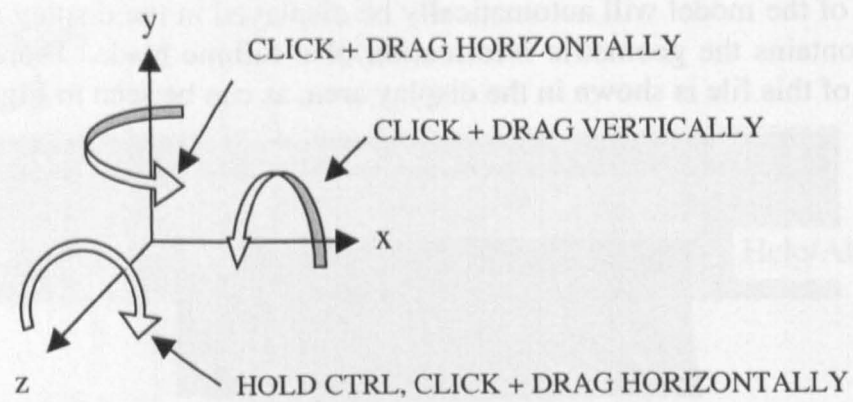

Figure 10-4: 3D coordinate system used by OpenGL and rotation of the component around each axis.

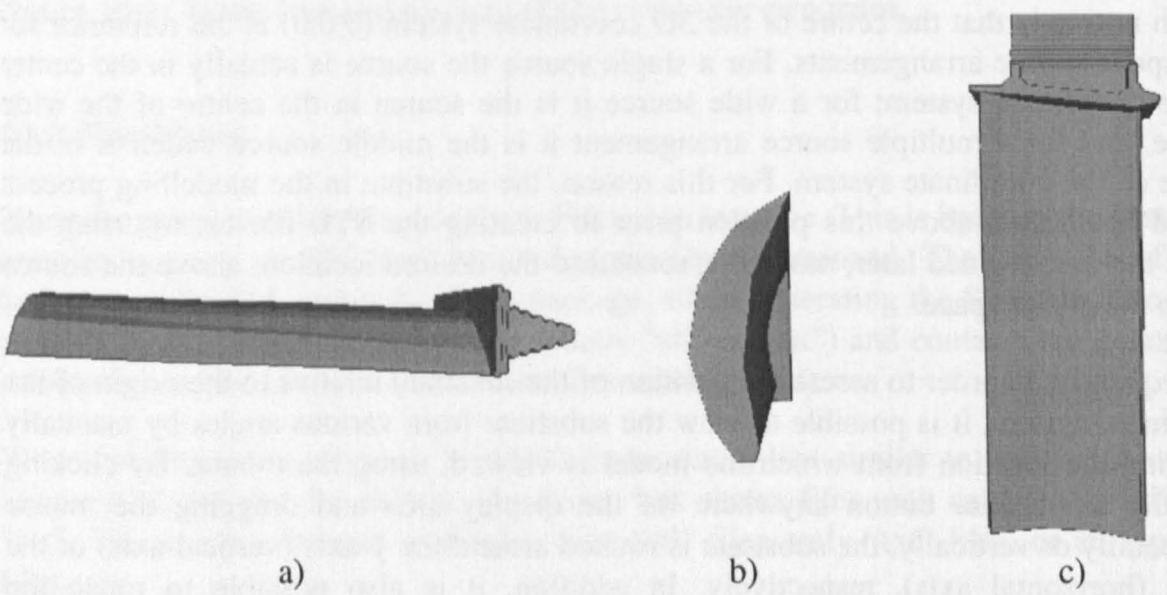

Figure 10-5: Turbine blade rotated manually by approximately 90° around each axis a) x-axis, b) y-axis, and c) z-axis (original position is shown in Figure 10-3).

From the File menu it is also possible to save the substrate using the "Save As" command. As explained later in the section "Tools Menu" on page 145, it is possible to move or rotate the substrate relative to the origin. This allows, for example, rotating the substrate and/or moving it to another position within the chamber and then analysing the results without having to create a new STL file for various distances. The "Save As" command saves the current geometric information of the part with the same or a different file name. In addition, the saved file may contain a finer mesh than the original by using the Tessellation menu, which will be explained later on page 143. The saved file is an STL file in text format, which, therefore, can be read again by the computer program. When saving the file, an extension "stl" or "txt" must be included in the filename in order for the file to be shown with the default file extensions.

10.3. View Menu

The View menu contains various commands that control how the substrate is displayed on the screen. Firstly, it is possible to toggle between "Solid" and "Wireframe". The default is Solid, which displays the substrate as a 3D solid. The previous figures of the turbine blade are all solid representations of the actual component. In addition, it is also possible to visualise the substrate as a set of triangles as shown in Figure 10-6. This command enables the user to interactively control the number of triangles that are used to represent the component, in this case an aerofoil component. From Figure 10-6 it is apparent that the pressure surface has relatively few and long triangles compared to the root part of the component (the triangles in the root are so small it appears as a solid). By analysing the number of triangles in critical areas such as the leading and trailing edges, the user can decide to increase the number of triangles to obtain a finer mesh. One way of achieving this is by using a CAD package to create the component with a lower facet deviation from the actual part, thus improving the model accuracy. However, if the component is made up of flat or nearly flat surfaces, using a lower facet deviation may not yield an increased number of triangles, which may be desirable in order to study the thickness variation in more detail. For example, a square, regardless of size and of the facet deviation used, is always represented with only two triangles. This is why visualising the number of triangles and allowing their number to be increased is important.

Figure 10-6: Turbine blade represented as a wireframe.

Other commands available from the View menu operate as follows:

- "Normal View". When the solid is manually rotated (See Figure 10-5) the original location from which the substrate was viewed is lost. However, it is possible to restore the original view by selecting "Normal View". This would display the substrate as shown in Figure 10-3.
- "Visible Facets" calculates, for a stationary substrate, which facets are visible from the source and only displays the visible facets.
- "All Facets" shows the whole component with all facets, for instance, after the "Visible Facets" command has been used.
- "Toolbar" and "Status bar" display or hide the toolbar and the status bar, respectively.

10.4. Tessellation Menu

Tessellation is a term used in OpenGL which means the break down or subdivision of complex objects into simple convex polygons (Woo, 1997). Within the computer

model, tessellation denotes the subdivision of each facet (triangle) into groups of smaller triangles, thus increasing the number of points for which the thickness will be calculated.

When creating an STL file using a CAD package it is possible to specify a parameter known as tolerance or absolute facet deviation (see page 135 for a detailed discussion of the STL file format). This gives the maximum distance from the facet to the part's surface (however, as discussed previously, as this value is reduced, the size of the STL file grows exponentially, and all calculations will require much more time). Therefore, choosing the facet deviation from the part itself is a compromise between speed (computing time) and accuracy of the model. Moreover, when the component surfaces can be approximated to flat surfaces the number of triangles needed to represent the surface are less than for more complex surfaces. For instance, a cube, regardless of size and of the facet deviation used, is represented with only 12 triangles (two per side); in this case the STL file is an exact representation of the actual part. However, few triangles may not be accurate enough to represent the thickness variation in critical areas such as the leading edge of a turbine blade. In the example of a turbine blade seen previously, both the pressure and suction surfaces are represented with relatively few and long triangles whereas the root of the component, which is usually masked to prevent deposition, contains a large percentage of all triangles. In conclusion, an STL file is an approximation to the part's surface. Therefore, when modelling nearly flat surfaces, each surface will be represented by as few as two triangles and this may not be adequate to represent the thickness distribution on that surface. That is why functions to tessellate the component were included in the computer model.

The default value for the tessellation is "1×", which means that each triangle that is read from the text file will be represented as a triangle on the screen. The Tessellation menu only allows the number of triangles to be increased from that specified in the text file. The other available options are: "2×", "3×", "4×", and "6×". Figure 10-7 shows a wireframe view of the turbine blade with six times as many triangles as the "original" file, which is represented in Figure 10-6.

For simplicity, each time a tessellation is selected, the procedure reopens the file and tessellates each triangle according to the chosen value. If, for example, the component is repositioned i.e. moved or rotated (as explained in the next section) and then tessellated, the effect of the move or rotate commands is lost. In other words, the selection of the tessellation value should take place before moving or rotating the substrate, or if the substrate is repositioned, the file saved and then opened before selecting a tessellation value.

In order to increase the tessellation value above the sixfold limit, the following steps should be taken:

1. Open the file;
2. Increase the tessellation to a value different than "1×";
3. Save the file using the same or a different name;
4. Open the file just saved (the number of triangles created per triangle in the file will be the square of the value used, for instance, the use of "6×" yields a tessellation of 36).

When tessellating a long triangle into, for instance, two smaller ones it is important that the centroids of the two smaller triangles are as far away as possible. If the two triangles are created by using a median from the shortest edge to the opposite vertex, then the centroids of the triangles will be relatively close thus not improving the spatial resolution of the thickness distribution. Therefore, the tessellate command calculates the longest edge and then divides the triangle by "drawing" a median to the opposite vertex.

In conclusion, if speed and memory use are of no concern, then the more triangles used the finer the mesh of thickness distribution produced. However, to obtain the best performance possible, the largest triangulation tolerance possible to meet the application's needs should be used.

Figure 10-7: Turbine blade represented as a wireframe with each triangle from the file represented as six smaller ones.

10.5. Tools Menu

The "Tools Menu" consists of two commands, the "Move" and the "Rotate" commands. These commands do not change the location from which the substrate (which can include a shadow-mask) is viewed; instead they change the substrate position relative to the source, hence modifying the thickness profile.

If a shadow-mask is used, then both the substrate and the shadow-mask behave as a single component. Using the "Move" or "Rotate" commands, moves or rotates both the shadow-mask and the substrate. This is discussed in more detail in "Advantages and Limitations" on page 152.

The "Move" command allows the substrate to be moved relative to its current position. This allows various substrate arrangements to be studied without the need to create an STL file for each substrate location. For instance, the effect of a substrate directly above the source or offset from the centreline, or at various source-to-substrate heights on the thickness distribution can be studied. The move dialog box (Figure 10-8) shows the minimum and maximum values for the x, y and z axes, and the user can enter the increment or relative distance (positive or negative) by which the component will be moved. From Figure 10-8 it can be seen that the minimum value for the z-axis is 5 units which means that the substrate is too close to the origin of the coordinate system (or source). Therefore, the substrate needs to be moved further away from the source, for instance another 100 units above the source. As mentioned earlier, units are typically expressed in centimetres but any other unit of measurement can be used (for example, inches).

The "Field of View" parameter controls the angle of view in the x-z plane; its value must be in the range [0.0, 180.0]. In other words, it allows the user to zoom in and out whenever the substrate appears too small or too large, respectively. In addition, it can also be used to analyse the coating thickness for individual facets as discussed in "Calculate Menu" on page 147. The bigger the angle the smaller the image will appear on the screen.

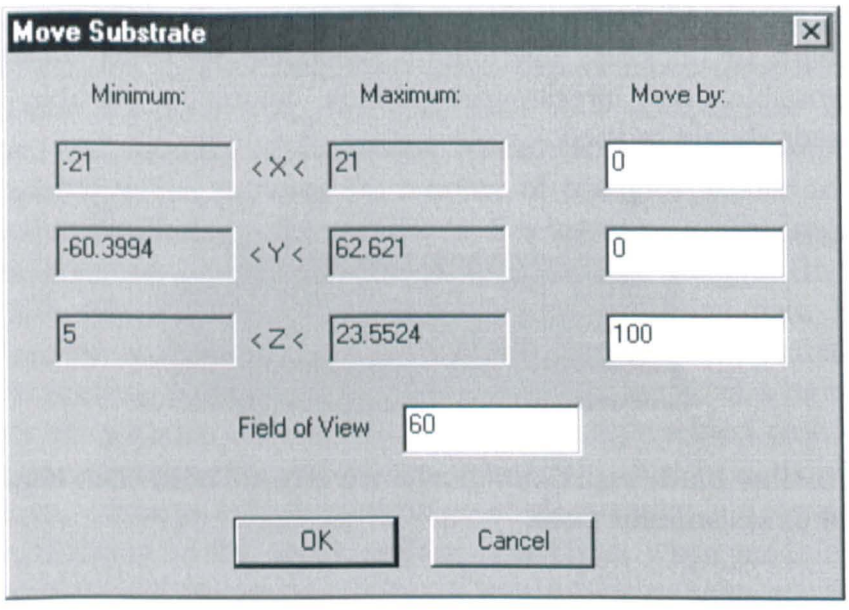

Figure 10-8: Move dialog box.

The rotate command can be used not only to define the position of the substrate when calculating the thickness distribution for a stationary substrate, but also to define the initial inclination when calculating the thickness distribution of a rotated substrate. The parameters controlling the rotation of the substrate are the angle of rotation in degrees, the point of rotation and the vector around which the substrate will be rotated. For a rotation around the origin the point of rotation should be (0,0,0). Figure 10-9 shows how to rotate a substrate by 90 degrees around a vector 60 units above the source and parallel to the y-axis.

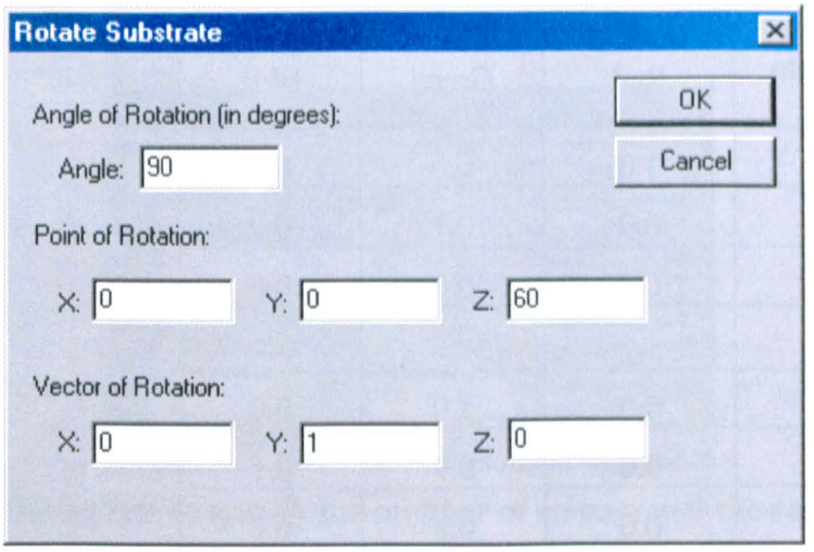

Figure 10-9: Rotate dialog box.

10.6. Calculate Menu

The Calculate menu computes the thickness distribution profile for the whole component, either stationary or rotating, and then represents the thickness with different colours.

The convention for colour used is similar to the colour gradients used by a CAD or finite element analysis tool to represent, for instance, stress distribution or surface temperature. The computer program sets the colour of each facet by specifying three components: red, green, and blue (RGB). The range of values is typically between zero and 255 for each component. In addition, a percentage range between 0.0 (zero intensity) and 1.0 (full intensity) is also common. For example, the colours red, green and blue are specified as a percentage by the ternary components (1.0, 0.0, 0.0), (0.0, 1.0, 0.0), and (0.0, 0.0, 1.0), respectively. The program represents coating thickness, therefore, by mapping the predicted coating thickness distribution to various colours.

In order to assess the coating thickness for each facet and because gradient colours can lead to confusion, the number of colours used to plot the thickness distribution can be varied from 2 to 20 colours. For simplicity, the thickness distribution is visualised as a percentage of the maximum deposition rate. All calculations are normalised such that the maximum deposition rate is represented as 100. Table 10-1 shows the relationship between the colour intensity (for each RGB value) and the deposition rate associated when using 20 colours. Figure 10-10 illustrates the actual gradient colours produced. Because the surface temperature of the component decreases with increasing coating thickness, the higher the red value the thinner the coating (hotter surfaces). Conversely, the higher the blue value the thicker the coating (cooler surfaces).

Table 10-1: Deposition rate v RGB Colour.

Deposition Rate (%)	Red	Green	Blue
0 – 5	1.0	0.0	0.0
5 – 10	0.9	0.1	0.0
10 – 15	0.8	0.2	0.0
...	...	...	...
50 – 55	0.0	1.0	0.0
55 – 60	0.0	0.9	0.1
60 – 65	0.0	0.8	0.2
...	...	...	...
95 – 100	0.0	0.0	1.0

Moreover, it is also possible to select a deposition range to plot by specifying both the minimum and maximum percentages of the deposition rate. For example, to visualise the whole substrate the range must be 0 to 100. However, other ranges may be visualised. For instance, it is possible to visualise only the facets with a deposition rate equal to or less than 50% or the facets with a deposition rate equal to or above 50%. Both the number of colours and the plot range, regardless of calculation type (stationary or rotated), are specified by using the dialog box shown in Figure 10-11.

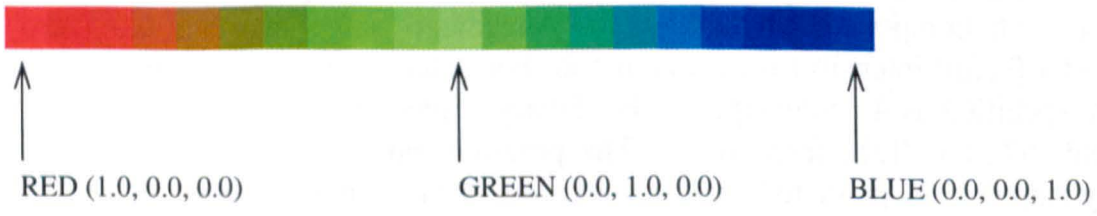

Figure 10-10: Colour gradient used to represent coating thickness.

Since both the number of colours and the plot range can be varied, it is evident that Table 10-1 only applies when 20 colours and the whole range (0-100%) are selected. From the above, it is apparent that the exact mapping of the colours to the deposition rate varies according to the parameters used. The deposition range represented by each colour is thus a function of the number of colours and the plotted range. For instance, if two colours are chosen to plot the full range of deposition thickness (from zero to 100%) then facets with a deposition rate between zero and 50% will be red and facets with a deposition rate above 50% will be blue; if twenty colours are used then each colour will represent a 5% deposition range, as shown in Table 10-1. From the above, it is evident that the colours used to represent coating thickness are relative to the range selected. In addition, the computer program always uses colours that are furthest apart,

i.e. if two colours are used then it is red and blue, if three colours are used then it is red, green and blue, and so on.

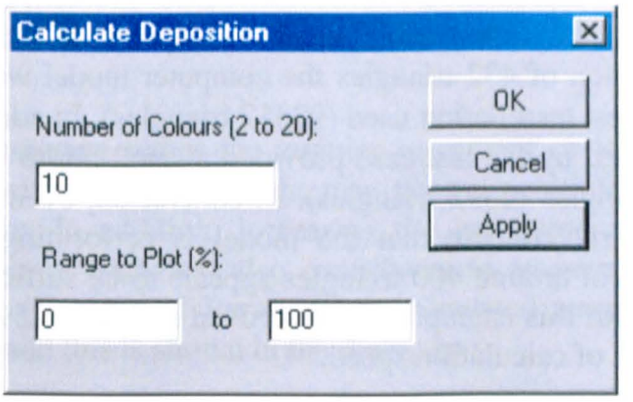

Figure 10-11: Dialog box to specify the number of colours and the range to plot.

In order to test whether the computer model was performing all calculations correctly, a flat plate (25 cm^2) was positioned 20 cm directly above the source (using the computer model) and the thickness profile calculated for the stationary component. The original STL file contained only two triangles and was created using Unigraphics (see Table 9-1 on page 137 for the STL file generated). The number of triangles was increased first to 72 (2×6×6) and then to 432, 2592, 15552, and 93312 (72×6×6×6×6). The result of the predicted thickness profile is shown in Figure 10-12 (the source is represented as a small dot in the centre of each figure):

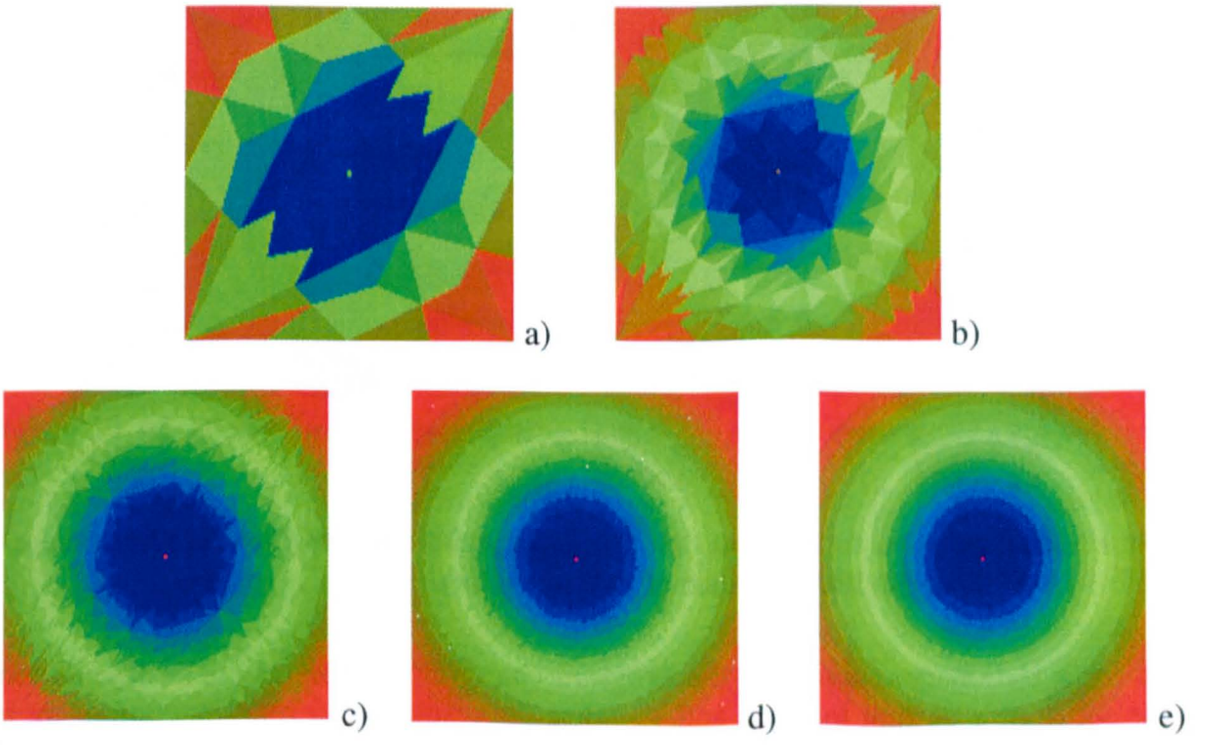

Figure 10-12: Predicted deposition rate for a stationary flat plate with various number of triangles a) 72; b) 432; c) 2592; d) 15552; e) 93312.

From the above, it is evident that the minimum tessellation used (72 triangles) does not provide enough accuracy to represent the circular symmetrical contour plot typical of a

stationary, flat component. With a sixfold increase in the number of triangles (Figure 10-12b) the circular symmetrical plot is represented reasonably well, even though the concentric circles are not represented. A smoother colour gradient is clearly possible, as shown especially in the last two cases, but at the expense of calculation speed. For example, for a tessellation of 432 triangles the computer model was around 200 times faster than for the highest tessellation used (93312 triangles). In addition, the smoothest colour gradient generated by the last case provided a small improvement over surfaces with relatively few triangles (2592 triangles). In conclusion, even though the last two cases investigated clearly confirm that the model is performing all calculations as expected, a tessellation of around 400 triangles appears to be sufficient to represent the thickness distribution, for this example. For improved accuracy 2592 triangles could be used, but at the expense of calculation speed.

After confirming that the computer model was predicting the thickness distribution for this simple case correctly, the turbine blade component was used in order to investigate the modifications in thickness profile onto a stationary component with a complex geometry. Figure 10-13 illustrates the results for the suction surface, which was facing the source, using ten colours. While Figure 10-13a represents all facets, Figure 10-13b and Figure 10-13c represent the facets with a deposition rate between 0 and 50% and between 50 and 100%, respectively. It can clearly be seen that, for this example, the coating exhibits a gradient in thickness from the leading edge to the trailing edge.

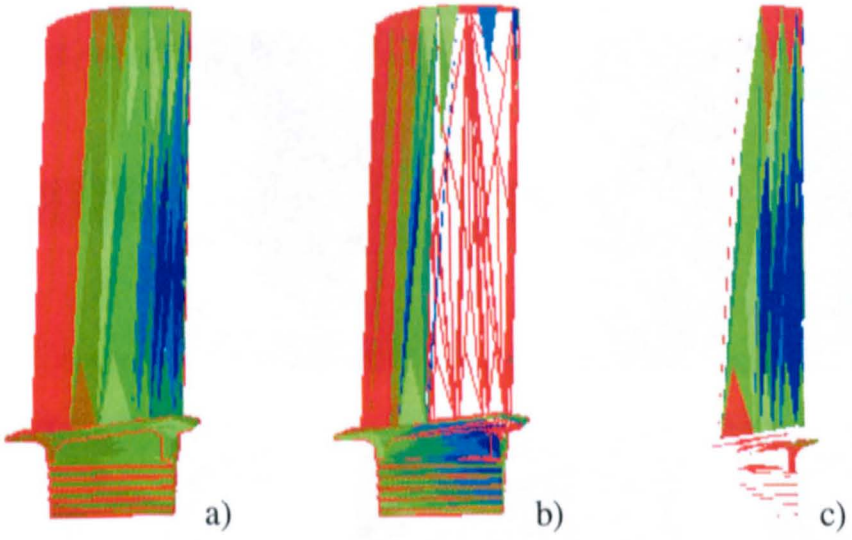

Figure 10-13: Predicted deposition rate for facets with a deposition rate between a) 0-100% b) 0-50% c) 50-100 (number of colours = 10).

While for a stationary component the program can compute the thickness distribution for the substrate's current location and visualise the results, for a rotating component it is necessary to enter some parameters such as the angular increment and the point and vector of rotation (Figure 10-14). This aspect of the calculation is computer intensive. As an example, for a turbine blade to give a reasonable accuracy, as can be seen in the example plotted in Figure 10-3, some 600 triangles were required. Rotation involves 72 iterations per rotational axis (5° increments). Thus, for a rotational speed of 6 r.p.m. and a deposition of a 240 μm coating at 6 μm per minute, calculation of the coating

thickness profiles will take just under 10 million iterations for a single axis of rotation. Each iteration involves calculating the new element position, determining whether the element is visible and then, if so, calculating the incremental increase in coating thickness. It is this visibility issue that is critical in the optimisation of shadow mask positions.

It is evident that decreasing either the angular increment or the deposition rate per minute, or increasing either the speed or the maximum deposition, increases the number of iterations necessary. In addition, increasing the resolution of the substrate mesh (increasing the number of triangles) also contributes to an increase in the number of iterations. This value (Number of Iterations) is calculated automatically each time a parameter is changed and this is shown in the dialog box.

Figure 10-15 illustrates the predicted thickness profile for a rotated substrate. For this example, the substrate was rotated in 15 degree increments for 24 iterations (360 degrees). From the above it is evident that the thickness distribution is a function of the location of the substrate, angular increment, and both the point and vector of rotation.

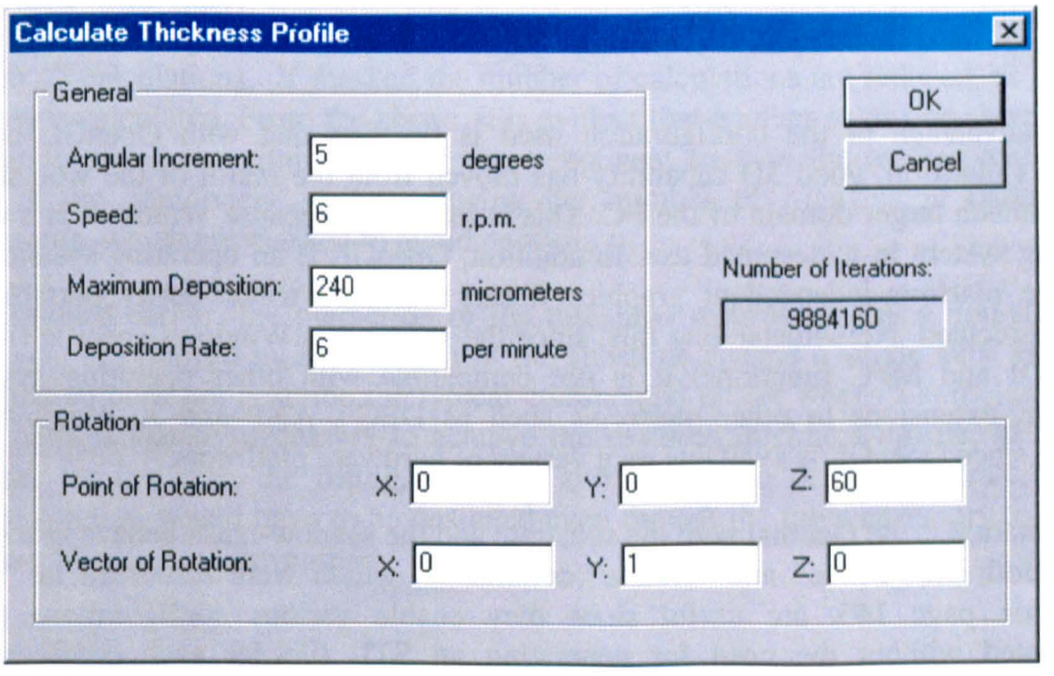

Figure 10-14: Dialog box for calculating thickness profile onto a rotating substrate.

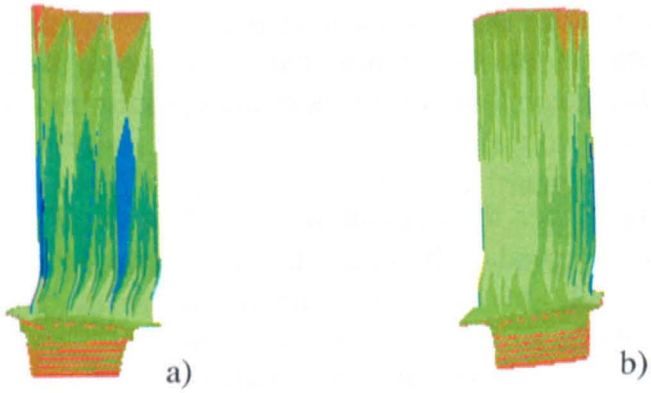

Figure 10-15: Predicted deposition rate for the rotated substrate a) pressure surface b) suction surface.

10.7. Advantages and Limitations

All computer models, without exception, have advantages and limitations of one form or another.

A first advantage of the configuration used is the fact that with OpenGL on the Windows platform, good 3D capability has moved from the realm of the workstation into the much larger domain of the PC. This is important because Windows is a cheap operating system in widespread use. In addition, OpenGL is an operating system- and hardware platform-independent graphics library designed to be easily portable yet rapidly executed. Notwithstanding this, since the software is Windows-specific (it uses both GDI and MFC functions) it is not compatible with other operating systems. However, extensions to other platforms such as DEC's AXP and X Windows are possible since OpenGL is available on a variety of hardware platforms.

One limitation is the fact that both the substrate and the shadow-mask behave as a single entity. Both the "Move" and "Rotate" commands, which were discussed in "Tools Menu" on page 145, are useful since they enable various configurations to be investigated without the need for generating an STL file for each configuration. However, another significant feature in allowing a higher degree of control of EB-PVD-deposited TBCs is the study of the effect of the shadow-mask on the thickness distribution. This is achieved by varying the position of the shadow-mask relative to the substrate in order to optimise the thickness profile. Therefore, an improvement of the computer model should allow the shadow-mask and the substrate to be moved or rotated independently. However, different substrate/shadow-mask arrangements can be studied by generating various STL files from within the CAD system. In addition, this limitation can be partly overcome if the geometric information of both the substrate and shadow-mask are in separate files allowing the shadow-mask to be moved or rotated using the software tool. The new position could then be saved to a different file. The file with the new shadow-mask position and the substrate could then be joined into a single file using a text editor thus enabling the combined arrangement to be analysed.

Another limitation of the computer model is that STL binary files are not recognised and thus cannot be read. Even though binary files are a more compact and efficient format, they require some translation in order to understand the data. However, the recognition of binary files by the software represents only a small advantage in the overall capabilities of the software tool. More important limitations concern the use of the tessellation menu and improving computer speed, as described in the following paragraphs.

Firstly, the choice of a new tessellation value overrides the Tools command. That is, if either the "Move" or "Rotate" commands from the Tools menu are executed and then a new tessellation chosen, the new position or inclination of the substrate will be lost since every time the tessellation command is executed the file is read from the hard-disk. In order to overcome this limitation, the choice of the tessellation value should take place before moving or rotating the substrate.

When executing a tessellation command, all triangles, without exception, are tessellated. This means that, for instance, the root part of the component, which is usually represented with many triangles due to its complex shape, but which is normally masked to avoid deposition, will account for a relatively high percentage of the time to perform all calculations. If masked the number of calculations are reduced, as only the visibility is calculated. From the above, it is evident that another extension should allow the user to tessellate certain areas of the component such as the leading and trailing edges of the component whilst reducing the number of triangles in parts of the components, which are masked to avoid deposition.

As mentioned earlier, the prediction of the thickness distribution for a non-stationary component is achieved by the rotation of the substrate around a single axis. However, this situation does not describe the typical commercial coater where a complex motion of the parts is usually necessary to achieve the required thickness profile. In order to simulate, for instance, the tilting, rotation, and translation of the substrate, a user-specific solution would have to be designed even though the tools necessary to achieve this have already been developed.

10.8. Improving Speed

This section discusses and describes issues concerning extensions to the computer model in order to improve the computational speed.

Complex models may require thousands of triangles to be represented accurately. As discussed earlier, it is usually possible to specify how much the straight-line sections of the STL file deviate from the actual curves of the part itself (usually known as tolerance or absolute facet deviation). As this value is decreased, the model is more accurate but the number of triangles needed to represent the part increases rapidly and all calculations take longer. Therefore, the first method to obtain the best performance possible is to use the largest triangulation tolerance possible to meet the application's needs. This ensures that the minimum number of triangles is used. However, nearly flat surfaces can be represented with very few triangles while more complex areas need relatively more triangles. This can be seen in the wireframe view of the turbine blade

(Figure 10-6): both the pressure and suction surfaces of the component are represented with relatively few and long triangles while the root part contains many triangles, which are not going to be coated. Therefore, another method to increase speed is by using a model without root and tip or the casting model, which represents the root as a lump of material, hence requiring less triangles.

As stated before, each iteration involves calculating the new element position, determining whether the element is visible and then, if so, calculating the incremental increase in coating thickness. In order to avoid wasting time by repeatedly calculating whether each element is visible, the model could create an array of 72 positions (one for each 5° increment) as follows: each array position would contain a list of pointers to the visible facets for that iteration. That is, position one of the array contains a list of the visible facets for the initial substrate position, position two contains the visible facets for the substrate inclined at 5°, position three the visible facets for the substrate inclined at 10°, and so on. The computer model would then only have to calculate the incremental increase in coating thickness for all the identified array elements (eliminating the time-consuming visibility issue). At run completion the total coating thickness for each element would be the values stored in the array of facets. This solution dramatically increases speed but at the expense of a small penalty in memory. However, computer memory does not appear to be a major problem due to its low cost.

Yet another method to increase speed, albeit probably the most complex solution is the use of parallel processing. Parallel processing has been defined by many authors such as Jones (1988), for example, as "a technique for increasing the computation speed for a task, by dividing the algorithm into several sub-tasks and allocating multiple processors to execute multiple sub-tasks simultaneously". De Bakker (1989) argued that parallel processing was the most promising answer to meeting the computational performance goals of many tasks. For many specific applications within numerous areas, it is possible to improve performance almost linearly by making use of a "transputer", a microprocessor with integral memory. A detailed discussion of parallel computing is beyond the scope of this work; however, this subject has been discussed in detail elsewhere (Siegel, 1985; Desrochers, 1987; Carling, 1988; Brain, 1988; Fleming, 1988; Mariani, 1988; America and Rutten, 1989; Freeman and Phillips, 1992).

In this study, no ordering is required by the algorithm when calculating the incremental increase in coating thickness for all the facets. Since each of the calculations is independent of the others, they could each be executed in parallel. The use of parallelism or concurrency offers the possibility of a significant increase in the performance of the computer model. Notwithstanding this fact, it would most likely mean having to rewrite some of the code into another computer language capable of concurrency. However, as noted by many investigators, parallel processing is still difficult to implement. Therefore, the previous method (creating an array with 72 positions) would be simpler to implement in different machines and would dramatically increase the performance of the software.

In conclusion, the methods to improve speed can be summarised as follows:

- Use the largest triangulation tolerance possible;
- Use a model without root and tip or the casting model, which represents the root as a lump of material. Alternatively, masking the root improves speed as only the visibility issue is performed;
- Extend the model to use an array of 72 positions. Each position contains a list of pointers to the visible facets for each iteration thus eliminating the time-consuming visibility issue;
- Extend the computer model to take advantage of parallel processing.

CHAPTER

11

11. Validation of the Computer Model

11.1. Introduction to the case-studies

As highlighted in the section on the "Deposition Model" on page 127, the issues that characterise the coating of gas turbine components include shadow-masks, substrate manipulation (rotation and translation, for example), cooling hole blockage, and the coating of clusters of blades. The case-studies chosen analysed the above issues by gradually increasing the complexity of the model. For instance, stationary cylinders were investigated first, then rotating cylinders, and then a cluster of three rotating cylinders. In addition, the effect of shadow-masks as well as cooling holes blockage were also investigated. All of the investigations were directed at determining the feasibility of predicting coating thickness, and column inclination, from a set of evaporation and deposition conditions. They are briefly described in the following paragraphs and in detail in separate sections.

Firstly, the thickness profile around an 18 cm long, 12 mm-diameter stationary cylinder, positioned at two heights, was investigated (Run I). This study should indicate whether one of the major assumptions was valid, and if so, to what extent. The assumption in question concerns the fact that particles undergo a line-of-sight transition. Therefore, for a stationary cylinder, the arc facing the source should receive coating, whereas the back of the cylinder should be free from coating. Moreover, it is also possible to analyse the column inclination as a function of angular displacement.

Run II analysed a cylinder positioned horizontally and with the same diameter as Run I, but this time rotated around its longitudinal axis. By rotating a cylinder at a constant speed (20 r.p.m. was used) a uniform coating would be expected.

Run III aimed at determining the effect of thickness variation on a cluster of three rotating cylinders, positioned longitudinally in a circle at an angular separation of 120°. This run studied the decrease in deposition rate as a result of the shadowing effect. The diameter of the cylinder, the rotational speed, and the point of rotation were the same as run two.

Run IV investigated the thickness profile on two flat plates, one acting as the component the other as a shadow-mask, rotated above the melt pool.

Run V evaluated the coating build up and the thickness profile down cooling holes. This is important because hole blockage reduces cooling air flow, which may have a detrimental effect on the life of the component.

For Run VI two turbine blade sections were coated using commercial equipment and an attempt was made to study the measured and predicted coating thickness for various locations on the component.

A detailed description of the specifications of the laboratory EB-PVD coater used for the physical experiments was given in Table 8-6 on page 123.

11.2. RUN I (Stationary Cylinders)

As discussed in the evaporation model, one assumption made was that the particles undergo a line-of-sight transition (see "Simplifying Assumptions" on page 99). Investigations to study the effects of line-of-sight deposition have been proposed. Rigney and co-workers (1995) analysed this effect by coating a stationary cylinder over a single source. Although they measured a very thin coating and a relatively thick coating on the backside and the head-on position, respectively, other important parameters such as the diameter of the cylinder, source-to-substrate distance, and the coating thickness at the tangency point of the vapour, were not included in this paper.

In order to study how close an EB-PVD laboratory coater approximates the true line-of-sight process, the thickness profile around an 18 cm long, 12 mm-diameter stationary cylinder, positioned along the centreline at 15 and 18.75 cm over the source, was investigated. Theory would predict no coating deposited on the backside of the cylinder, which faces away from source, up to and including the theoretical point tangent to the vapour flux. In addition, theory predicts a thin coating near the tangency point getting progressively thicker, being thickest at the head-on position. A comparison of both the measured and predicted results should indicate the error associated with the theoretical line-of-sight effect.

From the above, it is evident that one approach to predict a coating deposited on the backside of a component, as measured by Rigney et al., for example, is by using virtual sources (see "Virtual Sources" on page 121). The coating thickness, and the direction of growth of the columns, at any point on a component surface depends on integrating the complex vapour flux distributions from all sources, both virtual and real, onto a predefined surface element. If the modelling requires the virtual sources to be included, then two important questions must be answered: their position, and their charge (or power), which can be as a percentage of the real source. This is explained later in the section discussing the virtual source concept.

Moreover, the stationary cylinder allowed the study of the variation in coating thickness as a function of the vapour incidence angle (VIA). The value of VIA varies as the location of the substrate changes within the chamber and/or the angle between the vapour flux and the substrate surface is varied. It is clear, therefore, that for a cylinder the value of VIA varies from 0° (head-on position) to 90° (at the tangency point of the

vapour), while the coating thickness decreases as the VIA value increases, for a given source-to-substrate distance.

The inclination of the ceramic columns has also been of considerable interest in the last years. This is important because the growth direction of the columns is directly linked to the thermal conductivity, but more importantly to the erosion rate of the TBC. Ideally, the columns should be perpendicular to the substrate's surface in order for them to offer the best resistance to erosion and foreign object damage. Theoretically, the column inclination is a function of the VIA.

In conclusion, coating a stationary cylinder allowed the study of:

- Line-of-sight effect (front side versus backside);
- The need for virtual sources depending on the error of the line-of-sight effect;
- Variation in coating thickness for the side receiving coating (coating thickness as a function of both the source-to-substrate distance and VIA);
- Direction of column growth, which theoretically is only a function of the VIA.

Firstly a brief explanation to provide an overview of the different scenarios will be given, and then each case study is discussed in detail in a separate section.

The cross section illustrated in Figure 11-1 is typical of the thickness profile obtained in these coating trials for stationary cylinders, showing the thickness gradient from the head-on position (VIA = 0°) to the tangency of the vapour flux (VIA = 90°).

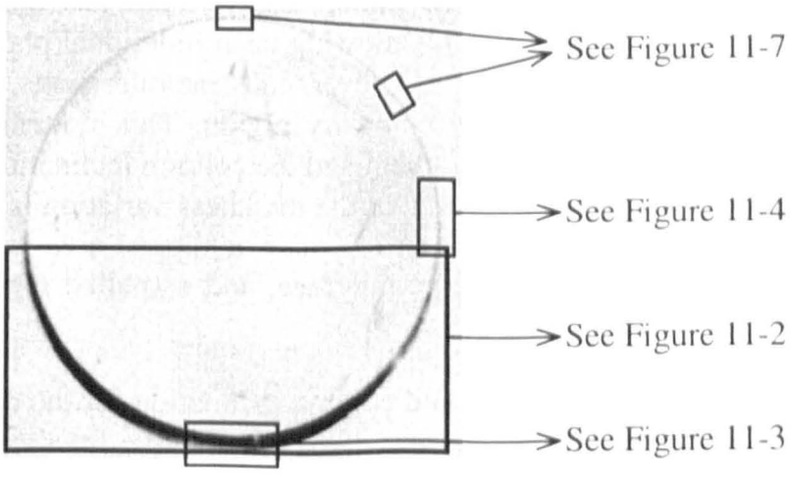

Figure 11-1: Cross section of the cylinder for a height of 18.75 cm directly above the source (negative image).

It is evident from both Figure 11-1 and Figure 11-2 that the distribution profile exhibits a thickness gradient. At the head-on position (VIA = 0°) the coating is thick with the ceramic columns perpendicular or nearly perpendicular to the component's surface (Figure 11-3). The maximum coating thickness was measured to be directly above the source (580 μm, for a height of 18.75 cm for a 90-minute deposition). A thinner porous coating, around 410 μm thick, was deposited about halfway between the head-on

position and the point tangent to the vapour (VIA = 45°) while at both positions near to the tangency point to the vapour (VIA ≈ 90°) the coating was relatively thin.

In the detailed view of the area directly above the source (Figure 11-3) two areas of abnormal growth, usually referred to as "flakes", are evident (Goward, 1974; Boone, 1986; Bettridge and Ubank, 1986). The removal of the "flake" type defects from the ceramic may result in the formation of "pits".

Figure 11-4 represents a typical area around the theoretical point where the vapour flux arrives at 90 degrees to the substrate's normal. Optical measurements showed a relatively thin coating for a VIA of around 85. As discussed in "Evaporation Model" on page 99, theory would predict no coating deposited for a VIA = 90°, in addition to the areas not visible from the source (backside of the substrate). However, measurements of the thickness showed a uniform thin coating (20-25 μm) on the backside of the substrate (Figure 11-7 illustrates the uniform coating in two areas hidden from the source). This value represents between 3 to 4% of the maximum coating thickness. Other investigations (Rigney et al., 1995) into the effects of line-of-sight deposition with a stationary cylinder indicated a similar value (<12 μm and >225 μm for the backside and for the head-on position, respectively). In addition, near the point of VIA = 90°, the inclination of the columns was at its highest. An inclination of 40° to the substrate's surface, for a VIA = 85°, was measured, as seen in Figure 11-4. For a VIA = 90° the ceramic spalled (completely on the right side and partially on the left) probably due to the very steep vapour-impact angle.

Figure 11-5 and Figure 11-6 illustrate an area for a VIA approximately between 25° and 65°. For a VIA = 25° it is clear that a coating thickness and morphology similar to the head-on position occurs (Figure 11-5). Worth noting is that while Figure 11-5 represents the actual curvature of the cylinder, Figure 11-6 has been "flattened" for ease of analysis. This was achieved by allowing each individual photograph to slightly overlap at a recognisable feature. However, all measurements were taken within each photograph and not at each boundary region. This flattening process was important because both the thickness gradient and the column inclination could be more accurately measured. Also, it can be seen that the thickness variation is smooth (dashed line). Two areas of defects can be seen: an irregular or dipped area in the centre of Figure 11-5, probably due to a defect at the interface, and a spalled region in the centre of Figure 11-6.

All thickness measurements and column inclination for the cylinder samples were taken using a software package written in the Quantitative Interactive Programming language (Quips), which is compatible with the Leica Q500 MC Image Analysis system. The software calculates, from a given set of positions, the centre point of the cylinder, and its radius. Then, based on the estimated centre point, it moves the motorised stage automatically, allowing the user to take equally spaced radial measurements at the interface around the perimeter. After the specimen was positioned at the various angles, the coating thickness, and column inclination, could be measured.

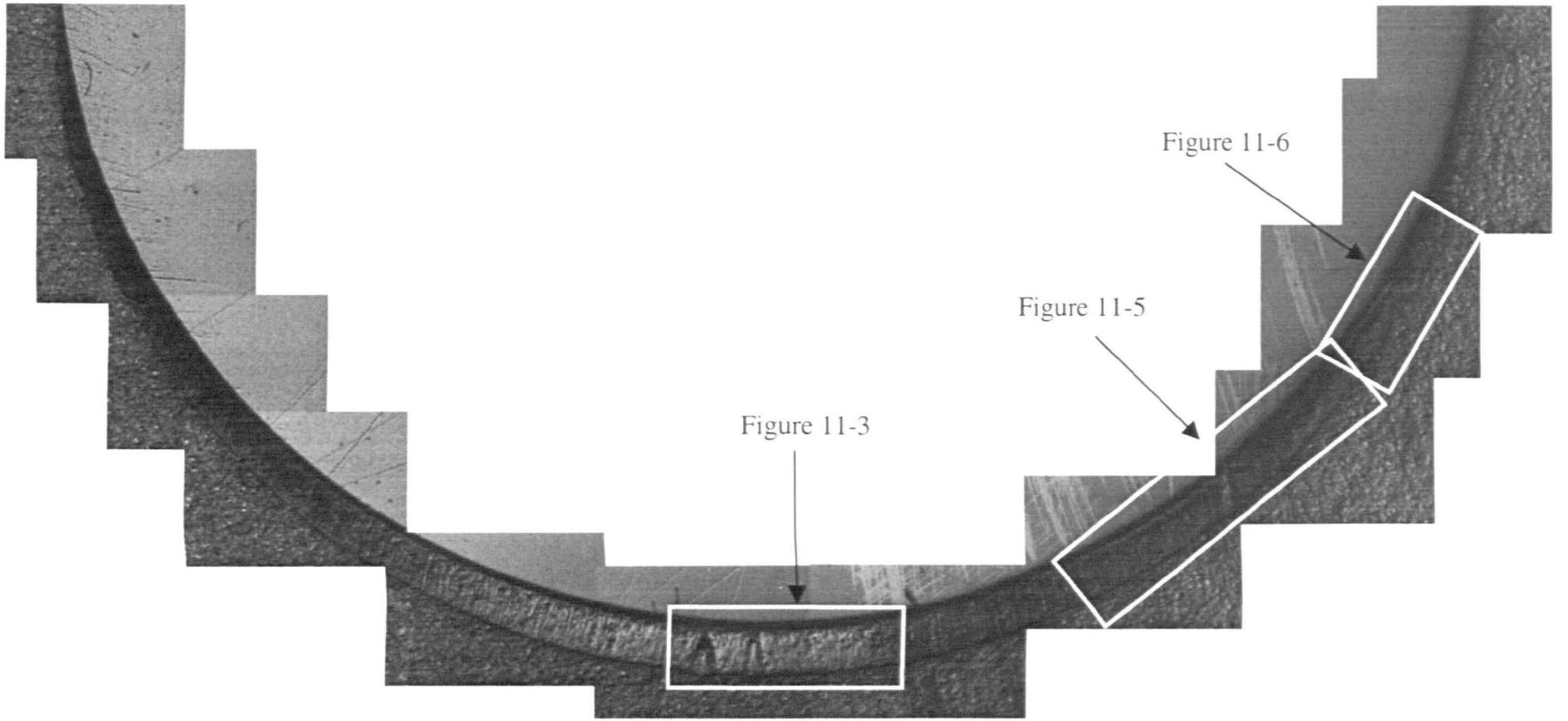

Figure 11-2: Thickness distribution for the side facing the source of a 12 mm diameter stationary cylinder 18.75 cm above the source.

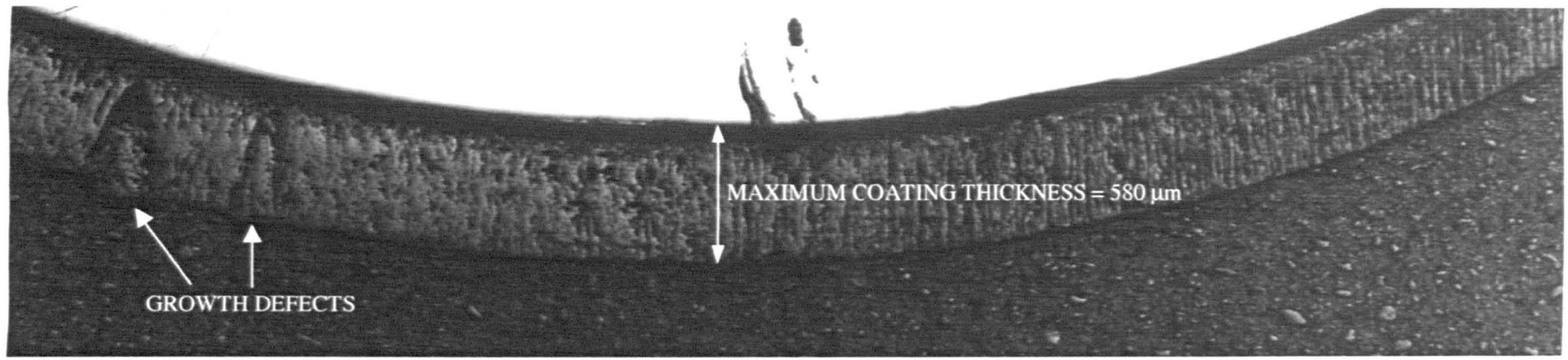

Figure 11-3: Detailed view of a typical coating for the head-on position (VIA = 0).

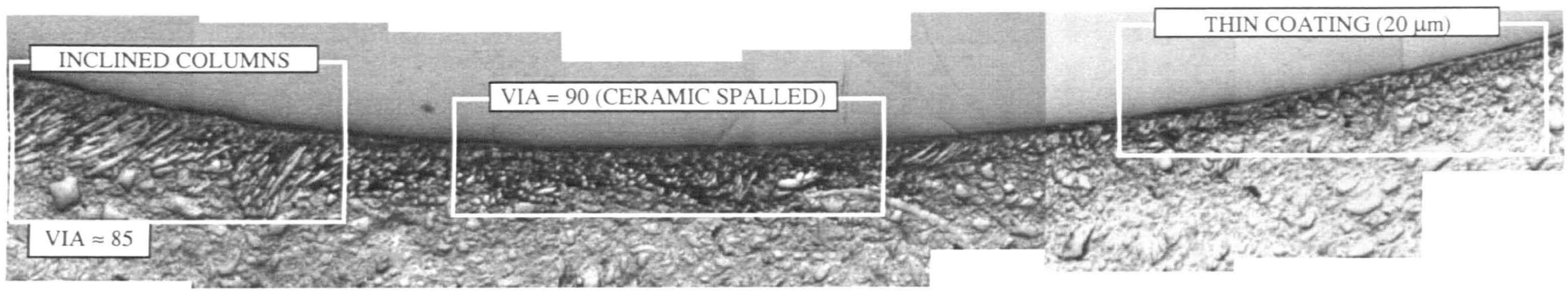

Figure 11-4: Thickness profile for an area around the tangency point of the vapour flux showing a thin coating (20 μm) in an area hidden from the source, and a thicker coating for a VIA of just less than 90°.

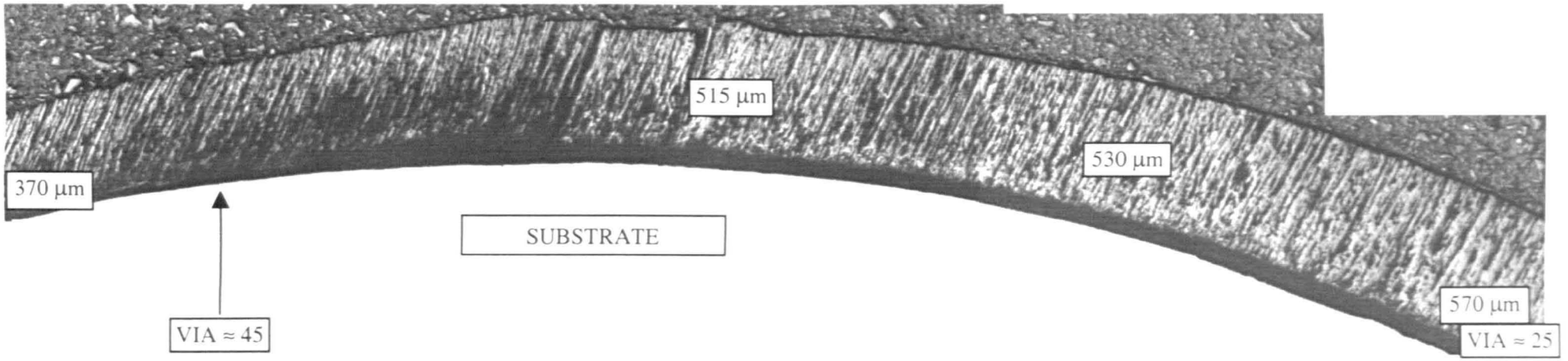

Figure 11-5: Thickness profile for a VIA of around 25 to 45° (width of area represented is approximately 5.3 mm).

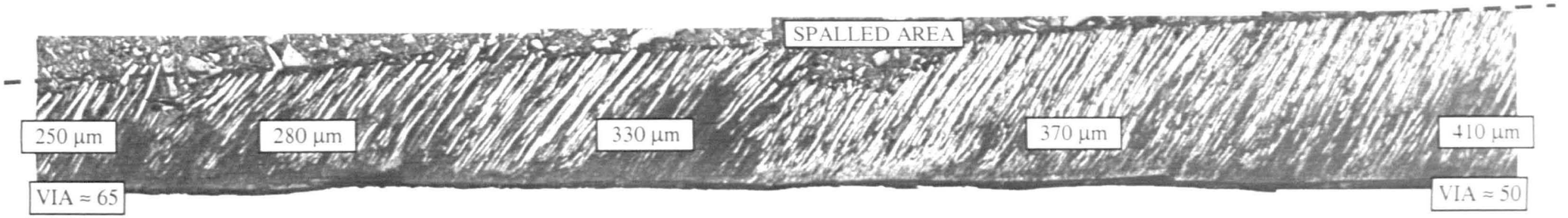

Figure 11-6: Thickness profile for a VIA of around 50 to 65° (width of area represented is approximately 3.4 mm).

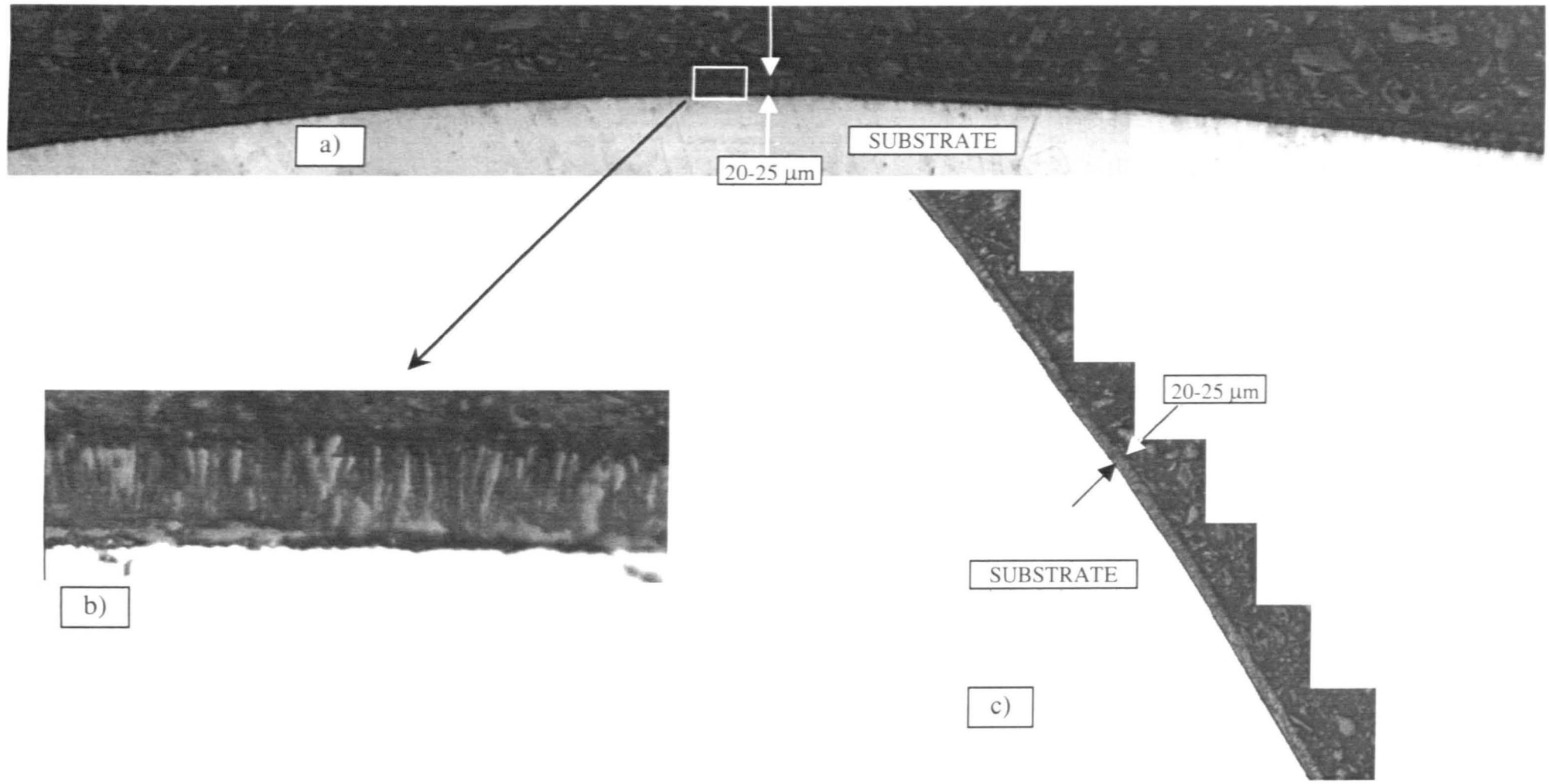

Figure 11-7: Thickness profile showing a 20-25 μm layer for areas not visible from the source a) and b) at the back of the cylinder; c) as shown in Figure 11-1.

11.2.1. Thickness Distribution

The coating thickness for the visible area of the stationary cylinders was measured in approximately 5° increments. In order to distinguish between the two tangent points to the vapour flux, a value of –90 and 90 was used to represent the right and left positions, respectively. A VIA = 0 represents the point directly above the source, which was used to normalise the measured coating thickness in order to allow a comparison to that predicted using the software tool.

A constant thickness distribution, representing a 3-4% deposition relative to the deposition directly above the source, was measured over the whole of the backside of the cylinder samples. As illustrated in Figure 11-7 this thin layer was between 20 and 25 μm thick for a height of 18.75 cm above the source.

Table 11-1 presents a detailed comparison between the measured and predicted coating thickness. As can be seen from Table 11-1, the measured coating thickness was normalised relative to the head-on position (point directly above the source). As explained later in the section on the virtual source concept, a three-zone model is proposed to improve the accuracy of the model. The differences between measured and predicted using both the cosine law and the three-zone model based on the cosine law are highlighted.

Figure 11-8 shows a comparison between predicted and measured coating thickness for the cosine law model, and the error associated with the predicted values. Figure 11-8 further illustrates that agreement is exceedingly good, ±5% for a VIA less than 35°. For positions nearer to the two tangent points of the vapour flux, the deposition rate measured and cosine law model agree within ±15%. Figure 11-9 plots a direct comparison between predicted and measured coating thickness irrespective of substrate inclination (a perfect fit would be the diagonal straight line included in the figure).

Although the accuracy of the predictions are some 15% lower than those measured for a VIA between 30° and 90°, this value was consistent for the deposition trials undertaken for the two working heights and various samples considered. An implication of this is that the gas scattering within the coater accounts for an increase in deposition rate, this being typically +15% for a VIA between 30° and 90°. As explained later in the section on virtual sources, further improvements in the accuracy are possible by adopting one or more virtual sources.

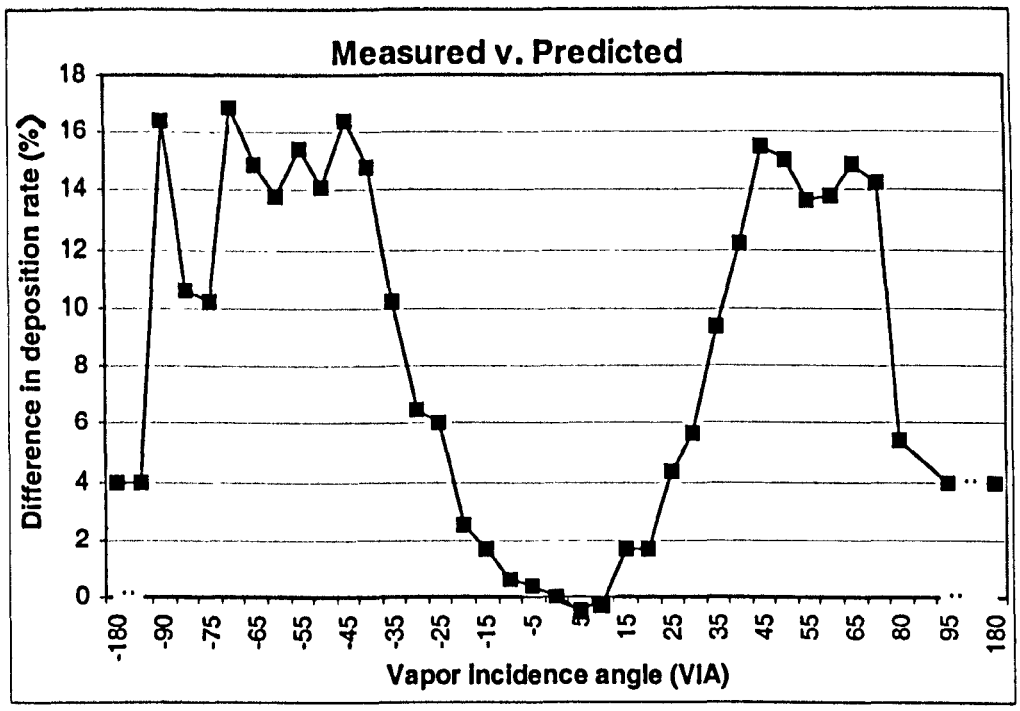

Figure 11-8: Difference in normalised coating thickness between measured and predicted deposition profiles, based on a cosine law model.

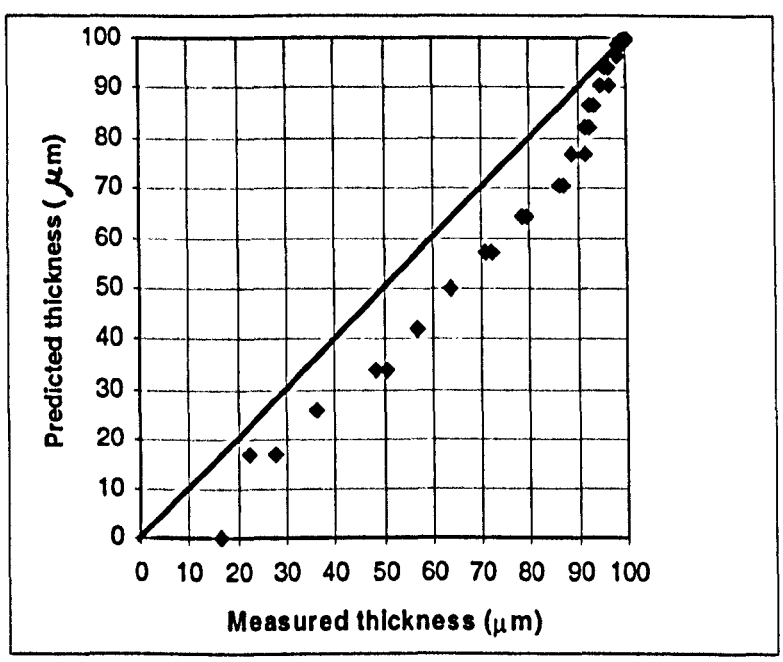

Figure 11-9: Scatter diagram demonstrating the degree of fit for the cosine law model.

Table 11-1: Measured and predicted coating thickness for the side facing the source of a stationary cylinder.

VIA	Measured (μm)	Measured [a] (normalised)	Predicted [b] (cosine law)	Predicted [c] (three-zone model)	Difference ([a-b])	Difference ([a-c])
-90	95	16.4	0	15	16.4	1.4
-80	160	27.6	17	32	10.6	-4.4
-75	210	36.2	26	41	10.2	-4.8
-70	295	50.9	34	49	16.9	1.9
-65	330	56.9	42	57	14.9	-0.1
-60	370	63.8	50	65	13.8	-1.2
-55	420	72.4	57	72	15.4	0.4
-50	455	78.4	64.3	79.3	14.1	-0.9
-45	505	87.1	70.7	85.7	16.4	1.4
-40	530	91.4	76.6	91.6	14.8	-0.2
-35	535	92.2	82	97	10.2	-4.8
-30	540	93.1	86.6	86.6	6.5	6.5
-25	560	96.6	90.5	90.5	6.1	6.1
-20	560	96.6	94	94	2.6	2.6
-15	570	98.3	96.6	96.6	1.7	1.7
-10	575	99.1	98.5	98.5	0.6	0.6
-5	580	100.0	99.6	99.6	0.4	0.4
0	**580**	**100.0**	**100**	**100**	**0.0**	**0.0**
5	575	99.1	99.6	99.6	-0.5	-0.5
10	570	98.3	98.5	98.5	-0.2	-0.2
15	570	98.3	96.6	96.6	1.7	1.7
20	555	95.7	94	94	1.7	1.7
25	550	94.8	90.5	90.5	4.3	4.3
30	535	92.2	86.6	86.6	5.6	5.6
35	530	91.4	82	97	9.4	-5.6
40	515	88.8	76.6	91.6	12.2	-2.8
45	500	86.2	70.7	85.7	15.5	0.5
50	460	79.3	64.3	79.3	15.0	0.0
55	410	70.7	57	72	13.7	-1.3
60	370	63.8	50	65	13.8	-1.2
65	330	56.9	42	57	14.9	-0.1
70	280	48.3	34	49	14.3	-0.7
80	130	22.4	17	32	5.4	-9.6
90	Ceramic Spalled		0			

11.2.2. Column Inclination

The inclination of the columns was measured all around the cylindrical samples in approximately 5° increments. At the backside of the cylinder the inclination of the columns was between 80 and 90° to the substrate's surface. The estimated error associated with the measurement of column inclination was 5°. This is due to the fact that the diameter of the cylinder was relatively small making it difficult to estimate the plane of the surface for a given position. In addition, the point where the measurement was taken was an approximation, and in some localised areas the inclination of the columns varies by a few degrees.

As previously mentioned, the VIA is defined as the angle between the substrate normal and the direction of the vapour flux. Thus, for the head-on position the VIA = 0 whereas for the point tangent to the vapour flux the VIA = 90. There are, therefore, two points on a stationary cylinder with a VIA = 90. Even though the VIA is a useful measurement, column inclination is usually measured relative to the component's surface, i.e. the complementary angle of the VIA.

Table 11-2 indicates the predicted column inclination, which is a function of the VIA, and the measured inclination relative to the component's surface. From Table 11-2 it is clear that for the position directly above the source the columns grow perpendicular relative to the substrate surface. For all other positions, however, the columns are inclined with respect to the substrate normal, being more inclined as the value of VIA increases. The lowest inclination measured, relative to the substrate's surface, was 40° for both points nearly tangent to the vapour flux. Around the area for a VIA = 90 (for both the left and right positions) the ceramic spalled presumably due to insufficient adhesion between the relatively low amount of vapour flux arriving at these angles and the substrate.

Table 11-2 further illustrates that the gas scattering effect offsets the directionality of the vapour cloud. Not only are no columns inclined at an angle below 40° to the surface, but also as the VIA increases, the inclination of the columns, measured relative to the surface, decreases but in a considerably more moderate way. For instance, the measured inclination for a VIA = 55 was 50°, relative to the substrate's surface, whereas for a VIA = 80 it was 40°. This means that a 25-degree separation rendered a small decrease (10°) in the column inclination.

Figure 11-10 plots a direct comparison between predicted and measured results. Both Table 11-2 and Figure 11-10 indicate, for a VIA less than 45°, a relatively small deviation of the predicted results compared to those measured. However, for a VIA = 80° this deviation can be as much as 30°. From the above, it is evident that the effect of at least one virtual source, offset from the point directly above the source, causes the characteristics of the real source to deviate from a simple cosine distribution. This is discussed in more detail in the section on virtual source concept on page 170.

Table 11-2: Measured versus predicted column inclination relative to the component's surface.

VIA	Measured Inclination (degrees)	Predicted Inclination (complementary angle of VIA)	Difference between measured and predicted (in degrees)
0	90	90	0
5	88	85	3
10	86	80	6
15	85	75	10
20	82	70	12
25	75	65	10
30	70	60	10
35	65	55	10
40	60	50	10
45	58	45	13
50	55	40	15
55	50	35	15
60	45	30	15
65	43	25	18
70	41	20	21
75	40	15	25
80	40	10	30
85/90	Ceramic Spalled		

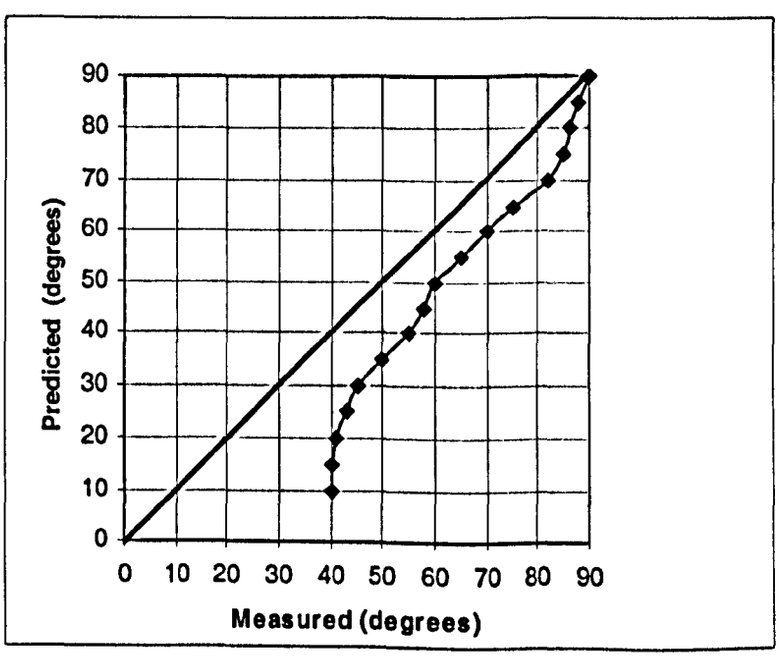

Figure 11-10: Scatter diagram demonstrating the degree of fit for the cosine law model.

11.2.3. Virtual Sources

The analysis of the coating thickness around stationary cylinders showed a thin coating at the backside of the component. This relatively thin layer accounted for 3 to 4% of the coating thickness measured directly above the source. Furthermore, the accuracy of the predictions of both the coating thickness and column inclination for the side facing the source was relatively poor as the VIA increases. This acknowledges that, as expected, the EB-PVD coating process is not a true line-of-sight process and that the gas scattering effect offsets the directionality of the vapour cloud. Moreover, this work is concurrent with the study by Rigney et al. (1995) as far as line-of-sight deposition is concerned, with an associated error of around 4%, over the whole of the back of the cylinder.

However, as seen previously, the virtual source concept may be used to increase the accuracy of the model. From the knowledge of coating distribution at the backside of stationary components, due to the atom-atom collisions or gas scattering, these sources are positioned usually where the vapour pressure is sufficiently high as to contribute to a deviation from the true line-of-sight process. It follows, therefore, that virtual sources may be positioned anywhere within the vacuum chamber, and not only on the plane where the real source or sources are. For example, for a two or three-source coater, the localised high vapour pressure in the region between the sources may result in a low mean free path, contributing to the presence of a virtual source. Because virtual sources can be positioned anywhere within the vapour cloud, they have a fundamental difference from the real source, i.e. their evaporation is typically omnidirectional (without preferential direction of evaporation; the n value, which defines the focus of the vapour flux, is zero).

Another important aspect is the power (or intensity) of the virtual source and will be defined as a percentage of the deposition rate of the real source for a given height (d_0). In addition, the intensity of the virtual source is expected to fall off as an inverse square law as the source-to-substrate distance increases. One approach to predict a 3-4% coating deposited at the backside of a cylindrical component could be using a virtual source with a power between 2-5%, depending on the separation to the substrate, and positioned directly behind the cylinder (Figure 11-13, Case 1). However, as discussed earlier, a uniform coating was measured over the whole of the backside of the cylinder. This means that a single virtual source is not adequate to predict a constant thickness directly at the back and near to both points (right and left) tangent to the vapour flux (although this depends upon the accuracy required). Also, the virtual source derives its "charge" from the primary sources and therefore must see the primary source. This is not possible for a source behind the component to be coated. Further improvements are possible by assuming two virtual sources with identical power and offset from the position directly behind the source (Figure 11-13, Case 2). Moreover, due to the circular profile of the cylinder, an increase in the number of virtual sources, say five, renders a more uniform thickness profile, as illustrated in Figure 11-13 (Case 3). In conclusion, it is apparent that the aggregate flux arriving at any point on a substrate surface is a function of the summation of the flux from a 3D omnidirectional shell (the summation of many virtual point sources displaced around the component in 3D).

It is also evident that the three cases shown in Figure 11-13 reflect a 2D concept. For the real 3D space, the number of virtual sources needed depends on the dimensions of the substrate, in addition to the required accuracy. Worth noting is that to obtain the best performance possible from the computer model, the least number of virtual sources should be used. Since a virtual source calculates distances, angles, visibility, etc. in the same way as a real source, the use of five virtual sources, for example, causes a fivefold penalty in operating speed, for the improvement in accuracy.

11.2.3.1. Thickness distribution

As reported earlier, the gas scattering within the coater accounted for an increase in deposition rate. This being +15% for a VIA between 35 and 90° and +4% for the whole of the backside of the cylinder. However, for a VIA less than 35° the cosine law model is accurate within ±5%. It follows, therefore, that further improvements in the degree of fit were possible by using a three-zone model as defined by the above limits. This zone model increases the fit of the model to that measured by around ±7% as is clear from Table 11-1. Predicted deposition rates are within an accuracy of generally better than ±8%, as evident in Figure 11-11, with many points actually matching the perfect fit (straight diagonal line).

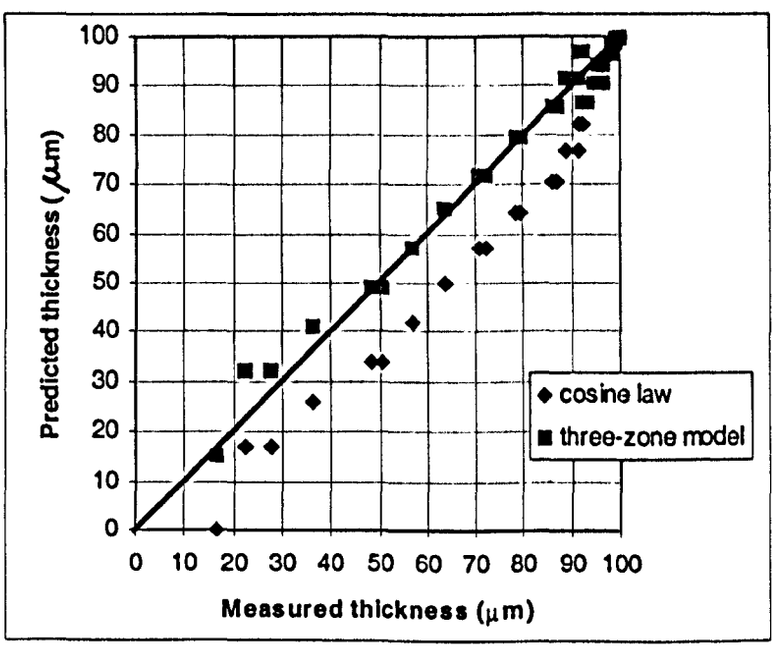

Figure 11-11: Scatter diagram demonstrating the degree of fit for both the cosine law and the three-zone model.

In addition, from the knowledge of coating distribution, based on an understanding of the physics of evaporation, it is possible to define the position, and intensity of one or more virtual sources (depending on the required accuracy) in order to predict the thickness distribution around stationary cylinders.

An investigation into modelling the coating thickness of a stationary cylinder 18.75 cm above the source was determined as follows. One method of modelling the uniform coating at the whole of the backside of the cylinder would be to position two virtual sources (two being enough due to the relatively small-diameter cylinder) offset from the

position directly behind the source, as shown in Figure 11-13 (Case 2). These two sources would be positioned 10 cm away from the cylinder and would have an intensity of 1% relative to the real source. This configuration represents a relative coating thickness for the edge-on position of 3.5% ($\frac{1}{\left(\frac{10}{18.75}\right)^2}$), based on the inverse square law, and thus would be adequate to model the 4% backside deposition. Additionally, the n value (source characteristic) would be zero since an omnidirectional source is, by definition, non focused, and would thus match an almost uniform deposition around the cylinder surface. In addition, it is assumed that some interaction (or blending) of the two virtual sources occurs at the position directly behind the real source, as illustrated in Figure 11-12.

Furthermore, the 15% deviation for a VIA between 35 and 90° could be modelled by adopting another two virtual sources 5 cm away from the cylinder with an intensity of 1% relative to the real source (similar to the previous two virtual sources). A source with such a configuration would have a power of around 14% of that of the real source. Also very important is the fact that these two virtual sources, as opposed to the previous two, are slightly more focused, since they should affect the area for a VIA between 35 and 90° while their effect outside these limits should be close to zero.

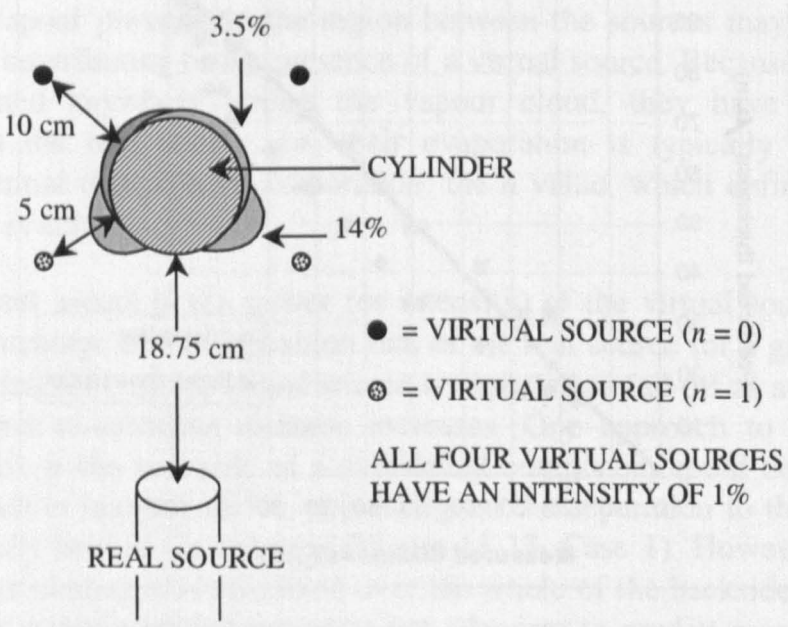

Figure 11-12: Determined configuration of virtual sources in order to increase the accuracy of the predictions of that of the cosine law model showing the deposition profiles for each virtual source.

The above configuration illustrates the physics of evaporation behind the deviation from the cosine law model, for the laboratory coater available at Cranfield University. As reported earlier, the modelling of gas scattering is not only desirable to further understand the evaporation process, but also necessary in order to increase the accuracy of the predictions.

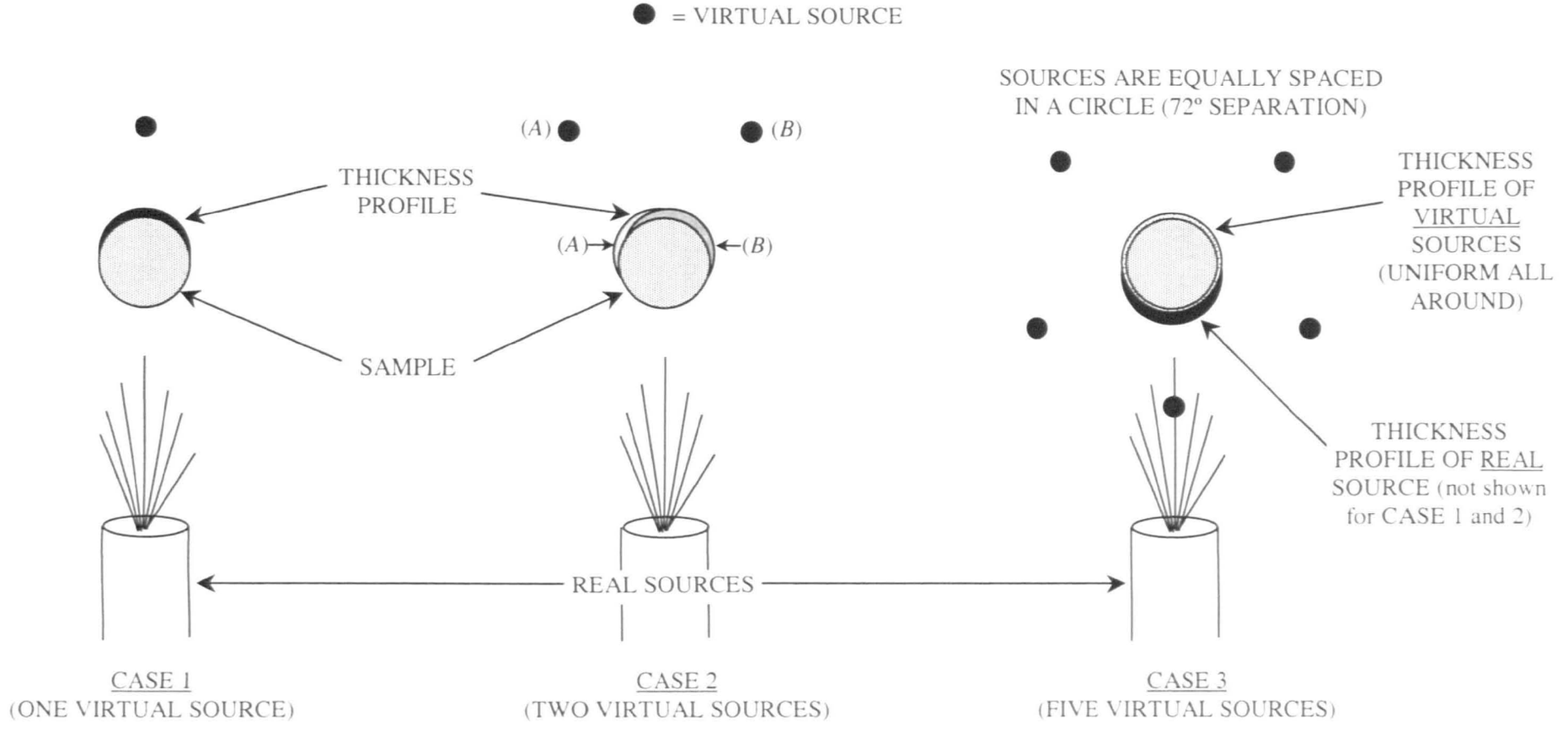

Figure 11-13: Virtual source configuration for predicting a uniform deposition at the back of a cylinder (CASE 1 **is physically not possible because virtual sources derive their "charge" from the primary source and in this case the virtual source is hidden from the primary source).**

11.2.3.2. Column Inclination

It was evident, from the results for column inclination discussed previously, that the accuracy of the predictions around a stationary cylinder, using the cosine law, are relatively poor. However, the virtual source modelling concept may be used to improve the accuracy of the predictions, as shown for the thickness distribution case. From Table 11-3 it is possible to identify various zones, for the visible side of the cylinder, with an almost constant difference between measured and predicted. For example, for a VIA between 15 and 45° the discrepancy between measured and predicted was around 10°, while for a VIA between 50 and 65° it was around 15°. For this reason, the position, intensity, and characteristic of the virtual source(s) should reflect the experimental conditions and the knowledge of column inclination around the stationary cylinder. From Table 11-3 four zones are evident, as follows:

- Zone 1: for a VIA $\leq$ 10, the predicted inclination (P_i) is equal to the VIA;
- Zone 2: for 10 < VIA $\leq$ 45, P_i = VIA + 10°;
- Zone 3: for 45 < VIA $\leq$ 65, P_i = VIA + 15°;
- Zone 4: for 65 < VIA $\leq$ 80, P_i = VIA + 25°;

For a VIA between 80 and 90° there was insufficient data but some areas where the ceramic did not spall suggest an inclination of around 40° relative to the component's surface. In addition, for the whole of the back of the cylinders the column inclination was nearly perpendicular to the substrate's surface (between 80 and 90°). The results for the whole of the back of the cylinder thus suggest that the measured column inclination is the summation of many virtual point sources displaced around the component in 3D, which is concurrent with the results for the thickness distribution.

Table 11-3 indicates the differences between the measured column inclination and that predicted using the cosine law model and the four-zone model. The degree of fit for both the predicted results by the cosine law and the four-zone model are illustrated in Figure 11-16. From Table 11-3 it is clear that the virtual source should account for a relatively low deviation for a low VIA (10° for a VIA between 15 and 45°), while for a higher VIA the deviation from the cosine law model is higher (20° for a VIA = 70, and 30° for a VIA = 80, for example).

From the calculations of the measured and predicted inclinations for various points for a VIA between 0 and 90° it is possible to determine the positions and intensities of the virtual sources. For example, the measured column inclinations for the whole of the back of the cylinder indicate, as reported above, many virtual sources displaced around the component in 3D. For the visible side of the cylinder calculations of vector directions and magnitudes allowed the virtual source characteristics to be identified. For instance, from Figure 11-14 it is evident that if the predicted and measured column inclination have a vector $\vec{a} = (0, -1)$ and $\vec{b} = (1, -1)$, respectively, then the virtual source accounts for a vector $\vec{c} = (1, 0)$ (i.e. $\vec{c} = \vec{b} - \vec{a}$). Figure 11-15 schematically shows the theoretical column inclination of both the real and virtual source (dashed line), the

predicted thickness of the columns (solid arrows; two from each type of source) and the resulting (or measured) column inclination on the cylinder specimens for a VIA=45 and 80°.

Table 11-3: Difference between measured and predicted column inclination for both the cosine law model and the four-zone model.

VIA	Difference between measured and predicted (in degrees)	Predicted Inclination (Four-Zone Model)	Differences between measured and four-zone model (in degrees)
0	0	90	0
5	3	85	3
10	6	80	6
15	10	85	0
20	12	80	2
25	10	75	0
30	10	70	0
35	10	65	0
40	10	60	0
45	13	55	3
50	15	55	0
55	15	50	0
60	15	45	0
65	18	40	3
70	21	45	-4
75	25	40	0
80	30	35	5
85	Ceramic Spalled		
90	Ceramic Spalled		

The calculations of inclinations suggest, therefore, that the virtual sources (one for each side) are displaced approximately 5 cm from the sample for a VIA=80° with an intensity of 2% relative to the real source (Figure 11-15). This configuration would have a power of approximately 30 and 15% for a VIA=80 and 20°, respectively, accurate within ±10% with the measured results. The degree of fit represented by the four-zone model (Figure 11-16) is typical of the results attainable with the above configuration.

Although the results agreed reasonably well with the four-zone model for the trial runs performed, further research is required with substrates at various other heights both directly above the source and offset from the centreline. Moreover, studies on other equipment, both laboratory and commercial coaters, for instance, would be useful to define this behaviour precisely.

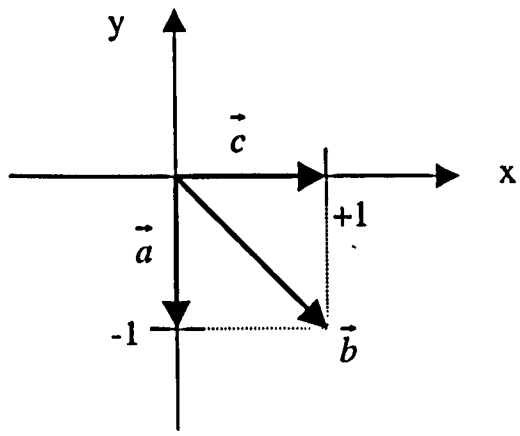

$\vec{a}$ = PREDICTED COLUMN INCLINATION

$\vec{b}$ = MEASURED COLUMN INCLINATION

$\vec{c}$ = COLUMN INCLINATION OF VIRTUAL SOURCE

Figure 11-14: Locating the virtual sources from the calculations of inclinations.

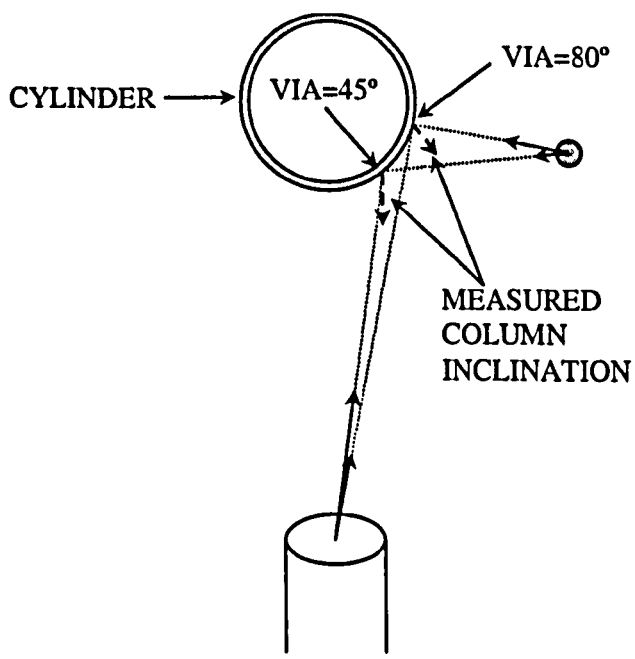

Figure 11-15: Position and power of the virtual source as a function of both the direction and intensity (coating thickness) of columns measured.

Worth noting is that the results of both the thickness distribution and column inclination indicate similar configurations for the virtual sources including multiple single point sources at the whole of the back of the cylinder, and two for the side facing the source, although with slightly different intensities.

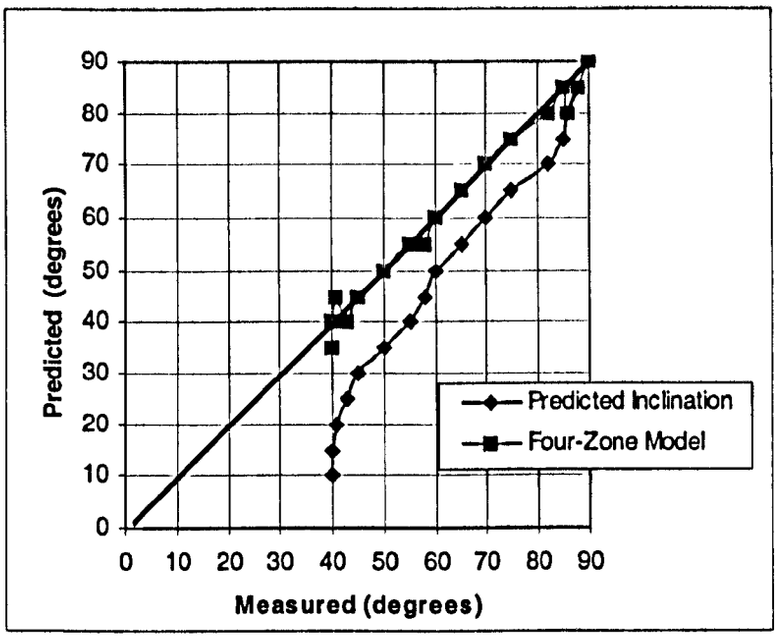

Figure 11-16: Scatter diagram demonstrating the degree of fit for both the cosine law and the proposed four-zone model.

11.3. Run II (Rotating Cylinder)

At the vacuum levels used within a commercial coater the vapour deposition of ceramic is effectively a line-of-sight process. The components to be coated are continuously rotated, usually about their longitudinal axis, while being moved, tilted or oscillated about a second axis. This planetary motion is necessary to ensure not only that all surfaces where coating is required are coated with ceramic, but also that a given EB-PVD thickness profile is met.

The laboratory coater used for the physical experiments has two rotating fixtures for substrate rotation 15 cm above the source (see Table 8-6 on page 123 for more information on the specifications of the laboratory coater). A macrophotograph of the rotating pin after deposition is given in APPENDIX B.

In order to analyse the thickness profile of a rotated component an 8 mm diameter cylinder was rotated around its longitudinal axis. The cylinder was positioned horizontally and parallel to the line formed by the EB-gun and the source. In addition, it was displaced 5 cm relative to the normal to the source, due to the configuration of the rotating fixtures. A constant rotational speed of 20 r.p.m. was used. Since all the surfaces see the vapour flux for the same time period, a uniform coating was expected.

A 2 mm^2 reference sample (stationary) was positioned 10 cm directly above the source. For the 90 minute deposition time allowed, the coating thickness measured on this sample was 740 μm. It follows, therefore, that a deposition rate of around 8 μm per minute for a height of 10 cm directly above the source was achieved. Based on the

cosine equation (inverse square law) a coating thickness of 330 μm (740×44.4%) was predicted for the same height as the cylindrical samples (15 cm).

Two samples were analysed and the coating thickness measured. Both samples were displaced 5 cm along the x-axis relative to the source (to the right of the source). In addition, SAMPLE 2 was also displaced 3 cm towards the back of the chamber (y-axis). This displacement was measured relative to the normal to the source. It was, therefore, important to calculate the predicted coating thickness for the two samples, relative to the point directly above the source (330 μm). The predicted deposition rate for a stationary sample on the positions investigated was approximately 240 and 215 μm (330×72% and 330×65%, respectively).

However, not only were the samples offset from the centre point, but they were also rotated, contributing to an effective decrease in the deposition rate. Thus, the decrease in coating thickness for rotated samples had to be predicted relative to stationary samples, as illustrated in Figure 11-17. The predicted deposition rate for a small-diameter rotated component relative to a stationary component is 63%. Therefore, the predicted deposition rate for the rotating samples was 151 and 135, respectively (240×0.63 and 215×0.63).

Figure 11-18 represents a comparison between measured and predicted deposition profiles, as a function of angular displacement, for both samples. A perfect fit would be the horizontal straight lines included in the figure. Figure 11-19 illustrates the constant thickness distribution, for four points on the sample, typical of those measured over the whole of the specimens. Computer generated values agreed very well with the measured coating thickness, for the samples analysed. With the exception of two points in SAMPLE 1, which had about half the expected thickness (80 and 70 μm), both samples have a uniform deposition, generally better than ±5%. The degree of fit of the model is, therefore, extremely good for the EB evaporation source used within the Cranfield coater. In addition, the effect of gas scattering (virtual source) is negligible for rotating specimens.

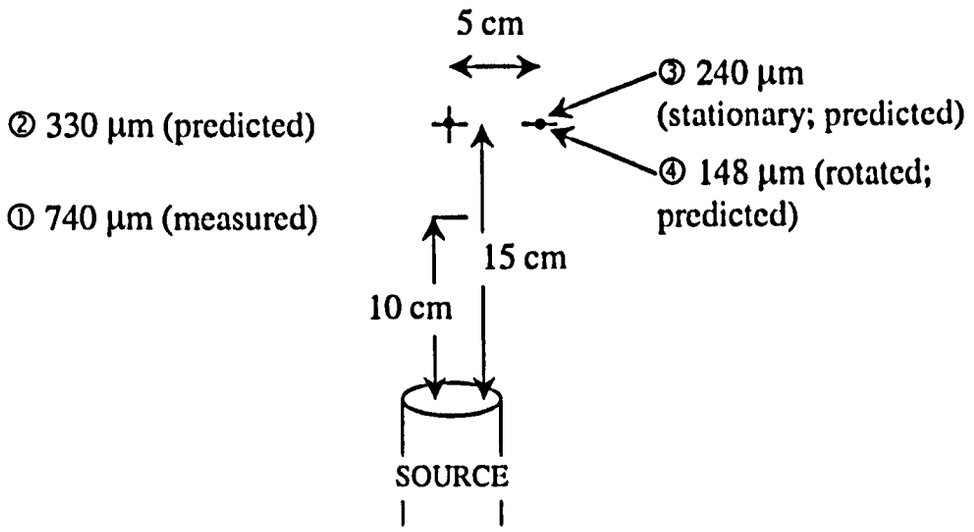

Figure 11-17: Predicted deposition rate for a rotated sample 15 cm above the source and displaced 5 cm relative to the normal to the source.

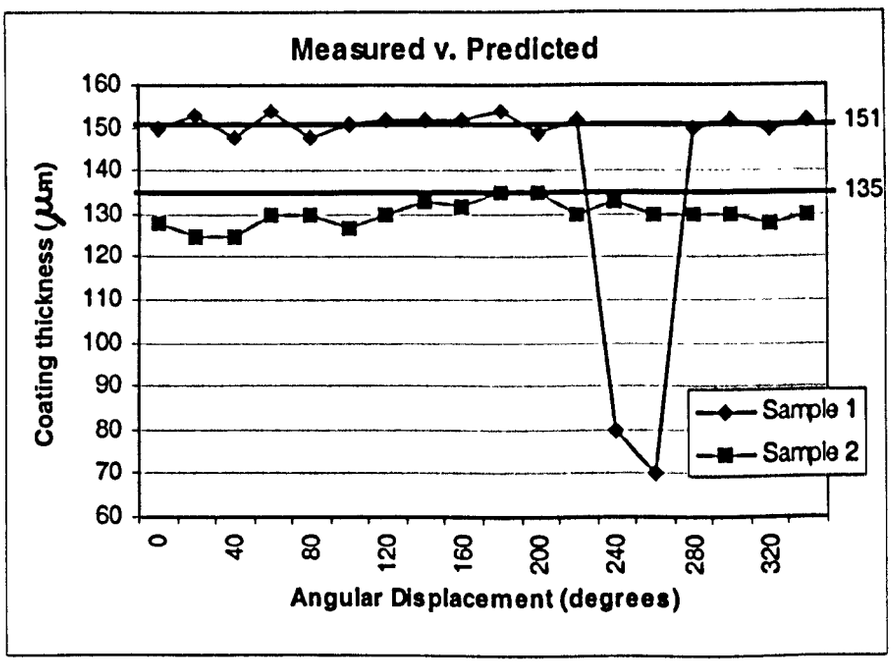

Figure 11-18: A comparison between measured and predicted deposition profiles (points with an angular displacement of 240 and 260° are considered erroneous).

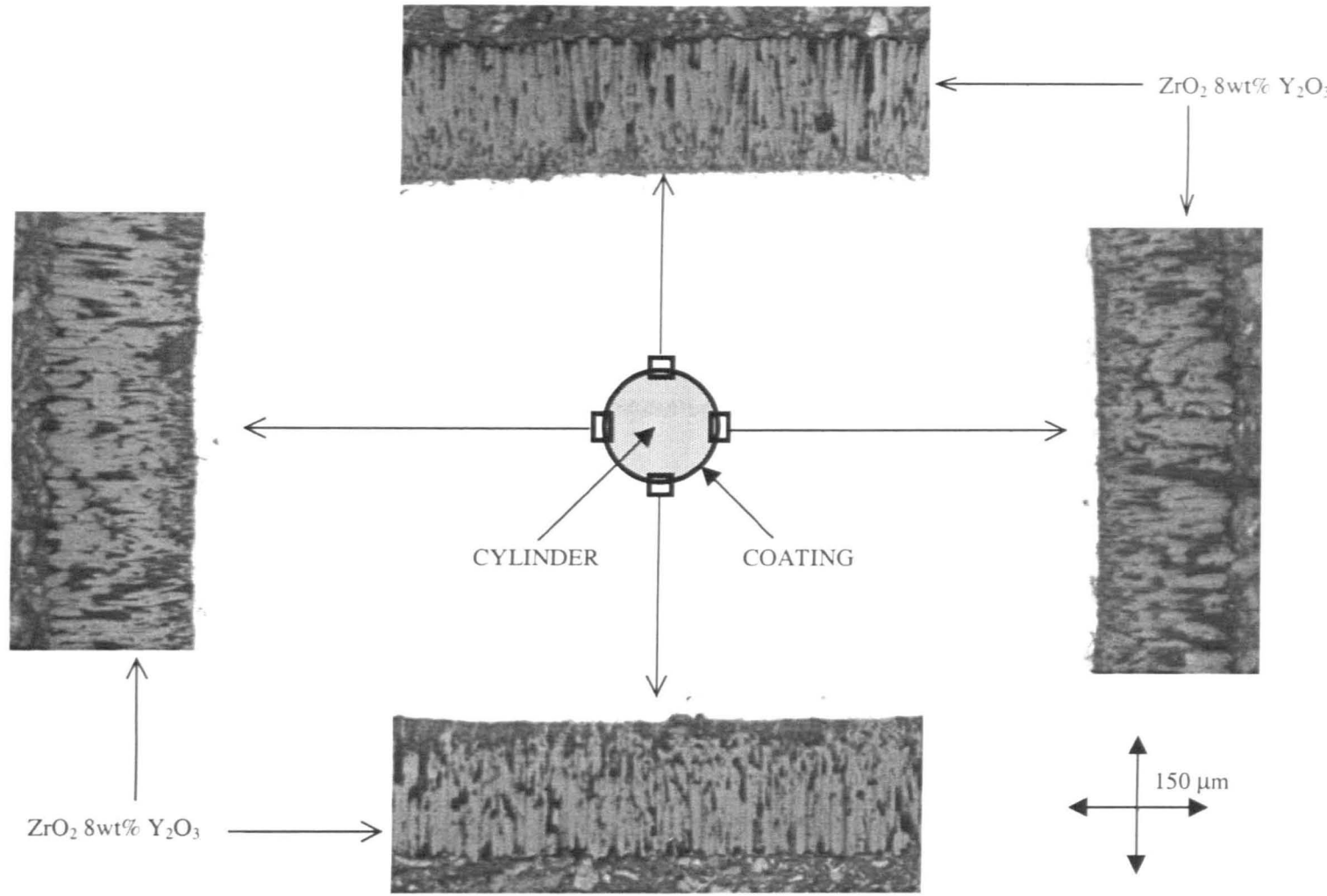

Figure 11-19: Photomicrographs showing the uniform deposition, for four points on the sample, typical of the uniform deposition measured for the whole specimen.

11.4. Run III (Cluster of Three Rotating Cylinders)

In order to evaluate the feasibility of coating a cluster of blades, to increase throughput and reduce coating cost, three pins were welded to a 6 cm diameter disc in order to study both the rotational and shadowing effects on the thickness distribution. The pins were 8 mm in diameter and 10 cm long positioned in a circle 1.5 cm away from the centre of the disc and at an angular separation of 120°.

The STL file used as an input file for the software tool was generated using Unigraphics v.14. Both an isometric and a top view of the arrangement, including all dimensions, can be found in APPENDIX B. Furthermore, two triangulated views of the arrangement, one as generated by the CAD/STL translator using a tolerance of 0.8 mm, and the other one with a sixfold increase in the number of triangles, which was performed by the software tool, can also be found in APPENDIX B.

The centre of the disc was used as the point of rotation of the structure. In addition, the vector of rotation was parallel to the disc's normal, i.e. parallel to the pins, as shown in Figure 11-20. A rotational speed of 20 r.p.m. was used. This arrangement is of interest because turbine blades can be positioned with their trailing edge pointing to the centre of the disk, in order to limit the thickness, whereas the leading edge, which points away from the other two blades, does not get shadowed by the adjacent blades (See "Cluster of Blades" on page 130).

From the above, it is evident that for a given pin, the area not shadowed by other pins will receive the highest deposition whereas the area closest to the centre of the disc will receive the lowest deposition (Figure 11-20).

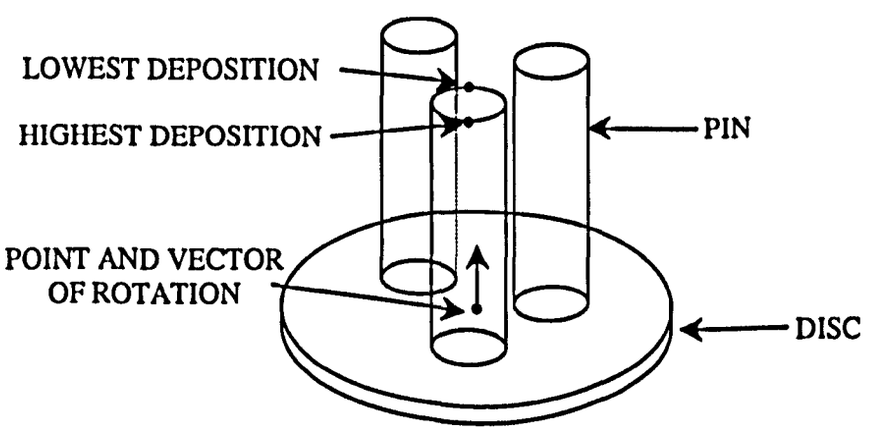

Figure 11-20: Arrangement of a cluster of three pins.

Since the point of rotation was 15 cm above the source, for cylinders 8 mm in diameter and 1.5 cm away from the centre of the disk, the closest and the furthest away the surfaces of the cylinders get to the source is 13.1 cm and 16.9 cm, respectively. This is important because, for instance, for a normalised deposition rate of 100% at 15 cm above the source, the points closest and furthest away from the source have a deposition

rate of 133% and 78%, respectively. In other words, the coating thickness for a rotating cluster of blades changes not only because the inclination of the substrate changes, but also because the source-to-substrate distance also changes considerably (over 50% for this example).

Each iteration of the rotation involves calculating the new element position, determining whether the element is visible and then if so calculating the incremental increase in coating thickness based on the above parameters (i.e. inclination of the substrate and source-to-substrate distance). Due to the simultaneous rotation and shadowing effect, the deposition rate for the area closest to the centre of the disk was relatively low compared to areas not affected by the shadowing of other cylinders. Deposition rates between 0.4 and 1 μm/min were achieved for the lowest and highest deposition areas, respectively, for the cluster of cylinders.

Two samples were analysed and the coating thickness measured all around the circular profile. Both samples were taken from the same pin (they were positioned 1 and 3 cm from the end of the pin, respectively). Figure 11-21 presents a comparison between measured and predicted deposition profiles. In addition, it illustrates the thickness distribution around the specimens, as a function of angular displacement. A value of 0 and 180° represent the point of highest and lowest deposition, respectively, as shown in Figure 11-20. From Figure 11-21 it is evident that the predicted coating thickness for the point of lowest deposition (point affected by the shadowing) is approximately 50% that of the point of highest deposition.

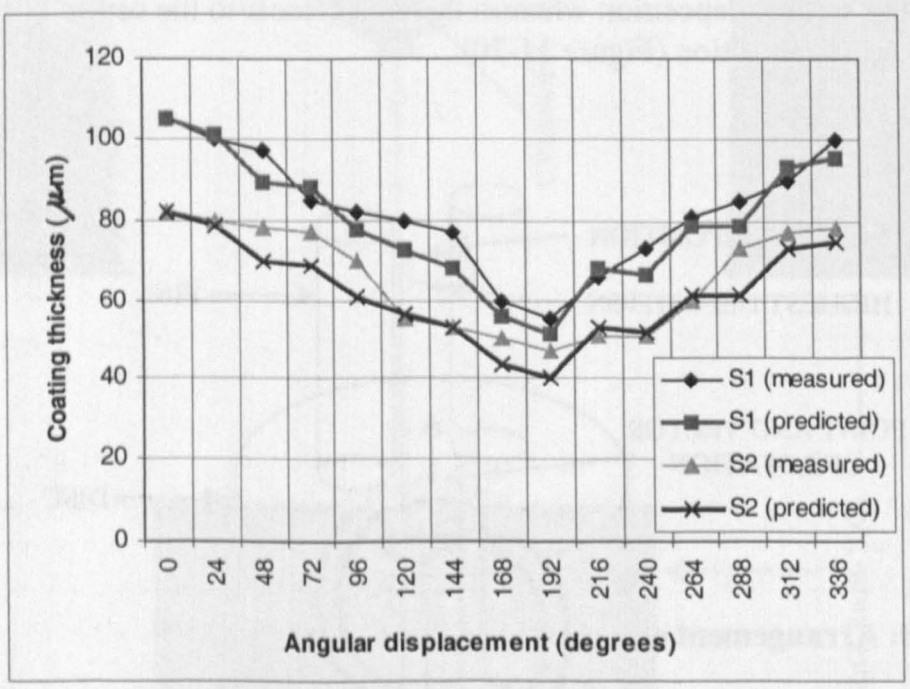

Figure 11-21: Comparison between measured and predicted deposition profiles for two samples (S1 and S2) in a cluster of cylinders.

Figure 11-22 demonstrates the degree of fit between measured and predicted results, using the computer model, irrespective of angular displacement and source-to-substrate

distance. A perfect fit would be the diagonal straight line included in the figure. Agreement of the predicted coating thickness to the measured is reasonably good. As can be seen from Figure 11-22, the coating thickness could be modelled to within an accuracy of around 15%, for this example. Figure 11-22 further acknowledges that the measured thickness is generally higher than that predicted, as with other previous deposition trials, which may also reflect gas scattering effects within the coater as discussed earlier.

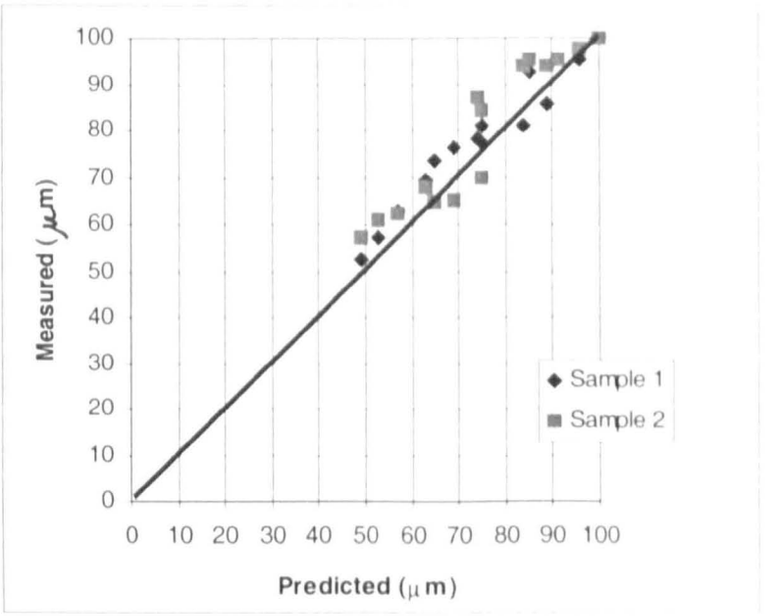

Figure 11-22: Scatter diagram presenting a comparison between predicted and measured results.

11.5. Run IV (Shadow Masks)

The effect of shadow-masks on the thickness profile was addressed by using the arrangement illustrated in Figure 11-23. In addition to the study of the masking effect, this structure also allowed the degree of fit of the inverse square law to be investigated by analysing areas not shadowed by the mask. Figure 11-23 further shows both the masked and non-masked areas perpendicular to the normal to the source.

An isometric view of the arrangement is given in APPENDIX B, in addition to a top and a side view showing all dimensions in millimetres. Note that because all surfaces were flat, the CAD/STL generator only required two triangles to approximate each surface, regardless of the tolerance specified. For this reason, the tessellation menu within the computer program was used to increase the mesh of the triangles in order to provide a better accuracy in the predicted values.

The coating thickness was measured around a section profile, and the predicted values calculated using the computer model. The predicted coating thickness was calculated by positioning the substrate within the computer model's coating space in order to match the expected component movement. Rotation of the substrate involved 72 iterations (5°

increments) around a vector shown in Figure 11-23. Figure 11-24 summarises the coating thickness measured around the sample (all measurements are in micrometres).

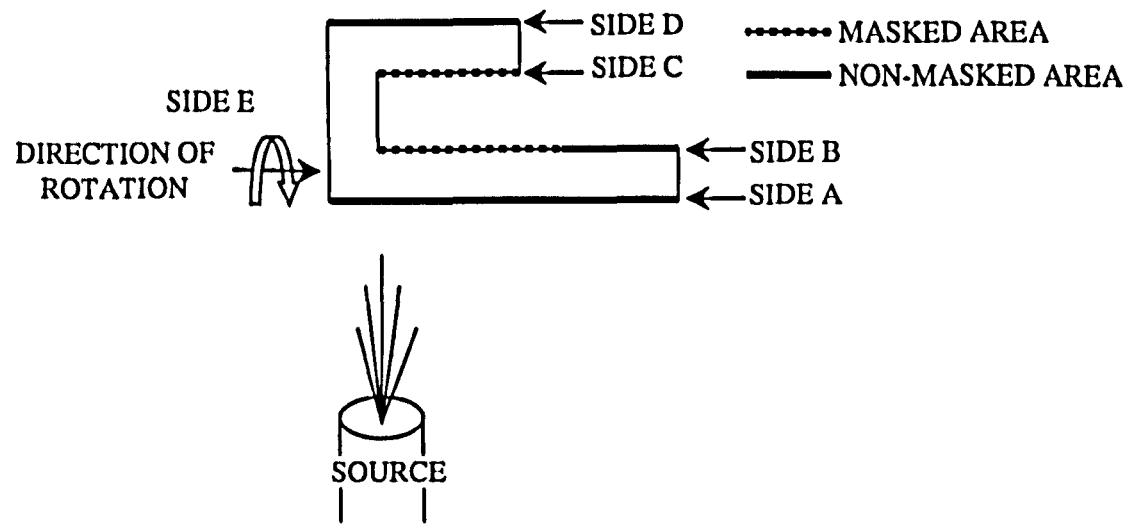

Figure 11-23: Arrangement to study the shadow-mask effect.

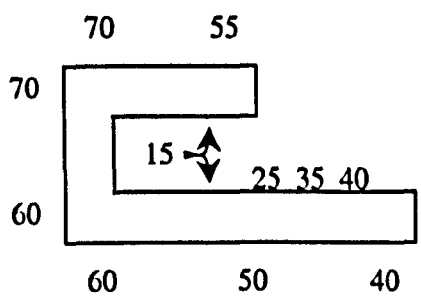

Figure 11-24: Summary of measured thickness for the shadow-mask arrangement (all values in micrometres.

From Figure 11-23 it is clear that SIDE A and SIDE D were not subjected to any shadowing effect, in addition to part of SIDE B, represented as a solid thick line. On the other hand, for SIDE C and part of SIDE B the expected thickness profile was modified by the shadow mask. Worth noting is that the masked area of SIDE B and all SIDE C did see some of the vapour flux due to the rotation of the substrate. A thin coating, around 15 μm thick, was measured on this area. SIDE E and SIDE D have the thickest coatings due to the fact that they get closer to the source than all other sides. Because both SIDE A and SIDE D are not affected by the shadow-mask, the coating thickness profile on these sides increases as the source-to-substrate distance decreases; for SIDE B, however, the opposite occurs because of the shadowing effect. Figure 11-25 shows a comparison of thickness (measured and predicted) versus linear displacement for the various sides. As expected, SIDE B and SIDE C, affected by the shadow-mask, exhibit a measured coating thickness higher than that predicted, probably due to the gas scattering within the coater.

Figure 11-26 presents a comparison between the predicted and measured results irrespective of source-to-substrate distance. Agreement is good, within an accuracy of ±20%. It is evident that the coating thickness, especially for the thinnest areas, are

relatively low, which emphasises the fact that further experimental research is required in order to quantify the effect of shadow-masking. As can be seen from Figure 11-24, the thinnest coating was measured for the area affected by the shadow-mask; from Figure 11-26 it is evident that the measured coating thickness for this area was higher than that predicted, similar to other deposition trials undertaken using the laboratory coater at Cranfield University (for instance, measurements on the stationary cylinder revealed a thicker coating than that predicted, in addition to a thin coating at the backside of the component, as a result of gas scattering effects).

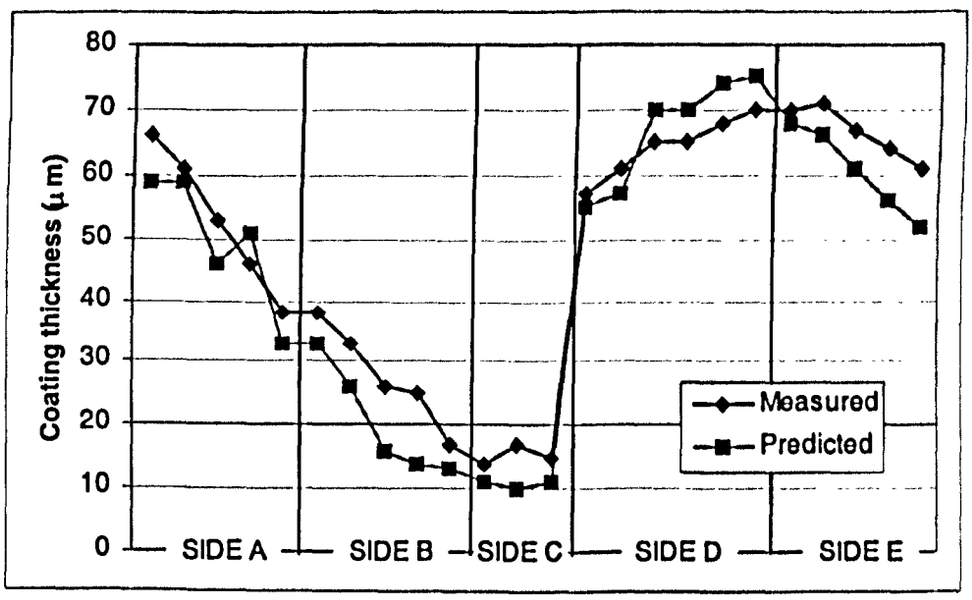

Figure 11-25: Comparison between measured and predicted deposition profiles around the shadow-mask arrangement.

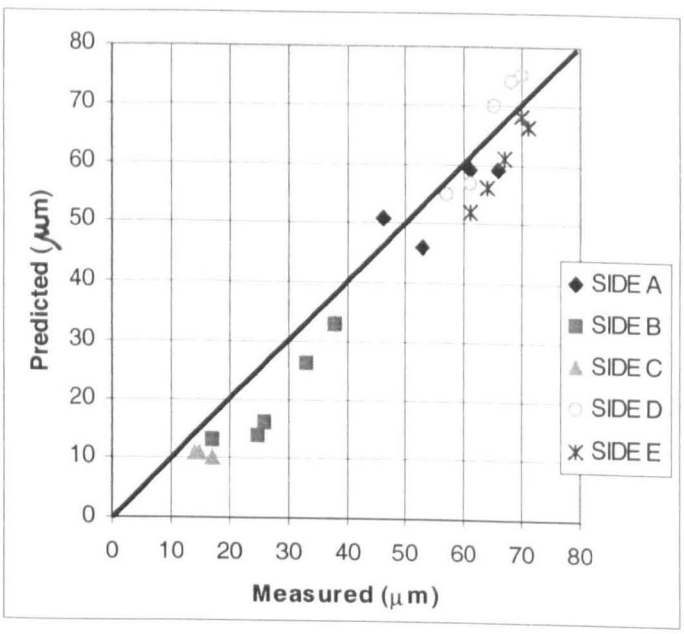

Figure 11-26: Scatter diagram demonstrating the degree of fit for the shadow mask arrangement.

11.6. Run V (Cooling Holes Blockage)

As stated before, the EB-PVD process is not usually used to coat internal passages. However, small diameter holes used for cooling in most high-pressure turbine blades can be partly blocked by the build-up of coating at their entrance. Therefore, predicting hole closure is important because cooling air flow is reduced, which may have a detrimental effect on the lives of the components.

One first attempt at comparing measured and predicted coating thickness was undertaken using a cylinder-shaped substrate with holes inclined at different angles. Figure 11-27 illustrates a solid STL file of a component with a hole normal to the surface and two others inclined at 45° relative to the surface. Prediction of hole closure and the thickness profile down cooling holes is a function of hole diameter, angle of hole relative to the surface, coating thickness, source-to-substrate distance, and substrate rotation.

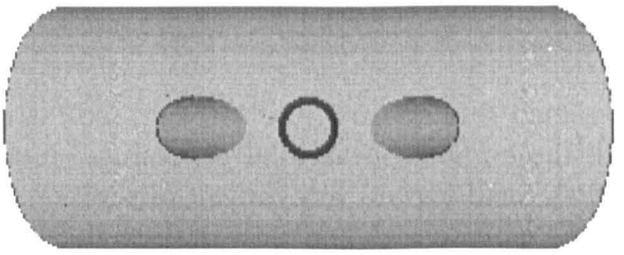

Figure 11-27: Cylinder-shaped component with a hole in the centre normal to the surface and two holes inclined at 45° to the surface.

Figure 11-28 shows a comparison of the measured and predicted results for a hole inclined at 45° to the component's surface. Evaluation of the coating thickness, using an optical microscope, showed that the ceramic spalled in places from the side facing the source. In addition, for the side hidden from the source a very thin coating, less than 7 μm thick, was measured. This was due to the thickness deposited on the flat part, which was relatively thin (around 70 μm thick) not enabling the build up of coating to occur at the hole entrance and further down the hole. In conclusion, it appears that in order for the results to be more significant the coating time allowed should be increased. Figure 11-28 further indicates that, even though the coating thickness is relatively thin, it is possible to predict thickness distribution down cooling holes. Accuracy was approximately ±25% but the results suggest that the computer-generated values agree reasonably well with those measured. In addition, defining the edge of the hole accurately is important since it is apparent that displacing this position would increase the accuracy of the predictions.

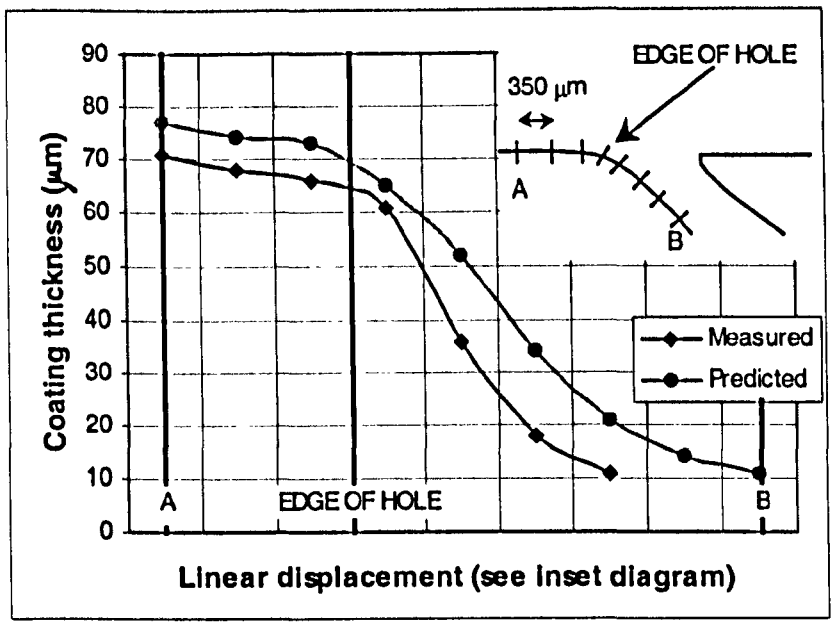

Figure 11-28: Comparison of measured and predicted deposition profiles versus linear displacement from the hole entrance.

Visualisation of the predicted results, using the software tool, is easy to perform. After selecting the position of the component and the general and rotational parameters, the use of the number of colours and various plot ranges, in addition to the zoom, move and rotate features, allows the component and any desired detail to be seen from any position. For example, Figure 11-29a represents the thickness distribution for the above component using ten colours. From Figure 11-29a it is difficult to analyse the coating thickness at the entrance of the cooling holes. However, by using the zoom command (see chapter on the computer program), and selecting a different plot range and number of colours, it is possible to highlight small variations in coating thickness (Figure 11-29b,c). In addition, it is possible to translate or rotate the component in order to look at it from any arbitrary point to get a good view of it. This was achieved by using an OpenGL-related library known as OpenGL Utility Toolkit (GLUT)[6]. Figure 11-29d illustrates a view with the "camera" inside the component and looking out of the hole (the source is represented by the small green dot in the centre of the hole).

When plotting the thickness profile, facets with a deposition rate within the selected range are represented as a solid area whereas wireframe facets have a deposition rate within the selected range but represent the backside of the facet. In addition, facets with a deposition rate outside the plot range are not drawn by the computer model.

Worth noting is that by varying both the number of colours and plot range, the colour used to represent a given facet also varies. This does not mean that the coating thickness changes with the above parameters. What it means is that the colours used are always relative to the plot range. That is, red and blue are used to represent the facets with the

[6] See http://reality.sgi.com/opengl/glut3/glut3.html for more information about OpenGL Utility Toolkit.

lowest and highest deposition rate specified by the plot range, respectively. If ten colours are used to plot the range between 0-50%, then red and blue represent facets with a deposition rate of between 0-5% and 45-50%, respectively. If the same number of colours is used to plot the range between 50-100%, then red and blue represent facets with a deposition rate of between 50-55% and 95-100%, respectively.

From Figure 11-29b-d it can clearly be seen that the coating exhibits, for this example, a graduation in thickness from the hole entrance to the bottom of the hole. The area in the hole that is hidden from the source is shown as red (Figure 11-29d).

An important aspect of the modelling concerns the accuracy of the predictions. For small features, such as cooling holes, the accuracy of the predictions is a function of the number of iterations. In other words, the more iterations that are performed by the model the more accurate the results should be. This is important because, for instance, a 300 μm thick coating is relatively big compared to a 1 mm diameter hole. It follows, therefore, that to predict a coating thickness around small features with reasonable accuracy the coating must be integrated as part of the component geometry taking into full consideration its effect on the predicted results for the next iteration (i.e. it is important to recalculate the component shape). A development of the computer model could, therefore, include the possibility for the user to select the number of iterations or accuracy and also, importantly, the estimated time associated with each option so that the user can select an accuracy based on how long that option takes. For example, it may be viable to run the software tool for 1 hour to achieve an accuracy of ±20% but impractical to achieve ±10% accuracy, if the computer model takes 6 hours.

From the above, it is clear that further experimental research is required in order to predict the percentage of hole closure and thickness distribution, as a function of the above parameters.

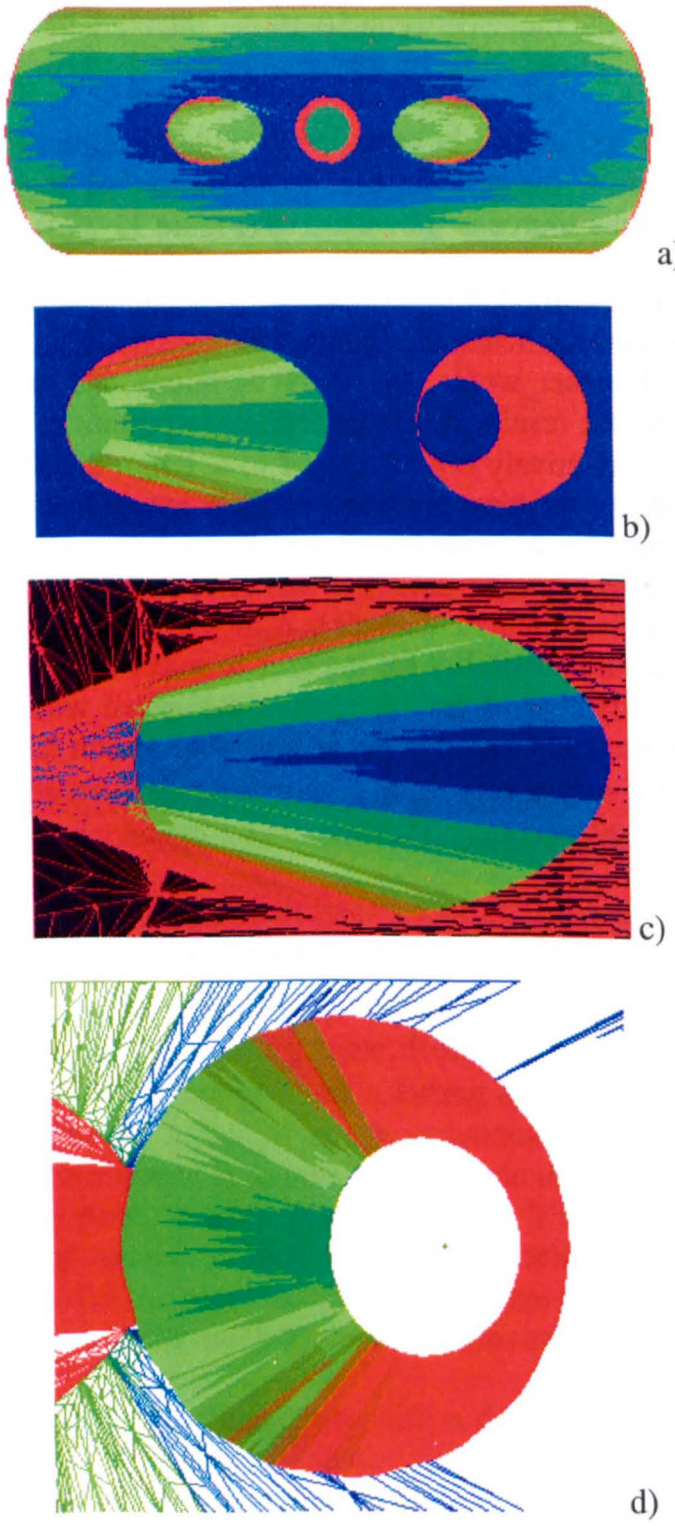

Figure 11-29: Thickness distribution for a cylinder-shaped component with three cooling holes a) whole component; b)-c) detailed view of an inclined hole; d) looking out of the hole (the source is represented by a dot in the centre of the hole).

11.7. Run VI (Commercial Equipment)

Two turbine blade sections were coated using commercial equipment by a leading company in the coating technology field for aircraft and industrial turbine engines. The blade sections were taken from an industrial turbine with both samples identical in terms of design profile, with a length of around 15 cm, but slightly different in transversal width, as illustrated in Figure 11-30.

In order to compare the measured thickness to that predicted, the computer model needs, as mentioned earlier, the STL representation of the part, in addition to the planetary motion associated with the rotation of the component. However, the majority of evaporation parameters associated with the characteristics of coating equipment are considered highly proprietary. Some of the confidential information include, but are not limited to, working height, source separation (for a multiple source arrangement), source diameter (may lie between 2.5 and 7 cm), source rotational speed (if used), scanning pattern, path and speed of translation, and rotational speed of the substrates. None of this information was therefore provided by the commercial coater company.

Neither the STL file of the part nor the planetary motion was provided either; therefore the coating thickness could not be predicted accurately using the software tool and compared to that measured. However, the point of rotation was known, as was the measured coating thickness around both turbine sections, as shown in Figure 11-31. All measurements are expressed in micrometres. In addition, rotation of the turbine blade seen in the computer model section is of the same proportions as the blade sections thus allowing a comparison between measured and predicted for various locations around the component.

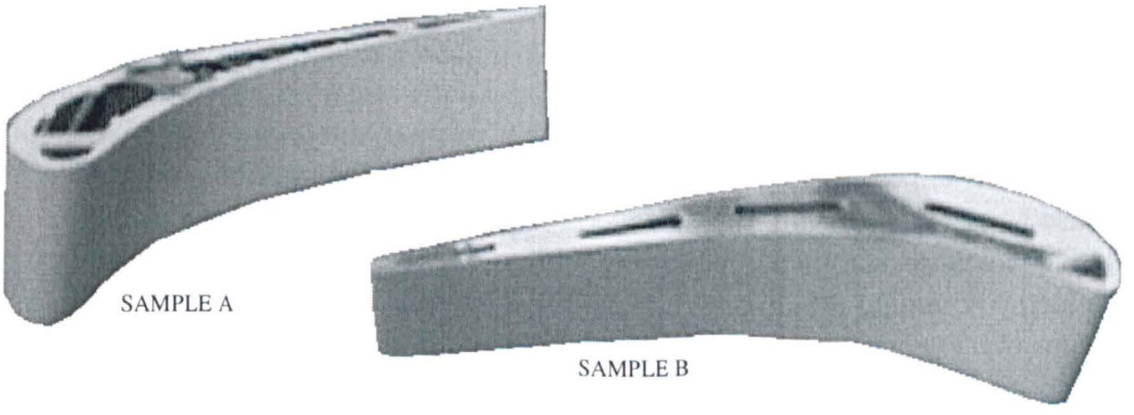

Figure 11-30: Turbine blade sections coated with a TBC under production conditions.

Figure 11-31 presents the measured coating thickness around the turbine blade sections. Uniformity is accurate to within ±20%, which, due to the size of the components, suggests a complex planetary motion of the parts, such as rotation around the longitudinal axis of the components, in addition to translation and/or tilt. Also, due to

the size of the components, the coating equipment used should have been a multisource coater, possibly a two or three-source coater. Worth noting is that the coating at the trailing edge is slightly thicker than that at the leading edge, which is contrary to aerodynamic performance. One hypothesis is that the above thickness profile is suitable for stator vanes of industrial gas turbines, which are more prone to higher temperatures. Assuming that both samples were coated concurrently and the same coating time was allowed, it appears that SAMPLE B was either further away from the centre of the vapour flux or a different planetary motion was used.

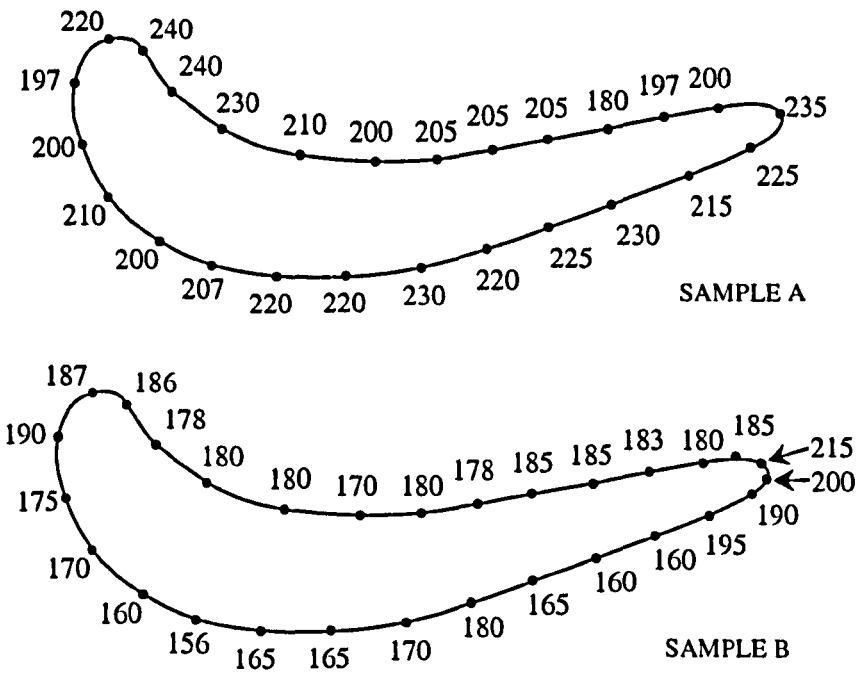

Figure 11-31: Measured thickness distribution for two turbine blade sections coated under production conditions (all measurements in micrometres).

A simulation of the predicted thickness, using the computer model, for a turbine blade was performed, rotated around the same point and in the same proportions as the two turbine blade sections. In order to achieve a uniform thickness distribution onto a component 15 cm long rotated around a single axis of rotation, as is the case of the software tool, it appears that the component must be positioned remote from the source or, as the results appear to indicate, a more complex planetary motion should have been used. Based on the deposition rate achieved for previous experiments (8 $\mu m/min^{-1}$ at 10 cm above the source, stationary), theory would predict, based on the inverse square law, for a rotated component 30 cm above the source, a deposition rate of just 0.5 $\mu m/min^{-1}$. This means that the substrate is remotely enough so that minor changes in the source-to-substrate distance have a small influence on the deposition rate.

Therefore, from the various calculations performed it appears that the point of rotation was around 30 cm above the source. A typical predicted coating thickness for such a component is shown in Table 11-4. Since the point of rotation was closer to the leading edge (about one-third of the length of the blade), the predicted coating thickness for the trailing edge was higher than that measured (the trailing edge gets closer to the source). However, the geometry of the trailing edge has a small radius compared to the leading edge and, therefore, the vapour flux arrives at a steeper angle than at the leading edge.

This is important because, even though the trailing edge gets considerably closer to the source, the overall deposition was uniform within ±20%.

For a source-to-substrate distance of 30 cm, it is estimated that the source separation was around 24 cm in order for a uniform deposition to be achieved, whilst permitting a greater component throughput. Nevertheless, a uniform deposition can also be achieved for parameters different to those mentioned above by varying the planetary motion design.

Table 11-4: Predicted versus measured coating thickness for the turbine blade sections based on a turbine blade geometry (all measurements in micrometres).

SAMPLE A	Measured	Predicted
Leading Edge	220	224
Point of rotation (pressure surface)	220	210
Point of rotation (suction surface)	212	238
Trailing Edge	235	279
SAMPLE B	Measured	Predicted
Leading Edge	187	192
Point of rotation (pressure surface)	180	172
Point of rotation (suction surface)	156	175
Trailing Edge	215	256

Contacts and visits have been made to major engine manufacturers, both in the UK and abroad. However, because of confidentiality issues due to the proprietary nature of the information, no other details were disclosed. Nevertheless, it is clear that this software tool holds great promise, although difficulties have been recognised in extending the model to user-specific requirements due to confidentiality issues. In the next section, a discussion of the major aspects concerning the extension of the software tool as it is perceived to fit into the manufacturing process of turbine blades is provided.

11.8. Incorporation into the Manufacturing Process

Because the software tool was developed for experimental evaluation, the planetary motion of the part simulated within the computer model reflects the laboratory coater existent at Cranfield University. Therefore, other planetary motions such as translation, rotation and butterfly action, typical of commercial coaters, have still to be incorporated in the model, even though the necessary tools for substrate rotation and translation have already been developed. In other words, programming a complex motion of parts such as rotation of the substrates around their longitudinal axis, translation or rotation around a second axis, and tilting of the substrate holder can be achieved by calling the modelling transformation functions (rotation and translation) in the required order.

Prediction of the coating thickness should be performed to various user-defined accuracies as this can be traded off for calculation speed. In addition, it should be possible to visualise the predicted coating thickness for certain areas of the substrate such as all around the aerofoil section and for various positions along the height of the blade.

Another important aspect of the software tool is visualisation of the results. Since the colour gradient may be confusing or if it is not accurate enough then a data visualisation tool could be used. One such product is SigmaPlot[7]. SigmaPlot provides tools to acquire data and then analyse and manage a full range of graph options to create technical graphs. Also important is the fact that SigmaPlot scripts can be embedded in custom C++ or Visual Basic programs allowing SigmaPlot to be used from within these applications[8]. It follows, therefore, that the software tool could use the capabilities of SigmaPlot to present the results in a user-friendlier manner than colour gradients.

Still another far-reaching feature would be exporting the predicted results to a file in order to perform studies on the integrated component and coating layer. Relevant studies, which turbine blade engineers carry out, include cooling airflow, stress distribution, and surface temperature, for instance. One solution would be exporting both the geometric information of the substrate and the predicted coating thickness to an STL file. The STL file could then be used by any application that supports facetted data like Finite Element Analysis (FEA) and Computer-Aided Manufacturing (CAM) applications, but not usually CAD application since they do not generally understand STL files. For this reason, it is important either to create a file that can be read by CAD systems, such as a neutral file format, or use a program to translate STL files into such a file format. A bi-directional IGES/STL translator is already available on the market[9] capable of performing the required translation. Since IGES is a neutral file format for exchange of CAD data between heterogeneous systems, the aforementioned studies could thus be performed.

[7] See http://www.spssscience.com/SigmaPlot for more product information or to download the SigmaPlot demo.
[8] *Eureka!* Volume 2 Issue 3. The Computer Algebra Centre Ltd. http://www.clecom.co.uk
[9] http://www.compunix-usa.com

CHAPTER

12

12. Conclusions

A software tool has been developed based on the Knudsen cosine law and aimed at calculating the coating thickness distribution around any component, but typically turbine blades. This study then proceeded to verify the computer model by first measuring the coating thickness for experimental trial runs and then comparing the calculated coating thickness to that measured using a laboratory coater.

The following principal conclusions have been drawn as a result of this study:

- To a first approximation, the EB-PVD evaporation source can be considered as a point source evaporator, but with evaporation characteristics that vary with the material being evaporated, the shape of the source and the geometry of the e-beam scan pattern. These source variations have been accommodated in the computer model by developing a generalised point source evaporation model that involves real and virtual sources operating in a 3D semisphere above the melt. The computer program developed in Visual C++ can simulate this behaviour including sources with large dimensions, asymmetric evaporation behaviour, the inclusion of multiple sources within a vacuum coating system, and the virtual source concept.

- Substrates with complex geometry can be modelled by generating an STL file from a CAD package with the geometric information of the component, which may include shadow-masks. The influence of shadow-mask size, orientation and geometry can then be assessed through successive runs of the computer model. Visualisation of the coated thickness distributions around components was achieved using OpenGL library functions within the computer model.

- Coating thickness profile and column inclination is a combination of both the evaporation and deposition models. In other words, the rate of coating deposition, and the direction of growth, at any point on a component surface depends on integrating the complex vapour flux distributions from all sources, both virtual and real, onto a predefined, inclined surface element (which may be rotated within the evaporation vapour flux and affected by non contact masks).

- Investigations of various arrangements indicate that the gas scattering within the coater offsets the directionality of the vapour flux. From the results, the effect of various virtual sources at the backside of a stationary cylinder was evident - (a deposition rate 3 – 4% that of the leading edge position was measured). In addition, for the side facing the source, a virtual source offset was apparent, from the point

directly above the source, increasing its effect as the vapour incidence angle increased.

- The applicability of the computer model, developed to characterise the thickness distribution around rotated components, through the use of non-contact masks, as a function of both the evaporation and deposition conditions, was evident from the various runs undertaken. The software tool can, consequently, reduce the number of iterations that are necessary to set up the various process parameters in order to achieve a desired thickness distribution on a component. From the knowledge of the predicted vapour flux distributions it should be possible to design masks capable of limiting the undesirable deposition of coatings on parts of a component and thus profiling the coating thickness in order for the deposit to follow a specified thickness distribution over the substrate surface. Optimisation of process parameters may contribute simultaneously to an increase in the deposition rate and increase in component throughput, hence reducing unit coating cost.

One can foresee computer models similar to that proposed being used to design mask geometry and component planetary motion, allowing the custom profiling of EB-PVD TBCs on aerofoil sections for both optimal thermal resistance and good erosion behaviour without compromising the aerodynamic performance of the turbine blade or vane. Other applications, where coating uniformity is critical to component performance, would benefit from the use of this software if the coatings are deposited by EB-PVD methods, for example, optical coatings on lenses and mirrors, and multi-layered wear-resistant coatings on cutting tools.

CHAPTER

13

13. Further Work

It is recommended that further development of the software tool incorporates the following:

- Programming of a parts manipulator with planetary motion other than one-axis rotation. In order for the software tool to match a specified planetary motion, such as the typical complex motion of commercial equipment, for example, the sequence of movements have to be matched by calling the modelling transformation functions (rotation and translation) in the required order.

- Programming of the positioning of two or more models (either substrates or shadow-masks), within the coater space, relative to one another. Currently, substrates and shadow-masks are treated as a single entity and thus one part cannot be positioned or moved relative to the another. This limitation can be partly overcome if the geometric information of the various parts are stored in separate files thus allowing each part to be moved or rotated independently, using the software tool, and then recombining the parts by joining them into a single file using a text editor.

- Visualisation of the predicted coating thickness could be performed for certain areas of the substrate such as both the leading and trailing edges and for other pre-defined positions around the aerofoil section. In addition, these results could be predicted for various position along the height of the blade (for a height of 25, 50 and 75% from the root, for example). Moreover, visualisation of the results could be improved. For example, SigmaPlot provides tools to manage a full range of graph options and SigmaPlot scripts can be embedded in custom C++ programs allowing SigmaPlot to be used from within these applications.

- Development of the user-interface allowing the end-user to specify all source variation characteristics with appropriate dialog boxes. For example, if tests performed on a certain source indicate that an asymmetric wide source arrangement is preferred over the single point source, then the user should be able to select, using an user-friendly interface, the number of point sources, their distance from the centre of the source, and for each point source, its emitting properties (focus of the vapour flux).

- Tessellation could be performed for certain areas of the component such as the leading and trailing edges of the component whilst reducing the number of triangles in parts of the components which are masked to avoid deposition.

- If calculation speed is of concern, methods to improve speed have been discussed in the section about the computer model. In particular, the user should try an reduce the number of triangles required to represent the part, for example, by using a model without root and tip or using the casting model, which represents the root as a lump of material, hence requiring fewer triangles. Furthermore, it is possible to eliminate the time-consuming visibility check by creating an array of 72 pointers (for a 5-degree increment), each position containing a list of the visible facets for that iteration.

Studies on other equipment, including both laboratory and commercial coaters, would be useful to define the accuracy of the predictions further and to evaluate the feasibility of complex geometry coating, in addition to contributing to knowledge on how to control process parameters more precisely. Recommendations for further work include:

- Coating of both stationary and rotated real parts within a laboratory coater. Whilst the former would facilitate the definition of any virtual sources present, the latter would test a simple planetary motion.

- Coating of a real part within a coater with a more complex planetary motion, such as rotation of the blade around its longitudinal axis and translation about a second axis. This requires the computer model's planetary motion facility being extended by calling the modelling transformation functions (rotation and translation) in the required order.

- Coating of simple parts (flat plates, stationary and rotating cylinders) within a multi-source coater, for example, a two or three-source coater. This type of configuration would ideally require each source to be studied independently in order for the behaviour of each vapour plume to be precisely defined. This study would characterise whether each source could be modelled as a single point source or as a wide source, any virtual sources present and their configuration (location and intensity), and also importantly any asymmetry effects of the source. In addition, the additive effects of the two or three sources could also be addressed.

- Coating of a real part within a commercial coater with a complex planetary motion. These coaters typically have up to three movements including rotation, translation and tilting, the latter being either butterfly or tandem. This would represent the most complex planetary system and all movements would have to be programmed including positions, accelerations, velocities, and dwell times.

All of the above investigations would require simulation using the computer model, of the predicted thickness distribution using the associated STL file and then a comparison of the measured and predicted results. Various other studies, which have to be performed on the integrated component and coating layer system, are relevant to the fields of aircraft engine manufacturers and manufacturers of stationary gas turbines. Such studies include cooling airflow, stress distribution, and surface temperature. Therefore, the predicted coating thickness could be integrated as part of the component geometry (STL file) and an IGES file created using an IGES/STL translator (http://www.compunix-usa.com) to perform the above studies.

References

AGARD, Proceedings of the 85th Meeting of the Advisory Group for Aerospace Research & Development (AGARD) Structures and Materials Panel on "Thermal Barrier Coatings". AGARD-R-823, ISBN 92-836-1073-3. Aalborg, Denmark 15-16 October 1997.

Alpérine, S.; Derrien, M.; Jaslier, Y.; Mévrel, R. **Thermal Barrier Coatings: the Thermal Conductivity Challenge.** Proceedings of the 85th Meeting of the AGARD Structures and Materials Panel on "Thermal Barrier Coatings". (Published April 1998). Aalborg, Denmark 15-16 October 1997, 1.1-1.10.

Alpérine, S.; Lelait L. **Microstructural Investigations of Plasma-Sprayed Yttria Partially Stabilized Zirconia TBC (In Relation to Thermomechanical Resistance and High-Temperature Oxidation Mechanisms).** *Journal of Engineering for Gas Turbines and Power*, Vol. 116, January 1994, 258-265.

Amagasa, S.; Shimomura, K.; Kadowaki, M.; Takeishi, K.; Kawai, H.; Aoki, S.; Aoyama, K. **Study on the Turbine Vane and Blade for a 1500°C Class Industrial Gas Turbine.** *Journal of Engineering for Gas Turbines and Power*, Vol. 116, July 1994, 597-604.

America, P. H. M.; Rutten, J. J. M. M. **A Parallel Object-Oriented Language: Design and Semantic Foundations.** Chapter 1. IN: de Bakker, 1989.

An, K.; Ravichandran, K. S.; Dutton, R. E.; Semiatin, S. L. **Microstructure, Texture, and Thermal Conductivity of Single-Layer and Multilayer Thermal Barrier Coatings of Y_2O_3-Stabilized ZrO_2 and Al_2O_3 Made by Physical Vapor Deposition.** *Journal of the American Ceramic Society*, Vol. 82, No. 2, Feb. 1999, 399-406.

Andritschky, M.; Teixeira, V.; Rebouta, L.; Buchkremer, H. P.; Stöver, D. **Adherence of Combined Physically Vapour-Deposited and Plasma-Sprayed Ceramic Coatings.** *Surface and Coatings Technology*, Vol. 76, 1995, 101-105.

Anklam, T. M. **Evaporation Rate and Composition Monitoring of Electron Beam PVD Processes.** Workshop Proceedings on "Electron Beam-Physical Vapor Deposition". PennState University, Applied Research Laboratory, 10-11 June 1998.

Anklam, T. M.; Berzins, L. V.; Braun, D. G.; Haynam, C.; Meier, T.; McClelland, M. A. **Evaporation Rate and Composition Monitoring of Electron-Beam Physical Vapor-Deposition Processes.** *Surface and Coatings Technology*, Vol. 77, No. 1-3, December 1995, 681-686.

Azad, F. H.; Skelly, D. W.; Rigney, D. V. **Electron Beam Physical Vapor Deposition Method.** US Patent No. 5,698,273. 1997.

Baghurst, D. J. *Notes on the Optimisation of Evaporation Process Conditions.* Prince of Wales Ind Est, Abercarn, Gwent, 1987.

Bartz, A.; Maricocchi, A.; Wortman, D. J. *PVD TBC experience on GE Aircraft Engines.* General Electric CO., Cincinnati, OH. Aircraft Engines, March 1995

Baxter, D. J.; Gilliand, D.; Lanza, F.; Toledo, G. P.; Bregani, F. **The Oxidative and Corrosive Degradation of Vacuum Plasma Sprayed Coatings in Industrial Gas Turbine Environments.** *Materials Science Forum*, vols. 251-254 (2), 1997, 801-808.

Beele, W. *Erosion/Corrosion Protective Coating for High-Temperature Components.* World Patent WO 96/31636, 1996.

Bennett, A. **Properties of Thermal Barrier Coatings.** *Materials Science and Technology*, Vol. 2, March 1986, 257-261.

Bertamini, L.; Di Gianfrancesco, A. *Thermal Testing of High Performance Thermal Barrier Coatings for Turbine Blades.* International Organization, November 1994, 33-1 to 33-11.

Bettridge, D. F.; Ubank, R. G. **Quality Control of High-Temperature Protective Coatings.** *Materials Science and Technology*, Vol. 2, March 1986, 232-242.

Blake, J. W. PHIGS and PHIGS+. Academic Press Limited, ISBN 0-12-103515-8, 1993.

Blocher, Jr. J. M. **Chemical Vapor Deposition.** IN: Bunshah, R. F. *et al* Deposition Technologies for Films and Coatings. ISBN 0-8155-0906-5, Noyes Publications, New Jersey, 1982.

Boeing. **Fuel: Burn Less, Spend Less.** *Airliner.* Boeing Commercial Airplane Group. January-March 1997, 2-3.

Boone, D. H. **Physical Vapour Deposition Processes.** *Materials Science and Technology*, Vol. 2, March 1986, 220-224.

Boone, D. H.; Strangman, T. E.; Wilson, L. W. **Some Effects of Structure and Composition on the Properties of Electron Beam Vapor Deposited Coatings for Gas Turbine Superalloys.** *Journal of Vacuum Science Technology*, Vol. 11, No. 4, July/August 1974, 641-646.

Bosch, S. **Lens Coating in Thermal Evaporation Physical Vapour Deposition Chambers: Optimization of the Geometrical Configuration.** *Journal of Physics D: Applied Physics,* Vol. 26, January 1993, 124-129.

Bose, S.; DeMasi-Marcin, J. *Thermal Barrier Coatings Experience in Gas Turbine Engine at Pratt & Whitney.* In NASA. Lewis Research Centre, Thermal Barrier Coating Workshop, March 1995, 63-78.

Brain, S. **The Mapping of Occam onto the Transputer Architecture.** Proceedings of the workshop on "Parallel Processing and Control – The Transputer and other Architectures", University College of North Wales, Bangor, 4-6 July 1988, 7.1-7.11.

Bratton, R. J.; Lau, S. K.; Andersson, C. A.; Lee, S. Y. **Studies of Thermal Barrier Coatings for Heat Engines.** Proceedings of the Second Conference on Advanced Materials for Alternative-Fuel-Capable Heat Engines. (Published May 1982). EPRI, RD-2369-SR, California, August 24-28, 1981, 6.82-6.101.

Brown, A. S. **Breaking the Turbine Temperature Barrier with TBCs.** *Aerospace America*, October 1996, 22-23.

Bruce, R. W.; Skelly, D. W.; Minnear, W. P.; Nardi, Jr. R. A.; Wortman, D. J.; Maricocchi, A. F.; Viguie, R.; Rigney, D. V. **Vapor Deposition of Ceramic Materials.** US Patent No. 5,418,003. 1995.

Bunshah, R. F. *et al* Deposition Technologies for Films and Coatings. ISBN 0-8155-0906-5, Noyes Publications, New Jersey, 1982.

Bunshah, R. F. **High-Rate Evaporation/Deposition Processes of Metals, Alloys, and Ceramics for Vacuum Metallurgical Applications.** *Journal of Vacuum Science Technology*, Vol. 11, No. 4, July/August 1974, 814-819.

Bürgel, R. **Coating Service Experience with Industrial Gas Turbines.** *Materials Science and Technology*, Vol. 2, March 1986, 302-308.

Carling, A. Parallel Processing – the Transputer and Occam. Sigma Press, ISBN 1-85058-077-4, 1988.

Cernuschi, F.; Bianchi, P.; Leoni, M.; Scardi, P. **Thermal Diffusivity/Microstructure Relationship in Y-PSZ Thermal Barrier Coatigns.** *Journal of Thermal Spray Technology*, Vol. 8(1), March 1999, 102-109.

Chan, K. S.; Cheruvu, N. S.; Leverant, G. R. **Coating Life Prediction for Combustion Turbine Blades.** *Journal of Engineering for Gas Turbines and Power*, Vol. 121, July 1999, 484-488.

Chang, P.; Halnan, W. K.; Hill, R. J. **Improvements in Equipment for the Evaporation of Subliming Materials in Reactive Gas Conditions.** Workshop Proceedings on "Electron Beam-Physical Vapor Deposition". PennState University, Applied Research Laboratory, 10-11 June 1998.

Chen, Q. F.; Peng, X.; Ma, X. Q.; Yuan, K. Q.; Li, T. F. **Thermal Stress Analysis of Ceramic Thermal Barrier Coatings under Loading.** *Chinese Academy of Sciences, Inst. of Corrosion & Protection of Metals.* Proceeding (A95-43894 12-27), Singapore, World Scientific, *1995, 683-686.*

Chevillard, S.; Drawin, S.; Vidal-Sétif, M. H. **Plasma Assisted CVD of Thick Yttria Partially Stabilized Zirconia Coatings.** Proceeding of the 85th Meeting of the AGARD Structures and Materials Panel on "Thermal Barrier Coatings". (Published April 1998). Aalborg, Denmark, 15-16 October 1997, 11.1-11.9.

Chow, R.; Bunshah, R. F. **Model for Calculating the Deposit Temperature in High-Rate Physical-Vapor-Deposition Process.** *The Journal of Vacuum Science and Technology*, Vol. 8, No. 6, 1971, VM73-VM78.

Conner, J. A.; Connor, W. B. **Ranking Protective Coatings: Laboratory vs. Field Experience.** *Journal of Metals*, December 1994, 35-38.

Cooper, S. P.; Strang, A. **Properties of Thermal Barrier Coatings.** (summary) *Materials Science and Technology*, Vol. 2, March 1986, 257.

Cosack, T.; Pawlowski, L.; Schneiderbanger, S.; Sturlese, S. **Thermal Barrier Coatings on Turbine Blades by Plasma Spraying With Improved Cooling.** *Journal of Engineering for Gas Turbines and Power*, Vol. 116, January 1994, 272-276.

Crostack, H.-A.; Beller, U. **Investigation of Damage Behaviour of Thermally Sprayed Coatings Depending on Coating Thickness.** Proceedings of the 8th National Thermal Spray Conference, 11-15 September 1995, Houston, Texas, 1995, 433-438.

Cruse, T. A.; Stewart, S. E.; Ortiz, M. **Thermal Barrier Coating Life Prediction Model Development.** *Journal of Engineering for Gas Turbines and Power*, Vol. 110, October 1988, 610-616.

Dapkunas, S. **Evaluation of the Hot-Corrosion Behaviour of Thermal Barrier Coatings.** Proceedings of 1974 Gas Turbine Materials in the Marine Environment Conference, 24-26 July 1974, 481-502.

De Bakker, J. W. Languages for Parallel Architectures – design, semantics, implementation models. John Wiley & Sons, ISBN 0-471-92177-7, 1989.

Demaray, R. E. **Adherent Ceramic Coatings.** US Patent No. 4,676,994. 1987.

Demaray, R. E.; Halnan, W. K.; Shen, S. **Development of Electron Beam Physical Vapor Deposition of Ceramic Coatings.** Proceedings of the Second Conference on Advanced Materials for Alternative-Fuel-Capable Heat Engines. (Published May 1982). EPRI, RD-2369-SR, California, August 24-28, 1981, 6.151-6.184.

Demaray, R. E; Fairbanks, J. W; Boone, D. H. *Physical Vapor Deposition of Ceramic Coatings for Gas Turbine Engine Components.* ASME Paper 82-GT-264, 1982.

DeMasi-Marcin, J. T.; Sheffler, K. D.; Bose, S. **Mechanisms of Degradation and Failure in a Plasma-Deposited Thermal Barrier Coating.** *Journal of Engineering for Gas Turbines and Power*, Vol. 112, No. 4, October 1990, 521-526.

Desrochers, G. R. Principles of Parallel and Multiprocessing. Intertext Publications, Inc. McGraw-Hill Book Company, ISBN 0-07-016579-3, 1987.

Driver, D.; Hall, D. W.; Meetham, G. W. **The Gas Turbine Engine.** Chapter 1. IN: Meetham, G. W. The Development of Gas Turbine Materials. 1981, 1-30.

Duderstadt, E. C. **Thermal Barrier Coating System With Hardenable Bond Coat.** US Patent No. 5,498,484. 1996.

Duderstadt, E. C.; Nagaraj, B. A. **Thermal Barrier Coating System With Intermetallic Overlay Bond Coat.** US Patent No. 5,238,752. 1993.

Duret, C.; Pichoir, R. **Protective Coatings for High Temperature Materials: Chemical Vapour Deposition and Pack Cementation Processes.** IN: Proceedings of the seminar "Coatings for High Temperature Applications". Edited by E. Lang. Applied Science Publishers. CEC High Temperature Materials Information Centre, Petten, The Netherlands, ISBN 0-85334-221-0, 1983, 33-78.

Durham, S.; Meier, S. M.; Gupta, D. K.; Sheffler, K. D. **Ceramic Thermal Barrier Coatings.** In: Advances in High Temperature Structural Materials and Protective Coatings. National Research Council of Canada, 1994, 226-236.

Duvall, D. A.; Ruckle, D. L. *Ceramic Thermal Barrier Coatings for Turbine Engine Components.* ASME Paper 82-GT-322, 1982.

Duvall, D. S. **Processing Technology for Advanced Metallic and Ceramic Turbine Airfoils Coatings.** Proceedings of the Second Conference on Advanced Materials for Alternative-Fuel-Capable Heat Engines. (Published May 1982). EPRI, RD-2369-SR, California, August 24-28, 1981, 6.102-6.117.

Eastman, C. G. **Is a Standard Possible for Engineering Data?** *Inform.* October 1988, 18-21.

EPRI, Proceedings of the Second Conference on Advanced Materials for Alternative-Fuel-Capable Heat Engines. RD-2369-SR, Monterey, California, 24-28 August 1981 (Published May 1982).

Fauchais, P.; Vardelle, A.; Vardelle, M. **Recent Developments in Plasma Sprayed Thermal Barrier Coatings.** Proceedings of the 85th Meeting of the AGARD Structures and Materials Panel on "Thermal Barrier Coatings". (Published April 1998). Aalborg, Denmark 15-16 October 1997, 3.1-3.12.

Fleming. P. J. **Occam Model of Parallelism.** Proceedings of the workshop on "Parallel Processing and Control – The Transputer and other Architectures", University College of North Wales, Bangor, 4-6 July 1988, 3.1-3.15.

Fosner, R. OpenGL Programming for Windows 95 and Windows NT. Addison-Wesley Developers Press, ISBN 0-201-40709-4, 1997.

Freborg, A. M.; Ferguson, B. L.; Brindley, W. J.; Petrus, G. J. **Bond Coat Considerations for Thermal Barrier Coatings.** Proceeding of the 85th Meeting of the AGARD Structures and Materials Panel on "Thermal Barrier Coatings". (Published April 1998). Aalborg, Denmark, 15-16 October 1997, 17.1-17.9.

Freborg, A. M.; Ferguson, B. L.; Brindley, W. J.; Petrus, G.J. **Modeling Oxidation Induced Stresses in Thermal Barrier Coatings.** *Materials Science and Engineering A* - Structural Materials: Properties, Microstructure and Processing, Vol. A245, No. 2, 1 May 1998, 182-190.

Freeman, T. L.; Phillips, C. Parallel Numerical Algorithms. Prentice Hall, ISBN 0-13-651597-5, 1992.

Fritscher, K.; Schmuecker, M.; Leyens, C.; Schulz, U. **TEM investigation on the adhesion of YPSZ EB-PVD TBCs.** *Materials Science Forum*, vols. 251-254 (2), 1997, 965-70.

Gedwill, M. A. *Burner Rig Evaluation of Thermal Barrier Coating System for Nickel-Base Alloys.* NASA TM-81684, February 1981.

Gell, M. **Applying Nanostructured Materials to Future Gas Turbine Engines.** *Journal of Metals*, October 1994, 30-34.

Gell, M. **The Potential for Nanostructured Materials in Gas Turbine Engines,** Proceedings of the 2nd International Conference on Nanostructured Materials, (October 1994) Vol. 6, 1995, 997-1000.

Gell, M.; Duhl, D. N.; Gupta, D. K.; Sheffler, K. D. **Advanced Superalloy Airfoils.** *Journal of Metals*, July 1987, 11-15.

Gell, M.; Vaidyanathan, K.; Barber, B.; Cheng, J.; Jordan, E. **Mechanisms of Spallation in Platinum Aluminide/Electron Beam Physical Vapor-Deposited Thermal Barrier Coatings.** *Metallurgical and Materials Transactions A*, Vol. 30A, February 1999, 427-435.

Gill, B. J.; Tucker, Jr R. C. **Plasma Spray Coating Processes.** *Materials Science and Technology*, Vol. 2, March 1986, 207-213.

Gladden H. J.; Liebert C. H. *Effects of a Ceramic Coating on Metal Temperatures of an Air-Cooled Turbine Vane.* NASA TP-1598, February 1980.

Glang, R. **Vacuum Evaporation.** Chapter 1. IN: Maissel L. I.; Glang R. Handbook of Thin Film Technology. New York: McGraw-Hill, ISBN 0-07-039742-2, 1970.

Goward, G. W. **Coatings and Coating Processing for Gas Turbine Airfoils Operating in a Marine Environment.** Proceedings of 1974 Gas Turbine Materials in the Marine Environment Conference. 24-26 July 1974, 277-296.

Goward, G. W. **Progress in Coatings for Gas Turbine Airfoils.** *Surface and Coatings Technology*, Vol. 109, No. 1-3, Oct. 10 1998, 73-79.

Goward, G. W. **Protective Coatings - Purpose, Role and Design.** *Materials Science and Technology*, Vol. 2, March 1986, 194-200.

Goward, G. W. **Recent Developments in High Temperature Coatings for Gas Turbines Airfoils.** Proceedings of the Conference on "High Temperature Corrosion". (Published 1983), California, Vol. NACE-6, March 2-6, 1981, 553-560.

Goward, G. W.; Grey, D. A.; Krutenat, R. C. **Thermal Barrier Coating for Nickel and Cobalt Base Super Alloys.** US Patent No. 4,248,940. 1981.

Graper, E. B. **Evaporation Characteristics of Materials from an Electron-Beam Gun.** *The Journal of Vacuum Science and Technology*, Vol. 8, No. 1, 1971, 333-337.

Grovenor, C. R. M., Hentzell, H. T. G.; Smith, D. A. **The Development of Grain Structure During Growth of Metallic Films.** *Acta Metall.*, Vol. 32, 1984, 773-781.

Gruner, H. **Vacuum Plasma Spray Quality Control.** *Thin Solid Films*, Vol. 118, 1984, 409-420.

Gruninger, M. F.; Borls M. V., **Thermal Barrier Ceramics for Gas Turbine and Reciprocating Heat Engine Applications.** Proceedings of the International Thermal Spray Conference & Exposition, Orlando, Florida, USA, 28 May - 5 June, 1992

Grünling, H. W.; MannsMann, W. **Plasma Sprayed Thermal Barrier Coatings for Industrial Gas Turbines: Morphology, Processing and Properties.** *Journal de Physique IV*, Vol. 3, November 1993, 903-912.

Gupta, B. K.; Farmer, G.; Walker, A. **Thick Thermal Barrier Coating Having Grooves for Enhanced Strain Tolerance.** US Patent No. 5,558,922. 1996.

Gupta, B. K.; Reeves, J. D.; Nagaraj, B. A. **Thermal Barrier Coating.** US Patent No. 5,403,669. 1995.

Hague, D.; Appleby, J. A.; Wortman, D. J.; McLaughlin, M. H.; Azad, F. H.; Archacki, R.; Guile, R. W.; Lawton, P. F. **Vapor Phase Intelligent Processing of Materials - Thermal Barrier Coatings.** Workshop Proceedings on "Electron Beam-Physical Vapor Deposition". PennState University, Applied Research Laboratory, 17-18 September 1996.

Hancock, P. **Future Direction of Research on High-Temperature Coatings.** *Materials Science and Technology*, Vol. 2, March 1986, 310-313.

Hancock, P. **Summary of the Mechanisms of Hot Corrosion in Marine Gas Turbines and the Role of Scale Failure.** Proceedings of 1974 Gas Turbine Materials in the Marine Environment Conference. 24-26 July 1974, 225-236.

Harmsworth, P. D.; Stevens, R. *The Microstructure of Zirconia Thermal Barrier Coatings.* The Institute of Ceramics, Leeds, Issue No. 42, March 1989, 123-131.

Haubold, T.; Gans, H.; Schwingel, D.; Taylor, R. **On Thick Thermal Barriers for Combustor Applications.** Proceedings of the 85th Meeting of the AGARD Structures and Materials Panel on "Thermal Barrier Coatings". (Published April 1998). Aalborg, Denmark 15-16 October 1997, 5.1-5.7.

Hertz, H. *Ann. Physik.*, Vol. 17, 1882, 177.

Holland, L. Vacuum Deposition of Thin Films. Chapman and Hall Ltd, London, 1966.

Hopgood, F. R. A.; Duce, D. A.; Johnston, D. J. A Primer for PHIGS - C Programmers' Edition. John Wiley & Sons, ISBN 0-471-93330-9, 1992.

Howard, T. L. J.; Hewitt, W. T.; Hubbold, R. J.; Wyrwas, K. M. A Practical Introduction to PHIGS and PHIGS Plus. Addison-Wesley Publishing Company, ISBN 0-201-41641-7, 1991.

Howse, M. G. J. W. *Technology Trends for Large Gas Turbine Engines.* Royal Aeronautical Society Inaugural Sir Roy Fedden Lecture. Presented at Cranfield University, Monday 2nd March 1998.

Immarigeon, J-P.; Parameswaran, V. R.; Chow, D.; Morphy, D. D.; Gougeon, P.; Prystay, M.; Moreau, C. **Evaluation of Thermal Barrier Coatings for Burner Rig Tests.** Proceeding of the 85th Meeting of the AGARD Structures and Materials Panel on "Thermal Barrier Coatings". (Published April 1998). Aalborg, Denmark, 15-16 October 1997, 15.1-15.10.

Itoh, Y.; Tamura, M. **Reaction Diffusion Behaviours for Interface Between Ni-Based Super Alloys and Vacuum Plasma Sprayed MCrAlY Coatings.** *Journal of Engineering for Gas Turbines and Power* - Transactions of the ASME, Vol. 121, No. 3, July. 1999, 476-483.

Jacobson, B. E. **Microstructure of PVD-Deposited Films Characterized by Transmission Electron Microscopy.** IN: Bunshah, R. F. *et al* Deposition Technologies for Films and Coatings. ISBN 0-8155-0906-5, Noyes Publications, New Jersey, 1982.

Jaslier, Y.; Alpérine, S. **Electron Beam Physical Vapour Deposition Thermal Barrier Coatings: A Comparative Evaluation of Competing Deposition Technologies.** Proceeding of the 85th Meeting of the AGARD Structures and Materials Panel on "Thermal Barrier Coatings". (Published April 1998). Aalborg, Denmark, 15-16 October 1997, 8.1-8.10.

Johnson, C. A., Ruud, J. A.; Bruce, R.; Wortman, D. **Relationships Between Residual Stress, Microstructure and Mechanical Properties of Electron Beam Physical Vapor Deposition Thermal Barrier Coatings.** *Surface and Coatings Technology*, Vol. 109, No. 1-3, Oct. 10 1998, 80-85.

Jones, R. L. **Experiences in Seeking Hot Corrosion-Resistant Stabilizers for Zirconia**. Proceedings of the Symposium: "High Temperature Coatings II", Elevated Temperature Coatings: Science and Technology II, ch.39, 1996, 127-138.

Jones, R. L.; Reidy, R. F. **Development of Hot Corrosion Resistant Scandia-Stabilized Zirconia Thermal Barrier Coatings.** Elevated Temperature Coatings: Science and Technology, The Minerals, Metals & Materials Society, October 1994, 23-30.

Jones, S. R. **Parallel Processing Computer Architectures.** Proceedings of the workshop on "Parallel Processing and Control – The Transputer and other Architectures", University College of North Wales, Bangor, 4-6 July 1988, 1.1-1.9.

Jordan, D. W. *Failure of Ceramic Thermal Barrier Coatings.* PhD Thesis, Northwestern University, Evanston, Illinois, December 1994.

Jue, J-F.; Nageswaran, R.; Virkar, A. **Characterization of Yttria and Rare Earth-Oxide Doped Zirconia Materials for High Temperature Applications.** Proceedings of the Symposium: "High Temperature Coatings II", Elevated Temperature Coatings: Science and Technology I, ch.37, 1995, 125-134.

Kaysser, W. A.; Peters, M.; Fritscher, K.; Schulz, U. **Processing, Characterisation and Testing of EB-PVD Thermal Barrier Coatings.** Proceeding of the 85th Meeting of the AGARD Structures and Materials Panel on "Thermal Barrier Coatings". (Published April 1998). Aalborg, Denmark, 15-16 October 1997, 9.1-9.11.

Kennard, E. H. The Kinetic Theory of Gases. McGraw-Hill Book Co. Inc. New York, 1938.

Knudsen, M. The Kinetic Theory of Gases. Methuen & Co. Ltd, London, 1934.

Kokini, K.; Takeuchi, Y. R. **Initiation of Surface Cracks in Multilayer Ceramic Thermal Barrier Coatings under Thermal Loads.** *Materials Science and Engineering, 1994, 301-309.*

Kvernes, I.; Lugscheider, E.; Lindblom, Y. *Protection Materials: Coatings for Thermal Barrier and Wear Resistance.* 2nd European Symposium on Engineering Ceramics. Elsevier Science Publishers LTD, Crown House, Essex, 1989, 45-79.

Lankin, Y. **New Results of EB-PVD Equipment Control System Modernization.** Poster in Workshop Proceedings on "Electron Beam-Physical Vapor Deposition". PennState University, Applied Research Laboratory, 17-18 September 1996.

Lardon, M.; Buhl, R.; Signer, H.; Pulker, H. K.; Moll, E. **Morphology of Ion-Plated Titanium and Aluminum Films Deposited at Various Substrate Temperatures.** *Thin Solid Films,* Vol. 54, No. 3, November 1978, 317-322.

Lart, G. *Comparison of Rapid Prototype Systems.* MSc Thesis, Cranfield University, 1991.

Lawson, K. J.; Nicholls, J. R.; Rickerby, D. S. **The Effect of Coating Thickness on the Thermal Conductivity of CVD and PVD Coatings.** 4th International Conference on "Advances in Surface Engineering", Newcastle, UK, 1996.

Leverant, G. R. **Diffusion Barrier for Protective Coatings.** US Patent No. 5,556,713. 1996.

Levine, S. R.; Clark, J. S. *Thermal Barrier Coatings - A Near Term High Payoff Technology.* NASA TM X-73586, 1977.

Levine, S. R.; Miller, R. A.; Stecura, S. **Improved Performance Thermal Barrier Coatings.** Proceedings of the Conference on "High Temperature Corrosion". (Published 1983), California, Vol. NACE-6, March 2-6, 1981b, 621-627.

Liebert, C. H.; Jacobs, R. E.; Stecura, S.; Robert Morse, C. *Durability of Zirconia Thermal-Barrier Ceramic Coatings on Air-Cooled Turbine Blades in Cyclic Jet Engine Operation.* NASA TM X-3410, September 1976.

Liebert, C. H.; Stepka, F. S. *Industry Tests of NASA Ceramic Thermal Barrier Coating.* NASA TP-1425, June 1979.

Liebert, C. H.; Stepka, F. S. *Potential use of Ceramic Coating as a Thermal Insulation on Cooled Turbine Hardware.* NASA TM X-3352, February 1976.

Liège, Series of Conference Proceedings held in Liège, Belgium. High Temperature Alloys for Gas Turbines. Applied Science Publishers, ISBN 0-85334-815-4, 25-27 September 1978.
High Temperature Alloys for Gas Turbines 1982. D. Reidel Publishing Company, ISBN 90-277-1468-1, 4-6 October 1982.
High Temperature Alloys for Gas Turbines and other Applications 1986. D. Reidel Publishing Company, ISBN 90-277-2347-8 (Part I), 90-277-2348-6 (Part II), 90-277-2304-4 (Set), 6-9 October 1986.

Lima, C. R. C.; da Exaltação Trevisan, R. **Temperature Measurements and Adhesion Properties of Plasma Sprayed Thermal Barrier Coatings.** *Journal of Thermal Spray Technology*, Vol. 8(2), June 1999, 323-327.

Litchfield, W. B.; Gent, J. T.; Graham, J. A. S. **Coating Material.** US Patent No. 4,303,737. 1981.

Maissel L. I.; Glang R. Handbook of Thin Film Technology. New York: McGraw-Hill, ISBN 0-07-039742-2, 1970.

Mariani, J. A. **Comparing Parallel Programming Languages and Architectures.** Proceedings of the workshop on "Parallel Processing and Control – The Transputer and other Architectures", University College of North Wales, Bangor, 4-6 July 1988, 2.1-2.8.

Maricocchi, A. F. **Method for Repair and Restoration of a Ceramic Thermal Barrier-Coated Substrate by Providing an Intermetallic Coating.** US Patent No. 5,254,413. 1993.

MARINE, Proceedings of 1974 Gas Turbine Materials in the Marine Environment Conference. Marine Maritime Academy, Castine, Maine. Organised by Army Materials and Mechanics Research Center, Massachusetts, 24-26 July 1974.

Marinski, G. S. **New EB-PVD Equipment by the International Center for Electron Beam Technologies (ICEBT).** Workshop Proceedings on "Electron Beam-Physical Vapor Deposition". PennState University, Applied Research Laboratory, 17-18 September 1996.

Marynsky, G. S. **Full Service EB-PVD Capacity.** Workshop Proceedings on "Electron Beam-Physical Vapor Deposition". PennState University, Applied Research Laboratory, 10-11 June 1998.

Mazars, P.; Manesse, D.; Lopvet, C. **Interdiffusion of MCrAlY Coating with the Substrate.** See Liège, 1986, Part II, 1183-1192.

McMinn, A. *Coatings Technology for Hot Component of Industrial Combustion Turbines. A Review of the State of the Art.* Electrical Power Research Institute (EPRI) - Report AP-5078, February 1987.

McMinn, A.; Viswanathan, R.; Knaup, C. L. **Field Evaluation of Gas Turbine Protective Coatings.** *Journal of Engineering for Gas Turbines and Power*, Vol. 110, January 1988, 142-149.

Meetham, G. W. The Development of Gas Turbine Materials. Applied Science Publishers Ltd, ISBN 0-85334-952-5, 1981.

Meetham, G. W. **Use of Protective Coatings in Aero Gas Turbine Engines.** *Materials Science and Technology*, Vol. 2, March 1986b, 290-294.

Meier, S. M.; Gupta, D. K. **The Evolution of Thermal Barrier Coatings in Gas Turbine Engine Applications.** *Journal of Engineering for Gas Turbines and Power*, Vol. 116, January 1994, 250-257.

Meier, S. M.; Gupta, D. K.; Sheffler, K. D. **Ceramic Thermal Barrier Coatings for Commercial Gas Turbine Engines.** *Journal of Metals*, Vol. 43, March 1991a, 50-53.

Meier, S. M.; Nissley, D. M.; Sheffler, K. D. *Thermal Barrier Coating Life Prediction Model Development.* NASA-CR-189111, July 1991b.

Meier, S. M; Nissley, D. M.; Sheffler, K. D.; Cruse, T. A. **Thermal Barrier Coating Life Prediction Model Development.** *Journal of Engineering for Gas Turbines and Power*, Vol. 114, April 1992, 258-263.

Meitner, P. L. *Analysis of Metal Temperature and Coolant Flow With a Thermal-Barrier Coating on a Full-Coverage-Film-Cooled Turbine Vane.* NASA TP-1310, August 1978.

Mévrel, R.; Duret, C.; Pichoir, R. **Pack Cementation Processes.** *Materials Science and Technology*, Vol. 2, March 1986, 210-206.

Miller, R. A.; Leissler, G. W.; Marcus Jobe, J. *Characterization and Durability Testing of Plasma-Sprayed Zirconia-Yttria and Hafnia-Yttria Thermal Barrier Coatings.* NASA TP-3295, February 1993.

Mogro-Campero, A.; Johnson, C. A.; Bednarczyk, P. J.; Dinwiddie, R. B.; Wang, H. **Effect of Gas Pressure on Thermal Conductivity of Zirconia Thermal Barrier Coatings.** *Surface and Coatings Technology*, Vol. 94-5, No. 1-3, October 1997, 102-105.

Morrell, P.; Rickerby, D. S. **Advantages/Disadvantages of Various TBC Systems as Perceived by the Engine Manufacturer.** Proceeding of the 85th Meeting of the AGARD Structures and Materials Panel on "Thermal Barrier Coatings". (Published April 1998). Aalborg, Denmark, 15-16 October 1997, 20.1-20.9.

Movchan, B. A. **EB-PVD Technology in the Gas Turbine Industry: Present and Future.** *Journal of Metals*, November 1996a, 40-45.

Movchan, B. A. **Gradient Coatings Produced by the EB-PVD Process.** Workshop Proceedings on "Electron Beam-Physical Vapor Deposition". PennState University, Applied Research Laboratory, 17-18 September 1996b.

Movchan, B. A. **New Non-Organic Coatings by EB-PVD.** Workshop Proceedings on "Electron Beam-Physical Vapor Deposition". PennState University, Applied Research Laboratory, 10-11 June 1998.

Movchan, B. A.; Demchishin, A. V. **Study of the Structure and Properties of Thick Vacuum Condensates of Nickel, Titanium, Tungsten, Aluminium Oxide and Zirconium Dioxide.** *Physics Metals Metallurgic*, Vol. 28, 1969, 83-90.

Movchan, B. A.; Malashenko, I. S.; Yakovchuk, K. Yu.; Rybnikov, A. I.; Tchizhik, A. A. **Two- and Three-Layer Coatings Produced by Deposition in Vacuum for Gas Turbine Blade Protection.** *Surface and Coatings Technology*, Vol. 67, 1994, 55-63.

Mukherjee, D. K. **State-of-the-art Gas Turbines - a Brief Update.** *ABB Review*, Vol. 2, 1997, 4-14.

Musset, A. **Uniformity of Coating Thickness on the Insides of Rotating Cylinders.** Proceedings of the 33rd Annual Technological Conference. Society of Vacuum Coaters, 29 April-4 May 1990, 243-245.

Mutasim, Z.; Brentnall, W. **Thermal Barrier Coatings for Industrial Gas Turbine Applications: An Industrial Note.** *Journal of Thermal Spray Technology*, Vol. 6, No. 1, March 1997, 105-108.

NACE, Proceedings of the Conference "High Temperature Corrosion". National Association of Corrosion Engineers, Houston, Texas, March 2-6 1981, San Diego, California (Published 1983).

Nagaraj, B. A.; Connor, W. B.; Jendrix, R.W.; Wortman, D. J.; Plemmons, L. W. **Platinum, Rhodium, or Palladium Protective Coatings in Thermal Barrier Coating Systems.** US Patent No. 5,427,866. 1995.

Nagaraj, B. A.; Wortman, D. J. **Burner Rig Evaluation of Ceramic Coatings With Vanadium-Contaminated Fuels.** *Journal of Engineering for Gas Turbines and Power*, Vol. 112, No. 4, October 1990, 536-542.

Nakamori, M.; Kayano, I.; Tsukuda, Y.; Takahashi, K.; Torigoe, T. **Hot Corrosion and its Prevention in High Temperature Heavy Oil Firing Gas Turbines.** *Materials Science Forum*, vols. 251-254 (2), 1997, 633-639.

Nathanael, N. *Viewing Optimization of Stereolithography Data Files for Integrity Evaluation Using PHIGS.* MSc Thesis, Cranfield University, 1993.

Nazeri, A.; Qadri, S. B. **Alumina-Stabilized Zirconia Coatings for High-Temperature Protection of Turbine-Blades.** *Surface and Coatings Technology*, Vol. 87-8, No. 1-3, December 1 1996, 166-169.

Nicholls, J. R. **Designing Oxidation-Resistant Coatings.** *Journal of Metals*, Vol. 52, No. 1, January 2000, 28-35.

Nicholls, J. R. Private Communication. 1999.

Nicholls, J. R.; Deakin, M. J. To be published. 2000.

Nicholls, J. R.; Jaslier, Y; Rickerby, D. S. **Erosion and Foreign Object Damage of Thermal Barrier Coatings.** *Materials Science Forum*, vols. 251-254 (2), 1997a, 935-948.

Nicholls, J. R.; Lawson, K. J.; Rickerby, D. S.; P. Morrell. **Advanced Processing of TBC's for Reduced Thermal Conductivity.** Proceeding of the 85th Meeting of the AGARD Structures and Materials Panel on "Thermal Barrier Coatings". (Published April 1998). Aalborg, Denmark, 15-16 October 1997b, 6.1-6.9.

Nicholls, J. R.; Pereira, V.; Lawson, K. J.; Rickerby, D. S. **Process Control of Deposition Profiles in the Manufacture of EB-PVD Thermal Barrier Coatings.** Proceedings of the Research and Technology Organization (RTO, NATO) Meeting on "Intelligent Processing of High Performance Materials". Brussels, Belgium, 13-14 May 1998, 16.1-16.11.

Nicoll, A. R.; Gruner, H; Wuest, G.; Keller, S. **Future Developments in Plasma Spray Coating.** *Materials Science and Technology*, Vol. 2, March 1986, 214-219.

Nied, H. A. **Ceramic Coating Edge Failure Due to Thermal Expansion Interference.** *Journal of Engineering for Gas Turbines and Power* - Transactions of the ASME, Vol. 120, No. 4, Oct. 1998, 820-824.

Nimmagadda, R.; Bunshah, R. F. **Temperature and Thickness Distribution on the Substrate during High-Rate Physical Vapor Deposition of Materials.** *The Journal of Vacuum Science and Technology*, Vol. 8, No. 6, 1971, VM85-VM94.

Nissley, D. M. *Thermal Barrier Coating Life Modeling in Aircraft Gas Turbine Engines.* In NASA. Lewis Research Center, Thermal Barrier Coating Workshop, March 1995, 265-281.

NMAB. *Coatings for High-Temperature Structural Materials Trends and Opportunities.* National Materials Advisory Board. National Research Council, ISBN 0-309-05381-1, National Academy Press, 1996.

Novak, R. C. *Coating Development and Use: Case Studies.* Presentation to the Committee on Coatings for High-Temperature Structural Materials, National Materials Advisory Board, National Research Council, Irvine, California, April 18-19, 1994.

Ohring, M. The Materials Science of Thin Films. Academic Press Limited, ISBN 0-12-524990-X, 1992.

Parks, W. P.; Hoffman, E. E.; Lee, W. Y.; Wright, I. G. **Thermal Barrier Coatings Issues in Advanced Land-Based Gas Turbines.** *Journal of Thermal Spray Technology*, Vol. 6(2), June 1997, 187-192.

PennState, Workshop Proceedings on "Electron Beam-Physical Vapor Deposition", PennState University, Applied Research Laboratory, 17-18 September 1996.

PennState, Workshop Proceedings on "Electron Beam-Physical Vapor Deposition", PennState University, Applied Research Laboratory, 10-11 June 1998.

Pereira, V. *Computer Model to Predict Vapour Deposition.* MSc Thesis, Cranfield University, 1996.

Pettit, F. S.; Goward, G. W. **Gas Turbine Applications.** IN: Proceedings of the seminar "Coatings for High Temperature Applications", Edited by E. Lang. Applied Science Publishers. CEC High Temperature Materials Information Centre, Petten, The Netherlands, ISBN 0-85334-221-0, 1983a, 341-359.

Pettit, F. S.; Goward, G. W. **Oxidation-Corrosion-Erosion Mechanisms of Environmental Degradation of High Temperature Materials.** IN: Proceedings of the seminar "Coatings for High Temperature Applications". Edited by E. Lang. Applied Science Publishers. CEC High Temperature Materials Information Centre, Petten, The Netherlands, ISBN 0-85334-221-0, 1983b, 1-32.

Pichoir, R. **Aluminide Coatings on Ni- or Co-Base Superalloys: Main Factors Determining their Morphology and Composition.** See Liège, 1978, 191-208.

Pint, B. A.; Nagaraj, B. A.; Rosenzweig, M. A. **Evaluation of TBC-coated β-NiAl Substrates Without a Bond Coat.** Proceedings of the Symposium: "High Temperature Coatings II", Elevated Temperature Coatings: Science and Technology II, ch.39, 1996, 163-174.

Quadakkers, W. J.; Tyagi, A. K.; Clemens, D.; Anton, R.; Singheiser, L. **The Significance of Bond Coat Oxidation for The Life of TBC Coatings.** Proceedings of the Symposium: "High Temperature Coatings II", Elevated Temperature Coatings: Science and Technology III, ch.36, 1999, 119-130.

Rairden, III, J. R. **Protective Coatings for Superalloys.** US Patent No. 3,998,603. 1976.

Ravichandran, K. S.; An, K.; Dutton, R. E.; Semiatin, S. L. **Microstructure and Thermal Conductivity of Layered Thermal Barrier Coatings Processed by Plasma Spray and Physical Vapor Deposition Techniques.** Proceeding of the 85th Meeting of the AGARD Structures and Materials Panel on "Thermal Barrier Coatings". (Published April 1998). Aalborg, Denmark, 15-16 October 1997, 14.1-14.12.

Reinhold, E.; Deus, C.; Wenzel, B. D.; Wolkers, L. **EB-Preheating of Turbine Blades - the Completion of EB-Technology for Thermal Barrier Coating.** *Surface and Coatings Technology*, Vol. 111, No. 1, Jan. 10 1999, 10-15.

Restall, J. E.; Malik, M.; Singheiser, L. **Metallic Diffusion and Overlay Coatings.** See Liège, 1986, Part I, 357-404.

Restall, J. E.; Wood, M. I. **Alternative Processes and Treatments.** *Materials Science and Technology*, Vol. 2, March 1986, 225-231.

Rhys-Jones, T. N.; Toriz, F. C. **Thermal Barrier Coatings for Turbine Applications in Aero Engines.** *High Temperature Technology*, Vol. 7, No. 2, May 1989, 73-81.

Ribeiro, A. F. M. *Automated Off-Line Programming for Rapid Prototyping Using Gas Metal Arc Welding.* PhD Thesis, Cranfield University, 1995.

Rickerby, D. S.; Bell, S. R.; White, D. K. **Thermal Barrier Coating for a Superalloy Article and Method of Application.** European Patent No. EP0718419B1. 1995.

Rigney, D. V.; Viguie, R.; Wortman, D. J. Skelly, D. W. *PVD Thermal Barrier Coating Applications and Process Development for Aircraft Engines.* NASA Conference 3312, 1995, 135-149.

Robson, J.; James, A. S.; Matthews, A.; Lewis, B. **The Deposition of Yttria Partially Stabilised Zirconia (PYSZ) onto Aluminium Alloy Substrates Using PVD Techniques.** *Surface and Coating Technology*, Vol. 60, 1993, 536-540.

Rolls-Royce. The Jet Engine. ISBN 0-902121-2-35, Fifth edition, 1986.

Royal Society, Proceedings of Conference on Protective Coating Systems for High Temperature Gas Turbines. Royal Society, London, *Materials Science and Technology*, Vol. 2, No. 3, March 1986.

Rybnikov, A. I.; Getsov, L. B.; Malashenko, I. S. **Thermal cyclic Response of EB PVD Yttria-Stabilized Zirconia/CoCrAlY Coatings.** *Thin Solid Films*, Vol. 270, 1995, 247-252.

Rybnikov, A. I.; Osyka, A. S.; Malashenko, I. S.; Getsov, L. B.; Tchizhik, A. A.; Leontiev, S. A. **Coated Blade Operation Experience with a Peak Load Power Gas Turbine.** *Surface and Coatings Technology*, Vol. 68, 1994, 38-44.

Schaffer, J. C.; Murphy, W. H.; Connor, W. B.; Nagaraj, B. A.; Vakil, H. B. **Thermal Barrier Coating System Having No Bond Coat.** US Patent No. 5,538,796. 1996.

Schiller, S.; Heisig, U.; Panzer, S. Electron Beam Technology. John Wiley & Sons, ISBN 0-471-06056-9, 1982.

Schiller, S.; Jaesch, G; Neumann, M. **High Rate Electron Beam Evaporation.** *Thin Solid Films*, Vol. 110, 1983, 149-164.

Schmitt-Thomas, Kh. G.; Dietl, U.; Haindl, H. **New Developments in Thermal Barrier Coatings (TBC) for Gas Turbine Use.** *Industrial Ceramics*, Vol. 16, No. 3, 1996, 195-198.

Schmitt-Thomas, Kh. G.; Dietl, U.; Haindl, H. **Thermal Barrier Coatings for Airbreathing Combustion Systems.** Z. Flugwiss. Weltraumforsch, Vol. 19, 1995, 41-46.

Schulz, U.; Fritscher, K.; Leyens, C.; Peters, M.; Kaysser, W. A. **The Thermocyclic Behavior of Differently Stabilized and Structured EB-PVD TBCs.** *Journal of Metals,* Vol. 49, No. 10, October 1997a, http://www.tms.org/pubs/journals/JOM/9710/Schulz/Schulz-9710.html

Schulz, U.; Fritscher, K.; Rätzer-Scheibe, H.-J.; Kaysser, W. A.; Peters, M.. **Thermocyclic Behaviour of Microstructurally Modified EB-PVD Thermal Barrier Coatings.** *Materials Science Forum*, vols. 251-254 (2), 1997b, 957-964.

Schulz, U.; Krell, T.; Leushake, U.; Peters, M. **Graded Design of EB-PVD Thermal Barrier Coating Systems.** Proceeding of the 85th Meeting of the AGARD Structures and Materials Panel on "Thermal Barrier Coatings". (Published April 1998). Aalborg, Denmark, 15-16 October 1997c, 16.1-16.10.

Schulz, U.; Peters, M. **Single Source Versus Dual Source Jumping Beam Evaporation for EB-PVD Thermal Barrier Coatings.** Workshop Proceedings on "Electron Beam-Physical Vapor Deposition". PennState University, Applied Research Laboratory, 10-11 June 1998.

Senf, J.; Wenzel, B. D.; Lenk, P. **Thermal Barrier Coatings - A Research Coater and a Concept for an Industrial Coater.** Workshop Proceedings on "Electron Beam-Physical Vapor Deposition". PennState University, Applied Research Laboratory, 17-18 September 1996.

Shaw, B.; Sikora, E.; Kennedy, K.; Miller, P.; Principe, E.; Scammon, K.; Heidersbach, K.; Miller, T.; Singh, J. **Corrosion Resistant Alloys and Coatings Produced by Physical Vapor Deposition.** Proceedings of a Symposium on "Advances in Coatings Technology for Surface Engineering" Edited by Clive R. Clayton et al., A publication of The Minerals, Metals & Materials Society. ISBN 0-87339-371-6, 1997, 287-304.

Sheffler, K. D.; Gupta, D. K. **Current Status and Future Trends in Turbine Application of Thermal Barrier Coatings.** *Journal of Engineering for Gas Turbines and Power*, Vol. 110, October 1988, 605-609.

Shillington, E. A. G.; Clarke, D. R. **Spalling Failure of a Thermal Barrier Coating Associated With Aluminum Depletion in the Bond-Coat.** *Acta-Materialia*, Vol. 47, No. 4, 10 March 1999, 1297-1305.

Siegel, H. J. Interconnection Networks for Large-Scale Parallel Processing. Lexington Books, ISBN 0-669-03594-7, 1985.

Siegel, R.; Spuckler, C. M. **Analysis of Thermal Radiation Effects on Temperatures in Turbine Engine Thermal Barrier Coatings.** *Materials Science and Engineering A* - Structural Materials: Properties, Microstructure and Processing, Vol. 245, No. 2, May 1 1998, 150-159.

Simpson, H. G. **Future EB-PVD Requirements for Navy Applications.** Workshop Proceedings on "Electron Beam-Physical Vapor Deposition". PennState University, Applied Research Laboratory, 10-11 June 1998.

Sims, C. T.; Stoloff, N. S.; Hagel, W. C. Superalloys II - High-Temperature Materials for Aerospace and Industrial Power. ISBN 0-471-01147-9, John Wiles & Sons, 1987.

Singh, J. **Electron Beam-Physical Vapor Deposition (EB-PVD) Coating Technology: Present and Future Applications.** Workshop Proceedings on "Electron Beam-Physical Vapor Deposition". PennState University, Applied Research Laboratory, 10-11 June 1998.

Singh, J. *Multilayer Ceramic/Metallic Coatings by Ion Beam-Assisted, Electron Beam Physical Vapor (EB-PVD) Deposition.* The Applied Researcg Laboratory, Pennsylvania State University, http://www.psu.edu, 1997.

Skelly, D. W.; Nagaraj, B. A.; Wortman, D. J.; Rigney, D. V.; Mannava, S. R.; Viguie, R.; Bruce, R. W.; Nelson, W. A.; Johnson, C. A.; Gupta, B. K. **Enhanced Thermal Barrier Coating System.** US Patent No. 5,419,971. 1995.

Slifka, A. J.; Filla, B. J.; Phelps, J. M.; Bancke, G; Berndt, C. C. **Thermal Conductivity of a Zirconia Thermal Barrier Coating.** *Journal of Thermal Spray Technology*, Vol. 7(1), March 1998, 43-46.

Smialek, J. L. **Toward optimum scale and TBC adhesion on single Crystal superalloys.** Proceedings of the Symposium on High Temperature Corrosion And Materials Chemistry, Electrochemical Society, Pennington, NJ, USA, Vol. 98, ch.52, No. 9, 1998, 211-220.

Smilgys, R. **Front Surface Mirror Protected by an Alumina Coating for Solar Thermal Power Generation.** Workshop Proceedings on "Electron Beam-Physical Vapor Deposition". PennState University, Applied Research Laboratory, 17-18 September 1996.

Smith, D. L. Thin-Film Deposition - Principals & Practice. McGraw-Hill, ISBN 0-07-058502-4, 1995.

Sohn, Y. H. *Characterization and Life Prediction of Physical Vapor Deposited Partially Stabilized Zirconia Thermal Barrier Coatings.* MSc Thesis, Worcester Polytechnic Institute, 1993.

Sohn, Y. H.; Biederman, R. R.; Sisson Jr., R. D. **Isothermal Oxidation of Physical Vapor Deposited Partially Stabilized Zirconia Thermal Barrier Coatings.** *Journal of Materials Engineering and Performance,* Vol. 3(1), February 1994a, 55-60.

Sohn, Y. H.; Biederman, R. R.; Sisson Jr., R. D. **Microstructural Development in Physical Vapour-Deposited Partially Stabilized Zirconia Thermal Barrier Coatings.** *Thin Solid Films,* Vol. 250, 1994b, 1-7.

Solfest, P. A.; Strangman, T. E. **Titania Doped Ceramic Thermal Barrier Coatings.** US Patent No. 4,916,022. 1990.

Spengler, C. J.; Whitlow, G. A. **Spalling and Corrosion Resistant Ceramic Coating for Land and Marine Combustion Turbines.** US Patent No. 4,576,874. 1986.

Srinivasan, V. **High-Temperature Corrosion and Erosion in Gas Turbine Engines - Where Do We Stand?** *Journal of Metals*, December 1994, 34.

Stabe, R. G.; Liebert, C. H. *Aerodynamic Performance of a Ceramic-Coated Core Turbine Vane Tested with Cold Air in a Two-Dimensional Cascade.* NASA TM X-3191, January 1975.

Staia, M. H.; Deleal, C. L.; Hidalgo, C. **Evaluation of the Hot Corrosion Protection of Commercial Aluminide Coatings for Turbine-Blades.** Proceedings of the Symposium: "High Temperature Coatings II", Elevated Temperature Coatings: Science and Technology I, ch.37, 1995, 241-252.

Stecura, S. *Effects of Compositional Changes on the Performance of a Thermal Barrier Coating System.* NASA TM-78976, August 1978.

Stecura, S. *Optimization of the NiCrAl-Y/ZrO_2-Y_2O_3 Thermal Barrier System.* NASA-TM-86905, 1985.

Stecura, S. *Two-Layer Thermal Barrier Coating for Turbine Airfoils - Furnace and Burner Rig Test Results.* NASA TM X-3425, September 1976.

Stecura, S. **Two-Layer Thermal Barrier Coatings I: Effects of Composition and Temperature on Oxidation Behaviour and Failure.** *Thin Solid Films*, Vol. 182, 1989, 121-139.

Stiger, M. J.; Yanar, N. M.; Pettit, F. S.; Meier, G. H. **Mechanisms for the Failure of Electron Beam Physical Vapor Deposited Thermal Barrier Coatings Induced by High Temperature Oxidation.** Proceedings of the Symposium: "High Temperature Coatings II", Elevated Temperature Coatings: Science and Technology III, ch.36, 1999, 51-65.

Strangman, T. E. **Columnar Grain Ceramic Thermal Barrier Coatings.** US Patent No. 4,321,311. 1982.

Strangman, T. E. **Durable Thermal Barrier Coating.** US Patent No. 5,562,998. 1996a.

Strangman, T. E. **Porous Thermal Barrier Coating.** US Patent No. 5,512,382. 1996b.

Strangman, T. E. **Thermal Barrier Coating System for Superalloy Components.** US Patent No. 5,514,482. 1996c.

Strangman, T. E.; Schienle, J. L. **Tailoring Zirconia Coatings for Performance in a Marine Gas Turbine Environment.** *Journal of Engineering for Gas Turbines and Power*, Vol. 112, No. 4, October 1990, 531-535.

Strangman, T. E.; Solfest, P. A. **Ceramic Thermal Barrier Coating with Alumina Interlayer.** US Patent No. 5,015,502. 1991.

Strangman, T. E.; Solfest, P. A. **Ceramic Thermal Barrier Coating with Alumina Interlayer.** US Patent No. 4,880,614. 1989.

Strangman, T. E.; Vonk, S. J. **Oxidation Resistant Protective Coating System For Gas Turbine Components, and Process for Preparation of Coated Components.** US Patent No. 4,743,514. 1988.

Stringer, J. **High Temperature Corrosion in Heat Engines.** Proceedings of the Second Conference on Advanced Materials for Alternative-Fuel-Capable Heat Engines. (Published May 1982). EPRI, RD-2369-SR, California, August 24-28, 1981, 4.1-4.26.

Stringer, J.; El Dashshan, M. E. **The Role of Sulphur in Hot Corrosion.** Proceedings of 1974 Gas Turbine Materials in the Marine Environment Conference. 24-26 July 1974, 161-182.

Tabakoff, W. **Investigation of Coatings at High temperature for use in Turbomachinery.** *Surface and Coatings Technology*, Vol. 39/40, 1989, 97-115.

Tabakoff, W.; Metwally, M.; Hamed, A. **High-Temperature Coatings for Protection Against Turbine Deterioration.** *Journal of Engineering for Gas Turbines and Power* - Transactions of the ASME, Vol. 117, No. 1, Jan. 1995, 146-151.

Talboom, F. P.; Elam, R. O.; Wilson, L. W. *Evaluation of Advanced Superalloy Protection Systems.* NASA CR 72813, December 1970.

Talboom, F. P.; Grafwallner, J. **Nickel or Cobalt Base with a Coating Containing Iron Chromium and Aluminum.** US Patent No. 3,542,530. November 1970.

Tamarin, Y. A.; Kachanov, E. B.; Zherzdev, S. V. **Thermophysical properties of ceramic layers in TBC-EB.** *Materials Science Forum*, vols. 251-254 (2), 1997, 949-56.

Tamura, M.; Takahashi, M.; Ishii, J.; Sizuki, K.; Sato, M.; Shimomura, K. **Multilayered Thermal Barrier Coating for Land-Based Gas Turbines.** *Journal of Thermal Spray Technology*, Vol. 8(1), March 1999, 68-72.

Taylor, R. E. **Thermal Conductivity Determinations of Thermal Barrier Coatings.** *Materials Science and Engineering A* - Structural Materials: Properties, Microstructure and Processing, Vol. A245, No. 2, 1 May 1998, 160-167.

Taylor, T. A.; Bettridge, D. F.; Tucker, Jr., R. C. **Coating Composition Having Good Corrosion and Oxidation Resistance.** US Patent No. 5,455,119. 1995.

Taylor, T. A.; Price, M. O.; Tucker, Jr. R. C. **Response of Plasma Sprayed $MgO.ZrO_2$ and ZrO_2-6.6Y_2O_3 Thermal Barrier Coatings to Thermal Fatigue and Hot Corrosion.** Proceedings of the Second Conference on Advanced Materials for Alternative-Fuel-Capable Heat Engines. (Published May 1982). EPRI, RD-2369-SR, California, August 24-28, 1981, 6.131-6.150.

Tchizhik, A. A.; Getsov, L. B.; Rybnikov, A. I.; Malashenko, I.S. **Creep Studies of the EB PVD Coatings with a Ceramic Layer.** *Thin Solid Films,* Vol. 270, 1995, 243-246.

Teer, D. G. **Evaporation and Sputter Techniques.** IN: Proceedings of the seminar "Coatings for High Temperature Applications". Edited by E. Lang. Applied Science Publishers. CEC High Temperature Materials Information Centre, Petten, The Netherlands, ISBN 0-85334-221-0, 1983, 79-120.

Teer, D. G.; Delcea, B. L. **Grain Structure of Ion-Plated Coatings.** *Thin Solid Films,* Vol. 54, No. 3, November 1978, 295-301.

Teixeira, V.; Andritschky, M.; Gruhn, H.; Malléner, W.; Buchkremer, H.; Stöver, D. **Failure of PVD/Plasma Sprayed Thermal Barrier Coatings During Thermal Cycling.** Proceedings of the 8th National Thermal Spray Conference, 11-15 September 1995, Houston, Texas, 1995, 515-520.

Telama, A.; Torkkell, K.; Mäntylä, T.; Kettunen, P. **Vapour Deposited TiN and TiC Diffusion Barriers.** See Liège, 1986, Part II, 1081-1090.

Thornton, J. A. **High Rate Thick Film Growth.** *Annual Review Material Science,* Vol. 7, 1977, 239-260.

Thornton, J. A. **Influence of Apparatus Geometry and Deposition Conditions on the Structure and Topography of Thick Sputtered Coatings.** *Journal of Vacuum Science Technology*, Vol. 11, No. 4, July/August 1974, 666-670.

Tin, S.; Madey, D. A.; Ritter, A. M.; Jackson, M. R.; Skelly, D. W.; Rutkowski, S.; Azad, F. H.; Nardi, R. A.; Coderman, R. R.; Dupree, P. L.; Wark, D. **Electron Beam Evaporation of High Temperature Materials.** Workshop Proceedings on "Electron Beam-Physical Vapor Deposition". PennState University, Applied Research Laboratory, 17-18 September 1996.

Toriz, F. C.; Thakker, A. B.; Gupta, S. K. *Flight Service Evaluation of Thermal Barrier Coatings by Physical Vapor Deposition at 5200 H.* 16th International Conference on Metallurgical Coatings, San Diego, California, USA, 17-21 April 1989, 161-172.

Toriz, F. C.; Thakker, A. B.; Gupta, S. K. *Thermal Barrier Coatings for Jet Engines.* ASME Paper 88-GT-279, 1988.

Trice, R. W.; Jennifer Su, Y.; Faber, K. T.; Hsin Wang, Wally Porter **The Role of NZP Additions in Plasma-Sprayed YSZ: Microstructure, Thermal Conductivity and Phase Stability Effects.** *Materials Science and Engineering A272*, 1999, 284-291.

Tsantrizos, P. G.; Kim, G. E.; Brzezinski, T. A. **TBCs on Free-Standing Multilayer Components.** Proceeding of the 85th Meeting of the AGARD Structures and Materials Panel on "Thermal Barrier Coatings". (Published April 1998). Aalborg, Denmark, 15-16 October 1997, 7.1-7.8.

Ulion, N. E.; Anderson, N. P. **Advanced Thermal Barrier Coated Superalloy Components.** US Patent No. 5,262,245. 1993.

Ulion, N. E.; Ruckle, D. L. **Columnar Grain Ceramic Thermal Barrier Coatings on Polished Substrates.** US Patent No. 4,321,310. 1982.

Ulion, N. E.; Ruckle, D. L. **Method for Producing Metallic Articles Having Durable Ceramic Thermal Barrier Coatings.** US Patent No. 4,414,249. 1983.

Unal, O.; Mitchell, T. E.; Heuer, A. H. **Microstructure of Y_2O_3-Stabilized ZrO_2 Electron Beam-Physical Vapor Deposition Coatings on Ni-Base Superalloys.** *Journal of the American Ceramic Society,* Vol. 77, No. 4, 1994, 984-992

Unigraphics, Unigraphics V14.0.2. Help Manual (http://www.ugsolutions.com) 2000.

Vossen J. L.; Kern W. Thin Film Processes. Academic Press, ISBN 0-12-728250-5, 1978.

Voyer, J.; Gitzhofer, F.; Boulos, M. I.; Durham, S. **Thermally Induced Acoustic Emissions in Thermal Barrier Coatings.** Proceedings of the 8th National Thermal Spray Conference, 11-15 September 1995, Houston, Texas, 1995, 457.

Wadley, H. N. G.; Groves, J. F. **Directed Vapor Deposition of Electron Beam Evaporant.** US Patent No. 5,534,314. 1996.

Walsh, P. N.; Quets, J. M.; Tucker, R. C. **Coatings For The Protection of Turbine-Blades From Erosion.** *Journal of Engineering for Gas Turbines and Power* - Transactions of the ASME, Vol. 117, No. 1, Jan. 1995, 152-155.

Watt, R. M.; Allen, J. L.; Baines, N. C.; Simons, J. P., George, M. **A Study of the Effects of Thermal Barrier Coating Surface Roughness on the Boundary Layer Characteristics of Gas Turbine Aerofoils.** *Journal of Turbomachinery*, Vol. 110, January 1988, 88-93.

Wisskirchen, P. Object-Oriented Graphics - from GKS and PHIGS to Object-Oriented Systems. Springer-Verlag, ISBN 3-540-52859-8, 1990.

Wix, J. **Common Standards for Data Exchange.** *Construction Computing.* Spring 1989, 13-15.

Wolfe, D. E.; Movchan, M. B.; Singh, J. **Architecture of Functionally Graded Ceramic/Metallic Coatings by Electron Beam-Physical Vapor Deposition.** Proceedings of a Symposium on "Advances in Coatings Technology for Surface Engineering" Edited by Clive R. Clayton et al., A publication of The Minerals, Metals & Materials Society. ISBN 0-87339-371-6, 1997, 93-110.

Woo, M.; Neider, J.; Davis, T. OpenGL Programming Guide - Second Edition - the official guide to learning OpenGL, Version 1.1. 2nd Edition, ISBN 0-201-46138-2, 1997.

Wood, J. H.; Goldman, E. H. **Protective Coatings.** Chapter 13. IN: Sims, C. T. et al. Superalloys II - High-Temperature Materials for Aerospace and Industrial Power. 1987, 359-384.

Wortman, D. J.; Duderstadt, E. C.; Nelson, W. A. **Bond Coat Development for Thermal Barrier Coating.** *Journal of Engineering for Gas Turbines and Power*, Vol. 112, No. 4, October 1990, 527-530.

Wortmann, J. **Ceramics in Aero-Engines.** *Designing with Structural Ceramics*, Petten, The Netherlands, 3-6 April 1990, 258-272.

Wright Jr., R. S.; Sweet, M. OpenGL Superbible - The complete guide to OpenGL programming for Windows NT and Windows 95. Waite Group Press, ISBN 1-57169-073-5, 1996.

Wright, P.K. **Influence of Cyclic Strain on Life of a PVD TBC.** *Materials Science and Engineering A* - Structural Materials: Properties, Microstructure and Processing, Vol. 245, No. 2, May 1 1998, 191-200.

Youchison, D. L. **Large Area EB-PVD Processing at Sandia National Laboratories using Digital Rastering.** Poster in Workshop Proceedings on "Electron Beam-Physical Vapor Deposition". PennState University, Applied Research Laboratory, 17-18 September 1996.

Zhu, D; Ghosn, L. J.; Miller, R. A. **Effect of Layer-Graded Bond Coats on Edge Stress Concentration and Oxidation Behaviour of Thermal Barrier Coatings.** Proceedings of the Symposium on High Temperature Corrosion And Materials Chemistry, Electrochemical Society, Pennington, NJ, USA, Vol. 98, ch.52, No. 9, 1998, 170-189.

A

This appendix contains a diagram of the procedure to calculate the coating thickness and lists the files and the main Classes developed for the computer program. In addition, it shows, with examples, how to use some of the Classes' functions. The "workspace" of the project comprises 13 Classes in 28 files (13 .cpp, 14 .h and 1 .rc) with a total of approximately 4000 lines of code.

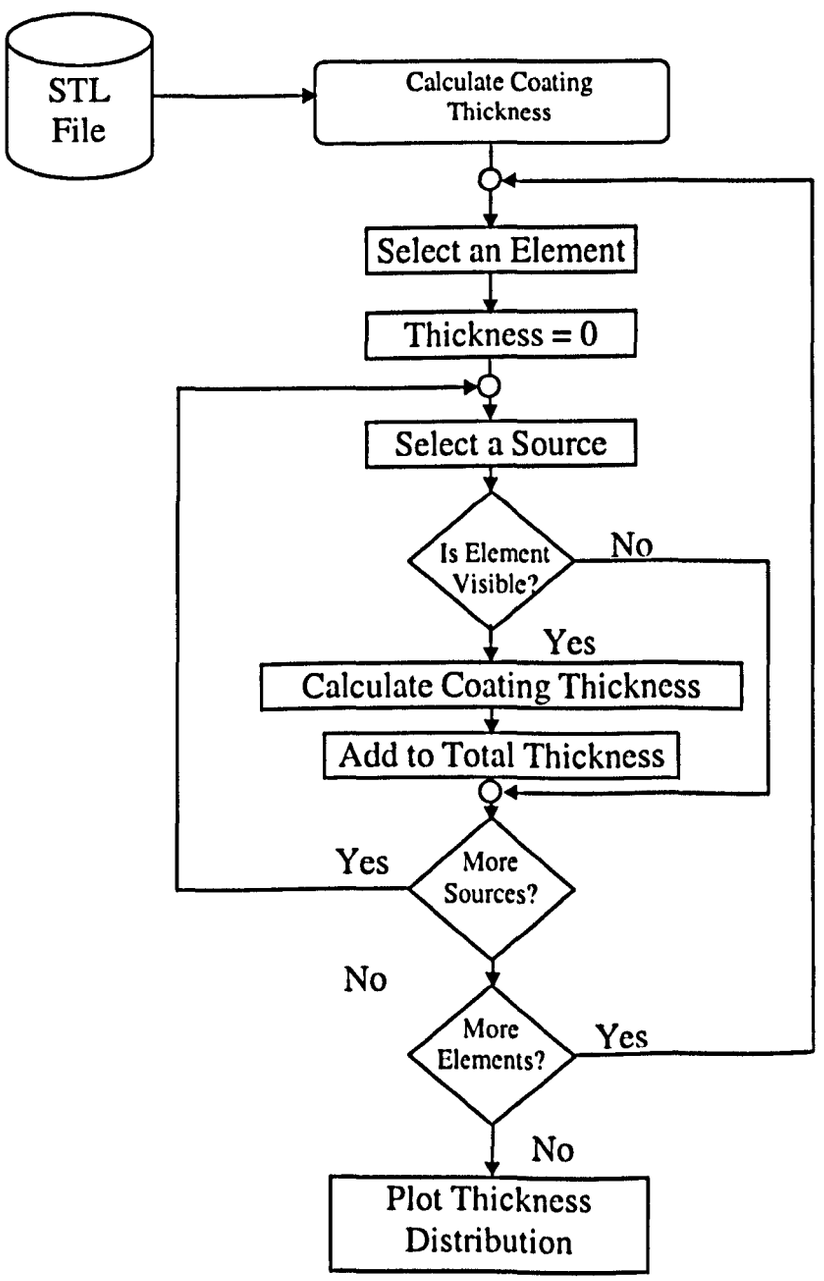

- Project files

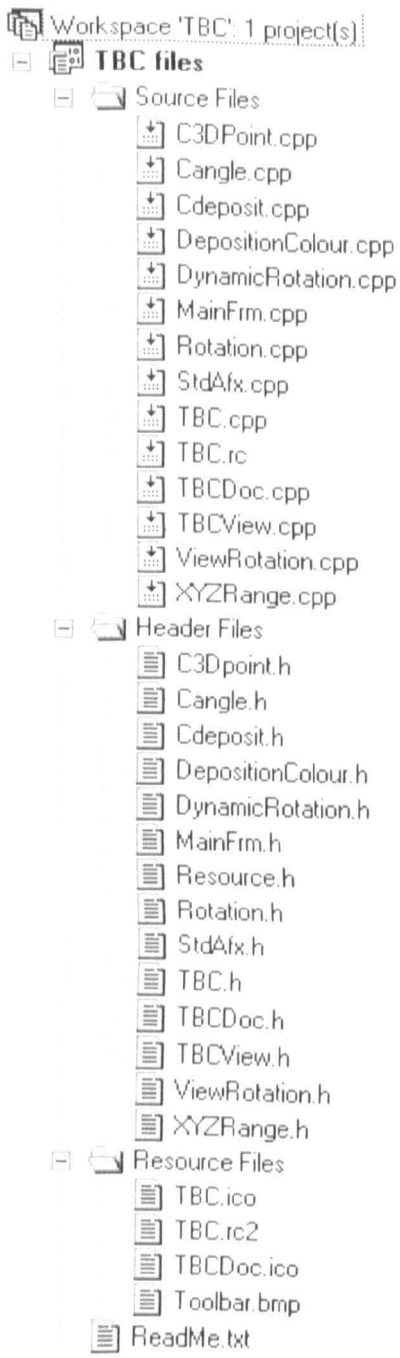

- Classes

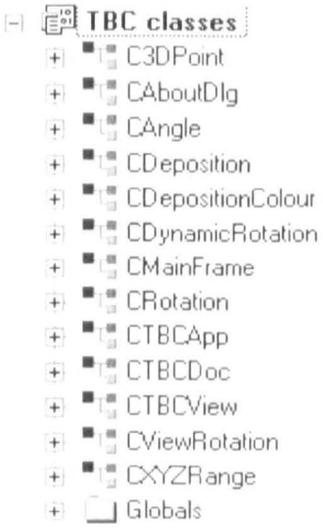

- C3DPoint

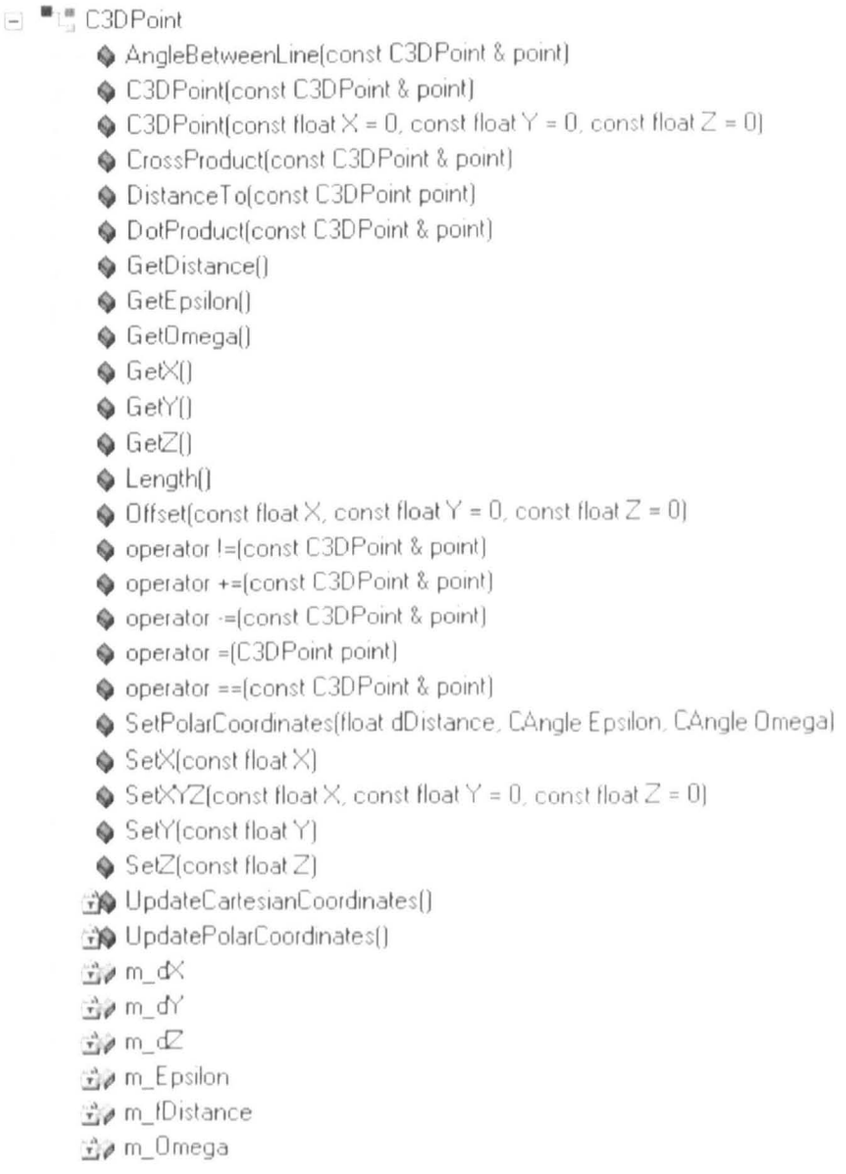

Example Usage (C3DPoint)

```
CPoint mypoint1(1, 1, 1);
CPoint mypoint2(-1, -1, 1);

float h = mypoint1.GetDistance(); // retrieves the distance between the origin of the
   // coordinate system and mypoint1 (used in the Polar coordinate system)

printf ("Point in Polar Coordinates: (h=%lf, Epsilon=%lf, Omega=%lf)\n", h,
mypoint1.GetEpsilon().Degrees(), mypoint1.GetOmega().Degrees());
   // angles in Degrees
printf ("Angle between mypoint1 and mypoint2=%lf (in degrees)\n",
   mypoint1.AngleBetweenLine(mypoint2).Degrees());
```

Output

```
Point in Polar Coordinates: (h=1.732051, Epsilon=45.0, Omega=35.264390)

Angle between mypoint1 and mypoint2=70.528779 (in degrees)
```

- CAngle

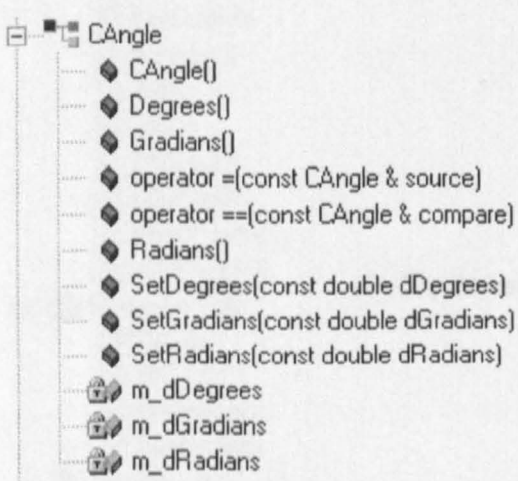

Example Usage (CAngle)

```
CAngle myangle;
myangle.SetDegrees(45);
printf ("Angle is: %lf degrees, %lf radians or %lf gradians\n", myangle.Degrees(),
   myangle.Radians(), myangle.Gradians());
```

Output

```
Angle is: 45.0 degrees, 0.785398 radians or 50.0 gradians
```

- CDeposition

- CRotation

- CTBCDoc (Document Class)

The Document Class handles the information of the model (substrate). For instance, it reads the geometric information of the component (ReadFile function) and updates the display area (RenderScene function).

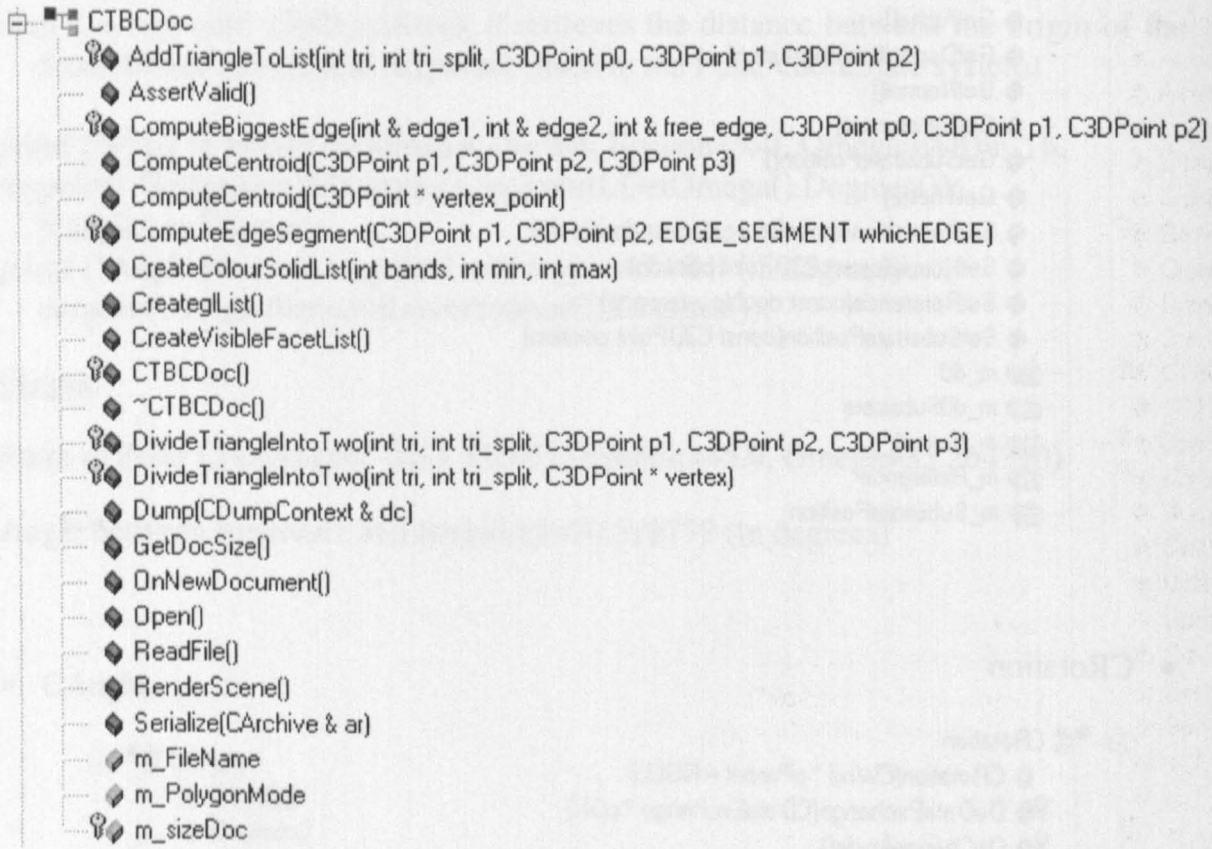

- CViewRotation

This Class rotates the model based on three parameters: an angle (in degrees), a point and a vector of rotation.

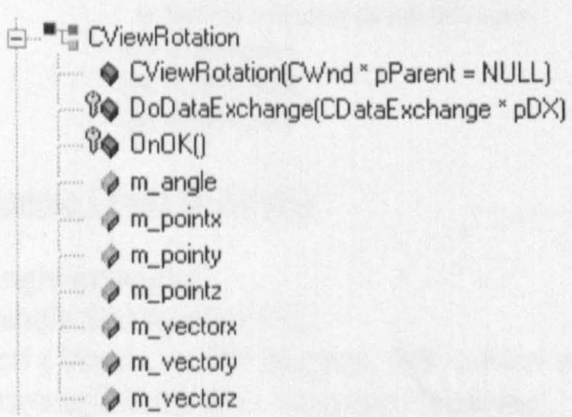

- CTBCView (View Class)

The View Class interprets user inputs and operations upon the *document*. For example, it handles all menu commands (File, View, Tessellation, Tools, Calculate, and Help) as well as mouse clicks on the display area to rotate the location from which the model is viewed (*click and drag* operations on the display area).

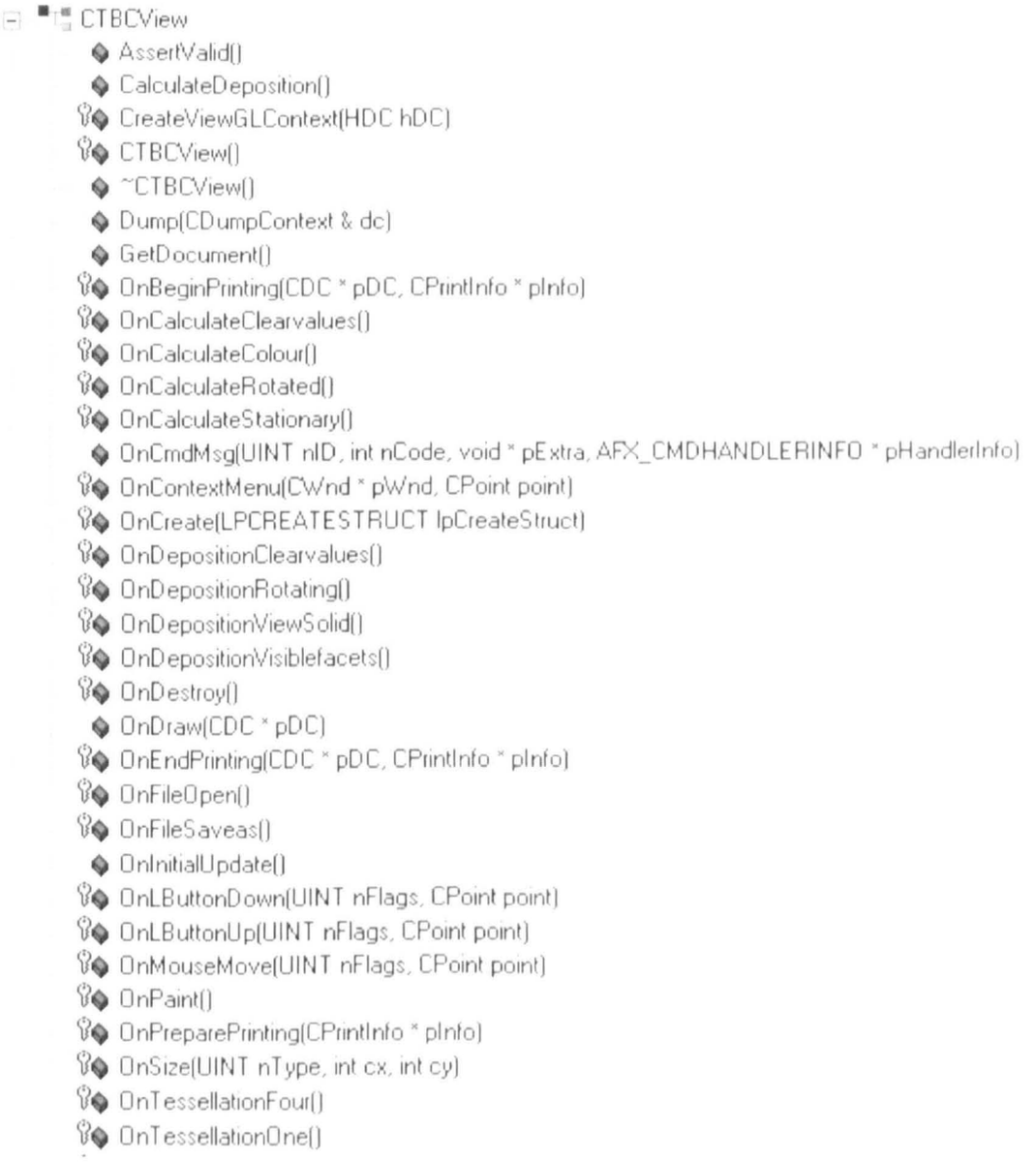

CONTINUED

CONTINUED

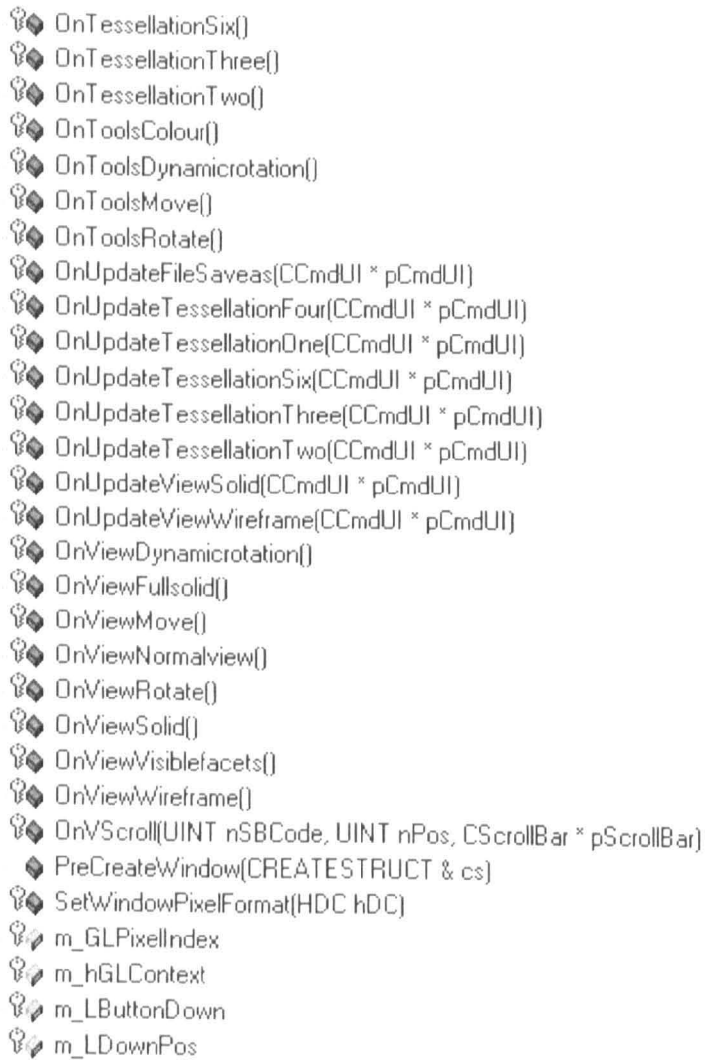

- CXYZRange

This Class translates the substrate by an offset relative to the components X, Y, and Z. In addition, it changes the "field of view" parameter which represents the degree of zoom.

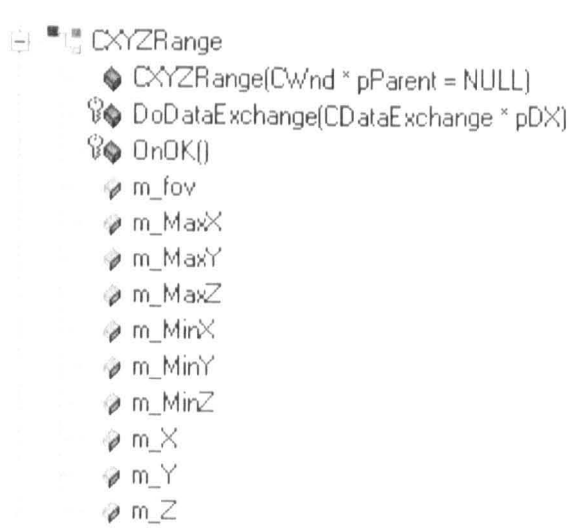

B

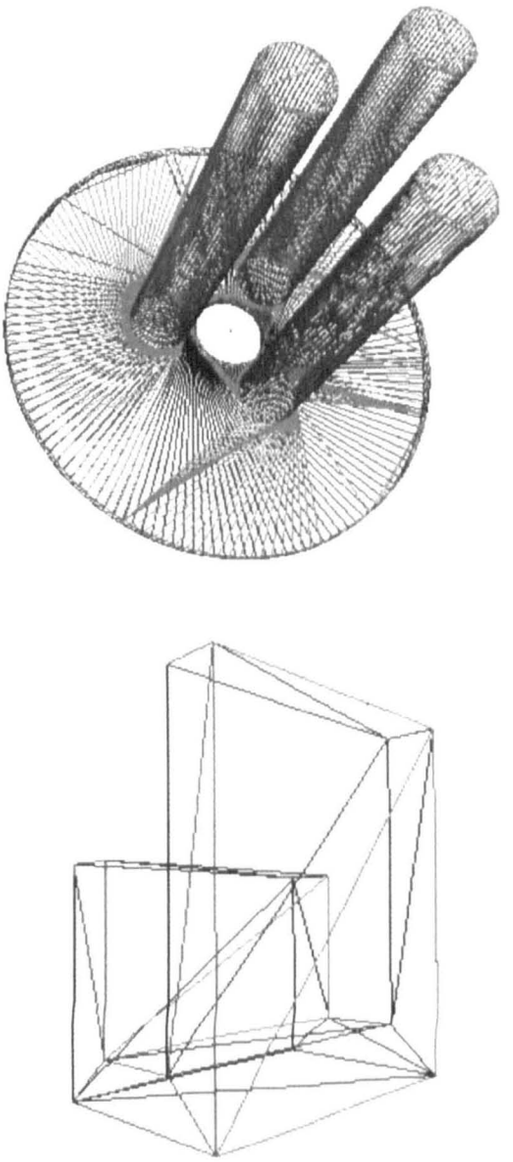

STL files generated using Unigraphics V14 with a tolerance of 0.8 mm (not shown at original size).

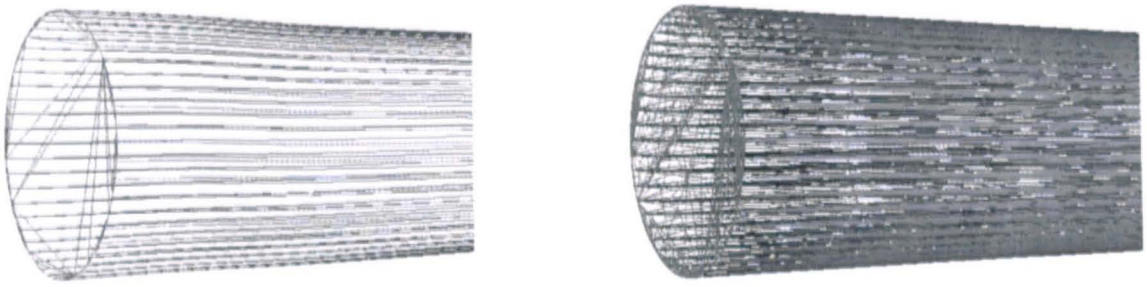

Detailed view of the end of a pin showing the difference in spatial resolution between the default tolerance and a model with a 6× increase in the number of triangles performed by the computer model.

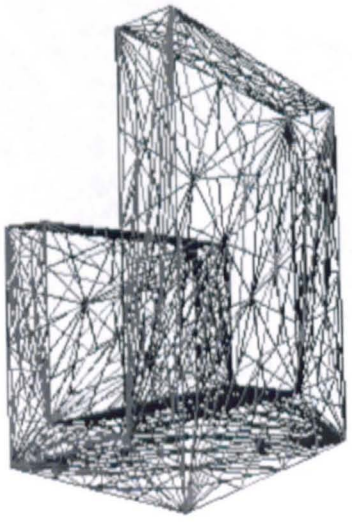

Shadow-mask arrangement with a 36× increase in the number of triangles.

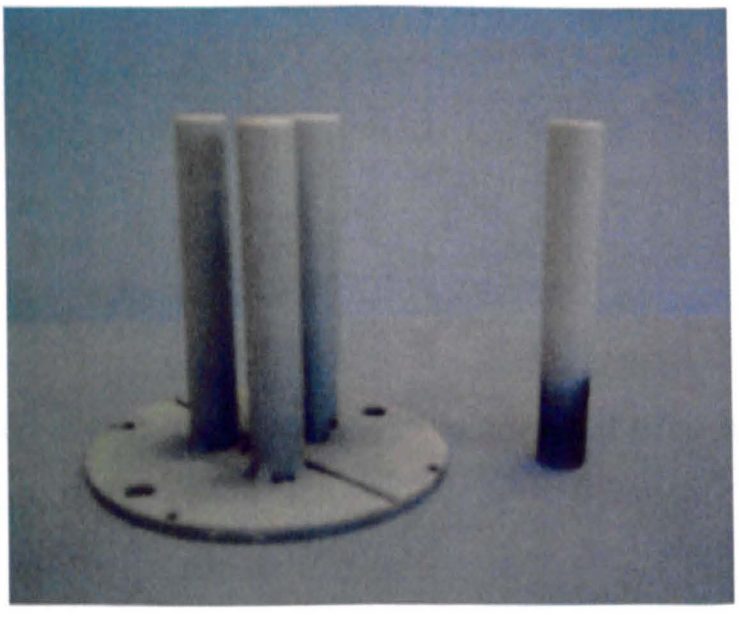

Macrophotograph of the rotating pin and the cluster of three pins after deposition.

Vacuum chamber of Cranfield University's EB-PVD coater showing the chamber and surrounding accessories, the 38 mm diameter ceramic ingot (8YSZ), and a close-up of rotating fixtures and substrate holders

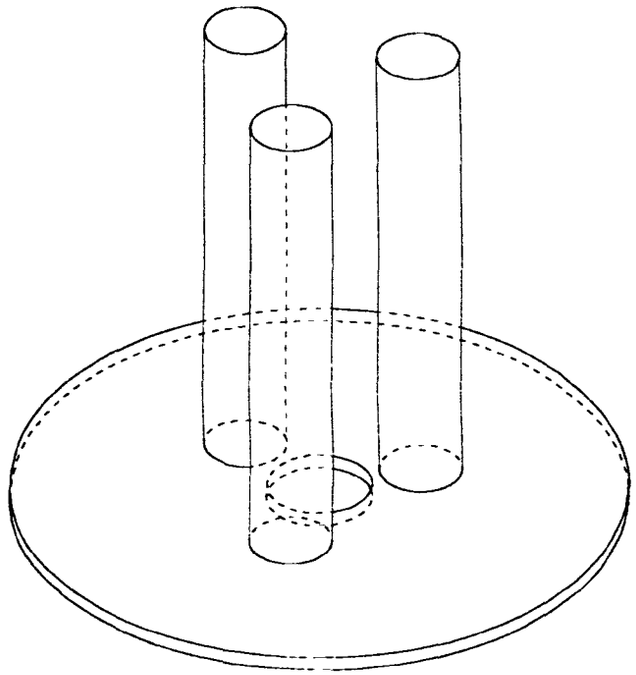

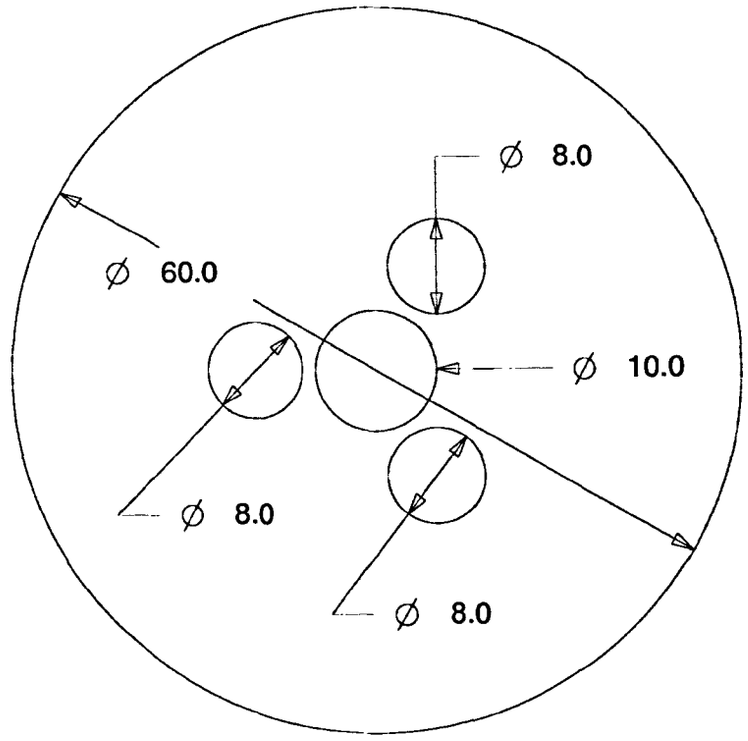
Ø 8.0
Ø 60.0
Ø 10.0
Ø 8.0
Ø 8.0

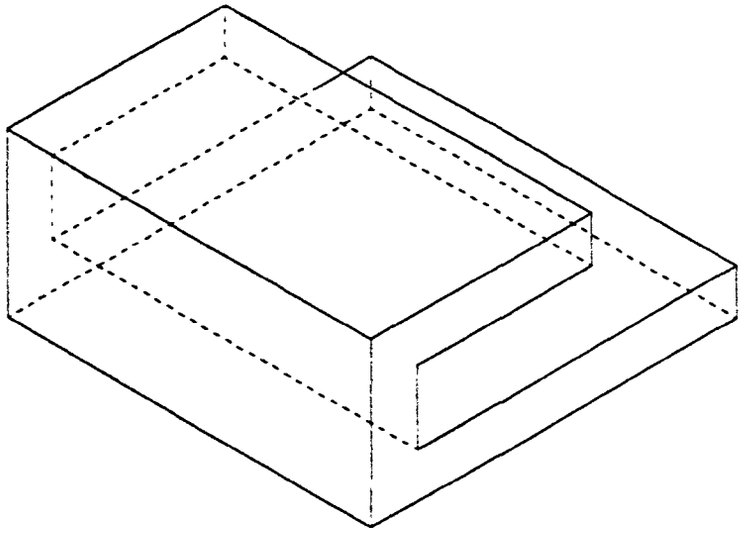

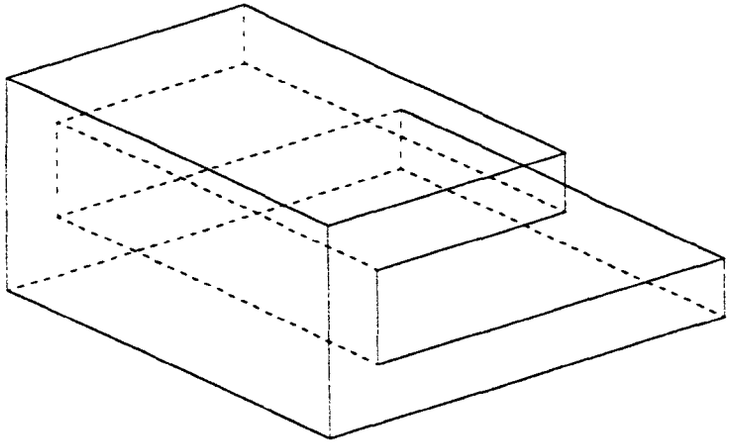

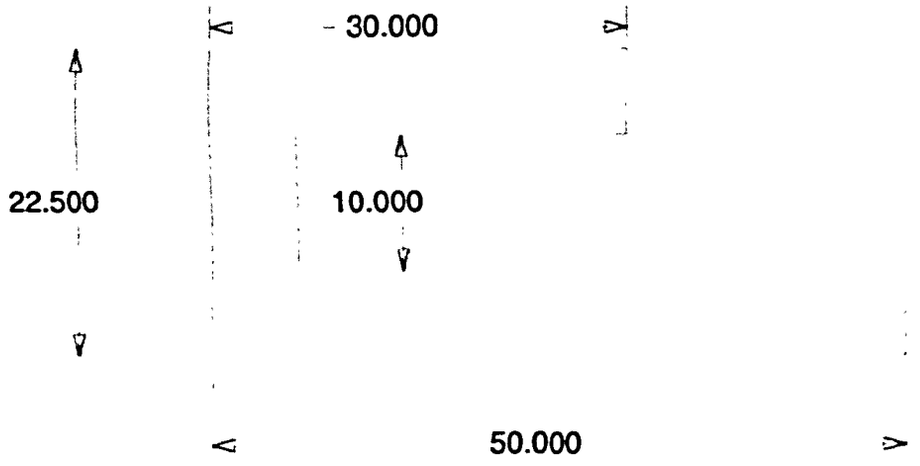
30.000
22.500
10.000
50.000

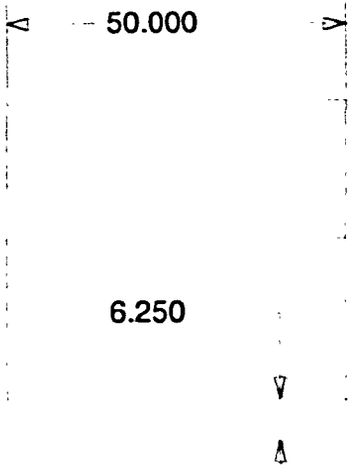
50.000
6.250

Author Index

I

J

K

L

M

N

O

P

Q

R

S

T

U

V

W

Y

Z